Investigation and Empirical Evaluation of Inputs to Optimization-Based Biomechanical Trunk Models

by

Mark L. McMulkin

Dissertation Submitted to the Faculty of the
Virginia Polytechnic Institute and State University
in Partial Fulfillment of the Requirements for
the Degree of

Doctor of Philosophy

in

Industrial and Systems Engineering

APPROVED:

K.H.E. Kroemer, Co-Chair

J.C. Woldstad, Co-Chair

J.G. Casali

R.E. Hughes

C.P. Koelling

April, 1996

Blacksburg, Virginia

Keywords: Biomechanics, Low Back, Optimization Models, Electromyography, Trunk, Lumbar Muscle Groups

INVESTIGATION AND EMPIRICAL EVALUATION OF INPUTS TO OPTIMIZATION-BASED BIOMECHANICAL TRUNK MODELS

by

Mark Lee McMulkin

Jeffrey C. Woldstad and Karl H.E. Kroemer, Co-Chairmen

Industrial and Systems Engineering

(ABSTRACT)

This dissertation investigated the ability of optimization-based biomechanical models to predict torso muscular activity. Two optimization models were considered: the Minimum Intensity Compression (MIC) model and the Sum of the Cubed Intensities (SCI) model. For each model, two sets of muscle geometries (moment arms, lines of action, and cross-sectional areas) were used as inputs: one was a compilation of several studies and one was reported by Han, Ahn, Goel, Takeuchi, and McGowan (1992). For each of the four model combinations, either 10 or 18 muscles were used to formulate predictions.

With computer simulations, the four models were used to predict muscle forces under loading conditions including three types of moments, flexion/extension, lateral bending, and torsional. The results indicated large differences in the predicted forces due to the different models and muscle geometries. Changes in force predictions for identical muscles were also found when the number of muscles in the formulation increased from 10 to 18. The models also predicted varying active and inactive regions of the muscles in response to changing moments.

To determine empirically the activity of muscles and test the accuracy of optimization-based models and inputs, combinations of the three moments were also applied to subjects through loads held in the hands. The subjects maintained a static posture during physical exertions while attempting flexion/extension, lateral bending, and torsion to counter the external loads. Results indicated little improvement in prediction of actual muscle activity by including 18 muscles instead of 10. The SCI model with compilation geometry provided the best predictions of actual muscle activity judged by overall R^2 values for each muscle and by the number of subjects the model accounted for over 50% of the variation. Actual activities of five of the eight muscles monitored were well predicted: left and right rectus abdominus, left external oblique, and left and right erector spinae. The left and right latissimus dorsi were poorly predicted by the models, which was due to the use of the muscle in shoulder stability which was not accounted for in trunk optimization models.

The experimental method included application of moments to subjects through loads held by the hands and by loads attached to a harness mounted at the shoulder level. The left and right erector spinae were the only muscles which exhibited the same activity for both apparatuses used to apply moments. The left and right latissimus dorsi showed the largest increase in activity when loads were held with the hands instead of applied via the harness. Differences between hand and harness loading were also found for the left and right rectus abdominus muscles and left and right external obliques at varying moment conditions.

This dissertation dedicated to my mother, Virginia Marie McMulkin, and to the memory of my father, Francis William McMulkin.

ACKNOWLEDGEMENTS

Support and facilities for this research were provided by the Industrial Ergonomics Laboratory in Industrial and Systems Engineering. I am extremely grateful to my Co-Chairmen, Jeffrey Woldstad and Karl Kroemer for their guidance and support through out this dissertation and my entire graduate career. I would also like to extend my appreciation to my remaining committee members, John Casali, Richard Hughes, and Pat Koelling, for their insight and advice in completing this dissertation.

This work could not have been completed with out the help of Randy Waldron, Jeff Snyder, and Will Vest who built and modified the apparatus used for the experiment.

Special thanks are due to Bethany Joseph, whose help, patience, understanding, and support were endless. I would like to recognize the valued contribution of my fellow graduate students for the help they provided during my graduate studies, and the relief they provided from work. In particular, I would like to thank Dan Mauney, Keith Tyeryar, Greg Stewart, Brad Schilling, Cortney Martin, Megan Jones, Sarah Fahey, Terry Fairbanks, Andy Gellatly, and Jon Kies.

Finally, my family deserves recognition for their constant and unending support of my graduate education. My mother, Virginia McMulkin, provided me with the strength to complete this long process. My brother, Kevin McMulkin, and sister, Kay Gasseling, were major influences through out my entire education.

TABLE OF CONTENTS

Chapter Page

LIST OF TABLES

LIST OF FIGURES

1. INTRODUCTION

Low back problems are a major health and economic burden in the United States. According to Andersson, Pope, Frymoyer, and Snook (1991), there are 4.8 million adults in the United States with low back disabilities, and 28.6 work days per hundred workers are lost each year due to low back disabilities. The costs of these low back problems are staggering, totaling $4.6 billion per year in workers' compensation costs, and estimated at $26.8 to $56 billion total cost to industries.

1.1 Optimization-based Biomechanical Models

If jobs and tasks likely to cause injuries to the low back region could be identified, then these jobs could be redesigned. Optimization-based biomechanical low back modeling is one technique aimed at identifying tasks and jobs that are likely to be hazardous to perform. For a given task, the tensions of the trunk muscles are estimated and used to calculate the resultant forces on the spinal column. If the estimated disc compression from completing a task is large, then the task may be deemed to be hazardous. The assumption in assessing tasks with this approach is that the models used to estimate trunk muscular activity are accurate.

This dissertation is concerned with the evaluation of biomechanical models used to estimate the trunk muscle forces and spinal compression. The foundation of optimization-based biomechanical models begins by applying engineering mechanics to the human body. The body is modeled as a series of rigid links. When an external force is applied to one of the links, muscles

produce force to counteract the external force and maintain a static posture. The compression, shear, and torsional forces on the spinal discs can be estimated by summing the external and internal (muscular) forces.

A planar diagram of a person holding a load is shown in Figure 1.1. A plane of reference must be established about which the forces and moments are summed. The reference system and its origin can be defined using body landmarks and features. Schultz and Andersson (1981) suggested defining a cutting plane through the L3/L4 disc, so the forces and moments can be determined at this joint.

The free body diagram of the torso above a L3/L4 cutting plane is shown in Figure 1.2. The external load and the weight of the upper torso create a compression force and generate a moment about the L3/L4 disc. The muscles of the trunk generate force to counteract the moment generated by the external load. (Note that the resultant muscle force shown on the diagram is a simplification of several muscles with different lines of action.) The combined forces of the muscles, external load, and weight of the body sum to equal the compression force on the spinal discs (as well as shear force). Reaction forces are generated by anatomical structures such as the disc, facets, and ligaments to keep the system in static equilibrium.

The forces of the individual muscles necessary to maintain a static posture are unknown. Since the number of muscles in the trunk region is generally greater than the number of moment and force equilibrium equations, the problem is statically indeterminate. There exists an infinite number of

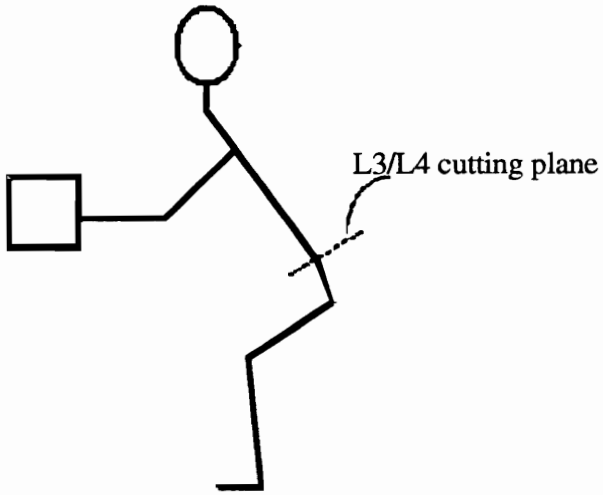

Figure 1.1 Cutting plane through L3/L4 disc

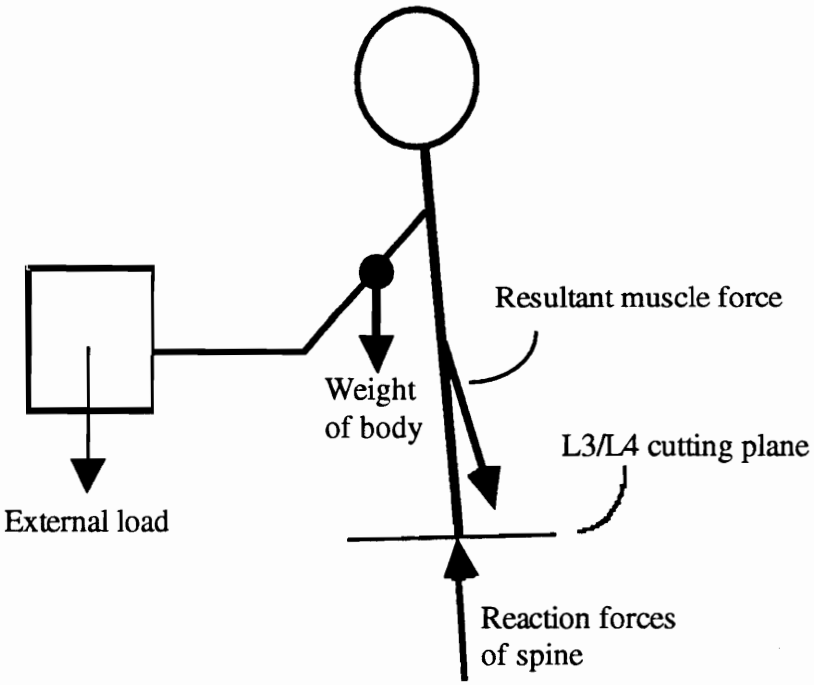

Figure 1.2 Free body diagram of forces about L3/L4 joint

combinations of muscle tensions to satisfy the moment equilibrium constraints. To solve the problem, optimization techniques can be employed to estimate the tension of the trunk muscles. Given an objective function and a set of constraints, the unknown muscle forces can be determined.

Biomechanical optimization models of the trunk must be tested and validated for their accuracy in predicting muscle activity. Previous modeling efforts have concentrated on selecting an objective function subject to constraints, then empirically testing the model to check its validity. Two models which have been used to predict the trunk muscle tensions are the Minimum-Intensity-Compression (MIC) model and the Sum of the Cubed Intensities (SCI) model. They will be discussed in the following sections.

1.2 The Minimum-Intensity-Compression (MIC) Model

The MIC model, developed by Bean, Chaffin, and Schultz (1988) as a reformulation of the iterative linear programming model of Schultz, Haderspeck, Warwick, and Portillo (1983) involves two steps. The first step is to minimize the intensity or tension that any one muscle can sustain subject to the moment equilibrium constraints. Intensity is defined as force of the muscle divided by cross-sectional area. The first step is a linear programming problem formulated as follows:

$$\text{Minimize} \quad I \tag{1.1}$$

$$\text{Subject to} \quad \sum_{i=1}^{m} \| f_i \| (r_i x \tau_i) + M^E + M^J = 0 \tag{1.2}$$

$$\frac{f_i}{A_i} \leq I \tag{1.3}$$

$$f_i \geq 0 \tag{1.4}$$

where I is the maximum intensity a muscle can sustain, m is the number of muscles, f_i is the tension in each muscle and $||f_i||$ is the magnitude of the tension (no direction), r_i is the moment arm vector with respect to the cutting plane origin (thus has the three-dimensional components of x, y, and z), τ_i is the muscle line of action with respect to the cutting plane origin (thus has the three-dimensional components of x, y, and z), M^E are the externally applied moments in three dimensions, and M^J are the moments due to joint contact and ligament forces. The $f_i \geq 0$ constraints are included because muscles cannot sustain compression. In addition, muscles cannot exert an infinite amount of force, so the $f_i / A_i \leq I$ constraints limit the muscle tension.

In the first step, intensity was minimized so that the maximum tension a muscle can assume was determined. The first step determines the set of feasible muscle forces with the determined intensity which satisfies the moment equilibrium constraints. The second step is to minimize the compression force on the disc (which is the sum of the muscle forces orthogonal to the cutting plane of the disc). The constraints are the moment equilibrium equations and the tension constraints. If there is only one optimum set of muscle forces determined in the first step, this is the only feasible solution for the second step and thus the optimum for the second step. The second step is necessary when multiple optimum sets of muscle forces are found in the first step. The second

step then chooses among the multiple optima to minimize the spinal compression. The second step is formulated as follows:

$$\text{Minimize} \quad \sum_{i=1}^{m} \|f_i\| \tau_i^z \tag{1.5}$$

$$\text{Subject to} \quad \sum_{i=1}^{m} \|f_i\| (r_i x \tau_i) + M^E + M^J = 0 \tag{1.6}$$

$$\frac{f_i}{A_i} \leq I \tag{1.7}$$

$$f_i \geq 0 \tag{1.8}$$

where τ^z is the unit direction orthogonal to the cutting plane of the disc, I is the maximum muscle intensity determined in the first step, and all other variables are the same as in the first step.

1.3 The Sum of the Cubed Intensities (SCI) Model

The SCI model was proposed by Crowninshield and Brand (1981) to predict the muscle activity of the lower extremities in locomotion. The SCI model can be applied to other body portions including the trunk. The objective is to minimize the sum of the cubed muscle intensities subject to the moment equilibrium constraints. Therefore, the optimization problem is formulated as follows:

$$\text{Minimize} \quad \sum_{i=1}^{m} \left(\frac{f_i}{A_i} \right)^3 \tag{1.9}$$

$$\text{Subject to} \quad \sum_{i=1}^{m} \|f_i\| (r_i x \tau_i) + M^E + M^J = 0 \tag{1.10}$$

$$f_i \geq 0 \qquad (1.11)$$

where the variables are defined as in the MIC model.

This objective function for this formulation was chosen based on muscular endurance capabilities. This model assumes that muscle forces are selected based on endurance restrictions. Further, Crowninshield and Brand (1981) based muscular endurance on a cubic relationship of the force divided by the cross-sectional area.

1.4 Research Objectives

This dissertation investigated optimization-based models using three new unique approaches. First, the muscle geometric inputs (moment arms, lines of action, and cross-sectional areas) were varied. Past investigations primarily used one set of muscle geometries. Second, combinations of three moments (torsional, flexion/extension, and lateral bending) were used for simulations of the models and empirical experimentation to test muscle activity. Third, moments were applied to subjects via different apparatuses: loads held in the hands and loads attached to a shoulder harness.

This dissertation had five objectives.

Objective 1: Summarize the current knowledge of the trunk muscle moment arms from the vertebrae, lines of action, and cross-sectional areas. To predict the trunk muscle forces, the Minimum Intensity Compression and Sum of the Cubed Intensities models require that the moment arms, r_i,

the muscle lines of action, τ_i, and the cross-sectional areas, A_i, are known.

Objective 2: Summarize the assumptions for solving optimization models applied to the trunk to predict muscle forces. The Minimum Intensity Compression and Sum of the Cubed Intensities models are convex so that solutions found will be global optimum. Convex models require assumptions about the human body.

Objective 3: Investigate the effect of input parameters on the muscle force predictions of the Minimum Intensity Compression (MIC) and Sum of the Cubed Intensities (SCI) low back optimization models and test the following hypotheses.

Hypothesis 3.1: Muscles with the same geometries will be predicted active or inactive differently by the MIC and SCI models (including equal number of muscles) under identical external loading conditions.

Hypothesis 3.2: The same muscle will be predicted active or inactive differently by two sets of muscle geometries reported in the literature using the same model, MIC or SCI, with identical loading conditions.

Hypothesis 3.3: Muscles with the same geometries will be predicted active or inactive differently by the same model, MIC or SCI, as the number of muscles included in the model is changed from 10 to 18 with identical loading conditions.

Objective 4: Compare the predictions of combinations of competing models, number of muscles, and muscle geometric data with experimentally obtained actual muscle activity to answer the following hypotheses.

Hypothesis 4.1: One of two models, the MIC or the SCI model, will predict muscle forces, as matched with actual muscle activity, significantly better.

Hypothesis 4.2: One of two muscle geometries, reported by Han et al. (1992) and reported by a compilation of authors, used in the MIC and SCI models will predict muscle forces, as matched with actual muscle activity, significantly better.

Hypothesis 4.3: One of the four combinations of model and geometry set, the MIC with Han et al. geometry, the MIC with compilation geometry, the SCI with Han et al. geometry, or the SCI with compilation geometry will predict muscle forces, as matched with actual muscle activity, significantly better than the rest.

Hypothesis 4.4: One of two numbers of muscles used in the MIC and SCI models, 10 or 18, will predict muscle forces which have unchanged geometry, as matched with actual muscle activity, significantly better.

Objective 5: Test the apparatus used to create combinations of moments at the L3/L4 disc. The hypothesis is that a shoulder harness used to apply moments will create different muscle activity from moments applied via weights held with the hands.

1.5 Dissertation Organization

The remainder of this dissertation has been divided into seven chapters. Chapters 2 and 3 consist of a literature review of the important topics in optimization-based biomechanical modeling of the trunk. Chapter 2 is a review of the functional anatomy of the trunk region. Chapter 3 is a detailed review of the development of low back optimization models. Chapter 4 presents the implementation of low back optimization models to predict muscle forces given varying input parameters. Chapter 5 covers the experiment used to test the accuracy of the models and input parameters. The results of the experiment are reported in the Chapter 6, followed by a discussion of the results in Chapter 7, and finally the conclusions of this study in Chapter 8.

2. FUNCTIONAL ANATOMY OF THE TRUNK

To implement an optimization-based model to predict muscle forces, a functional understanding of the musculo-skeletal system of the trunk is needed. In the formulation of an optimization model, the moment equilibrium equations are included as constraints:

$$\sum_{i=1}^{m} \|f_i\|(r_i x \tau_i) + M^E + M^J = 0 \qquad (2.1),$$

where m is the number of muscles, f_i is the tension in each muscle, r_i is the moment arm vector (thus has the three-dimensional components of x, y, and z), τ_i is the muscle line of action (thus has the three-dimensional components of x, y, and z), M^E are the externally applied moments in three-dimensions, and M^J are the moments due to joint contact and ligament forces. The tensions in each muscle, f_i, are the unknown quantities determined in solving the problem. All the other quantities are assumed to be known.

A reference system is established about which the forces and moments are summed. The reference system and its origin can be defined using body landmarks and features. The muscle moment arms and lines of action are dependent on the reference plane (or cutting plane) necessitating a consistent coordinate system be maintained. Schultz and Andersson (1981) suggested defining a cutting plane through the L3/L4 disc, so the forces and moments could be determined at this joint.

After determining a cutting plane, a coordinate system is placed at the origin. The directions of the x, y, and z axes are arbitrary, although a right-handed coordinate system should be selected. For consistency, the coordinate

system shown in Figure 2.1 is adopted. The x-axis runs laterally through the body and is positive to the right side. The y-axis runs anteriorly and posteriorly, with the positive direction toward the anterior. The z-axis runs foot to head, the positive direction toward the head. Trunk anatomy studies have adopted different coordinate systems since the axis directions are arbitrary. All values reported in this review correspond to the coordinate system established by Figure 2.1.

The anatomy literature was reviewed to determine the appropriate muscles to include in the model (m in the above constraints), the moment arm vector (r_i), lines of action (τ_i), area of each muscle (A_i), and finally the relative contribution of disc and ligament forces. Because the line of action, moment arm, and area of each muscle depend on the cutting plane, it is important to consider this when reviewing studies.

2.1 Skeletal System of the Trunk

Two of the major functions of human bones are to provide the framework of the body and provide the lever arms to which muscles attach (via tendons) to create torque about the joints (Kroemer, Kroemer, and Kroemer-Elbert, 1990). The origin and insertion points of the tendons (from the muscles) on the bones are important anatomical considerations in determining muscle lines of action. The joint along the spinal column selected to apply the moment equilibrium equations affects muscle lines of action, moment arms, and cross-sectional areas.

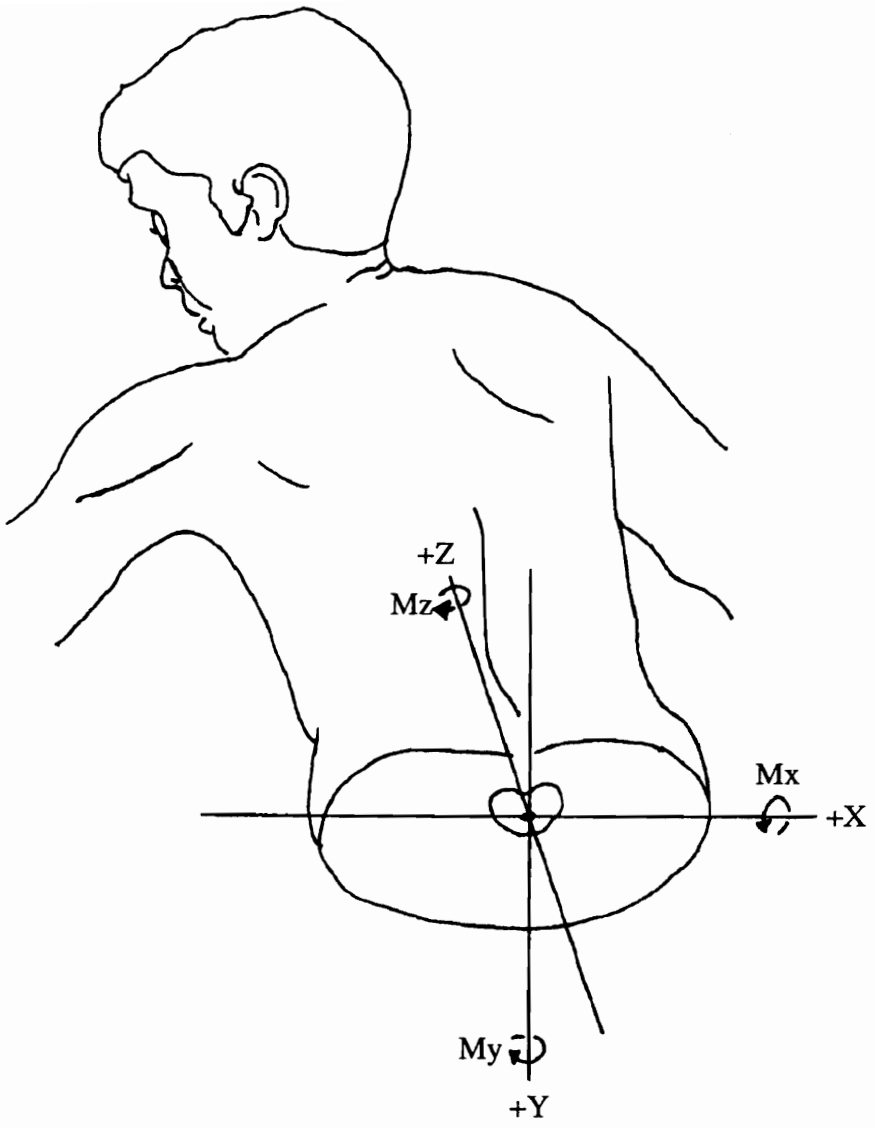

Figure 2.1 Coordinate system adopted for the low back (Hughes, 1991).

The spinal column consists of seven cervical vertebrae, twelve thoracic vertebrae, five lumbar vertebrae, and the sacrum and coccyx. Between each of the vertebrae are fibrocartilage discs which form the joints between the vertebrae. Although there is limited movement in the joints of the spinal column, any one of these could be used as a center of rotation about which the moments created by the muscles, external forces, and contact and ligament forces are summed. The joint chosen affects which muscles should be included in the model, the moment arm lengths of the muscles, the lines of action, and the area.

The cutting plane is generally defined to pass through the lumbar section of the spine. More specifically, the cutting plane is usually selected to pass through the L1/L2, L2/L3, L3/L4, L4/L5, or L5/S1 discs. Since the lumbar section of the spine is curved, cutting planes through these discs are not parallel. The selection of the cutting plane determines the coordinate system to be used. Non-parallel cutting planes result in different coordinate systems, although the relative distances between vertebrae, muscles, and ligaments does change.

The muscles connect to the vertebrae, ribs, and pelvic bones via tendons. The origin and insertion points as well as the path traversed by the muscles determines the line of action and moment arm length. These two topics will be discussed in following sections.

2.2 Number of Muscles Used in Modeling

The purpose of this section is to present the different muscles and their representations used in the formulation of various biomechanical trunk models.

It is not intended to present a detailed review of the muscle anatomy of the trunk. For a thorough review of trunk muscle anatomy, sources such as Williams, Warwick, Dyson, and Bannister (1989) or Anderson (1978) are appropriate.

Determining which muscles to include in a biomechanical model of the trunk area has perhaps the largest impact on the complexity of the model. As the number of muscles used in a model increases, the accuracy of the representation of the body may increase. However, the details of the muscle area, line of action, and moment arms are also necessary. Determining these values may not always be possible. In addition, a static biomechanical model of the forces and moments about one of the vertebrae is often an indeterminate system (the number of unknowns is larger than the number of equations). Therefore, adding more muscles simply adds more unknowns to an already statically indeterminate problem.

The number of muscles to include in a biomechanical model of the trunk is a function of several factors. First, the relative contribution of each muscle should be considered. This is a function of the cross-sectional area of the muscle and the distance from the point of rotation on the vertebrae. Muscles which can contribute negligible moment due to size, orientation, or location do not necessarily need to be included in a model. Second, the area, line of action, and moment arm of individual muscles must be known to be included. This information can not always be obtained for muscles that may be distinct but are located in close proximity to each other in the trunk. Third, practical

considerations such as the ability to mathematically state and solve the model need to be taken in to account.

McGill and Norman (1986) studied the relative moment generation contributed by the trunk muscles, ligaments, and disc about the L4/L5 joint in performing a dynamic lift. The model estimated the forces of 48 muscles and 7 ligaments. The force of each muscle was estimated by the following formula:

$$F_m = G[(EMG/EMG_m)(P_o)(\Omega)(\delta) + F_{pec}]$$

where

F_m = muscle force for each of the m (48) muscles,
G = error term or gain,
EMG = EMG amplitude (arbitrary units), measured by 1 of 6 electrode locations,
EMG_m = MVC (maximum voluntary contraction) EMG amplitude (arbitrary units),
P_o = maximum isometric force,
Ω = coefficient for velocity modulation,
δ = coefficient of active length modulation,
F_{pec} = force due to passive elasticity.

The force calculated by this formula was multiplied by the moment arm to obtain the moment contribution of each muscle. McGill and Norman (1986) used a detailed model including a large number of muscles and incorporating muscle length and velocity considerations. Several problems with the model existed. First, McGill and Norman were not specific about how the moment arms from the L4/L5 disc to each muscle are determined. For active length modulation, they indicated that the muscle length is calculated by an equation using a straight line between the origin and insertion. The path of the trunk muscles can follow a nonlinear path and a straight line may not be an accurate estimate of the

moment arm distance or length of the muscle. Second, the equation used to calculate muscle force relied on an EMG input from one of six locations on the trunk. Predicting 48 individual muscles from only six inputs was admitted by the authors to be a problem. Third, the equation to calculate muscle forces used the maximum isometric force as an input; the maximum isometric force was assumed to be the cross-sectional area of the muscle multiplied by the maximum muscle intensity, assumed to be from 35 to 55 N/cm^2. There was no agreement on the maximum intensity a muscle can assume. McGill, Patt and Norman (1988) state that it has been reported to range from 30 to 90 N/cm^2. Finally, the purpose of this model and study was to evaluate the relative contributions of the muscles, ligaments, and disc in generating moment about the L4/L5 disc. This study was not aimed at predicting muscle forces and disc compression in response to an external load. Establishing 48 moment arms and lines of action needed for an optimization model is very difficult, and McGill and Norman do not report the exact values or method they used.

In a study to compare static versus dynamic torsion about the L4/L5 disc, McGill and Hoodless (1990) and McGill (1991) used 50 muscles in their model. The 50 individual muscles employed in the model were reported but the associated moment arms were not listed. The force of each muscle was calculated as the cross-sectional area multiplied by a maximum intensity, assumed to be 35 to 50 N/cm^2. Their study is effective in identifying the differences in moment due to static and dynamic tasks. However, to implement 50 individual muscles into an optimization model, the lines of action and moment arms of each muscle are needed.

Ladin, Murthy, and De Luca (1989) used an optimization model developed by Schultz, Haderspeck, Warwick, and Portillo (1983) to predict the forces of 22 muscles during static exertion tasks. The 22 muscles consisted of the following 11 muscles for both the left and right sides: iliocostalis, multifidus, longissimus, quadratus, psoas, latissimus dorsi, medial portion of the external oblique, lateral portion of the external oblique, medial portion of the internal oblique, lateral portion of the internal oblique, and rectus abdominus. The muscles counteracted external loads in the flexion and lateral bending directions. Ladin et al. (1989) chose a cutting plane at the L3 level. The moment arms for each of the muscles at the L3 level were taken from Eycleshymer and Schoemaker (1911), but not specifically reported in their article. I assume they measured the moment arms from diagrams in this reference. Ladin et. al. (1989) proposed a 'switching curve' concept for each muscle. A muscle was considered either active or inactive during an external load. The switching curve divided the possible external loading moment conditions (combinations of flexion/extension and lateral bending) into regions in which the muscle was predicted to be active or inactive. Through experiments to verify proposed switching curves, Ladin et al. (1989) assert that the 11 pairs of muscles can be functionally grouped into a reduced set of 5 pairs

1) Erector spinae: consisting of the longissimus, multifidus, latissimus dorsi, and iliocostalis;
2) Paraspinal: consisting of the psoas and quadratus;
3) Medial abdominal: consisting of the medial portions of the external and internal obliques;

4) Lateral abdominal; consisting of the lateral portions of the external and internal obliques;

5) Rectus abdominus.

The concept of functionally grouping muscles had been used earlier by Maton and Bouisset (1977) and Bouisset, Lestienne, and Maton (1977) for the flexor muscles of the elbow. Maton and Bouisset (1977) measured the EMG activity of four elbow flexor muscles during six isometric force levels. They determined that the four muscles became active at the same loading conditions and their relative activity varied by a constant coefficient. Because of these results, Maton and Bouisset (1977) stated that using the biceps brachii as the "muscle equivalent" of all four muscles was justified. Bouisset et al. (1977) measured the EMG activity of three elbow flexors during movement tasks. Their results showed a constant relationship between the excitation levels of the three flexors, and the activity of the biceps muscle began and ended at nearly the same time as the other muscles. The flexor muscles of the elbow can be grouped into a muscle equivalent because of the activity relationships and timing of onset and cessation. Bozec, Maton, and Cnockaert (1980) and Bouisset (1973) found similar results for the elbow extensor muscles. An equivalent muscle group for the elbow extensors can be assumed because of the constant relationship between excitations of the different muscles. The concept of an equivalent muscle system implies that the group of muscles is under some common neural control mechanism.

The work of Maton and Bouisset (1977) and Bouisset et al. (1977) concentrated on two-dimensional loading of the elbow and not three-

dimensional loading as in the trunk. Maton and Bouisset (1977) and Bouisset et al. (1977) considered whether multiple muscles acted simultaneously to flex the elbow, but none of the muscles were considered to produced a three-dimensional force and moment. The muscles of the trunk, which create forces and moments in three-dimensions, might not be grouped together because they do not act in similar unit directions. However, even though the components of a muscle act in different unit directions, the components may act together to form an equivalent muscle group. For example, the fascicles of the erector spinae act in different unit directions (Macintosh and Norman, 1991), but they may act together to form an equivalent muscle group.

Schultz and Andersson (1981) presented two techniques to determine the muscle forces in response to externally generated moments. They included 10 muscles in their model, 5 on each side of the trunk: latissimus dorsi, erector spinae, external oblique, internal oblique, and rectus abdominus. Because this system was statically indeterminate, one method to finding a solution was to assume enough of the muscles were inactive until a determinate problem resulted. The second method was to apply optimization techniques. When applying linear optimization techniques, the number of non-zero muscle forces are equal to at most the number of constraint equations. Limiting non-zero forces presents a difficulty even when the number of muscles was ten as in the study reported by Schultz and Andersson (1991).

An iterative model to predict trunk muscle forces, developed by Schultz et al. (1983), minimized the maximum required muscle intensity. The model began with a maximum muscle intensity of 10 kPa (1 N/cm^2). A solution of

muscle forces in response to some external load was sought to minimize spinal compression. If no solution was possible, the intensity was increased by 10 kPa until a feasible solution was found. Schultz et al. (1983) used three sets of muscles at the L3 cutting plane: the first contained 22 muscles, the second 14, and the third 10. The 22-muscle model consisted of 11 bilateral pairs (left and right side) spanning the lumbar region: the rectus abdominus muscles, the lateral and medial external oblique abdominal muscles, the lateral and medial internal oblique abdominal muscles, the psoas, the quadratus lumborum, the latissimus dorsi, and the multifidus, longissimus, and iliocostalis groups of the erector spinae. For the 14-muscle model, the psoas and quadratus muscle were deleted and the three groups of erector spinae muscles (the multifidus, longissimus, and iliocostalis groups) were grouped into a single equivalent muscle. For the 10-muscle model, the 14-muscle model was further reduced. The lateral and medial external oblique abdominal muscles were combined into a single external oblique abdominal muscle equivalent. The lateral and medial internal oblique abdominal muscles were combined into a single internal oblique abdominal muscle equivalent. The authors stated that the muscle force predictions and disc compression of the 14- and 10-muscle models were consistent with the 22-muscle models. The combined erector spinae muscle was roughly the sum of the three individual muscles in the 22-muscle model. Similarly, in the 10-muscle model, the combined external and internal oblique abdominal muscles, were approximately the sum of the distributed forces in the 14- and 22-muscle models.

Several other studies with varying objectives employed optimization-based biomechanical models to estimate the muscle forces in the trunk. Hughes (1991), Johnson (1992), Schultz, Andersson, Örtengren, Haderspeck, and Nachemson (1982) selected a set of 10 muscles (5 from each side) to represent the muscular anatomy of the trunk: rectus abdominus, internal oblique, external oblique, latissimus dorsi, and erector spinae. Other studies have chosen from 14 to 171 muscles to model the trunk musculature (Schultz, Cromwell, Warwick, and Andersson, 1987; Schultz, Haderspeck-Grib, Sinkora, and Warwick, 1985; Takashima, Singh, Haderspeck, and Schultz, 1979; Yettram, Bai, and Jackman, 1989; Zetterberg, Andersson, and Schultz, 1987). The level of detail selected was dependent on the objective of the study, the mathematical modeling of the trunk, and the ability to solve and verify muscle force predictions. Zetterberg et al. (1987) employed 22 muscles in their optimization model to predict muscle forces. However, in verifying the predictions, they selected a subset of 10 muscles on which to collect EMG data. Yettram et al. (1980) included 171 muscles, but were concerned with analyzing multiple segments of the back, the forces for 17 vertebrae (T1 to C5). For example, Yettram et al. (1980) included 40 fascicles (20 each on the left and right sides) of the multifidus muscle. Only a portion of the 40 multifidus fascicles crossed each of the vertebrae.

The trunk of the body has a complex musculo-skeletal structure. An exact model of the lumbar region would include every muscle. However, to implement an optimization model to predict the muscle forces, cross-sectional areas, lines of actions, and moment arms for each individual muscle must be

known. Currently, the knowledge of these variables simply does not exist for a model including individual fascicles of each muscle. Therefore, a model including a reduced number of muscles and known geometries is used.

2.2.1 Detailed Anatomy of the Erector Spinae

The anatomy of the erector spinae muscle and its components have been studied in detail by Bogduk, Macintosh, and colleagues (Bogduk, 1980; Bogduk, Macintosh, and Pearcy, 1992; Macintosh and Bogduk, 1986, 1987, 1991; Macintosh, Bogduk, and Pearcy, 1993; Macintosh, Valencia, Bogduk, and Munro, 1986).

Bogduk (1980) dissected four cadavers while Macintosh and Bogduk (1987) dissected eight cadavers to determine the detailed anatomy of the erector spinae muscle. These authors defined the erector spinae to consist of the iliocostalis and longissimus muscles. They concluded that the erector spinae be considered to have four components: two columns of muscles (the iliocostalis and longissimus) each with thoracic and lumbar parts. They referred to the four components as follows: longissimus thoracis pars thoracis, iliocostalis lumborum pars thoracis, longissimus thoracis pars lumborum, and iliocostalis lumborum pars lumborum. Essentially, the longissimus thoracis pars thoracis and iliocostalis lumborum pars thoracis arise from the transverse processes and ribs of the thoracic region of the trunk. They join a common tendon which passes posteriorly to the erector spinae muscle in the lumbar region. Although the muscle bellies originate in the thoracic region, the tendon still creates force at a cutting plane through the L3/L4 disc, yet would have a

larger moment arm and thus require less force to resist an external load. The longissimus thoracis pars lumborum and iliocostalis lumborum pars lumborum arise from the transverse processes of the lumbar vertebrae. They form the soft muscle tissue generally considered to be the erector spinae in the lumbar region. The results provided by Bogduk (1980) and Macintosh and Bogduk (1987) were generally qualitative descriptions of the erector spinae. Graphical lines of action of the erector spinae components in the frontal plane were provided. Assuming there is no angular rotation of the muscles in the sagittal plane, the lines of action could be measured from the graphs. Quantitative moment arms values for the erector spinae components were not provided by Macintosh and Bogduk (1987).

A model which incorporated an increased moment arm for the thoracic erector spinae due to the common tendon passing posterior to the lumbar erector spinae soft tissue was investigated by McGill and Norman (1987). Through computed tomograghy scans of living subjects, McGill and Norman (1987) estimated the moment arm of the longissimus thoracis pars thoracis and iliocostalis lumborum pars thoracis tendon to be approximately 9 cm. They used a biomechanical model which allocated force to the lumbar erector spinae at a given maximum intensity (30 to 90 N/cm^2). Any remaining external load that was not counteracted by the lumbar erector spinae was then allocated to the thoracic erector spinae via a common tendon at a moment arm ranging from 7 to 10 cm. McGill and Norman (1987) demonstrated that this load sharing does reduce the estimate of spinal compression due to the general moment arm increase. A disadvantage of the model employed by McGill and Norman (1987)

was that muscle and tendon forces acting at the same cutting plane were not predicted simultaneously, but in a serial fashion. Specific three-dimensional moment arms and lines of action were not provided by McGill and Norman (1987), instead a two-dimensional view was given.

The attachments of each fascicle of the thoracic and lumbar erector spinae were reported by Macintosh and Bogduk (1991). The information provided was quite detailed, but difficult to incorporate into a biomechanical model. First, the line of action of each fascicle was given by Macintosh and Bogduk (1991) with respect to the vertebrae to which it attached. However, the line of action of each fascicle with respect to a given vertebrae cutting plane was not provided. Second, including each fascicle of the erector spinae into a model provides great detail of the erector spinae, yet leaves the other muscles more grossly represented. It appears that the erector spinae has been more closely studied than other muscles.

The anatomy of the multifidus muscle has been detailed by Macintosh et al. (1986) and Macintosh and Bogduk (1986). From cadaver dissections, Macintosh et al. (1986) qualitatively described the multifidus as consisting of five bands, one each emanating from the five lumbar vertebrae spinous processes. Using radiographs of 21 living subjects, Macintosh and Bogduk (1986) quantitatively report the line of action of each component of the multifidus muscle. The lines of action of each component are reported with respect to each vertebrae. Although the lines of action are given in detail, associated moment arms and areas are not provided. The difficulty of including

detailed descriptions of a few muscles without complete information or without detailed information on all trunk muscles still remains.

Bogduk et al. (1992a) developed a detailed model of the lumbar trunk to include the multifidus and erector spinae muscles. They incorporated individual fascicles of the multifidus and erector spinae muscles. However, the model was limited to two-dimensional sagittal plane motion. Lateral information such as moment arms and direction in the frontal plane were not included.

2.2.2 Detailed Anatomy of the Psoas Muscle

A qualitative and quantitative depiction of the psoas muscle was provided by Bogduk, Pearcy, and Hadfield (1992b). From the dissection of three cadavers, Bogduk et al. (1992b) reported the psoas consists of 10 fascicles. Five of these arise from the T12/L1 to L4/L5 discs and five arise from the L1 to L5 transverse processes. The fascicles join to form a common psoas tendon. Using radiographic scans of living subjects, moment arms and lines of action for each fascicle were given for the sagittal plane assuming, any lumbar disc as the reference frame. Without further three-dimensional information and equivalent information for the remaining torso muscles, it is difficult to input this information into a biomechanical model.

2.3 Muscle Moment Arms

To implement an optimization model, the moment arms from the muscles to the assumed origin are needed. A cutting plane establishes a reference

coordinate system. Given a reference coordinate system, values for the moment arms are stated in terms of x, y, and z lengths.

Tracy, Gibson, Szypryt, Rutherford, and Corlett (1989) measured the cross-sectional area and position of the lumbar muscles using magnetic resonancing imaging (MRI). Twenty-six males were included in their study which were under investigation for intervertebral disc degeneration or protrusion. This restriction might have caused some reduction in muscle size, but no subjects had been immobilized, leading to a gross change. Transverse MRI's were taken at each lumbar disc level. The moments arms for each of the right side muscles at the L3/L4 level are listed in Table 2.1. The values and directions correspond to the coordinate system previously shown in Figure 2.1. Tracy et al. (1989) only measured the right side muscles. The left side muscles are assumed to be symmetrical for implementation into a model. The moment arms for the muscles are a three-dimensional vector with r_x, r_y, and r_z, components; r_z is equal to zero for each muscle because the lengths are for a cutting plane which, by definition is perpendicular to the z-axis.

The only cutting plane at which Tracy et al. were able to discern the oblique muscles individually was the L3/L4 level. If another cutting plane is used, alternative studies would need to be consulted. The technique employed by Tracy et al. was performed on relatively healthy and active adults, which was an advantage over the use of cadavers. Two main disadvantages to the study were that no female subjects were included, and although moment arm values for several muscles were reported, the sample size for some muscles were small.

TABLE 2.1 Moment Arms for the Right Side Trunk Muscles at the L3/L4 Level as Reported by Tracy et al. (1989). Values are in cm

Muscle	N	r_x	r_y	r_z
R. Erector Spinae	26	3.82	-5.76	0
medial (multifidus)	21	1.79	-6.10	0
intermediate (longissimus)	21	3.89	-6.05	0
lateral (iliocostalis)	21	5.86	-5.43	0
R. Rectus Abdominus	25	3.38	7.95	0
R. Obliques (overall)	13	12.21	1.72	0
R. Internal Oblique	3	11.39	0.96	0
R. External Oblique	3	12.62	1.09	0
R. Latissimus Dorsi	1	7.19	-5.42	0
R. Quadratus Lumborum	26	7.49	-3.48	0
R. Psoas	26	4.29	-0.59	0

Since each MRI taken by Tracy et al. (1989) was a transverse scan, they were not parallel to the intervertebral discs (due to lumbar lordosis). The angles of each lumbar disc relative to transverse plane of the body were also measured by Tracy et al. The angles for the L1/L2, L2/L3, L3/L4, L4/L5, L5/S1 discs were found to be 8.3, 4.1, -1.3, -12.1, and -31.4 degrees, respectively. Therefore, the L3/L4 disc is most closely parallel to the transverse plane of the body. The transverse plane used by Tracy et al. to measure the disc angles is not the same as the cutting plane defined in Figure 2.1. The L3/L4 disc has angle of 0 degrees with respect to the x-y plane in Figure 2.1. The transverse plane used by Tracy et al. was tilted -1.3 degrees with respect to the cutting plane defined in the current paper.

Han, Ahn, Goel, Takeuchi, and McGowan (1992) measured the moment arms of 20 muscles (10 for the left side and 10 for the right) using computed

axial tomography (CT scans). Ten Japanese patients, six male and four female, suffering from low-back, pain-related spinal disorders participated in the study. The centroid locations (or moment arms) at all disc levels from T12/L1 to L5/S1 were measured. The centroid locations for the muscles in this study were reported in non-dimensionalized terms. For example, the centroid location of the left rectus abdominus in the x-direction was reported as -0.1340, which equaled r_x divided by the trunk width at this level. Table 2.2 lists the mean moment arms for the ten muscles investigated by Han et al. (1992) at the L3/L4 level. The non-dimensionalized values were dimensioned (in cm) by multiplying by the mean trunk width and depth reported on the ten subjects. Han et al. (1992) measured the moment arms for both the right and left side muscles which accounts for the slight differences in values reported.

At the L4/L5 cutting plane level, McGill, Patt, and Norman (1988) measured the moment arms of eight muscles. They determined the moment arm values using transverse CT scans of 13 active men who received treatment for complaints of low back pain. Table 2.3 lists the eight muscles and the corresponding moment arms reported by McGill et al. Only data on the right side muscles are reported and symmetry for the left side was assumed.

McGill, Santaguida, and Stevens (1993) measured the moment arms of several muscles from the T5 to L5 levels. They determined moment arms using MRI on 15 active young men with no history of back disease or injury. Table 2.4 lists the muscles studied and the corresponding moment arms at the L3 and L4 levels. Moment arms corrected for fiber orientation were reported for muscles

TABLE 2.2 Dimensional Moment Arms at the L3/L4 Level Reported by Han et al. (1992). Values are in cm

	Left		Right	
Muscle	r_x	r_y	r_x	r_y
Multifidus	-1.640	-5.334	1.615	-5.470
Iliocostalis	-5.707	-4.893	5.509	-4.820
Longissimus	-3.497	-5.364	3.516	-5.311
Rectus Abdominus	-3.643	7.211	3.676	7.074
Internal Oblique	-10.569	2.671	10.718	2.414
External Oblique	-11.572	1.745	11.732	1.667
Latissimus Dorsi	-8.388	-4.346	8.046	-4.583
Quadratus Lumborum	-6.691	-2.958	6.670	-3.064
Psoas	-3.828	-0.529	3.929	-0.713
Transversus	-9.788	3.130	9.865	2.991

TABLE 2.3 Right Side Muscle Moment Arms Determined by McGill et al. (1988) at the L4/L5 level. Values are in cm

Muscle	r_x	r_y
R. Erector Spinae	3.26	-5.90
R. Erector Mass Common Tendon	1.98	-8.49
R. Rectus Abdominus	4.35	10.28
R. Internal Oblique (anterior)	10.77	6.92
R. Internal Oblique (posterior)	12.52	3.85
R. External Oblique (anterior)	12.86	5.94
R. External Oblique (posterior)	13.95	2.08
R. Psoas	4.88	0.58

TABLE 2.4 Moment Arms at the L3 and L4 Levels Reported by McGill et al. (1993). Values are in cm

Muscle	L3		L4		Corrected L3/L4	
	r_x	r_y	r_x	r_y	r_x	r_y
L. Erector Spinae	-3.8	-6.1	-3.3	-6.1		
R. Erector Spinae	4.0	-6.1	3.4	-6.1		
L. Multifidus	-1.4	-5.3				
R. Multifidus	1.1	-5.5				
L. Longissimus Thoracis	-1.9	-6.1				
R. Longissimus Thoracis	2.2	-6.1				
L. Iliocostalis Lumborum	-4.8	-5.5				
R. Iliocostalis Lumborum	5.2	-5.7				
L. Rectus Abdominus	-3.8	8.0	-3.6	7.3		
R. Rectus Abdominus	4.2	7.9	3.8	7.3		
L. Internal Oblique	-11.2	2.6	-10.3	4.1	-8.9	2.0
R. Internal Oblique	11.6	2.5	10.9	4.1	8.9	2.0
L. External Oblique	-12.5	1.9	-12.0	3.2	-11.0	1.7
R. External Oblique	13.0	2.0	12.5	3.5	11.0	1.7
L. Latissimus Dorsi	-10.4	-4.3				
R. Latissimus Dorsi	10.2	-4.5				
L. Psoas	-4.2	-0.6	-4.8	0.2		
R. Psoas	4.4	-0.7	5.0	0.1		
L. Quad. Lumborum	-7.3	-3.4	-7.8	-3.1	-5.9	-2.9
R. Quad. Lumborum	7.6	-3.7	8.1	-3.6	5.9	-2.9
L. Transversus	-10.7	2.3	-10.1	3.0		
R. Transversus	11.2	2.2	10.8	2.8		

that changed by 10%. Data on both the right side and left side muscles were reported.

Cholewicki and McGill (1996) implemented a model including 45 pairs of muscles. The 45 muscles were comprised of several fascicles. For example, 12 fascicles of the multifidus as well as 5 fascicles of the psoas were included. Moment arms of the 45 pairs of muscle were not reported, but the three-

dimensional coordinates of the origin and insertion of each muscle were reported. The moment arms could be calculated from the coordinates. Due to the amount of data reported, the original source should be consulted.

Chaffin, Redfern, Erig, and Goldstein (1990) measured the moment arms of 14 muscles (7 for the left side and 7 for the right) using CT scans. A group of 96 healthy, physically active women between 40 and 63 years participated in the study. The moment arms at the L2/L3, L3/L4, and L4/L5 disc levels were measured. Table 2.5 lists the mean moment arms for the seven muscles investigated by Chaffin et al. at the L3/L4 level. They measured the moment arms for both the right and left side muscles which accounted for the slight differences in the values reported.

TABLE 2.5 Moment Arms at the L3/L4 Level Reported by Chaffin et al. (1990). Values are in cm

	Left		Right	
Muscle	r_x	r_y	r_x	r_y
Erector Spinae	-3.4	-5.3	3.4	-5.2
Rectus Abdominus	-4.3	7.2	4.3	7.0
Internal Oblique	-11.4	2.0	11.3	2.1
External Oblique	-12.2	2.0	12.0	2.3
Latissimus Dorsi	-10.7	-3.0	10.6	-3.0
Quadratus Lumborum	-6.5	-3.3	6.5	-3.2
Psoas	-3.8	-0.8	3.7	-0.8

Using CT scans, Németh and Ohlsén (1986) measured the moment arms of four trunk muscles at the L5/S1 disc level. Eleven male and ten female patients participated in the study. Moment arms were measured for both the left and right side muscles and then reported in terms of an average of both, Table 2.6.

Reid, Livingston, and Pearsall (1994) determined geometric data of the psoas muscle using magnetic resonance imaging on 15 active males with no history of back pain. They measured the moment arms and cross-sectional areas of the left and right psoas muscles at nine vertebral and/or intervertebral

TABLE 2.6 Moment Arms Averaged Across the Left and Right Sides at the L5/S1 Level Reported by Németh and Ohlsén (1986). Values are in cm

	Left		Right	
Muscle	r_x	r_y	r_x	r_y
Males				
Erector Spinae	-2.3	-7.1	2.3	-7.1
Rectus Abdominus	-4.8	10.9	4.8	10.9
Oblique Abdominal	-13.4	6.4	13.4	6.4
Psoas	-5.7	1.3	5.7	1.3
Females				
Erector Spinae	-2.5	-6.5	2.5	-6.5
Rectus Abdominus	-4.0	8.0	4.0	8.0
Oblique Abdominal	-11.4	5.2	11.4	5.2
Psoas	-5.0	0.8	5.0	0.8

levels: L2, L2/L3, L3, L3/L4, L4, L4/L5, L5, L5/S1, and S1. At the L3/L4 disc level, r_x was -4.2 and 4.4 cm respectively for the left and right sides; r_y was -0.4 and -0.4 cm respectively for the left and right sides.

The moment arms of rectus abdominus and erector spinae were determined by Reid and Costigan (1985) in terms of percentage of the trunk depth and width. However, regression analyses performed by Chaffin et al. (1990) and Han et al. (1992) to predict muscle moment arms from parameters such as trunk depth or width exhibited low R^2 values. These studies indicated that predicting muscle moments arms from anthropometric inputs was relatively unsuccessful and unreliable. Rab, Chao, and Stauffer (1977) provided moment arms for seven trunk muscles in graphical representations. Due to difficulties in reading the graphs, these moment arms are not considered accurate enough to be used as inputs into a biomechanical model.

2.4 Lines of Muscle Action

The lines of action for ten trunk muscles were measured by Dumas, Poulin, Roy, Gagnon, and Jovanovic (1988) on one cadaver. External oblique, internal oblique, and transverse abdominus muscles were represented by curvilinear models while latissimus dorsi, rectus abdominus, transversus abdominus, quadratus lumborum, iliopsoas, and erector spinae (iliocostalis and longissimus) muscles were represented by linear models. Multiple vectors were also used to represent the main orientation of the fibers for the ten muscles. The lines of action for the ten muscles (an average of the vectors representing each muscle) at the L3/L4 disc level are listed in Table 2.7.

TABLE 2.7 Lines of Action Found by Dumas et al. (1988) at L3/L4

	Line of Action			
	I_x	I_y	I_z	
R. Erector Spinae				
R. Longissimus: origin to				
costa XII	-0.134	0.005	-0.991	
costa VIII	-0.103	0.016	-0.995	
costa VI	-0.063	-0.004	-0.998	
R. Iliocostalis: origin to				
costa XII	-0.281	-0.052	-0.958	
costa IX	-0.222	0.016	-0.975	
costa VII	-0.137	-0.004	-0.991	
R. Rectus Abdominus	-0.028	0.016	-0.9995	
R. Internal Oblique: to crest of illium from				
costa X	0.134	-0.574	-0.808	
costa XI	-0.284	-0.466	-0.837	
R. External Oblique: to crest of illium from				
costa IX	-0.477	0.160	-0.864	
costa X	-0.376	0.322	-0.870	
costa XI	-0.038	0.360	-0.932	
costa XII	0.028	0.227	-0.974	
R. Latissimus Dorsi	-0.340	-0.284	-0.897	
R. Quadratus Lumborum	0.125	0.134	-0.983	(7 others listed)
R. Psoas (iliopsoas)	0.166	0.357	-0.919	(6 others listed)

Dumas et al. measured the right side muscles only and assumed symmetry for the left side muscles.

Han et al. (1992) also determined the lines of action for 20 muscles (10 left and 10 right) in ten Japanese patients with back disorders at all levels from T12/L1 to L5/S1. Table 2.8 lists the muscles and both left and right lines of action at the L3/L4 disc found by Han et al. (The lines of action for both the left and right sides of the body were measured.)

TABLE 2.8 Lines of Action Found by Han et al. (1992) at L3/L4

Muscle	Left			Right		
	$\mathcal{I}_x$	$\mathcal{I}_y$	$\mathcal{I}_z$	$\mathcal{I}_x$	$\mathcal{I}_y$	$\mathcal{I}_z$
Multifidus	-0.1248	-0.0377	-0.9851	0.1065	-0.0275	-0.9906
Longissimus	-0.1508	0.1008	-0.9696	0.1834	0.1841	-0.9568
Iliocostalis	-0.0031	0.2054	-0.9555	-0.0506	0.2064	-0.9508
Rectus Abdominus	0.0125	-0.1182	-0.9789	0.0009	-0.1191	-0.9852
Internal Oblique	-0.1340	-0.5538	-0.8201	0.1340	-0.5538	-0.8201
External Oblique	0.3760	0.3406	-0.8617	-0.3760	0.3406	-0.8617
Latissimus Dorsi	0.3610	0.0125	-0.7061	-0.4179	-0.1619	-0.7832
Psoas	-0.1400	0.1098	-0.9758	0.1333	0.1262	-0.9729
Quad. Lumborum	-0.2576	0.1274	-0.9387	0.2879	0.0936	-0.9378

Cholewicki and McGill (1996) implemented a model including 45 pairs of muscles. The 45 muscles were comprised of several fascicles. For example, 12 fascicles of the multifidus as well as 5 fascicles of the psoas were included. Lines of action of the 45 pairs of muscle were not reported, but the three-dimensional coordinates of the origin and insertion of each muscle were reported. The line of action could be calculated from the coordinates. Due to the amount of data reported, the original source should be consulted.

A difficulty in modeling the trunk muscles is reducing the large fan like muscles, such as the obliques with large attachment sites, into a single line of action vector. Schultz et al. (1983) divided the internal and external oblique muscles into lateral and medial portions with separate lines of action. However, the lines of action used by Schultz et al. (1983) were stated only in the following terms: for the medial portion of the internal and external oblique the line of

action is in a plane 30° to the sagittal plane, and for the lateral portion of the internal and external oblique the line of action is in the sagittal plane. Although Schultz et al. (1983) divided the obliques into two portions, the lines of action were not as detailed as those given by Dumas et al. (1988) or Han et al. (1992).

Van der Helm and Veenbaas (1991) summarized the assumptions of using a single line of action to represent a muscle as follows: "The first assumption is that the force vector derived from the muscle line of action at a certain cross-section of the muscle is representative of the forces transmitted by the muscle at that particular cross-section (Andrews and Hay, 1983). A second assumption is that there are no moments exerted by the muscle around the muscle line of action. In addition, it is assumed that no shear forces exist in the particular cross-section." Van der Helm and Veenbaas (1991) discussed representing shoulder muscles with large attachment sites. They described the mechanical effects of a muscle when it is divided into a large number (200) and a reduced number (6) of muscle lines of action. They describe a procedure to reduce the number of lines of action from 200 and also evaluate the force and moment error in the reduction. They stress that an important feature of their method is that force vectors are positioned after the complete measurement of the attachments site of muscle bundles is made.

Van der Helm and Veenbaas (1991) listed some of the difficulties in representing muscles with large attachment sites with a single line of action. However, a complete description of the trunk muscle attachment sites required for their procedure has not been recorded for the trunk muscles such as the

obliques. Line of action data reported by Dumas et al. (1988) and Han et al. (1992) may be used with the assumption of using single lines of action to represent a muscle.

2.5 Muscle Area

Tension (or intensity) of a muscle is the force per unit area. The exact value of the maximum capable muscle intensity is not well established, but is assumed to be the same for all trunk muscles. Therefore, the relative amount of force that can be generated by each muscle is largely a function of the cross-sectional area of that muscle. Force alone does not determine the relative contributions of the muscles in resisting an externally applied moment. The moment arms of a muscle play a large role in determining moment generation as well.

Tracy et al. (1989) measured the cross-sectional area of the lumbar muscles at each lumbar disc level using magnetic resonancing imaging (MRI). Twenty-six males were included in their study which were under investigation for intervertebral disc degeneration or protrusion. The cross-sectional areas at the L3/L4 disc level for each of the muscles measured by Tracy et al. are listed in Table 2.9. Tracy et al. actually only measured the right side muscles. The left side muscles are assumed to be symmetrical for implementation into a model. The cross-sectional areas reported were not modified for fiber orientation because the transverse MRI taken by Tracy et al. were not perpendicular to the fiber orientation of the muscles. To obtain the effective muscle area, the z-

TABLE 2.9 Right Side Muscle Cross-Sectional Areas Reported by Tracy et al. (1989) at L3/L4 level

Muscle	N	Area (cm^2)
R. Erector spinae	26	26.0
R. Rectus Abdominus	25	6.6
R. Obliques (overall)	13	35.1
R. Latissimus dorsi	1	4.3
R. Quadratus lumborum	26	7.1
R. Psoas	26	14.8

component of the unit force vector (from Dumas et al., 1988 for example) was multiplied by the transverse area as in McGill et al. (1988).

Han et al. (1992) determined the muscle areas for 10 muscles in 10 Japanese patients with back disorders. Table 2.10 lists the effective muscle areas (or physiological cross-sectional area) for the left and right sides measured by Han et al. (1992). The gross area of the muscle was measured in the transverse CT scan, and then converted to the effective area by accounting for the angle of the muscle line of action with respect to transverse cut.

Stokes and Gardner-Morse (1995) studied the lumbar spine using physiological cross-sectional areas for the multifidus, iliocostalis, longissimus, and psoas muscles from Bogduk et al. (1992a) and Bogduk et al. (1992b). The cross-sectional areas were given for each fascicle of the muscles. The total area for the multifidus, iliocostalis, longissimus, and psoas muscles at the L3/L4 level used by Stokes and Gardner-Morse was difficult to determine. The

TABLE 2.10 Cross-Sectional Areas Found by Han et al. (1992) at L3/L4 Cutting Plane.

Muscle	Effective Cross-Sectional Area (cm^2)	
	Left	Right
Multifidus	5.06	5.31
Iliocostalis	7.39	6.89
Longissimus	6.13	6.05
Rectus Abdominus	4.62	4.73
Internal Oblique	4.92	4.80
External Oblique	5.56	5.48
Latissimus Dorsi	0.90	1.00
Quadratus Lumborum	3.90	3.63
Psoas	8.79	8.80
Transversus	1.54	1.62

muscles were broken down into lumbar and thoracic components. The lumbar components have muscle fibers in the L3/L4 cutting plane, but many of the thoracic fascicles attach to a common tendon at this cutting plane. The difference in the thoracic and lumbar portions of the erector spinae muscle was discussed previously in Section 2.2.1.

At the L4/L5 cutting plane level, McGill, Patt, and Norman (1988) measured the cross-sectional area of eight muscles. They determined the areas using transverse CT scans on 13 active men who received treatment for complaints of low back pain. Table 2.11 lists the eight muscles and the corresponding cross-sectional areas corrected for fiber orientation reported by McGill et al. Data on both the right side and left side muscles were reported.

TABLE 2.11 Cross-Sectional Area at L4/L5, McGill et al. (1988)

Muscle	Effective Cross-Sectional Area (cm^2) Left	Right
Erector Spinae(uncorrected)	23.4	21.7
Sacrospinalis	16.5	15.3
Multifidus	4.3	4.0
Rectus Abdominus	7.5	8.3
Internal Oblique	8.5	7.7
External Oblique	10.0	8.8
Psoas	18.0	17.2
Quadratus Lumborum	6.3	5.9
Transverse Abdominus	1.5	1.5

McGill, Santaguida, and Stevens (1993) measured the cross-sectional area of several muscles from the T5 to L5 levels. They determined the areas using MRI on 15 active young men with no history of back disease or injury. Table 2.12 lists the muscles studied and the corresponding raw cross-sectional areas at the L3 and L4 levels. Cross-sectional area corrected for fiber orientation were reported for muscles whose area changed by 10%. Data on both the right side and left side muscles were reported.

Cholewicki and McGill (1996) reported the physiological cross-sectional areas for 45 pairs of muscles. The 45 muscles were comprised of several fascicles. For example, 12 fascicles of the multifidus as well as 5 fascicles of the psoas were included. Due to the amount of data reported, the original source should be consulted.

TABLE 2.12 Cross-Sectional Area (cm^2) at L3 and L4 Levels, McGill et al. (1993)

	L3		L4		Corrected Area L3/L4
Muscle	Left	Right	Left	Right	
Erector Spinae	29.33	28.31	22.34	21.51	
Longissimus thoracis	7.82	7.47			
Iliocostalis lumborum	13.95	13.68			
Multifidus	4.72	4.47			
Rectus Abdominus	6.93	6.70	7.46	7.50	
Internal Oblique	14.24	15.15	9.00	9.03	11.54
External Oblique	13.35	12.76	9.92	9.15	11.21
Latissimus Dorsi	2.56	2.32			
Psoas	15.93	15.94	18.20	19.61	
Quadratus Lumborum	7.46	7.01	6.25	7.25	5.82
Transverse Abdominus	3.76	3.56	2.24	2.37	

Reid and Costigan (1985) determined the cross-sectional area of the rectus abdominus and erector spinae muscles for 28 subjects using CT scans. Values of 16.02 and 15.73 cm^2 were reported for the left and right erector spinae muscles, respectively. The total area for rectus abdominus muscle was given as 10.5 cm^2, or 5.25 cm^2 for the left and right sides each assuming symmetry. These areas were not corrected for fiber orientation.

Reid, Livingston, and Pearsall (1994) determined geometric data of the psoas muscle using magnetic resonance imaging on 15 active males with no history of back pain. They measured the moment arms and cross-sectional areas of the left and right psoas muscles at nine vertebral and/or intervertebral levels: L2, L2/L3, L3, L3/L4, L4, L4/L5, L5, L5/S1, and S1. At the L3/L4 disc

level, the psoas area was reported as 12.3 and 14.0 cm^2 for the left and right sides, respectively.

2.6 Anatomical Measurements for Non-Upright Postures

The muscles moment arms, lines of action, and cross-sectional areas to this point have only been considered for supine or upright postures. When the trunk is deviated from the neutral posture such as twisting or flexion, the moment arms, lines of action, and areas may change.

Tsuang, Novak, Schipplein, Hafezi, Trafimow, and Andersson (1993) determined the muscle moment arms, lines of action, and areas for 10 muscles (5 of each side) for the torso in a neutral posture and then twisted 25 and 50 degrees. The subjects were asked to lie supine for the non-twisting condition. Twisting was accomplished by passively rotating the shoulders of the subjects and placing wedges under their shoulders so that 25 and 50 degree twist conditions were achieved. The amount of twist was measured at the shoulder level so the rotation of the lumbar spine was much less (approximately 10 degrees) for the maximum twist of 50 degrees at the shoulders. Five males with no spinal problems, restricted physical activities, or recent history of back pain participated in the study. The data was obtained using MRI techniques.

Muscle geometry data was collected using two reference frames. First, a three-dimensional or absolute reference frame was used with the center of the L5/S1 disc chosen as the origin. Second, a relative reference frame at each disc level was established. Table 2.13 shows the moment arms for the muscles under study at each angle of twist for the L3/L4 disc. The moment arms shown

in Table 2.13 are all with respect to the L3/L4 disc, not an absolute reference frame.

TABLE 2.13 Moment Arms for the Left and Right Sides at the L3/L4 Level for Three Levels of Torso Rotation Reported by Tsuang et al. (1993). Values are in cm

	r_x		r_y	
Muscle	Left	Right	Left	Right
Erector Spinae				
0 degrees	-3.5	3.3	-4.9	-4.9
25 degrees	-3.5	3.4	-5.3	-5.3
50 degrees	-3.5	3.7	-5.1	-5.3
Rectus Abdominus				
0 degrees	-3.5	3.2	6.2	6.4
25 degrees	-1.9	5.0	6.7	6.5
50 degrees	-0.7	6.2	7.0	6.6
Obliques				
0 degrees	-10.9	10.2	1.5	2.1
25 degrees	-9.9	11.3	2.0	1.4
50 degrees	-9.3	12.1	2.3	1.0
Psoas				
0 degrees	-4.5	4.1	-0.3	-0.1
25 degrees	-4.5	4.2	-0.4	-0.3
50 degrees	-4.4	4.2	-0.5	-0.2
Quadratus Lumborum				
0 degrees	-7.7	7.4	-2.9	-2.6
25 degrees	-7.7	7.1	-2.9	-2.6
50 degrees	-7.6	7.1	-2.8	-2.7

The muscle lines of action were reported only with respect to the absolute reference frame. The lines of action, with respect to the local reference frame of the L3/L4 disc, were not given. In a biomechanical model, the data is needed with respect to the local cutting plane, even if that cutting plane is displaced due to trunk rotation.

The cross-sectional areas of the muscles examined in this study are listed in Table 2.14 for each angle of twist. The areas reported were not corrected for fiber orientation.

For biomechanical modeling where one of the spinal discs is selected as the reference, the relative reference frame described in this experiment is appropriate. Tsuang et al. (1993) reported that the moment arms of only the abdominal muscles (left and right rectus abdominus and left and right obliques) changed significantly in the relative reference frame. There was no significant displacement of the psoas, erector spinae, or quadratus lumborum muscles. The moment arms of the oblique muscles changed from 0.9 to 2.2 cm in the x-direction (an 8 - 21% change), while changes in the y-direction were numerically smaller, the percentage change was as high as 50%. For relative differences in cross-sectional area, only the oblique muscles changed significantly. The area of the right oblique increased about 20% at the L3/L4 level while the left oblique decreased by 13% at the same level. Changes in the muscle lines of action were only reported for the absolute reference system and were not available for the relative reference frames. It does not appear from this study that changes in the moment arms and cross-sectional areas occur for most muscles.

TABLE 2.14 Cross-Sectional Areas Found by Tsuang et al. (1993) at L3/L4 Cutting Plane for Three Angles of Trunk Twist.

Muscle	Effective Cross-Sectional Area (cm^2) Left	Right
Erector Spinae		
0 degrees	19.3	18.1
25 degrees	20.0	19.3
50 degrees	19.7	19.1
Rectus Abdominus		
0 degrees	7.1	7.0
25 degrees	6.7	6.4
50 degrees	6.9	6.6
Obliques		
0 degrees	27.8	26.6
25 degrees	24.8	30.2
50 degrees	23.8	32.6
Psoas		
0 degrees	14.7	13.4
25 degrees	13.6	12.4
50 degrees	14.4	12.4
Quadratus Lumborum		
0 degrees	5.9	6.5
25 degrees	6.0	6.1
50 degrees	6.0	6.9

Tveit, Daggfeldt, Hetland, and Thorstensson (1994) studied the changes in erector spinae moment arm with changes in the lumbar spine curvature. They had subjects perform simulated lift static while lying supine. The simulated lifting was performed with kyphosis and lordosis of the lumbar spine. Magnetic resonance images were used to determine the moment arm of the

erector spinae. The average moment arm lengths for the two postures of six males and five females are shown in Table 2.15. Tveit et al. (1994) reported that longer moment arms were found in lordosis as compared to kyphosis. No significant difference were found between males and females in the kyphosed position except at the L1/L2 level. Male moment arms were significantly greater than females in lordosis except at the L4/L5 level. Relative changes in moment are lengths were only significantly different between males and females at the L2/L3 level. For postures deviated from upright standing such as bending to lift weights, the results of Tveit et al. (1994) indicated changes in moment arms of the erector spinae muscle.

A model was reported by Nussbaum and Chaffin (1994) to determine a representation of spine motion segments and muscle geometries. The model was both scaleable and deformable. An initial geometry of the bony elements

TABLE 2.15 Average Moment Arms (mm) of the Erector Spinae for the Lumbar Spine in Kyphosis and Lordosis reported by Tveit et al. (1994)

	Males (n =6)		Females (n=5)	
Lumbar Level	Kyphosis	Lordosis	Kyphosis	Lordosis
L1/L2	52	64	45	56
L2/L3	53	63	52	57
L3/L4	56	62	55	59
L4/L5	55	64	56	62
L5/S1	57		57	

was resized based on 15 anthropometric measurements allowing the model to be scaleable. The model was also deformable based on motions of the spine such as flexion, extension, and lateral bending. The model reported by Nussbaum and Chaffin (1995) determines the muscle lines of action due to postural changes. However, due to weak relationships between anthropometric measures and muscle lines of action and moment arms, average sets of values were used for all subjects. The model accounted for changes in muscle geometry due to postural changes, but not anthropometric differences.

2.7 Joint Contact and Ligament Forces

2.7.1 Introduction to Ligaments

Ligaments are a connective tissue with the main function of connecting bone to bone to provide stability at the joints (Chaffin and Anderson, 1991). As joints articulate, the ligaments become stretched and create tensile force to pull the bones of the joint together. Ligaments possess only passive characteristics as opposed to muscles which have both passive and active force components. As the ligament elongates, it develops a higher amount of tension.

Ligaments connect the vertebrae of the spinal column as they do many other joints. Kroemer, Kroemer, and Kroemer-Elbert (1990) point out that the spinal column consists of cartilaginous joints which are tightly covered by ligaments. One of the functions of the ligaments in the trunk is to help maintain the structural integrity of the spinal column. This is accomplished by providing tensile forces between the vertebrae to which they are connected.

2.7.2 Role of Ligaments in Lifting

An investigation of only the ligamentum flavum was reported by Nachemson and Evans (1968). The ligamentum flavum between the L3 and L4 vertebrae of 10 cadavers (age 13 to 79) was subjected to tension tests to determine the stress-strain relationship of this ligament. Through other tests Nachemson and Evans (1968) found the ligamentum flavum to pre-stress the disc with a force ranging from 14.7 to 3.9 N. Finally, the ligamentum flavum was estimated to produce a moment of up to 2.9 Nm in full forward flexion and negligible moment in extension (possibly because it shortened to its resting position). This moment would provide only a small contribution in a lifting task. Based on these results, Nachemson and Evans (1968) concluded that the role of the ligamentum flavum is to provide protection for the nerve roots, and due to the pre-stressing, stabilize the spine. It should be noted that other ligaments in the trunk were not tested for the same characteristics.

Andersson, Chaffin, Herrin, and Matthews (1985) developed a biomechanical model to predict the forces of the muscles, ligaments, and intra-abdominal pressure (IAP) around the L5-S1 joint in response to isometric external forces. Seven ligaments were included in the model: lumbodorsal fascia, interspinous and supraspinous ligaments, articular ligament, ligamentum flavum, and iliolumbar and sacrolumbar ligaments. They employed a model to predict the restorative moments of the muscles, ligaments, and IAP when loads of 0 and 500 N were held in the hands. For each load, the torso was also rotated to 0, 30, 60, and 90 degrees flexion.

Anderson et al. (1985) developed methodologies to estimate the muscle, ligament, and IAP force contributions. The amount of restorative moment for the ligaments, muscles, and IAP predicted by the model are shown in Figure 2.2. The contribution of the ligaments predicted in this isometric mid-sagittal lifting task is very small compared to that of the muscles.

Cappozzo, Felici, Figura, and Gazzani (1985) estimated the compressive force acting on the L3-L4 joint during weight lifting exercises. Four subjects performed "half-squat" exercises with a barbell resting on the subject's shoulders. The moment about the L3-L4 joint of the subjects in the mid-sagittal plane was estimated to be between 110 to 250 Nm due to external forces and body weights. The internal muscular forces needed to resist this moment were then calculated. Cappozzo et al. (1985) did not include ligament tension in their model of internal resisting moments because it was considered negligible. They estimated a restorative moment due to the ligaments of 2.5 Nm/degree of rotation between two adjacent vertebrae (based on data from Panjabi, Krag, White, and Southwick, 1977 and Schultz, Warwick, Berskon, and Nachemson, 1979). They considered that the relative displacement between the L3 and L4 vertebrae would have to be larger than six degrees for the ligament moment to make a significant moment contribution. Although rotation of the vertebrae was not measured they assumed "with confidence" that it was less than six degrees. Through this analysis of the ligaments' limited capability to produce torque in a lifting task, Cappozzo et al. (1985) justified its exclusion from their model.

McGill and Norman (1986) estimated the moments generated by the muscles, ligaments, and disc components about the L4-L5 joint in response to

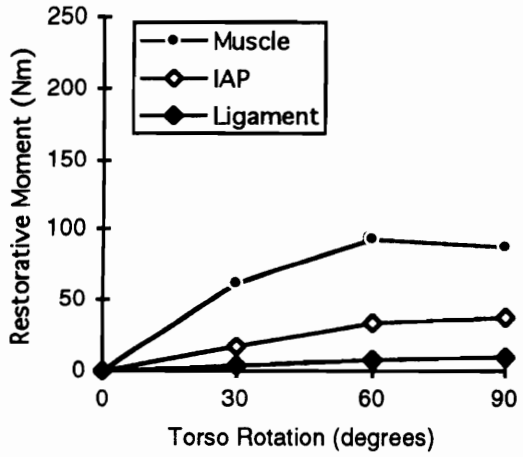

(a) External load equals 0 N, IAP = Intra-Abdominal Pressure

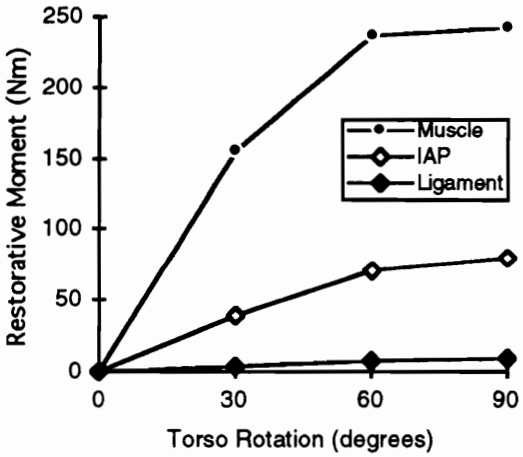

(b) External load equals 500 N, IAP = Intra-Abdominal Pressure

Figure 2.2 Estimated restorative moment vs. torso rotation by element at (a) 0 N, and (b) 500 N load in the hands with straight legs, adapted from Anderson et al. (1985).

external forces during a dynamic mid-sagittal plane lifting task. Three subjects performed six lifts consisting of combinations of varying loads and accelerations in the mid-sagittal plane. Through a motion monitoring system, assumed lines of action, moment arm lengths, and EMG data the restorative moments of 48 muscles were estimated. Eight ligaments were also included in the model: anterior and posterior longitudinal ligaments, ligamentum flavum, articular ligament, intertransverse ligament, interspinous and supraspinous ligaments, and the lumbodorsal fascia. The individual forces created by the ligaments were calculated using stress-strain relationships and pre-tension values found in the literature. The forces calculated were then converted to moments about the disc based on assumed moment arms and lines of action.

The estimated relative moment contributions of the ligaments, muscles, and disc components during the lifting task are shown in Figure 2.3 (McGill and Norman, 1986). The ligament and disc moments follow near the zero moment line indicating the amount of moment produced was negligible. McGill and Norman (1986) acknowledged that the ligament system may not have produced any moments because the subjects elected to assume a flat back posture. Since the ligaments are passive, they must be stretched to contribute force. Even though the subjects kept a mostly flat back posture, the ligament forces should not have been that greatly under estimated. Therefore, McGill and Norman (1986) concluded that the ligament and disc forces were not a significant component of the spinal lifting mechanism during stressful, mid-sagittal lifts under study.

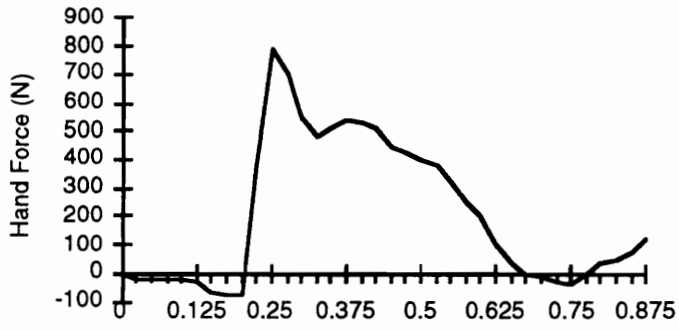

(a) Hand Force

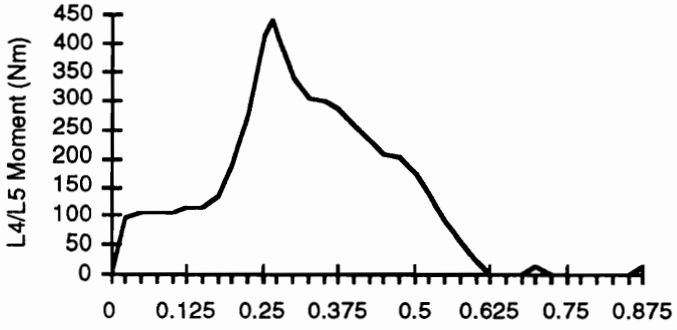

(b) Total L4/L5 Moment

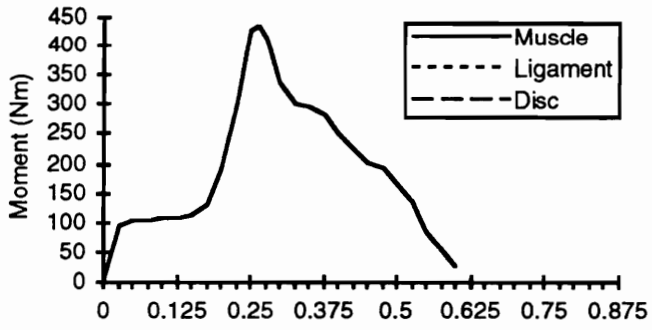

(c) Restorative Moments

Figure 2.3. Forces at the hands during a lift is shown in part A, and the calculated moment at the L4-L5 joint is shown in part B. Part C shows the estimated restorative moments due to the discs, ligaments, and muscles adapted from McGill and Norman (1986).

2.7.3 Summary: Ligament and Disc Force Contribution

The ability of the ligaments to generate restorative moments in mid-sagittal plane lifting is small and limited compared to the moments supplied by the muscles. This is best supported by the extensive modeling of isometric and dynamic lifting provided by Anderson et al. (1985) and McGill and Norman (1986). Their models did not predict significant moment generating capabilities for the ligaments of the back. The models are only estimations of the moments for the ligaments, but it seems unlikely that the estimates would be grossly incorrect.

The role of the ligaments in the back appears to be to provide protection and help maintain the alignment of vertebrae. Although the delicate structural integrity of the back is also accomplished through muscle activation, the ligaments accomplish alignment through passive means. No signals or control are required from the nervous system.

2.8 Summary of Trunk Anatomy

In developing an optimization-based biomechanical model of the trunk, geometric muscle inputs of cross-sectional area, moment arms to a center of rotation, and lines of action are needed. A review of the literature revealed that this information has been gathered in piece meal fashion. Only Han et al. (1992) collected muscle geometric inputs in a comprehensive manner. However, these data were collected only on Japanese patients. To obtain another set of muscle inputs, the formulations of several studies were combined.

Given the literature reviewed, four sets of muscle inputs were generated. The first two sets consisted of 18-muscle models. One was derived from the data of Han et al. (1992) while the second was from a compilation of several studies. The muscles included were the multifidus, longissimus, iliocostalis, rectus abdominus, internal oblique, external oblique, latissimus dorsi, psoas, and quadratus lumborum for the left and right sides. The third and fourth sets consisted of 10-muscle models. The third set was derived from the data of Han et al. (1992) while the fourth was from a compilation of several studies. The muscles included were the erector spinae, rectus abdominus, internal oblique, external oblique, and latissimus dorsi for the left and right sides. Having four muscle geometry sets allowed the effect of input parameters to the low back optimization models on muscle force predictions to be tested. The number of muscles was varied from 18 to 10 with associated geometries.

The geometric data for 18 muscles taken from data reported by Han et al. (1992) is shown in Table 2.16. The moment arms, lines of action, and cross-sectional areas were determined by averaging the left and right hand side values reported. In addition, the lines of action were scaled so that the resultant force is a unit vector. The values reported by Han et al. (1992) did form a resultant unit vector which was possibly due to measurement difficulties.

The second 18-muscle input data set was based on several studies. The moment arms for each of the 18 muscles was provided by Tracy et al. (1989). The lines of action for the longissimus, iliocostalis, rectus abdominus, internal oblique, external oblique, latissimus dorsi, psoas, and quadratus lumborum

TABLE 2.16 Geometric Muscle Inputs for 18 Muscles Reported by Han et al. (1992) at L3/L4: Moment Arms, r (cm), Unit Muscle Force Components, τ, and Physiological Cross-Sectional Areas, A (cm^2).

Muscle	r_x	r_y	r_z	τ_x	τ_y	τ_z	A
L. Multifidus	-1.63	-5.40	0	-0.116	-0.033	-0.993	5.19
R. Multifidus	1.63	-5.40	0	0.116	-0.033	-0.993	5.19
L. Longissimus	-3.51	-5.34	0	-0.169	0.144	-0.975	6.09
R. Longissimus	3.51	-5.34	0	0.169	0.144	-0.975	6.09
L. Iliocostalis	-5.61	-4.86	0	0.053	0.211	-0.976	7.14
R. Iliocostalis	5.61	-4.86	0	-0.053	0.211	-0.976	7.14
L. Rectus Abdominus	-3.66	7.14	0	0.013	-0.120	-0.993	4.68
R. Rectus Abdominus	3.66	7.14	0	-0.013	-0.120	-0.993	4.68
L. Internal Oblique	-10.64	2.54	0	-0.134	-0.555	-0.821	4.86
R. Internal Oblique	10.64	2.54	0	0.134	-0.555	-0.821	4.86
L. External Oblique	-11.65	1.71	0	0.376	0.341	-0.862	5.52
R. External Oblique	11.65	1.71	0	-0.376	0.341	-0.862	5.52
L. Latissimus Dorsi	-8.22	-4.46	0	0.453	-0.209	-0.867	0.95
R. Latissimus Dorsi	8.22	-4.46	0	-0.453	-0.209	-0.867	0.95
L. Psoas	-3.88	-0.62	0	-0.138	0.119	-0.983	8.80
R. Psoas	3.88	-0.62	0	0.138	0.119	-0.983	8.80
L. Quad. Lumborum	-6.68	-3.01	0	-0.277	0.112	-0.954	3.77
R. Quad. Lumborum	6.68	-3.01	0	0.277	0.112	-0.954	3.77

were taken from Dumas et al. (1988). The line of action of the multifidus was taken from Macintosh and Bogduk (1986). The area of the multifidus, longissimus, and iliocostalis was calculated by using the area of the erector spinae reported in Tracy et al. (1989) and dividing it into the proportions given in Schultz et al. (1983). The final physiological area was determined by multiplying the area by the z component of the unit force vector to account for fiber orientation as in McGill et al. (1988). The areas of the rectus abdominus, latissimus dorsi, psoas, and quadratus lumborum were taken from Tracy et al.

(1989). The overall oblique area reported by Tracy et al. (1989) was divided into the internal and external oblique portions using the ratios given by Chaffin et al. (1990). These areas were then multiplied by the z component of the unit force vector to account for fiber orientation. Table 2.17 lists the final muscle geometry for the compilation of studies discussed.

TABLE 2.17 Geometric Muscle Inputs for 18 muscles at L3/L4: Moment Arms, r (cm), Unit Muscle Force Components, τ, and Physiological Cross-Sectional Areas, A (cm^2). These Values are a Compilation of Tracy et al. (1989), Dumas et al. (1988), Macintosh and Bogduk (1986), Schultz et al. (1983), McGill et al. (1988), and Chaffin et al. (1990).

Muscle	r_x	r_y	r_z	τ_x	τ_y	τ_z	A
L. Multifidus	-1.79	-6.10	0	-0.309	0.000	-0.951	4.95
R. Multifidus	1.79	-6.10	0	0.309	0.000	-0.951	4.95
L. Longissimus	-3.89	-6.05	0	0.134	0.005	-0.991	10.31
R. Longissimus	3.89	-6.05	0	-0.134	0.005	-0.991	10.31
L. Iliocostalis	-5.86	-5.43	0	0.281	-0.052	-0.958	9.96
R. Iliocostalis	5.86	-5.43	0	-0.281	-0.052	-0.958	9.96
L. Rectus Abdominus	-3.38	7.95	0	-0.028	0.016	-0.9995	6.60
R. Rectus Abdominus	3.38	7.95	0	0.028	0.016	-0.9995	6.60
L. Internal Oblique	-11.39	0.96	0	-0.134	-0.574	-0.808	14.20
R. Internal Oblique	11.39	0.96	0	0.134	-0.574	-0.808	14.20
L. External Oblique	-12.62	1.09	0	0.376	0.322	-0.870	15.30
R. External Oblique	12.62	1.09	0	-0.376	0.322	-0.870	15.30
L. Latissimus Dorsi	-7.19	-5.42	0	0.340	-0.284	-0.897	3.90
R. Latissimus Dorsi	7.19	-5.42	0	-0.340	-0.284	-0.897	3.90
L. Psoas	-4.29	-0.59	0	-0.166	0.357	-0.919	14.80
R. Psoas	4.29	-0.59	0	0.166	0.357	-0.919	14.80
L. Quad. Lumborum	-7.49	-3.48	0	-0.125	0.134	-0.983	7.10
R. Quad. Lumborum	7.49	-3.48	0	0.125	0.134	-0.983	7.10

The 10-muscle input data set was determined by combining and eliminating muscles from the 18-muscle data set. The multifidus, longissimus, and iliocostalis muscles were combined into a single erector spinae muscle. The quadratus lumborum and psoas muscles were eliminated from the data set.

The first 10-muscle input data set was taken from Han et al. (1992). The moment arms and line of action for the erector spinae were determined by using the moment arms and line of action for the longissimus muscle. For the remaining muscles, the moment arms, lines of action, and cross-sectional areas were determined by averaging the left and right hand side values reported. In addition, the lines of action were scaled so that the resultant force is a unit vector. The values reported by Han et al. (1992) did form a resultant unit vector which was likely due to measurement difficulties. The geometric data for 10 muscles taken from Han et al. (1992) is shown in Table 2.18.

The second 10-muscle input data set was based on several studies. The moment arms for each of the 10 muscles was provided by Tracy et al. (1989). The lines of action for the 10 muscles were taken from Dumas et al. (1988). The areas of the erector spinae, rectus abdominus, and latissimus dorsi, were taken from Tracy et al. (1989). The final physiological area was determined by multiplying the area by the z component of the unit force vector to account for fiber orientation as in McGill et al. (1988). The overall oblique area was reported by Tracy et al. (1989) and was then divided into the internal and external oblique portions using the ratios given by Chaffin et al. (1990). These areas were then multiplied by the z component of the unit force vector to

account for fiber orientation. Table 2.19 lists the final 10-muscle geometry for the compilation of studies discussed.

TABLE 2.18 Geometric Muscle Inputs for 10 Muscles Reported by Han et al. (1992) at L3/L4: Moment Arms, r (cm), Unit Muscle Force Components, τ, and Physiological Cross-Sectional Areas, A (cm^2).

Muscle	r_x	r_y	r_z	τ_x	τ_y	τ_z	A_i
L. Erector Spinae	-3.51	-5.34	0	-0.169	0.144	-0.975	18.42
R. Erector Spinae	3.51	-5.34	0	0.169	0.144	-0.975	18.42
L. Rectus Abdominus	-3.66	7.14	0	0.013	-0.120	-0.993	4.68
R. Rectus Abdominus	3.66	7.14	0	-0.013	-0.120	-0.993	4.68
L. Internal Oblique	-10.64	2.54	0	-0.134	-0.555	-0.821	4.86
R. Internal Oblique	10.64	2.54	0	0.134	-0.555	-0.821	4.86
L. External Oblique	-11.65	1.71	0	0.376	0.341	-0.862	5.52
R. External Oblique	11.65	1.71	0	-0.376	0.341	-0.862	5.52
L. Latissimus Dorsi	-8.22	-4.46	0	0.453	-0.209	-0.867	0.95
R. Latissimus Dorsi	8.22	-4.46	0	-0.453	-0.209	-0.867	0.95

TABLE 2.19 Geometric Muscle Inputs for 10 Muscles at L3/L4: Moment Arms, r (cm), Unit Muscle Force Components, τ, and Physiological Cross-Sectional Areas, A (cm^2). These Values are a Compilation of Tracy et al. (1989), Dumas et al. (1988), McGill et al. (1988), and Chaffin et al. (1990).

Muscle	r_x	r_y	r_z	τ_x	τ_y	τ_z	A
L. Erector Spinae	-3.82	-5.76	0	0.281	-0.052	-0.958	24.9
R. Erector Spinae	3.82	-5.76	0	-0.281	-0.052	-0.958	24.9
L. Rectus Abdominus	-3.38	7.95	0	-0.028	0.016	-0.9995	6.6
R. Rectus Abdominus	3.38	7.95	0	0.028	0.016	-0.9995	6.6
L. Internal Oblique	-11.39	0.96	0	-0.134	-0.574	-0.808	14.2
R. Internal Oblique	11.39	0.96	0	0.134	-0.574	-0.808	14.2
L. External Oblique	-12.62	1.09	0	0.376	0.322	-0.870	15.3
R. External Oblique	12.62	1.09	0	-0.376	0.322	-0.870	15.3
L. Latissimus Dorsi	-7.19	-5.42	0	0.340	-0.284	-0.897	3.9
R. Latissimus Dorsi	7.19	-5.42	0	-0.340	-0.284	-0.897	3.9

3. LOW BACK OPTIMIZATION MODELS

The emphasis of this dissertation is to evaluate alternative optimization-based models used to predict the muscles forces in the trunk region. The general formulation of optimization-based models applied to the trunk are reviewed first in this chapter. The formulations of the two specific models, the Minimum Intensity Compression (MIC) and Sum of the Cubed Intensities (SCI) models, are then discussed.

3.1 Optimization-based Biomechanical Models

Using optimization models of the trunk, the tension of the trunk muscles are estimated and used to calculate the resultant forces on the spinal column. The foundation of optimization models begins by applying engineering mechanics to the human body. The body is modeled as a series of rigid links. When an external force is applied to one of the links the body produces reaction forces using the muscles to maintain a static posture. The compression, shear, and torsional forces on the spinal discs are estimated by summing the external and internal (muscular) forces.

A planar diagram of a person holding a load was shown previously in Figure 1.1. A plane of reference is established about which the forces and moments are summed. The reference system and its origin are defined using body landmarks and features. Schultz and Andersson (1981) suggested defining a cutting plane through the L3/L4 disc, so the forces and moments were determined at this joint.

The free body diagram of the torso above a L3/L4 cutting plane was shown previously in Figure 1.2. The external load and weight of the torso create a compression force at the L3/L4 disc. The muscles of the trunk generate force to counteract the moment generated by the external load. (Note the resultant muscle force shown on the diagram is a simplification of several muscles with different lines of action which actually exist.) The combined forces of the muscles, external load, and weight of the body sum to equal the compression force on the spinal discs (as well as shear forces). Reaction forces are generated by anatomical structures such as the disc, ligaments, and facet joints to keep the system in static equilibrium.

The forces of the individual muscles necessary to maintain a static posture are unknown. Since the number of muscles in the trunk region is generally greater than the number of moment and force equilibrium equations, the problem is statically indeterminate. There exists an infinite number of combinations of muscle tensions to satisfy the equilibrium constraints. To estimate the tension of the trunk muscles optimization techniques are employed. Given some objective function subject to a set of constraints, the unknown muscle forces are determined.

Models using a cutting plane approach are a limited set of model formulations. Another modeling approach, proposed by Gracovetsky, Farfan, and Lamy (1977), predicted trunk and ligament forces based on a multiple vertebrae model. The objective function proposed by Gracovetsky et al. (1977) was to minimize the sum of the squared shear forces on five lumbar discs.

Other approaches to estimate the forces of the trunk muscle and disc forces do not use optimization approaches. Reilly and Marras (1989) presented a method to estimate trunk forces using measured muscle EMG signals as inputs. Marras (1988) presented some of the difficulties in using optimization models to predict forces for dynamic conditions. Reilly and Marras (1989) assessed dynamic forces using muscle EMG signals as inputs. The major difficulty with using EMG signals as inputs is relating the signals to muscle forces.

Another approach to estimate muscle forces uses both EMG signals and optimization approaches. Cholewicki and McGill (1996) estimated muscle forces using EMG signals as inputs, and then adjusted the forces using a optimization algorithm. The major difficulty with using EMG signals of relating the signals to muscle forces initially still remains. The scope of this dissertation is limited to a set of cutting plane optimization models. Other modeling techniques such as those proposed by Gracovetsky et al. (1977) or Reilly and Marras (1989) are alternative approaches.

Biomechanical optimization models of the trunk must be tested and validated for their accuracy in predicting muscle activity. Two models which have been proposed to predict the trunk muscle tensions are the Minimum-Intensity-Compression (MIC) model (Bean, Chaffin, and Schultz, 1988) and the Sum of the Cubed Intensities (SCI) model (Crowninshield and Brand, 1981).

3.1.1 Generalized Optimization Model Formulation

For static optimization biomechanical models, the moment equilibrium equations in three-dimensions (and possibly the force equilibrium equations) are constraints. The muscles of the trunk act to resist the moments generated by an external load. Assuming a transverse cutting plane through the body, the moments are summed about one of the spinal discs as follows:

$$\sum_{i=1}^{m} \|f_i\|(r_i x \tau_i) + M^E + M^J = 0 \qquad (3.1)$$

where m is the number of muscles, f_i is the tension in each muscle, r_i is the moment arm vector, τ_i is the muscle line of action, M^E are the externally applied moments in three-dimensions, and M^J are the moments due to joint contact and ligament forces.

The force equilibrium equations can also be included as constraints as follows:

$$\sum_{i=1}^{m} \|f_i\|\tau_i + F^E + F^J = 0 \qquad (3.2)$$

where m is the number of muscles, f_i is the tension in each muscle, τ_i is the muscle line of action, F^E are the externally applied forces in three-dimensions, and F^J are the forces due to joint contact and ligament forces. Often the force equilibrium equations are not included in model formulations. The moments are generally summed about the joint. The joint reaction forces are assumed to pass through the point about which the moments are summed, and because of this assumption do not contribute any moment. The joint reaction forces (see

Figure 1.2) are then determined from the resultant muscle forces and external load. Assuming joint reaction forces pass through the point of rotation, reaction forces have no effect on the moment equilibrium equations. The reaction forces assume values to balance the muscle and external forces and thus satisfy the force equilibrium equations.

The muscles forces f_i can not sustain compression so additional constraints are:

$$f_i \geq L_i \tag{3.3}$$

where L_i is some lower non-negative bound (usually zero). In addition, muscles can not exert an infinite amount of force, so an upper limit of muscle tension can be included as constraints:

$$f_i \leq U_i \tag{3.4}$$

An objective function subject to the above constraints must be selected to complete the optimization problem. The objective function that the body selects to determine the trunk muscular forces is unknown. Modeling efforts have concentrated on selecting an objective function, then empirically testing the model to check its validity.

Of course, not all models use exactly the same constraint equations and often vary in the objective function used. However, the general structure of low back biomechanical models is to select some objective function subject to the constraints described above.

3.1.2 Characteristics of Solving Optimization Models

The general property of convex optimization problems will be discussed in the following section. Then the assumptions to make the set of feasible muscle forces convex are reviewed followed by the assumptions to make the objective function convex. The practical implications of these assumptions and convex models are then discussed.

3.1.2.1 Convexity

A region of space is considered to be convex set if the line segment joining any two points in the region also lies in the region (Williams, 1985). Figure 3.1 shows an example of a convex set and a nonconvex set in two-dimensions. The strict mathematical definition for a convex set is as follows: a set X is called a convex set if given any two points x_1 and x_2 in X, then $\lambda x_1 + (1 - \lambda)x_2 \in X$ for each $\lambda \in [0,1]$. Note that $\lambda x_1 + (1 - \lambda)x_2$ for λ in the interval [0,1] represents a point on the line segment joining x_1 and x_2, (Bazaraa, Jarvis, and Sherali, 1990).

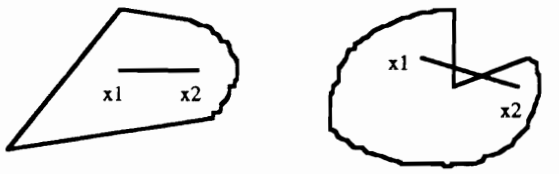

a. convex set b. nonconvex set

Figure 3.1 Example of convex and nonconvex sets.

The properties of a convex function are analogous to the properties of a convex set. Bazaraa, Sherali, and Shetty (1993) define a convex function as follows. Let f: S -> E_1, where S is a nonempty convex set in E_n. The function f is said to be convex on S if

$$f(\lambda x_1 + (1 - \lambda)x_2) \leq \lambda f(x_1) + (1 - \lambda)f(x_2) \qquad (3.5)$$

for each x_1 and $x_2 \in S$ and for each $\lambda \in (0,1)$. Figure 3.2 shows a convex function as well as a concave function and one that is neither convex nor concave. Note that a concave function is just the negative of the convex function.

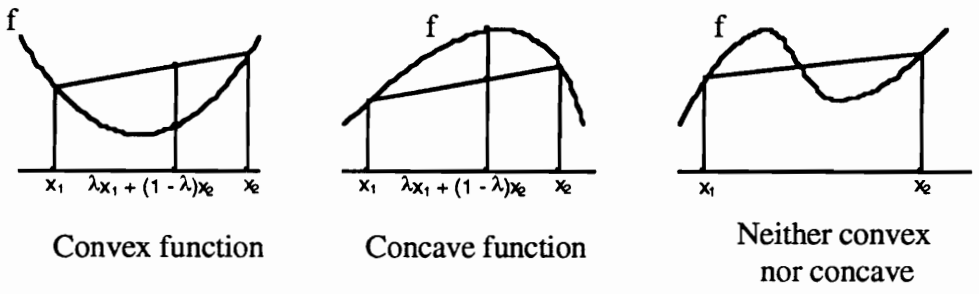

Figure 3.2 Examples of convex and concave functions. Adapted from Bazaraa, Sherali, and Shetty (1993).

The importance of establishing that a model is convex relates to the concept of local optima versus the global optimum. The global minimum of a function is the solution $\bar{x}$ such that $f(\bar{x}) \leq f(x)$, for all x. In other words, there is no other feasible solution which yields a lower objective function value. A local minimum occurs when, $f(\bar{x}) \leq f(x)$, for each x in a neighborhood of size ε

around $\bar{x}$. However, another local minimum might exist outside the neighborhood of $\bar{x}$ which has a lower objective function. A global minimum is always a local minimum.

Optimization seeks to find the global minimum (or maximum) given an objective function and set of constraints. If an optimization problem is a convex programming problem, then any optimum found must be a global optimum (Williams, 1985). However, for a nonconvex programming problem an optimum found is not necessarily a global optimum. (It may simply be a local minimum or maximum.) The concept of local optima is common from calculus. A function (f) can be differentiated to find the possible local minima and maxima (the points where f' equal zero are possible local minima or maxima). The second derivative of the function indicates whether it is a local minima, maxima, or inflection point. If a function is not convex, it is unknown if the local minima and maxima are the global minimum or maximum.

Optimization problems can be divided into linear and non-linear programming. The general form of a linear program is stated in the following terms (Bazaraa, Sherali, and Shetty, 1993):

$$\text{Minimize} \quad \sum_{j=1}^{n} c_j x_j \text{ , objective function} \tag{3.6}$$

$$\text{Subject to} \quad \sum_{j=1}^{n} a_{ij} x_j \geq b_i, \quad i = 1,2,\ldots,m \text{ , constraints} \tag{3.7}$$

$$x_j \geq 0, \quad j = 1,2,\ldots,n \tag{3.8}$$

where x_j are the decision variables, c_j are the cost coefficients, a_{ij} are the coefficients of the constraint equations, and b_i are the right hand side values.

Linear programming is a special case of convex programming. In other words, all linear programs are convex and the feasible region defined by a set of linear constraints is convex (Williams, 1985).

Optimization-based muscle force prediction models use the concepts of mathematical programming to estimate the muscle forces in the human body. However, to model the human body several assumptions and approximations are made in order to make the problem convex, solve the optimization problem, and achieve a global minimum prediction. In the following sections the general assumptions about the feasible muscle forces and objective functions to make the problem convex are reviewed and discussed.

3.1.2.2 Assumptions for a "Set of Feasible Muscle Forces to be Convex"

To make the set of feasible muscles forces convex, the general approach has been to make assumptions so that the constraint equations are linear. If the constraint equations are linear then the feasible solution set is convex as discussed in the previous section.

Muscle forces are greater than or equal to zero, and can produce only tensile forces. Every model has this assumption because muscles can not contract to create a negative force (can not sustain compression forces). This is a physiological assumption and not necessarily a mathematical assumption. Many optimization formulations use non-negativity assumptions for the decision variables. The physiological assumption that muscles forces be non-negative fits common optimization problems.

For a given cutting plane, muscles are assumed to transmit force in a straight line of action. This line is generally one that joins the muscle point of origin to the point of insertion. Seireg and Arvikar (1973) used this method to determine the muscle line of action. However, they also stated that this method requires considerable judgment because the muscles have innumerable shapes and do not originate and insert in a straight line fashion. Andrews and Hay (1983) pointed out that muscles do not follow straight paths between points of attachment for all joint configurations. They suggested a centroid line method to determine the line of action of the muscle force. Seireg and Arvikar (1973) indicated that because some muscles have very complex geometry and area of attachment, the muscle can be represented by more than one line of action.

An opposite approach reported by Pederson, Brand, Cheng, and Arora (1987) is to combine different muscle groups into one line of action (to reduce the number of unknowns). Regardless of the sophistication level of the method, the transmission of muscle force is assumed to occur along a line(s). The method to determine the line(s) of action might take into account the area and number of attachments, the path of the muscle (straight line versus curvilinear), the cross-sectional area of the muscle, and the length of the muscle. A review of the studies to determine muscle lines of action was discussed in Section 2.4. The end result is that muscle forces are be assumed to transmit force in a single direction vector denoted as τ_i^x, τ_i^y , τ_i^z. This vector represents the unit direction of force and not the magnitude. Solving for the decision variables in the optimization problem determines the magnitude of the muscle forces.

In addition to assuming the force line of action, the muscle moment arms about the joints under study are assumed. The moment arms, denoted by r_x, r_y, r_z, along with the lines of action are used to calculate the moments about a given joint. The moment arms have been estimated through studies of cadavers, magnetic resonancing, or computed tomography scans as reviewed in Section 2.3. Regardless of the method to determine the moment arms, they are assumed to remain constant and fixed. This assumption is generally made even in dynamic movements and changes in posture which can affect the moment arms through tissue movement and muscle shortening characteristics.

The cross-sectional area of the muscles can be used in the upper limit of muscle force constraint equations. Bean et al. (1988) used a constant value for the cross-sectional area in their examples. If the muscle cross-sectional area is assumed to be constant, the feasible set of muscle forces will be convex. Other convex formulations allowing the cross-sectional area to vary are possible, but beyond the scope of this discussion.

After selecting a cutting plane, constant values of the line of action, moment arm, and cross-sectional area for each muscle are assumed. They are assumed constant even with changes in body posture and lengthening or shortening of the muscles. Convex optimization problems could account for changes in the muscle characteristics through iterative formulations of the system. Each iterative formulation needs to remain convex.

Given these assumptions, a convex programming model can be developed. Hughes (1991) summarized static models which employ the relationships of the sum of forces and sum of moments must equal zero. The

externally applied forces, forces due to body mass, internal muscle forces, and joint reaction forces sum to zero to maintain equilibrium as follows:

$$\sum_{i=1}^{m} \| f_i \| \tau_i + F^E + F^J = 0 \qquad (3.9)$$

The moments about each axis are also in equilibrium as follows:

$$\sum_{i=1}^{m} \| f_i \| (r_i x \tau_i) + M^E = 0 \qquad (3.10)$$

F^J is the joint reaction force of the spinal disc. F^E and M^E are the forces and moments at the joint due to external forces and body mass. The assumed line of action is τ_i, and the assumed moment arm is r_i for each i-th muscle. The tension in the i-th muscle is represented by f_i, which are the values that the optimization problem is predicting.

R. E. Hughes (personal communication, May 6, 1995) pointed out that there is an implicit assumption in stating equation 3.10. The assumption is that the reaction force passes directly through the point about which moments are summed, and the position of the reaction force does not change with varying muscle and external loads. Suppose that as the muscle forces increase the position of the reaction forces changes due to elastic properties of spinal discs. This implies that the joint reaction forces need to be added to equation 3.10 with a moment arm vector that is a function of the muscle forces. In general, this would create a nonconvex solution space. If the joint reaction forces are assumed always to pass through the point about which moments are summed, the moment arm function is always equal to zero.

All models restrict the muscle force to be greater than a minimum value L_i (usually zero) and some require it to be less than some maximum value U_i (Hughes, 1991).

$$\|f_i\| \geq L_i \tag{3.11}$$

$$\|f_i\| \leq U_i \tag{3.12}$$

The force and moment equilibrium formulation is usually statically indeterminate and requires an optimization approach. The set of feasible muscles forces for this optimization problem are convex because the assumptions about the muscle functions make the constraints linear. To solve the formulation, an objective function is selected.

3.1.2.3 Assumptions Used to Justify Convex Objective Functions

The true objective function selected to determine the muscle forces is unknown. However, several convex objective functions assumed to be selected by the motor control systems have been proposed.

One assumption most optimization models make is that the selected objective function does not change. The human body is supposed to follow the criteria regardless of the task. As Redfern (1988) stated " a static task may use a different control strategy then a dynamic one, a slow dynamic movement may differ from a fast movement or a learned task may have a different control strategy than an unlearned one." Convex optimization problems can account for changes in the objective function through iterative formulations of the system. However, each iterative formulation needs to remain convex.

Seireg and Arvikar (1973) suggested several objective functions: 1) minimizing the forces in the muscles, 2) minimizing the work done by the muscles (the product of the force and the elongation of the muscle), 3) minimizing the vertical reactions at the joints, 4) minimizing the moments at the joints, and 5) some weighting scheme of the first four functions. They made two basic assumptions with any of these objective functions. First, the body selects muscles forces to optimize some criteria. Second, the body optimizes this function in a linear fashion (and therefore the objective function is convex).

An objective function that minimized the sum of the muscle forces was selected by Penrod, Davy, and Singh (1974). This objective function again assumes that the body selects some criteria to optimize and does so in a linear fashion. In minimizing the sum of forces, Crowninshield (1978) and Crowninshield and Brand (1981) argued that the muscle with the longest moment arm will be selected with a large force to satisfy the moment equilibrium equation. All other muscles will be predicted to have small or zero force. This uneven distribution of muscle forces is not necessarily observed *in vivo* and would highly stress those muscles predicted active (Bean et al., 1988).

To correct for this problem, Crowninshield and Brand (1981) included muscle cross-sectional area in the objective function. They selected a nonlinear objective function based on the inverse relationship of muscle force and contraction endurance. They stated that muscle selection to maximize activity endurance is reasonable for prolonged activities such as normal gait. However, this objective function may not apply to other forms of exertions where

for example, speed may be maximized or pain minimized. Their specific objective function is as follows:

$$\text{minimize} \sum_{i=1}^{m} \left(\frac{f_i}{A_i} \right)^3 \qquad (3.13)$$

where m is the number of muscles crossing the joint, f_i is the force in the i-th muscle, and A_i is the average cross-sectional area of the i-th muscle. Crowninshield and Brand (1981) assumed the power equal three based on a review of the literature to determine endurance time as a function of muscle stress. Since the muscle stresses are assumed to be positive (muscles create only tensile forces), the objective function is convex. A cubic function, e.g. $f(x) = x^3$, is not convex over all real numbers but is convex for $x \geq 0$ (Bazaraa, Sherali, and Shetty, 1993). Crowninshield and Brand (1981) assumed that the body optimizes some criteria. The objective function chosen is a convex function based on physiologic properties of muscle endurance.

Crowninshield and Brand (1981) recognized that the objective function that minimizes the cubic of muscle stress may not be applicable for all situations. For example, patients with painful arthritis might reduce pain by minimizing joint loading. The objective function for this situation could be to minimize the resultant force vector created by the activity of the muscles. They did not specifically test this scenario.

An, Kwak, Chao, and Morrey (1984) introduced the concept of predicting muscle forces by minimizing muscle stress in the objective function subject to the moment equilibrium constraints. Stress was defined as the muscle force divided by the physiological cross-sectional area. They applied their model to

predicting muscle forces at the elbow when external flexion-extension and pronation-supination moments were applied.

A model developed by Bean et al. (1988) used two objective functions in sequence to estimate the forces of the muscles in the trunk. First, their model minimizes the maximum intensity the muscles can transmit as proposed by An et al. (1984). If the maximum intensity of the muscles is not constrained, the maximum stabilizing forces are allocated to those muscles with the largest moment arm. In an attempt to avoid this unrealistic situation, the maximum intensity can be fixed but its exact value is unknown. Bean et al. (1988) assumed that muscles cannot create very large intensities and that the stabilizing muscle forces are distributed to several muscles by limiting the maximum intensity. Second, after establishing the maximum intensity of the muscles, the objective function is to minimize the compression on the joints. Bean et al. (1988) made some assumptions about the feasible intensities of the muscles, then used this to minimize another objective function. The second objective function assumes that the body selects muscle forces to minimize damage to the joints (disc compression in this case).

In summary, optimization models to predict muscle forces have used convex objective functions so a global minimum is found. All models assume that the human body is attempting to optimize some criteria. In general, the objective function criteria is assumed not to change with different tasks. The selection of different criteria to optimize were reported by several authors. In general, physiological assumptions are presented to keep the objective function convex. These assumptions included minimization of the forces on the joints,

limitations on the intensity of muscles, and relationships to muscular endurance capabilities.

3.1.2.4 Practical Implications of Convex Programming

If an optimization problem is convex (whether linear or nonlinear), it is possible to find an optimum solution which is also the global optimum. If the problem is not convex, a global optimum solution is not guaranteed if a solution is possible at all. The largest practical implication is that muscle forces and objective functions have been formulated as convex functions.

For example, muscles are assumed to transmit force along a straight line and joint reaction forces are assumed to act through the point about which moments are summed. Although this may not be entirely true, it is a necessary assumption so that the mathematical program may be easily solved. Even if a complex system of equations could be developed that modeled the activities of muscles and joint reaction forces, the implication is that the optimization problem may not readily be solved. Researchers balance the need to represent model components accurately with the ability to solve the mathematical representations quickly.

3.1.3 Implications from Varying Optimization Models

A study of varying linear and non-linear optimization models was conducted by Dul, Townsend, Shiavi, and Johnson (1984). They applied several optimization models to the redundant knee system to predict muscle forces during a static-isometric flexion task of the knee. Dul et al. (1984)

assumed three major muscle groups act about the knee to create flexion. The muscles and assumed moment arms and cross-sectional areas are shown in Table 3.1. They further assumed that the extensor muscles of the knee are not active during flexion.

TABLE 3.1 Knee Flexion Muscle Characteristics Used by Dul et al. (1984) to Evaluate Optimization Models

Muscle Group	Moment Arm (cm)*	Area (cm^2)†	Maximum Force (N)‡
1. Long hamstrings Long biceps femoris Semitendinosus Semimembranous	4.42	25.5 (40.0)	765 (1200)
2. Short hamstrings Short biceps femoris	3.16	5.2 (10.0)	156 (300)
3. Gastrocnemius Medial gastrocnemius Lateral gastrocnemius	2.83	35.0 (25.0)	1050 (750)

* Estimated moment arm with respect to joint center for Knee angle of 140^{o}.

† Estimated physiological cross-sectional area; in parentheses are the values used by Pedotti, Krishnan, and Stark (1978).

‡ Maximum muscle force for maximum muscle stress of 30 N/cm^2; in parentheses are the values used by Pedotti, Krishnan, and Stark (1978).

The general form of the optimization problems investigated by Dul et al. (1984) is as follows:

$$\text{Minimize} \sum_{i=1}^{3} x_i^p \tag{3.14}$$

$$\text{Subject to} \quad x_i \geq 0 \; ; \; i = 1,2,3 \tag{3.15}$$

$$\sum_{i=1}^{3} c_i x_i = M \tag{3.16}$$

$$x_i \leq x_{imax} \; ; \; i = 1,2,3 \tag{3.17}$$

$$x_i = K x_j \; ; \; i \neq j \tag{3.18}$$

where x_i = decision variable: force or stress in the i-th muscle (N or N/cm^2),
p = power,
c_i = constant from the moment equation (cm or cm^3),
M = resultant moment (Ncm),
x_{imax} = maximum force or stress in the i-th muscle (N or N/cm^2),
K = stress or force ratio.

Dul et al. (1984) investigated 13 variations of the above general model. All variations used constraint equations 3.15 and 3.16. The 13 different cases were obtained by including the additional constraints, varying the value of p, and changing the cross-sectional areas assumed for the muscles. Table 3.2 lists the formulations of the 13 cases.

The objective of Dul et al. (1984) was to determine some basic characteristics of linear and non-linear models as well as the effect of additional constraints. The results of each model were the predicted muscle forces or stresses. Using the first model, the sum of the muscle forces is minimized subject to the moment equilibrium constraints. The solution to this formulation is simply to select the muscle with the longest moment arm, the long hamstrings,

TABLE 3.2 Thirteen Optimization Models Investigated by Dul et al. (1984).

Case	Muscle Force or Stress Used	Constraint Equations	p =	Other
1	Force	3.15,3.16	1	
2	Force	3.15,3.16,3.17	1	
3	Stress	3.15,3.16,3.17	1	
4	Force	3.15,3.16,3.17,3.18	1	$S_{LH} = S_{SH}$*
5	Stress	3.15,3.16,3.17,3.18	1	$S_{LH} = S_{SH}$*
6	Force	3.15,3.16,3.17,3.18	1	$S_{LH} = S_{SH}$*, A_i from Pedotti et al. (1978)
7	Stress	3.15,3.16,3.17,3.18	1	$S_{LH} = S_{SH}$*, A_i from Pedotti et al. (1978)
8	Force	3.15,3.16,3.17	2	
9	Stress	3.15,3.16,3.17	2	
10	Force	3.15,3.16,3.17	3	
11	Stress	3.15,3.16,3.17	3	
12	Force	3.15,3.16,3.17,3.18	3	$S_{LH} = S_{SH}$*
13	Stress	3.15,3.16,3.17,3.18	3	$S_{LH} = S_{SH}$*

* S_{LH} = stress long hamstrings, S_{SH} = stress short hamstrings, the fourth constraint is added with the stress (force/area) equal for these two muscles.

and increase its force in response to increases in external loads. The lack of a limit on muscle tension will not predict synergistic muscle activity.

When a limit is placed on the maximum force or stress, as in cases 2 and 3, the muscle with the largest moment arm is again recruited first. Its force increases until the force or stress limit is reached while all other muscles remain inactive. The muscle with the second largest moment arm is then recruited until its limit is reached. Dul et al. (1984) asserted that it is unlikely that a previously

inactive muscle becomes active only when another muscle reaches its maximum stress.

In cases 4, 5, 6, and 7 synergistic muscle activity is enforced because an additional constraint relates the stresses of two muscles. Therefore, if the muscle with the largest moment arm is recruited first, another muscle with a related stress will be recruited due to the fourth constraint. As Dul et al. (1984) stated, it is questionable to assume that the force in a muscle which crosses two joints is always related to a muscle which crosses only one joint, since there are situations when one is active and the other inactive and vice versa. Table 3.3 summarizes the order of recruitment for the first seven cases.

TABLE 3.3 Order of Recruitment of Three Knee Muscles for Seven Models, Dul et al. (1984)

Case	Decision Variable	Constraints	Order of Recruitment of Muscle
1	F_i	3.15,3.16	LH only
2	F_i	3.15,3.16,3.17	LH, SH, G†
3	F_i/A_i	3.15,3.16,3.17	LH, G, SH
4	F_i	3.15,3.16,3.17,3.18	LH + SH, G
5	F_i/A_i	3.15,3.16,3.17,3.18	G, LH + SH
6	F_i*	3.15,3.16,3.17,3.18	LH + SH, G
7	F_i/A_i*	3.15,3.16,3.17,3.18	LH + SH, G

* A_i from Pedotti et al. (1978)
† LH - long hamstrings, SH - short hamstrings, G - gastrocnemius

For the non-linear models, synergistic muscle activity is predicted at the onset of the external load. Instead of a serial recruitment of muscles, all muscles are recruited at the onset of the load. However, the muscle with the largest moment arm or product of moment by cross-sectional area has the largest muscle force at initial recruitment.

For the cases studied by Dul et al. (1984), the predicted load sharing depends on choice of decision variable, constraints, and objective function. The conclusions drawn from this study of optimization models are as follows:

(1) When forces are the decision variables, there is a preference for muscles with large moment arms. When stresses are the decision variables, there is a preference for muscles with the largest product of moment arm by cross-sectional area.

(2) For linear optimization models, a preferred muscle is recruited before any other muscles, and there is an orderly recruitment of muscles. Synergistic muscle activity is only predicted by adding constraints to limit the maximum force (or stress) or to relate muscle activity of two or more muscles.

(3) For non-linear models, synergism is predicted over the entire range or loads, but a preferred muscle produces a larger force.

Another general characteristic of linear programming problems is that the number of non-negative muscle forces can be at most equal to the number of constraints. In linear programming, there can only be as many basic variables as there are constraints. Therefore, the number of muscle forces that can be basic variables (and take on positive values) is at most equal to the number of

constraints. Note in the first case derived by Dul et al. (1984), there are three unknown muscle forces and only one constraint, the moment equilibrium equation. Therefore, the linear program predicts at most only one positive muscle force which is selected as the muscle with the longest moment arm to minimize the objective function. In the succeeding cases, additional constraints are added so the total number of constraints is greater than three. In these cases, multiple positive muscle forces are not necessarily predicted, for example when the external loads are small. However, as the external loads are increased, multiple positive muscle forces are predicted because there are enough constraints.

Non-linear optimization models, unlike linear models, do not possess the characteristic that the number of positive muscle forces can be at most equal to the number of constraints. A non-linear model with an objective function to minimize the squared stresses with only the moment equilibrium equation as a constraint can predict positive forces for more than one muscle (Dul et al., 1984).

3.2 The Minimum-Intensity-Compression (MIC) Model

The MIC model, developed by Bean, Chaffin, and Schultz (1988), is a reformulation of the iterative linear programming model of Schultz, Haderspeck, Warwick, and Portillo (1983). Schultz et al. (1983) developed an iterative model to predict trunk muscle forces by minimizing the maximum required muscle *intensity*. The model began with a maximum muscle intensity of 1 N/cm^2, and a solution of muscle forces in response to some external load was sought to

minimize spinal compression. If no solution was possible the intensity was increased by 1 N/cm^2 until a feasible solution was found. A model from Schultz et al. (1983) used five pairs of muscles (left and right sides) at the L3 cutting plane: the rectus abdominus, the external oblique abdominal, the internal oblique abdominal, the latissimus dorsi, and the erector spinae. The authors stated that the muscle force predictions and disc compression of the 10-muscle model was consistent with the 14- and 22-muscle models which were also investigated.

The MIC model involves two steps. The first step is to minimize the intensity or tension that any one muscle can sustain subject to the moment equilibrium constraints (An et al., 1984). Intensity is defined as force of the muscle divided by cross-sectional area. The first step is equivalent to the iterative steps of Schultz et al. (1983) where the intensity was gradually increased until the first feasible solution was found. Bean et al. (1988) pointed out that the difficulties of the Schultz et al. (1983) approach are its substantial computations and instability of solutions as intensities are slightly changed. The first step of the MIC model which is a linear programming problem is formulated as follows, assuming the ligament and disc forces, M^J, are negligible as reviewed in Chapter 2.

$$\text{Minimize} \quad I \tag{3.19}$$

$$\text{Subject to} \quad \sum_{i=1}^{m} \| f_i \| (r_i x \tau_i) + M^E = 0 \tag{3.20}$$

$$\frac{f_i}{A_i} \leq I \tag{3.21}$$

$$f_i \geq 0 \qquad (3.22)$$

where m is the number of muscles, f_i is the tension in each muscle, r_i is the moment arm vector, τ_i is the muscle line of action, M^E are the externally applied moments in three-dimensions, M^J are the moments due to joint contact and ligament forces, A_i are the cross-sectional areas of each muscle, and I is the maximum intensity any muscle can assume.

In the first step, intensity is minimized so that the maximum tension any muscle can assume is determined. The first step determines the set of feasible muscle forces with the minimum intensity which will satisfy the moment equilibrium constraints. The second step is to minimize the compression force on the disc (which is the sum of the muscle forces orthogonal to the cutting plane of the disc). The constraints are the moment equilibrium equations and the tension constraints. The second step is necessary when multiple optimum sets of muscle forces are found in the first step. The second step then chooses a single solution from among the multiple optima to minimize the spinal compression. If there is only one optimum set of muscle forces determined in the first step, then the second step is not necessary. If there is only one optimum set in the first step, it is the only feasible solution for the second step and thus the optimum for the second step. The second step is formulated as follows:

$$\text{Minimize} \quad \sum_{i=1}^{m} \|f_i\| \tau_i^z \qquad (3.23)$$

Subject to $$\sum_{i=1}^{m} \|f_i\|(r_i x \tau_i) + M^E = 0 \quad (3.24)$$

$$\frac{f_i}{A_i} \leq I \quad (3.25)$$

$$f_i \geq 0 \quad (3.26)$$

where τ_z is the unit direction orthogonal to the cutting plane of the disc, I is the maximum muscle intensity determined in the first step, and all other variables are the same as the first step.

3.2.1 Convexity of the MIC Model

The minimum intensity compression model is a convex programming problem because the first and second steps are convex. A linear equation by itself defines a convex set, for example, $x_i \geq 0$. Take any two points greater than zero and a linear combination of those two points is greater than zero. Therefore, the constraint equations, which are all linear, define convex sets.

The intersection of a finite number of convex sets is a convex set (assuming it is nonempty). Assume there are two intersecting convex sets C_1 and C_2. Let A and B be points in set C_1. If A and B are in the intersection of the convex sets then they are also in C_2. The linear combination of A and B must also be in the intersection because all sets are convex. Therefore, the set of feasible solutions defined by the constraint equations is convex because it is the intersection of convex sets. The objective function is convex because it is a simple linear sum of the muscles forces. Since the feasible solution set is convex and the objective function is convex, the second step of the MIC model

is a convex programming problem. Since the MIC model is a convex problem, the minimum solution found is a global minimum.

The MIC model predicts synergistic muscle activity because the maximum intensity any one muscle can assume is minimized. Recall from Dul et al. (1984), when upper bound constraints are added (constraint 3 in Dul et al., 1984) synergistic activity is predicted at 'high enough' external loads. In the Bean et al. (1988) formulation, a 'high enough' external load is enforced by minimizing the stress in the objective function. Several muscles are predicted to be active in order to minimize the maximum stress any one muscle can sustain. From Dul et al. (1984) when a specific value is selected for the maximum stress, the preferred muscle is the only active muscle until it reaches its maximum stress. However, the MIC model predicts synergistic muscle activity and as the external load increases the force and stress of the synergistic muscles increase.

3.2.2 Example of the MIC Model

The following example of the MIC model is taken from Hughes (1991). An imaginary cutting plane is assumed at the L3/L4 disc. The coordinate system used for this example was shown previously in Figure 2.1. Given a 10-muscle model, the muscles, moment arms, lines of action, and cross-sectional areas are shown in Table 3.4.

Assume that an external load applied to the body results in the following moments: -15 Nm M_x (extension moment, requires body to exert attempted

TABLE 3.4 Data Used in the MIC Model Example: Moment Arms r_i (cm) and Unit Muscle Force Components τ_i, and Anatomical Cross-Sectional Areas A_i (cm^2).

Muscle	r_i^{x*}	r_i^{y*}	r_i^{z*}	τ_i^{x}†	τ_i^{y}†	τ_i^{z}†	A_i‡
L. Erector spinae (LES)	-3.82	-5.76	0.0	0.281	-0.052	-0.958	24.9
R. Erector spinae (RES)	3.82	-5.76	0.0	-0.281	-0.052	-0.958	24.9
L. Rectus abdominus (LRA)	-3.38	7.95	0.0	-0.028	0.016	-0.9995	6.6
R. Rectus abdominus (RRA)	3.38	7.95	0.0	0.028	0.016	-0.9995	6.6
L. Internal Oblique (LIO)	-11.39	0.96	0.0	-0.134	-0.574	-0.808	14.2
R. Internal Oblique (RIO)	11.39	0.96	0.0	0.134	-0.574	-0.808	14.2
L. External Oblique (LEO)	-12.62	1.09	0.0	0.376	0.322	-0.870	15.3
R. External Oblique (REO)	12.62	1.09	0.0	-0.376	0.322	-0.870	15.3
L. Latissimus Dorsi (LLD)	-7.19	-5.42	0.0	0.340	-0.284	-0.897	3.9
R. Latissimus Dorsi (RLD)	7.19	-5.42	0.0	-0.340	-0.284	-0.897	3.9

* The muscle moment arms are from Tracy, Gibson, Szypryt, Rutherford, and Corlett (1989).

† The lines of action are from Dumas, Poulin, Roy, Gagnon, and Jovanovic (1988).

‡ The anatomical cross-sectional area of Tracy et al. (1989) is multiplied by the z component of the unit force vector to account for the effect of fiber orientation on physiological cross-sectional area as in McGill, Patt, and Norman (1988). The oblique muscle area of Tracy et al. (1989) is partitioned into internal and external oblique areas according to the proportions determined from Chaffin, Redfern, Erig, and Goldstein (1990).

flexion), 0 Nm M_y, and 15 Nm M_z (torsion moment). The first step of the MIC model is now formulated as follows:

Minimize I (3.27)

Subject to:

$$0.05518f_{LES} + 0.05518f_{RES} - 0.07946f_{LRA} - 0.07946f_{RRA} - 0.00776f_{LIO} - 0.00776f_{RIO} - 0.00948f_{LEO} - 0.00948f_{REO} + 0.04862f_{LLD} + 0.04862f_{RLD} - 15 = 0 \quad (\Sigma M_x = 0) \tag{3.28}$$

$$-0.03660f_{LES} + 0.03660f_{RES} - 0.03378f_{LRA} + 0.03378f_{RRA} - 0.09203f_{LIO} + 0.09203f_{RIO} - 0.10979f_{LEO} + 0.10979f_{REO} - 0.06449f_{LLD} + 0.06449f_{RLD} = 0 \quad (\Sigma M_y = 0) \tag{3.29}$$

$$0.01817f_{LES} - 0.01817f_{RES} + 0.00169f_{LRA} - 0.00169f_{RRA} + 0.06667f_{LIO} - 0.06667f_{RIO} - 0.04473f_{LEO} + 0.04473f_{REO} + 0.03885f_{LLD} - 0.03885f_{RLD} + 15 = 0 \quad (\Sigma M_z = 0) \tag{3.30}$$

$$f_{LES}/24.9 \le I;\ f_{RES}/24.9 \le I;\ f_{LRA}/6.6 \le I;\ f_{RRA}/6.6 \le I;\ f_{LIO}/14.2 \le I;\ f_{RIO}/14.2 \le I;\ f_{LEO}/15.3 \le I;\ f_{REO}/15.3 \le I;\ f_{LLD}/3.9 \le I;\ f_{RLD}/3.9 \le I \tag{3.31 - 3.40}$$

$$f_{LES} \ge 0;\ f_{RES} \ge 0;\ f_{LRA} \ge 0;\ f_{RRA} \ge 0;\ f_{LIO} \ge 0;\ f_{RIO} \ge 0;\ f_{LEO} \ge 0;\ f_{REO} \ge 0;\ f_{LLD} \ge 0;\ f_{RLD} \ge 0 \tag{3.41 - 3.50}$$

The result from this first step is that maximum muscle intensity is minimized to a value of 11.07 N/cm^2. Values for the muscle forces are also determined because they are decision variables in the first step of the MIC model. The values for the muscle force decision variables of the first step are listed below:

Muscle	Force (N)
L. Erector spinae	0
R. Erector spinae	0
L. Rectus abdominus	72
R. Rectus abdominus	72
L. Internal Oblique	157
R. Internal Oblique	13
L. External Oblique	48
R. External Oblique	169
L. Latissimus Dorsi	0
R. Latissimus Dorsi	0

Given the value of intensity determined from the first step (11.07 N/cm^2), the second step is now formulated as follows:

$$\text{Minimize } | -0.958f_{LES} - 0.958f_{RES} - 0.9995f_{LRA} - 0.9995f_{RRA} - 0.808f_{LIO} - 0.808f_{RIO} - 0.870f_{LEO} - 0.870f_{REO} - 0.897f_{LLD} - 0.897f_{RLD} | \quad (3.51)$$

Subject to

$$0.05518f_{LES} + 0.05518f_{RES} - 0.07946f_{LRA} - 0.07946f_{RRA} - 0.00776f_{LIO} - 0.00776f_{RIO} - 0.00948f_{LEO} - 0.00948f_{REO} + 0.04862f_{LLD} + 0.04862f_{RLD} - 15 = 0 \quad (\Sigma M_x = 0) \quad (3.52)$$

$$-0.03660f_{LES} + 0.03660f_{RES} - 0.03378f_{LRA} + 0.03378f_{RRA} - 0.09203f_{LIO} + 0.09203f_{RIO} - 0.10979f_{LEO} + 0.10979f_{REO} - 0.06449f_{LLD} + 0.06449f_{RLD} = 0 \quad (\Sigma M_y = 0) \quad (3.53)$$

$$0.01817f_{LES} - 0.01817f_{RES} + 0.00169f_{LRA} - 0.00169f_{RRA} + 0.06667f_{LIO} - 0.06667f_{RIO} - 0.04473f_{LEO} + 0.04473f_{REO} + 0.03885f_{LLD} - 0.03885f_{RLD} + 15 = 0 \quad (\Sigma M_z = 0) \quad (3.54)$$

$f_{LES}/24.9 \leq 11.07$; $f_{RES}/24.9 \leq 11.07$; $f_{LRA}/6.6 \leq 11.07$; $f_{RRA}/6.6 \leq 11.07$; $f_{LIO}/14.2 \leq 11.07$; $f_{RIO}/14.2 \leq 11.07$; $f_{LEO}/15.3 \leq 11.07$; $f_{REO}/15.3 \leq 11.07$; $f_{LLD}/3.9 \leq 11.07$; $f_{RLD}/3.9 \leq 11.07$

(3.55 - 3.64)

$f_{LES} \geq 0$; $f_{RES} \geq 0$; $f_{LRA} \geq 0$; $f_{RRA} \geq 0$; $f_{LIO} \geq 0$; $f_{RIO} \geq 0$; $f_{LEO} \geq 0$; $f_{REO} \geq 0$; $f_{LLD} \geq 0$; $f_{RLD} \geq 0$ (3.65 - 3.74)

The result from the second step of the MIC model is the predicted muscle forces to counteract the external moments. For this example with M_x = -15 Nm, M_y = 0 Nm and M_z = 15 Nm, the muscle forces predicted by the MIC model are as follows:

Muscle	Force (N)
L. Erector spinae	0
R. Erector spinae	0
L. Rectus abdominus	72
R. Rectus abdominus	72
L. Internal Oblique	157
R. Internal Oblique	13
L. External Oblique	48
R. External Oblique	169
L. Latissimus Dorsi	0
R. Latissimus Dorsi	0

The muscle forces predicted from the second step of the MIC model did not change from those predicted in the first step. This is because for the selected example, a single optimum combination of muscle forces exists in the

first step. Since only one feasible solution exists in the first step to minimize the intensity, there is only one feasible solution in the second step, and it is selected to minimize the compression force on the spine. If multiple optimal solutions existed in the first step, the second step is required to select among the optimal solutions. The predicted muscle forces were the same in both steps of the MIC model example, which will occur often in other examples. After a maximum intensity is determined in the first step, the feasible solutions for the second step are limited. Among the feasible solutions, the one that minimizes the disc compression is selected. The solution for the second step coincides with the solution from the first step unless there are multiple optima in the first step.

3.3 The Sum of the Cubed Intensities (SCI) Model

The SCI model was proposed by Crowninshield and Brand (1981). They predicted the muscle activity of the lower extremities in locomotion as well as the muscle activity about the elbow in flexion using the SCI model. The objective function of the SCI model is to minimize the sum of the cubed muscle intensities subject to the moment equilibrium constraints. Intensity is defined as the force generated by the muscle divided by its cross-sectional area. Crowninshield and Brand (1981) selected a cubic objective function based on human muscular endurance capabilities. For example, relatively high muscle intensities can only be sustained for short durations, while lower muscle intensities can be sustained longer. A cubic function was selected to best represent this intensity-duration trade-off by Crowninshield and Brand (1981).

The SCI optimization problem is formulated as follows:

$$\text{Minimize} \quad \sum_{i=1}^{m}\left(\frac{f_i}{A_i}\right)^3 \tag{3.75}$$

$$\text{Subject to} \quad \sum_{i=1}^{m}\|f_i\|(r_i x \tau_i) + M^E = 0 \tag{3.76}$$

$$f_i \geq 0 \tag{3.77}$$

$$A_i \geq 0 \tag{3.78}$$

where m is the number of muscles, f_i is the tension in each muscle, A_i is the cross-sectional area of each muscle, r_i is the moment arm vector, τ_i is the muscle line of action, and M^E are the externally applied moments in three-dimensions. Note the that the moments due to joint contact and ligament forces are not included in the formulation because they are considered negligible (reviewed in Section 2.7).

3.3.1 Convexity of the SCI Model

The SCI model is also a convex programming problem. The constraints are linear equations which define a convex set. Therefore, the set of feasible solutions defined by the constraint equations is convex because it is the intersection of convex sets. The cubic objective function is also convex. In general, a cubic function, e.g. $f = x^3$, is not convex for x unrestricted. For the SCI formulation x is equivalent to (f/A). However, f and A are restricted to be greater

than or equal to 0, and the function x^3 is convex when x is restricted to be greater than or equal to 0. Therefore, the objective function of the SCI model is convex. Since the feasible solution set is convex and the objective function is convex, the SCI model is a convex programming problem. Since the SCI model is a convex problem the minimum solution found is a global minimum.

The SCI model can predict synergistic muscle activity because it has a non-linear objective function. Recall from Dul et al. (1984), one case studied was a cubic objective function subject to the moment equilibrium constraints. This is the same formulation as the SCI model. Dul et al. (1984) found synergistic muscle activity was predicted at the onset of the external load, instead of a serial recruitment of muscles.

3.3.2 Example of the SCI Model

The following example of the SCI model is taken from Hughes (1991). An imaginary cutting plane is assumed at the L3/L4 disc. The coordinate system used for this example was shown previously in Figure 2.1. Given a 10-muscle model, the muscles, moment arms, lines of action, and cross-sectional areas are the same as those used in the MIC model example, shown previously in Table 3.4.

Assuming that an external load applied to the body results in the following moments: -15 Nm M_x (extension moment, requires body to exert attempted flexion), 0 Nm M_y, and 15 Nm M_z (torsion moment). The SCI model is now formulated as follows:

Minimize $(f_{LES}/24.9)^3 + (f_{RES}/24.9)^3 + (f_{LRA}/6.6)^3 + (f_{RRA}/6.6)^3 + (f_{LIO}/14.2)^3 + (f_{RIO}/14.2)^3 + (f_{LEO}/15.3)^3 + (f_{REO}/15.3)^3 + (f_{LLD}/3.9)^3 + (f_{RLD}/3.9)^3$ (3.79)

Subject to

$0.05518f_{LES} + 0.05518f_{RES} - 0.07946f_{LRA} - 0.07946f_{RRA} - 0.00776f_{LIO} - 0.00776f_{RIO} - 0.00948f_{LEO} - 0.00948f_{REO} + 0.04862f_{LLD} + 0.04862f_{RLD} - 15 = 0 \ (\sum M_x = 0)$ (3.80)

$-0.03660f_{LES} + 0.03660f_{RES} - 0.03378f_{LRA} + 0.03378f_{RRA} - 0.09203f_{LIO} + 0.09203f_{RIO} - 0.10979f_{LEO} + 0.10979f_{REO} - 0.06449f_{LLD} + 0.06449f_{RLD} = 0 \ (\sum M_y = 0)$ (3.81)

$0.01817f_{LES} - 0.01817f_{RES} + 0.00169f_{LRA} - 0.00169f_{RRA} + 0.06667f_{LIO} - 0.06667f_{RIO} - 0.04473f_{LEO} + 0.04473f_{REO} + 0.03885f_{LLD} - 0.03885f_{RLD} + 15 = 0 \ (\sum M_z = 0)$ (3.82)

$f_{LES} \geq 0$; $f_{RES} \geq 0$; $f_{LRA} \geq 0$; $f_{RRA} \geq 0$; $f_{LIO} \geq 0$; $f_{RIO} \geq 0$; $f_{LEO} \geq 0$; $f_{REO} \geq 0$; $f_{LLD} \geq 0$; $f_{RLD} \geq 0$ (3.83 - 3.92)

The predicted muscle forces from this example of the SCI model are as follows:

Muscle	Force (N)
L. Erector spinae	0
R. Erector spinae	0
L. Rectus abdominus	78
R. Rectus abdominus	77
L. Internal Oblique	143
R. Internal Oblique	0
L. External Oblique	13
R. External Oblique	134
L. Latissimus Dorsi	0
R. Latissimus Dorsi	0

The predicted muscles forces for MIC and SCI models are similar except for the right internal oblique and left external oblique muscles. In the MIC model, the right internal oblique muscle is predicted to exert 13 N of force while the SCI model predicts inactivity. The left external oblique muscle is predicted to exert 48 N force in the MIC model while the SCI model predicts a lower value of 13 N.

3.4 Validation of the MIC and SCI Models

An investigation of competing low back optimization models was performed by Hughes (1991). He tested four low back optimization models at loading conditions in which the four models differed in their predictions of some of the muscle forces. The four models tested were the MIC, SCI, Sum of the Squared Intensities (SSI), and Eigenvector-Synergy (ES) models. Since human muscles forces cannot be measured *in vivo*, electromyography (EMG) activity of the muscles was selected to validate the accuracy the model predictions. Determining an EMG-force function is problematic, so Hughes (1991) tested the competing models at loading conditions where the predicted

muscle forces were markedly different. Gross differences in predicted muscle forces should be reflected in gross differences in EMG data and not rely on an exact EMG-force relation.

The results of Hughes's experiments indicated that the MIC, ES, and SSI models can be rejected due to inaccuracies at some loading conditions. During sagittal and frontal plane loads, the left external oblique force predicted by the ES model did not correspond to EMG data of that muscle. This result depends only on assuming a monotonic relationship between isometric force and EMG. During asymmetric loading, the MIC model's prediction of the erector spinae force did not match EMG data. The ES and SSI models were not supported under asymmetric loading due to oblique EMG data. Under an increasing torsion load with a constant attempted flexion moment, the MIC model predicted increasing force in the rectus abdominus while the SCI model predicted constant force in this muscle. EMG data did not support the MIC model. Together, the results did not support the MIC, ES, or SSI models. The SCI model was not rejected by the experiments. The SCI model was not necessarily validated because of difficulties in functionally relating force to EMG. However, the SCI model was not rejected.

Ladin, Murthy, and De Luca (1989) experimentally tested the model developed by Schultz et al. (1983). Recall that the MIC model is an optimization reformulation of the iterative model of Schultz et al. (1983). Ladin et al. (1989) used the iterative model to predict the forces for 22 muscles at external loading conditions with flexion and lateral bending moments. Ladin et al. (1989) varied the flexion moment from 0 to 100 Nm in 10 Nm increments and at each flexion

moment level varied the lateral bending from -100 to 100 Nm in 10 Nm increments for a total of 231 loading conditions. For each muscle, a graph was generated which showed the loading conditions in which the muscle was active. Figure 3.3 shows a curve for the longissimus muscle, above the curve are all loading conditions in which the muscle is predicted active while below the curve it is inactive. Because this curve divides the loading conditions between active and inactive regions, Ladin et al. (1989) termed it the 'switching curve'. The switching curve concept lends itself to experimental testing because loading conditions in the inactive zones should show resting EMG potential. Active loading zones should have positive EMG data. No assumptions about force-EMG functions are necessary.

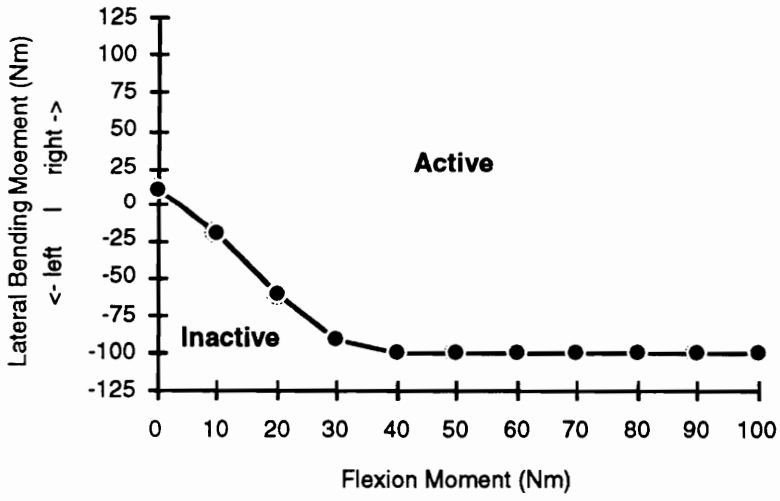

Figure 3.3 The switching curve of the left longissimus muscle adapted from Ladin et al. (1989), the area above the curve indicates loading conditions where the muscle is active, while those below the curve indicate conditions of inactivity

Ladin et al. (1989) tested each of six loading conditions on eight subjects equaling 48 observations; all conditions were repeated a second time for 48 more observations. Table 3.5 lists the number of predictions in which the muscle is predicted on and off and the corresponding empirical results. A Chi-square analysis of these results revealed that there was a strong correlation between the model predictions and the observed muscle activity for all but one muscle (the Ipsilateral RA on the first series of 48 trials).

This experiment evaluated the iterative model developed by Schultz et al. 1983), not the succeeding MIC model. However, the models are very similar. This experiment did not validate the MIC or iterative Schultz model as completely accurate. However, the Schultz model predictions were not rejected, and a switching curve method of evaluating the model was suggested. Ladin et al. (1989) also pointed out that the method of predicting muscles active and inactive became less stable as the loading condition was relatively close to the loading curve.

TABLE 3.5 Results of Ladin et al. (1989) evaluation of the Schultz et al. (1983) model. The first column indicates the number of predicted active and inactive conditions out of 48 and the last two columns represent actual activity.

	Experimental ON	Experimental OFF
Contralateral RA		
Predicted ON (16)	14	2
Predicted OFF (32)	2	30
Ipsilateral RA		
Predicted ON (16)	4	12
Predicted OFF (32)	0	32
Contralateral OB		
Predicted ON (32)	32	0
Predicted OFF (16)	2	14
Ipsilateral OB		
Predicted ON (0)	0	0
Predicted OFF (48)	15	33
Contralateral ES		
Predicted ON (48)	48	0
Predicted OFF (0)	0	0
Ipsilateral ES		
Predicted ON (32)	13	19
Predicted OFF (16)	0	16

RA = rectus abdominus; OB = oblique abdominal; ES = erector spinae

4. MUSCLE FORCES PREDICTED BY TRUNK OPTIMIZATION MODELS UNDER VARYING LOADING CONDITIONS

4.1 Introduction

Optimization-based biomechanical models have been developed for the trunk region to estimate the internal forces in response to an external load. For a given task, the tension of the trunk muscles are estimated and used to calculate the resultant forces on the spinal column. The foundation of optimization models begins by applying engineering mechanics to the human body. The body is modeled as a series of rigid links. When an external force is applied to one of the links, the body produces reaction forces using the muscles to maintain a static posture. The compression, shear, and torsional forces on the spinal discs can be estimated by summing the external and internal (muscular) forces.

The Minimum Intensity Compression (MIC) and Sum of the Cubed Intensities (SCI) models have been proposed to estimate the internal muscular forces. The formulations of these two models, the assumptions used to solve them, and examples of their implementation were discussed in Chapter 3.

Anatomical inputs are required by the MIC and SCI models to predict the muscle forces. If the joint contact and ligament forces are assumed negligible as reviewed in section 2.7, the required inputs are the number of muscles and their moment arms to the vertebrae, lines of action, and cross-sectional areas. Chapter 2 reviewed the studies conducted to determine geometric parameters

of the trunk muscles. From this review, sets of geometric inputs were determined.

A study to assess changes in the muscle lines of action on predicted muscle force was conducted by Nussbaum, Chaffin, and Rechtien (1995). They use the SCI model with five pairs of muscles (erector spinae, latissimus dorsi, external oblique, internal oblique, and rectus abdominus). The moment arms and cross-sectional areas of the muscles, taken from Moga, Erig, Chaffin, and Nussbaum (1993) and Hughes (1991) respectively, were kept constant throughout the study. Reference values for the muscle lines of action were taken from Moga, Erig, Chaffin, and Nussbaum (1992) (the current author was unable to obtain this article because the reference was incomplete). Nussbaum et al. (1995) varied lines of action for one pair (left and right sides) of muscles at a time, holding the lines of action for the remaining eight muscles. The forces for all 10 muscles were then predicted as the lines of action a single pair varied.

In varying the directions of the muscles, Nussbaum et al. (1995) projected the lines of action of each muscle into the sagittal and frontal planes. The assumed lines of action of a muscle in a single plane were rotated over a range ±20° in increments of 2°. All muscle forces were then predicted for five combinations of flexion/extension and lateral bending moments with a constant resultant moment of 140 Nm as a pair of muscle lines of action were varied.

Nussbaum et al. (1995) reported results chiefly concerned with the changes in forces (compression, lateral shear, and anterior-posterior shear) on the spinal column. However, they also reported changes in the predicted

activity/inactivity of the muscles as a load was rotated about the body. For example, the right external oblique was predicted to become active over a 15 degree span of load orientation with changes in its line of action. Another example, given by Nussbaum et al. (1995), pointed out that the activity of the internal oblique muscles changed substantially with changes in the line of action of the external oblique.

Another important result reported by Nussbaum et al. (1995) was that when a smaller resultant moment than 140 Nm was used, the model did not predict any qualitative changes in muscle recruitment patterns. Therefore, a lower resultant moment can be used in the moment equilibrium constraints without affecting the qualitative predictions of the muscle forces.

The study reported by Nussbaum et al. (1995) indicated the need to further investigate the effect of inputs to optimization based trunk models on muscle force predictions. First, Nussbaum et al. (1995) focused on spinal reaction forces and more study of changing muscle forces would be appropriate. Second, they performed a systematic change in the lines of action of a pair of muscles, but did not vary the line of actions of several pairs of muscles simultaneously. Finally, the moment arms and cross-sectional areas of each muscle were held constant.

The study reported in this dissertation differs from the method used by Nussbaum et al. (1995). The muscle geometric inputs for the current study were compiled from empirically measured data reported in the literature. The input parameters of areas, moment arms, and lines of action of the muscles for the current study were simultaneously varied because they were measured from

different samples. Model predictions of muscle forces were generated using two different geometry sets that represent actual measurements reported.

This chapter reports on a computer simulation conducted to determine the effects of different inputs into optimization-based biomechanical trunk models. The two models discussed earlier, the MIC and SCI, were included in the investigation. The number of muscles included in the development of the models were varied as well as the geometric parameters of the muscles (moment arms, the lines of action, and the cross-sectional areas).

4.2 Modeling Procedure

4.2.1 Inputs

Three variables were manipulated to determine the effects of input parameters on the muscle force predictions of torso biomechanical models. The first variable manipulated was the model used to predict the muscle forces, which had two levels. The first model employed was the Minimum Intensity Compression (MIC) model developed by Bean, Chaffin, and Schultz (1988). The second model used was the Sum of the Cubed Intensities (SCI) model proposed by Crowninshield and Brand (1981). The assumptions, descriptions, and development of both these models were reviewed in Chapter 3.

The second variable manipulated was the number of muscles included in the model formulation which had two levels. The first level consisted of 10 muscles, 5 each on the left and right sides as follows: erector spinae, rectus abdominus, internal oblique, external oblique, and latissimus dorsi. These were the same ten muscles used by several researchers (Hughes, 1991;

Johnson, 1992; and Schultz and Andersson, 1981). The second level consisted of 18 muscles, 9 each on the left and right sides as follows: multifidus, longissimus, iliocostalis, rectus abdominus, internal oblique, external oblique, latissimus dorsi, psoas, and quadratus lumborum. Increasing from 10 to 18 muscles was accomplished by splitting the erector spinae into its constituents of the multifidus, longissimus, and iliocostalis and adding the psoas and quadratus lumborum muscles.

The third variable manipulated was the geometry of the muscles included in the model which had two levels. Chapter 2 provided a review of the muscle moment arms, lines of action, and cross-sectional areas determined by several studies. Two geometry sets were developed from the literature. The first was taken from a study conducted by Han, Ahn, Goel, Takeuchi, and McGowan (1992) while the second was comprised from a compilation of several studies. When the models included 10 versus 18 muscles, the same general geometry sets were used by reducing the 18-muscle geometry set.

The geometric data for 18 muscles reported by Han et al. (1992) was shown previously in Table 2.16. The moment arms, lines of action, and cross-sectional areas were determined by averaging the left and right hand side values. In addition, the lines of action were scaled so that the resultant force was a unit vector. The values reported by Han et al. (1992) did not form a resultant unit vector which was possibly due to measurement difficulties.

The second 18-muscle input data set was comprised of several studies. The moment arms for each of the 18 muscles was provided by Tracy, Gibson, Szypryt, Rutherford, and Corlett (1989). The lines of action for the longissimus,

iliocostalis, rectus abdominus, internal oblique, external oblique, latissimus dorsi, psoas, and quadratus lumborum were taken from Dumas, Poulin, Roy, Gagnon, and Jovanovic (1988). The line of action of the multifidus was taken from Macintosh and Bogduk (1986). The area of the multifidus, longissimus, and iliocostalis was calculated by using the area of the erector spinae reported in Tracy et al. (1989) and dividing it into the proportions given in Schultz et al. (1983). The final physiological area was determined by multiplying the area by the z component of the unit force vector to account for fiber orientation as in McGill, Patt, and Norman (1988). The areas of the rectus abdominus, latissimus dorsi, psoas, and quadratus lumborum were taken from Tracy et al. (1989). The overall oblique area reported by Tracy et al. (1989) was divided into the internal and external oblique portions using the ratios given by Chaffin, Redfern, Erig, and Goldstein (1990). These areas were then multiplied by the z component of the unit force vector to account for fiber orientation. Table 2.17, shown previously, listed the final muscle geometry for the compilation of studies discussed.

The 10-muscle input data set was determined by combining and eliminating muscles from the 18-muscle data set. The multifidus, longissimus, and iliocostalis muscles were combined into a single erector spinae muscle. The quadratus lumborum and psoas muscles were eliminated from the data set.

The first 10-muscle input data set was taken from Han et al. (1992). The moment arms and line of action for the erector spinae were determined by using the moment arms and line of action for the longissimus muscle. For the remaining muscles, the moment arms, lines of action, and cross-sectional areas

were determined by averaging the left and right hand side values reported. In addition, the lines of action were scaled so that the resultant force was a unit vector. The geometric data for 10 muscles taken from Han et al. (1992) was shown previously in Table 2.18.

The second 10-muscle input data set was comprised of several studies. The moment arms for each of the 10 muscles was provided by Tracy et al. (1989). The lines of action for the 10 muscles were taken from Dumas et al. (1988). The areas of the erector spinae, rectus abdominus, and latissimus dorsi, were taken from Tracy et al. (1989). The overall oblique area was reported by Tracy et al. (1989) and was then divided into the internal and external oblique portions using the ratios given by Chaffin et al. (1990). The final physiological area was determined by multiplying the area by the z component of the unit force vector to account for fiber orientation as in McGill et al. (1988). Table 2.19, shown previously, listed the final 10-muscle geometry for the compilation of studies discussed.

4.2.2 Model Outputs

To determine the effect of input parameters on trunk optimization biomechanical models, the muscle forces were predicted for different external loads imposed on the body. The external load was expressed in terms of a three-dimensional moment consisting of x, y, and z components. According to the reference system, shown previously in Figure 2.1, a moment about the x-axis (M_x) was a flexion/extension moment. A positive external M_x would cause torso extension while a negative external M_x would cause torso flexion. A

moment about the y-axis (M_y) was a lateral bending moment. A positive external M_y would cause torso bending to the right while a negative external M_y would cause torso bending to the left. A moment about the z-axis (M_z) would be a twisting moment. A positive external M_z would cause torso twisting counter-clockwise while a negative external M_y would cause torso twisting clockwise.

The limits of M_x, M_y, and M_z were set to range from -50 to 50 Nm which was within the range investigated by Hughes (1991) and Ladin (1989) in other biomechanical model studies. A loading plane was created by combinations of M_x and M_y while M_z was held constant. M_x varied from -50 to 50 in increments of 2 Nm; at each level of M_x, M_y was varied from -50 to 50 Nm in increments of 2 Nm. The result was loading plane grid of 2601 external loading conditions for M_x and M_y while M_z was held constant at some level. M_z was varied from 0, 15, and 30 Nm levels.

Each of the eight combinations of model, number of muscles, and muscle geometry set (listed in Table 4.1) were used to predict the muscle forces, for each loading condition (a total of 7803). A Mathematica program was written to predict the muscle forces for conditions using the MIC model. The outputs of this program were the muscle forces predicted for each of the 10 or 18 muscles. The software MATLAB was used to predict the muscle forces for conditions involving the SCI model.

4.2.3 Graphing the Active Region

Ladin, Murthy, and De Luca (1989) experimentally tested the model developed by Schultz et al. (1983). The MIC model was an optimization

TABLE 4.1 Input Combinations Used to Predict Muscle Forces

Condition	Model	Number of Muscles	Geometry Set
1	MIC	10	Compilation
2	MIC	10	Han et al. (1989)
3	MIC	18	Compilation
4	MIC	18	Han et al. (1989)
5	SCI	10	Compilation
6	SCI	10	Han et al. (1989)
7	SCI	18	Compilation
8	SCI	18	Han et al. (1989)

reformulation of the iterative model of Schultz et al. (1983). Ladin et al. (1989) used the iterative model to predict the forces for 22 muscles at external loading conditions with flexion and lateral bending moments. Ladin et al. (1989) varied the flexion moment from 0 to 100 Nm in 10 Nm increments and at each flexion moment level varied the lateral bending from -100 to 100 Nm in 10 Nm increments for a total of 231 loading conditions. For each muscle, a graph was generated which showed the loading conditions in which the muscle was active. Figure 3.3 (shown previously) displays a curve for the longissimus muscle; above the curve were all loading conditions in which the muscle was predicted active while below the curve it was inactive. Because this curve divided the loading conditions between active and inactive regions, Ladin et al. (1989) termed it the 'switching curve.' The switching curve concept lent itself to

experimental testing because loading conditions in the inactive zones should have shown resting EMG potential. Active loading zones should have had positive EMG data. No assumptions about force-EMG functions were necessary.

Following the method forwarded by Ladin et al. (1989), graphs were generated depicting the loading conditions in which each muscle was predicted active and inactive. The muscle forces predicted at each loading condition were evaluated. If the muscle force was positive, it was active for that loading condition. Whereas if the muscle force was zero, it was predicted inactive. M_x represents the x-axis and M_y the y-axis while M_z was held constant so that a loading plane was established. Separate graphs were generated as M_z changed from 0 to 15 to 30 Nm.

4.3 Results

4.3.1 Muscle Force Predictions

Graphing the active/inactive regions for each muscle under all loading conditions would result in 336 separate graphs (2 models x 2 geometries x 18 muscles x 3 z-moments + 2 models x 2 geometries x 10 muscles x 3 z-moments). Four graphs were combined on each figure: MIC model with compilation geometry, MIC model with Han et al. geometry, SCI model with compilation geometry, and SCI model with Han et al. geometry. A total of 84 figures would show the active/inactive regions for each muscle in the 18- and 10-muscle models and the 3 M_z conditions. A few figures are presented in the results and not all 84 figures will be shown.

A typical active/inactive set of graphs is shown in Figure 4.1 for the Left Rectus Abdominus (LRA) Muscle in the 10-muscle model with 15 Nm twisting moment. The shaded regions represent a loading condition where the muscle force was predicted positive and therefore active. For example, at a loading condition of 10 Nm M_x, -30 Nm M_y, and 15 Nm M_z, the MIC model with the compilation geometry and the SCI model with the compilation geometry predicted the LRA active. The MIC model with the Han et al. geometry and the SCI model with the Han et al. geometry predicted the LRA inactive. Note that the graphs do not indicate the magnitude of activity. Other examples of active/inactive regions for three combinations input variables are shown in Figures 4.2 to 4.4.

To view the muscle forces predictions and activity using an alternative method, assume that an external load was applied to a person so that the resultant M_x-M_y moment was a constant of 30 Nm. A 100 N object held a distance of 30 cm from the center of the spinal disc would create a 30 Nm moment. If the load was rotated around the body, all combinations of M_x-M_y moments that create a resultant moment of 30 Nm would result. The muscle forces predicted by each model and muscle geometry were plotted versus the angle of rotation. Figure 4.5 shows the erector spinae muscle forces predicted by the MIC and SCI models using two different 10-muscle geometries for a load rotated about the body which creates a resultant 30 Nm M_x-M_y moment. Note that an angle of 0 degrees corresponds to 30 Nm M_x and 0 Nm M_y. Graphs plotting the predicted force for all muscles by angle of load were generated for both the 10- and 18-muscle models, Figures 4.5 to 4.18.

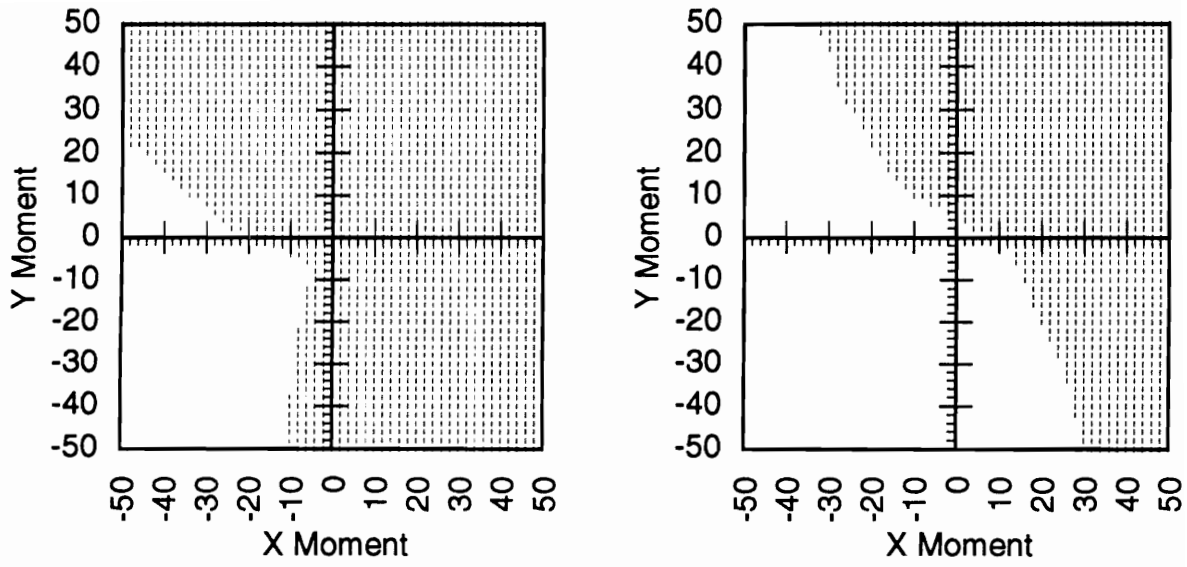

(a) MIC Model, Compilation Geometry

(b) MIC Model, Han et al. Geometry

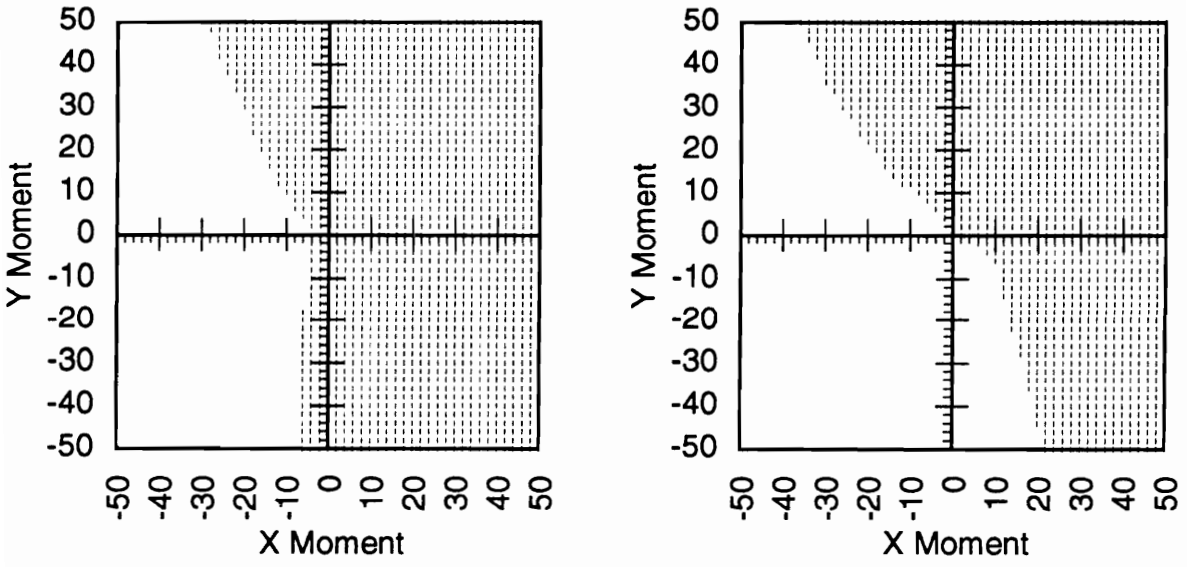

(c) SCI Model, Compilation Geometry

(d) SCI Model, Han et al. Geometry

Figure 4.1 Left rectus abdominus muscle for the 10-muscle geometries and 15 Z-moment. The shaded areas represent the regions where the muscle is active, while the unshaded regions represent inactivity.

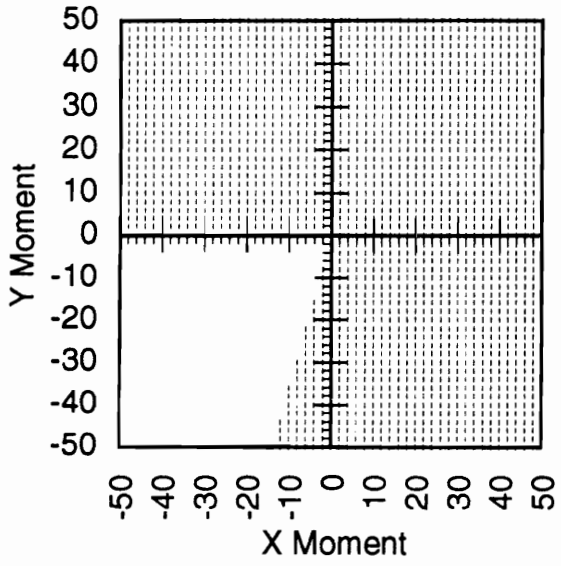

(a) MIC Model, Compilation Geometry

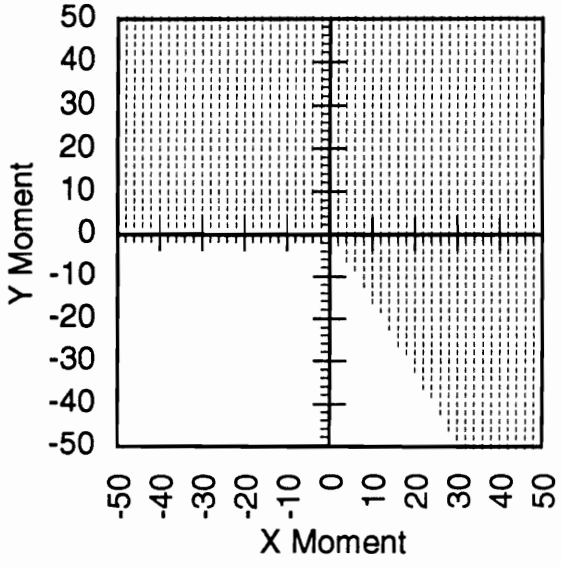

(b) MIC Model, Han et al. Geometry

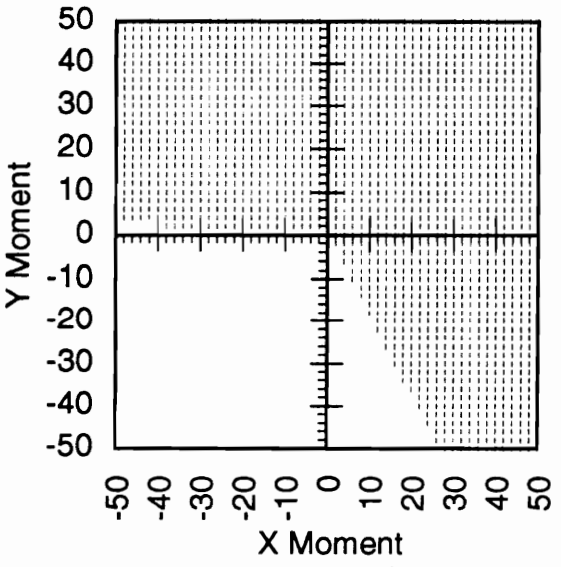

(c) SCI Model, Compilation Geometry

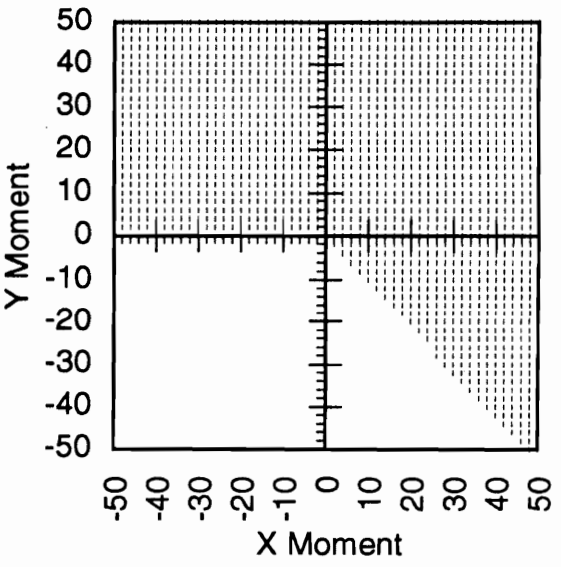

(d) SCI Model, Han et al. Geometry

Figure 4.2 Left internal oblique muscle for the 10-muscle geometries and 0 Z-moment. The shaded areas represent the regions where the muscle is active, while the unshaded regions represent inactivity.

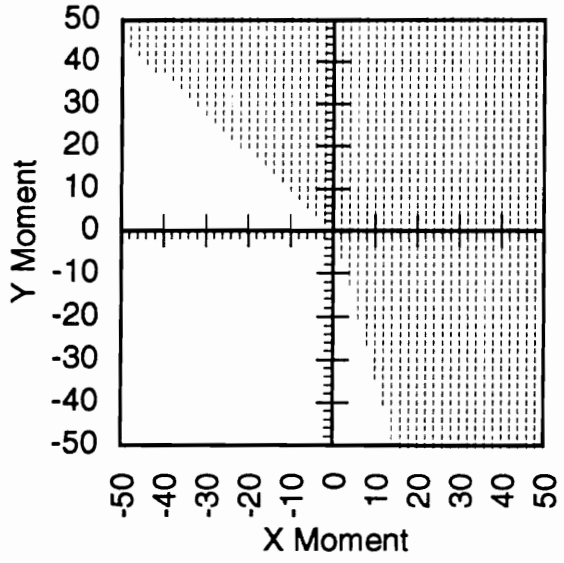

(a) MIC Model, Compilation Geometry

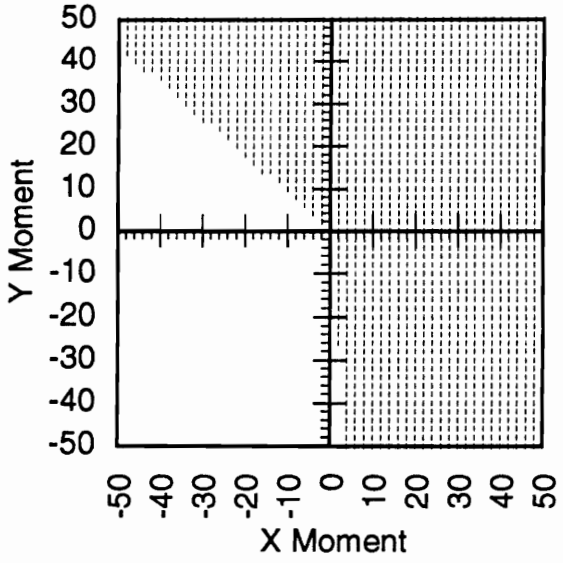

(b) MIC Model, Han et al. Geometry

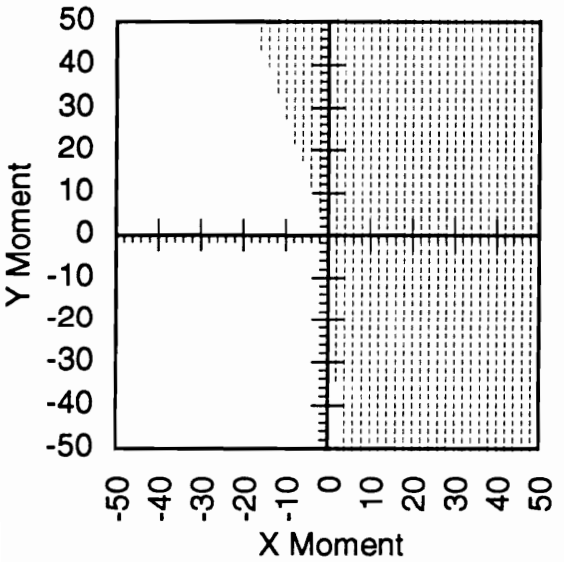

(c) SCI Model, Compilation Geometry

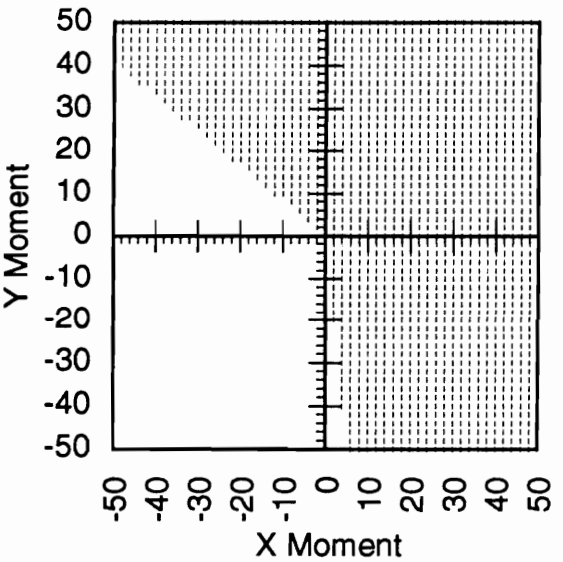

(d) SCI Model, Han et al. Geometry

Figure 4.3 Left rectus abdominus muscle for the 10-muscle geometries and 0 Z-moment. The shaded areas represent the regions where the muscle is active, while the unshaded regions represent inactivity.

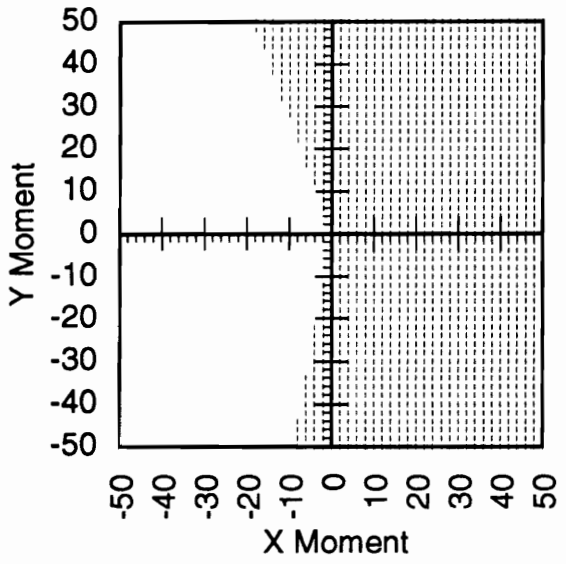

(a) MIC Model, Compilation Geometry

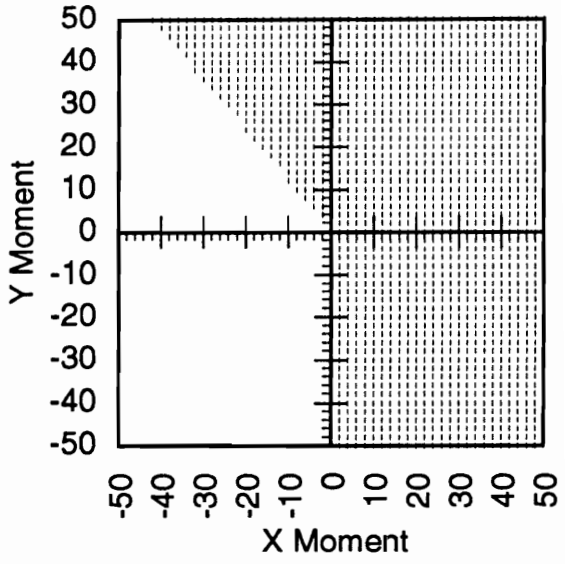

(b) MIC Model, Han et al. Geometry

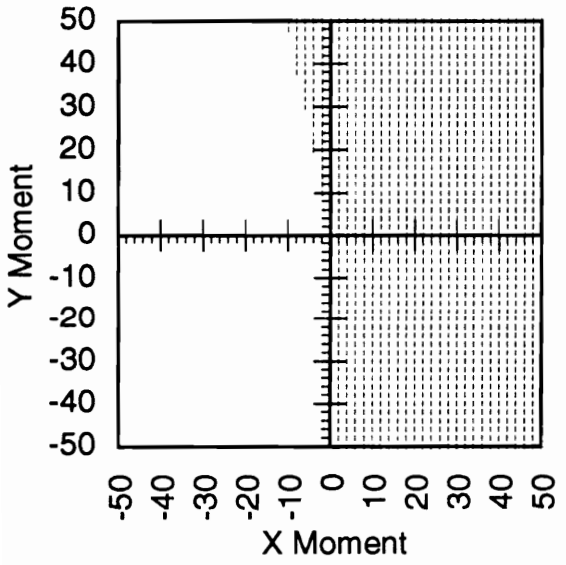

(c) SCI Model, Compilation Geometry

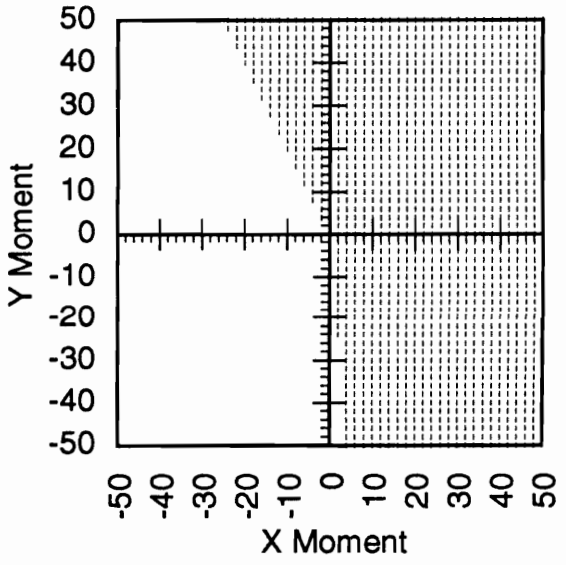

(d) SCI Model, Han et al. Geometry

Figure 4.4 Left rectus abdominus muscle for the 18-muscle geometries and 0 Z-moment. The shaded areas represent the regions where the muscle is active, while the unshaded regions represent inactivity.

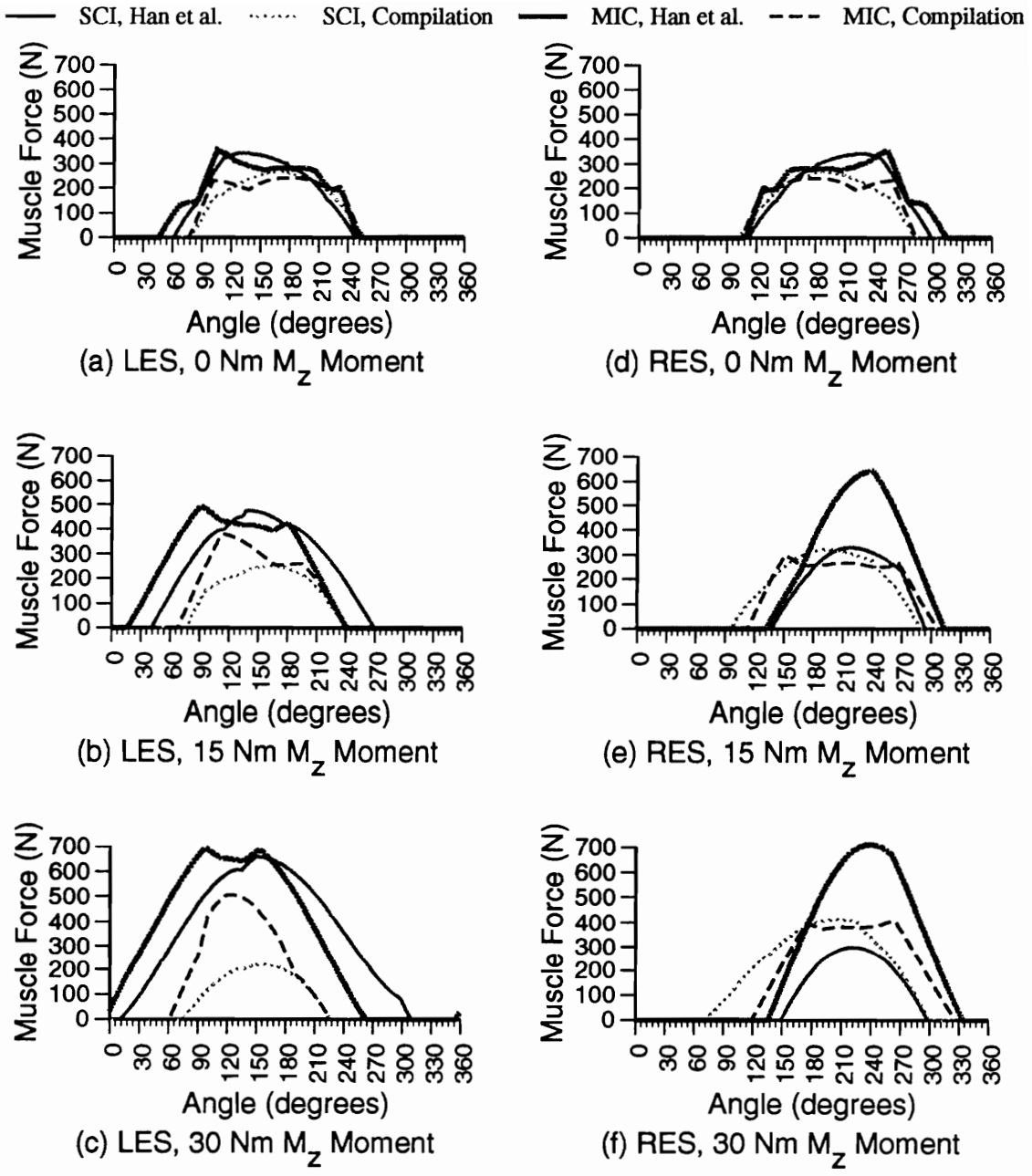

Figure 4.5 Left and right erector spinae muscle forces for 10-muscle inputs predicted by angle of rotation of a load which generates a resultant 30 Nm M_x-M_y moment. An angle of 0 degrees corresponds to 30 Nm M_x and 0 Nm M_y. The four lines on each graph represent the SCI and MIC models combined with muscle geometries reported by Han et al. (1992) and a compilation of other studies.

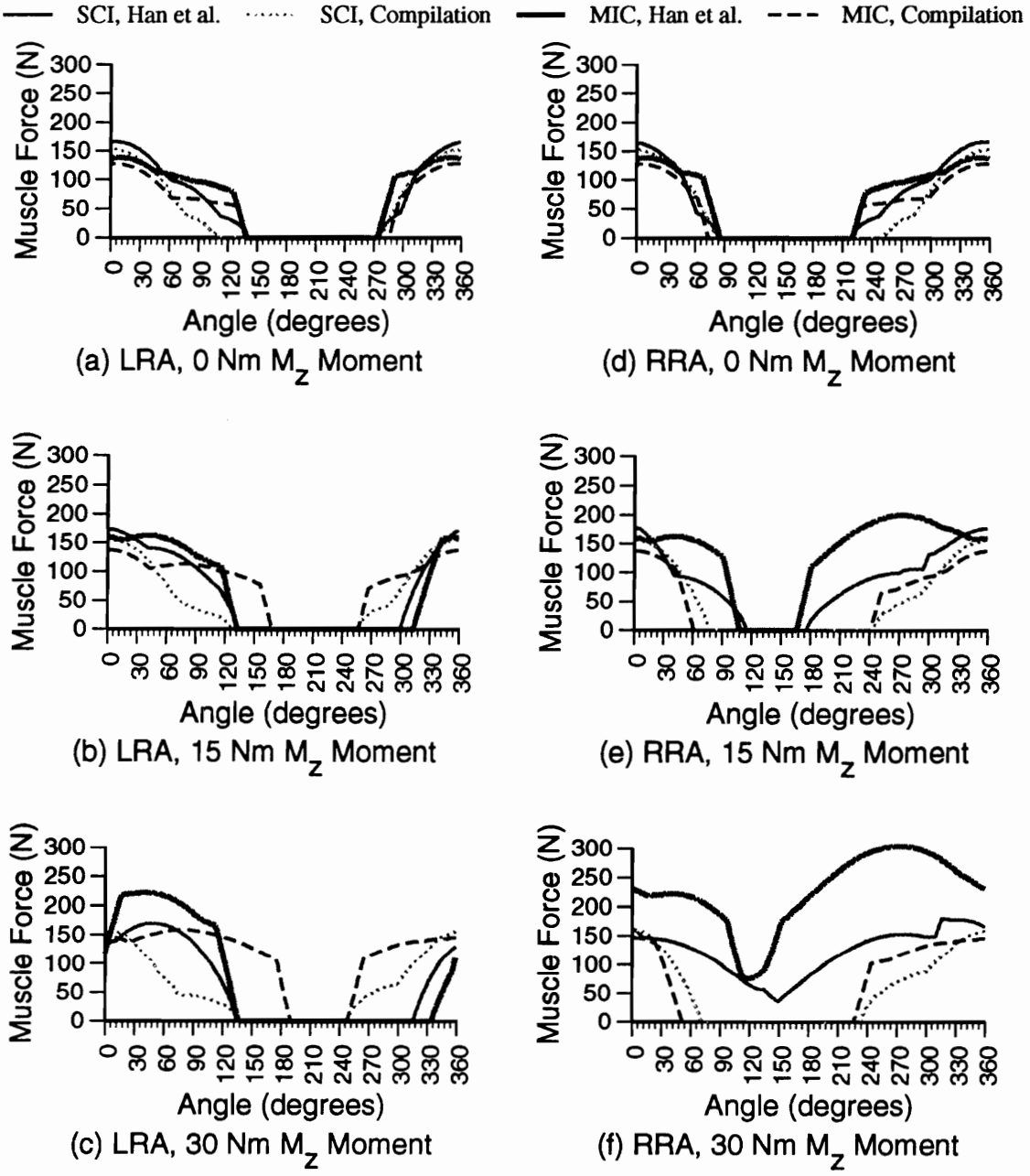

Figure 4.6 Left and right rectus abdominus muscle forces for 10-muscle inputs predicted by angle of rotation of a load which generates a resultant 30 Nm M_x-M_y moment. An angle of 0 degrees corresponds to 30 Nm M_x and 0 Nm M_y. The four lines on each graph represent the SCI and MIC models combined with muscle geometries reported by Han et al. (1992) and a compilation of other studies.

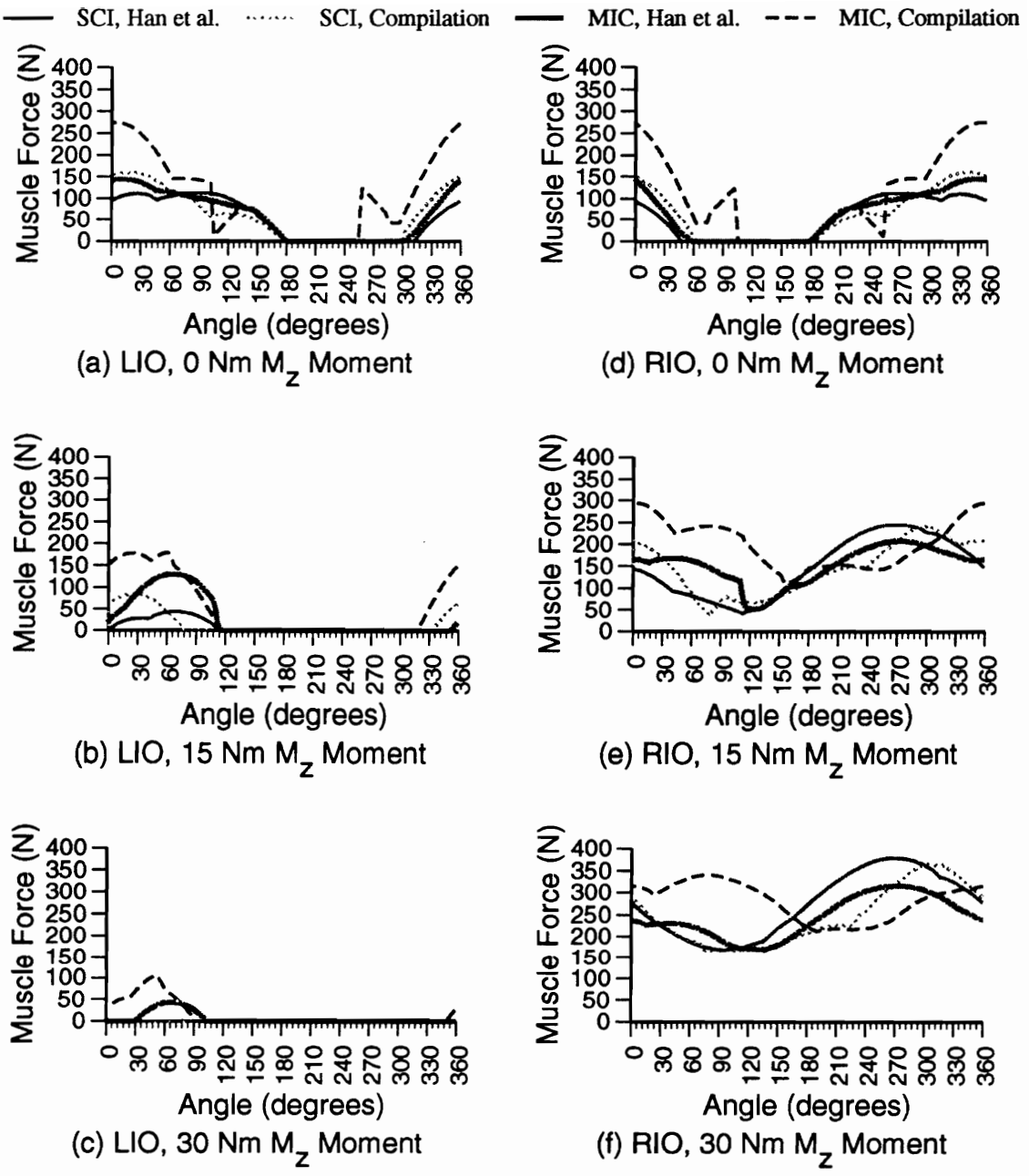

Figure 4.7 Left and right internal oblique muscle forces for 10-muscle inputs predicted by angle of rotation of a load which generates a resultant 30 Nm M_x-M_y moment. An angle of 0 degrees corresponds to 30 Nm M_x and 0 Nm M_y. The four lines on each graph represent the SCI and MIC models combined with muscle geometries reported by Han et al. (1992) and a compilation of other studies.

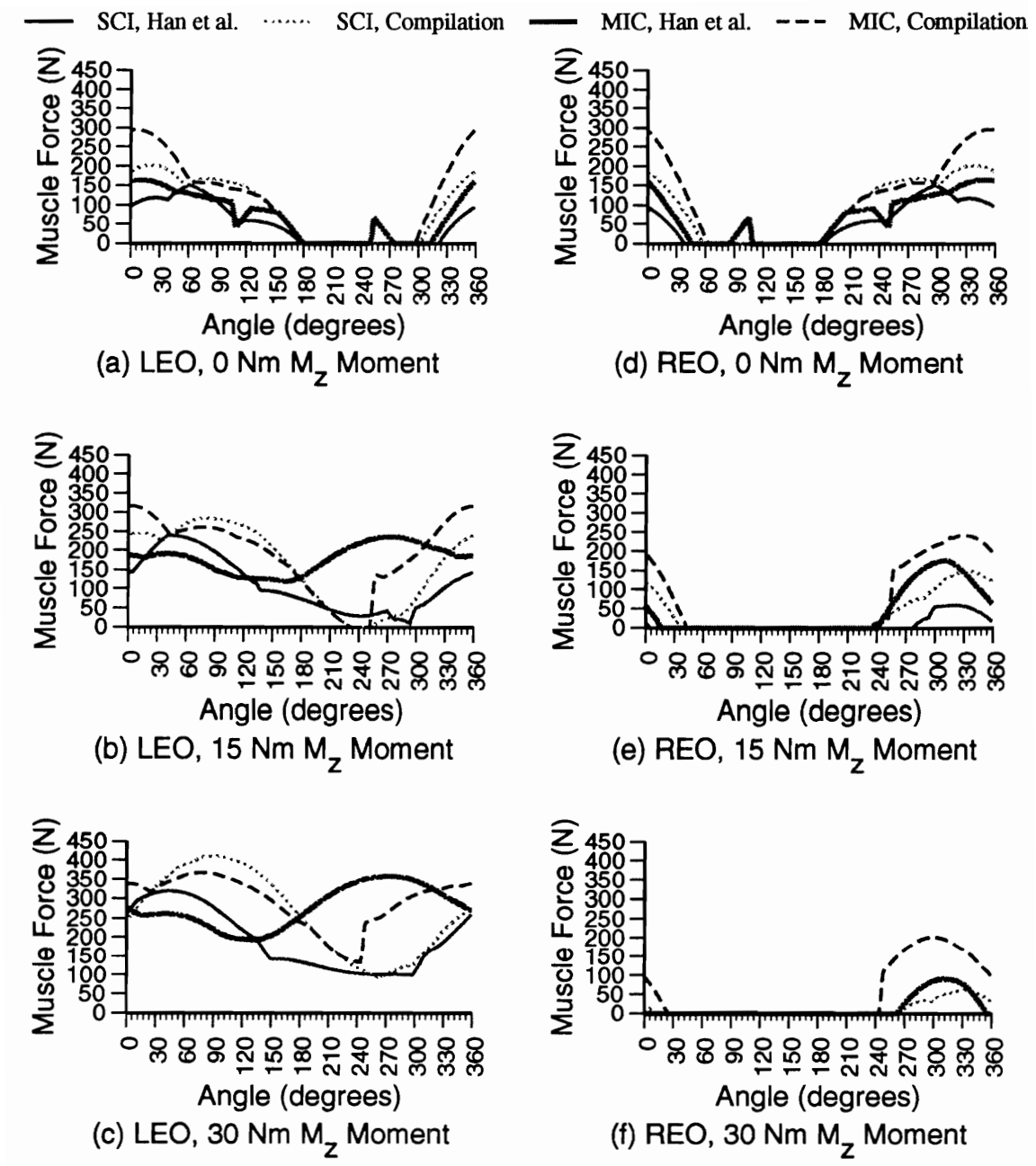

Figure 4.8 Left and right external oblique muscle forces for 10-muscle inputs predicted by angle of rotation of a load which generates a resultant 30 Nm M_x-M_y moment. An angle of 0 degrees corresponds to 30 Nm M_x and 0 Nm M_y. The four lines on each graph represent the SCI and MIC models combined with muscle geometries reported by Han et al. (1992) and a compilation of other studies.

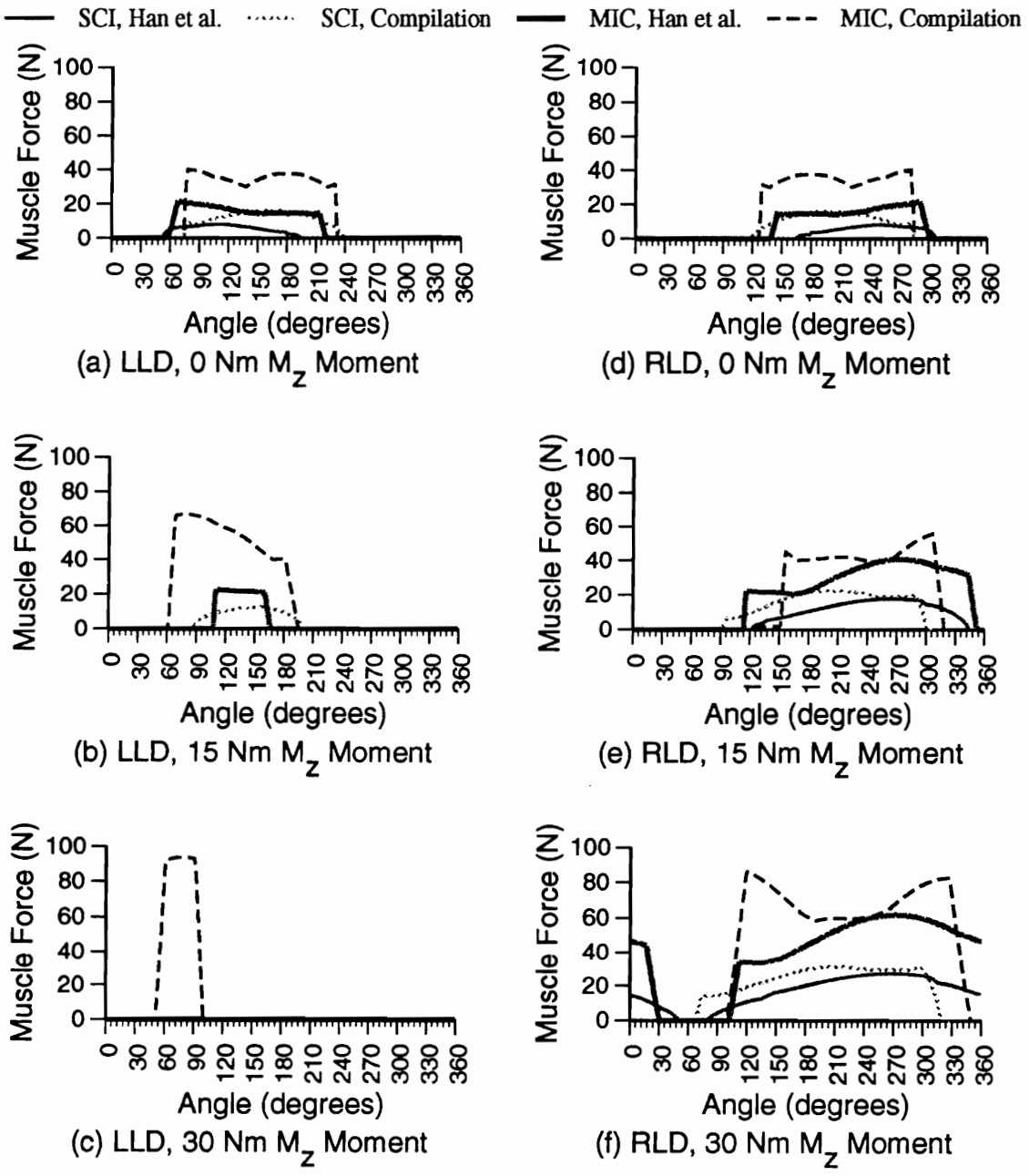

Figure 4.9 Left and right latissimus dorsi muscle forces for 10-muscle inputs predicted by angle of rotation of a load which generates a resultant 30 Nm M_x-M_y moment. An angle of 0 degrees corresponds to 30 Nm M_x and 0 Nm M_y. The four lines on each graph represent the SCI and MIC models combined with muscle geometries reported by Han et al. (1992) and a compilation of other studies.

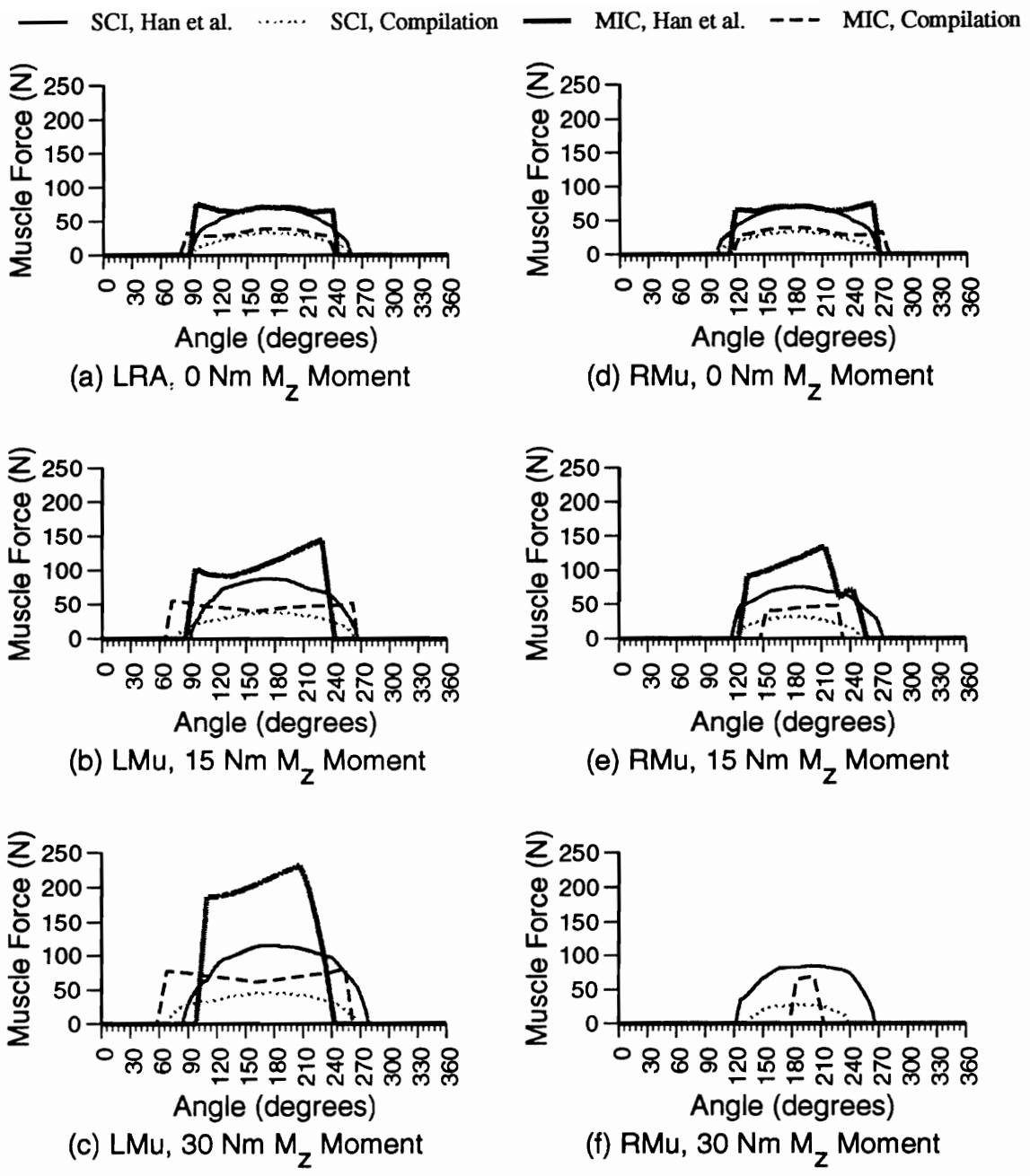

Figure 4.10 Left and right multifidus muscle forces for 18-muscle inputs predicted by angle of rotation of a load which generates a resultant 30 Nm M_x-M_y moment. An angle of 0 degrees corresponds to 30 Nm M_x and 0 Nm M_y. The four lines on each graph represent the SCI and MIC models combined with muscle geometries reported by Han et al. (1992) and a compilation of other studies.

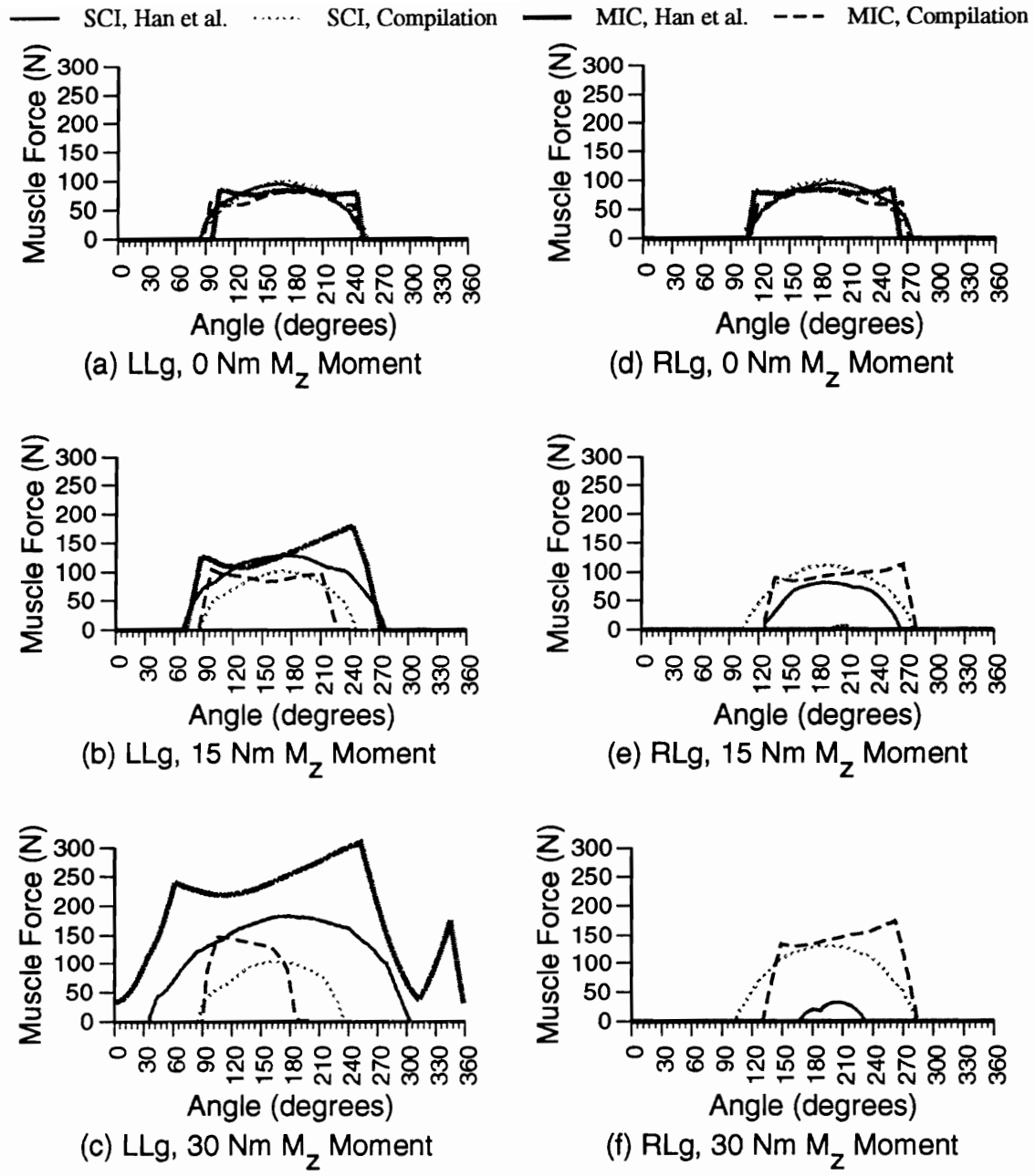

Figure 4.11 Left and right longissimus muscle forces for 18-muscle inputs predicted by angle of rotation of a load which generates a resultant 30 Nm M_x-M_y moment. An angle of 0 degrees corresponds to 30 Nm M_x and 0 Nm M_y. The four lines on each graph represent the SCI and MIC models combined with muscle geometries reported by Han et al. (1992) and a compilation of other studies.

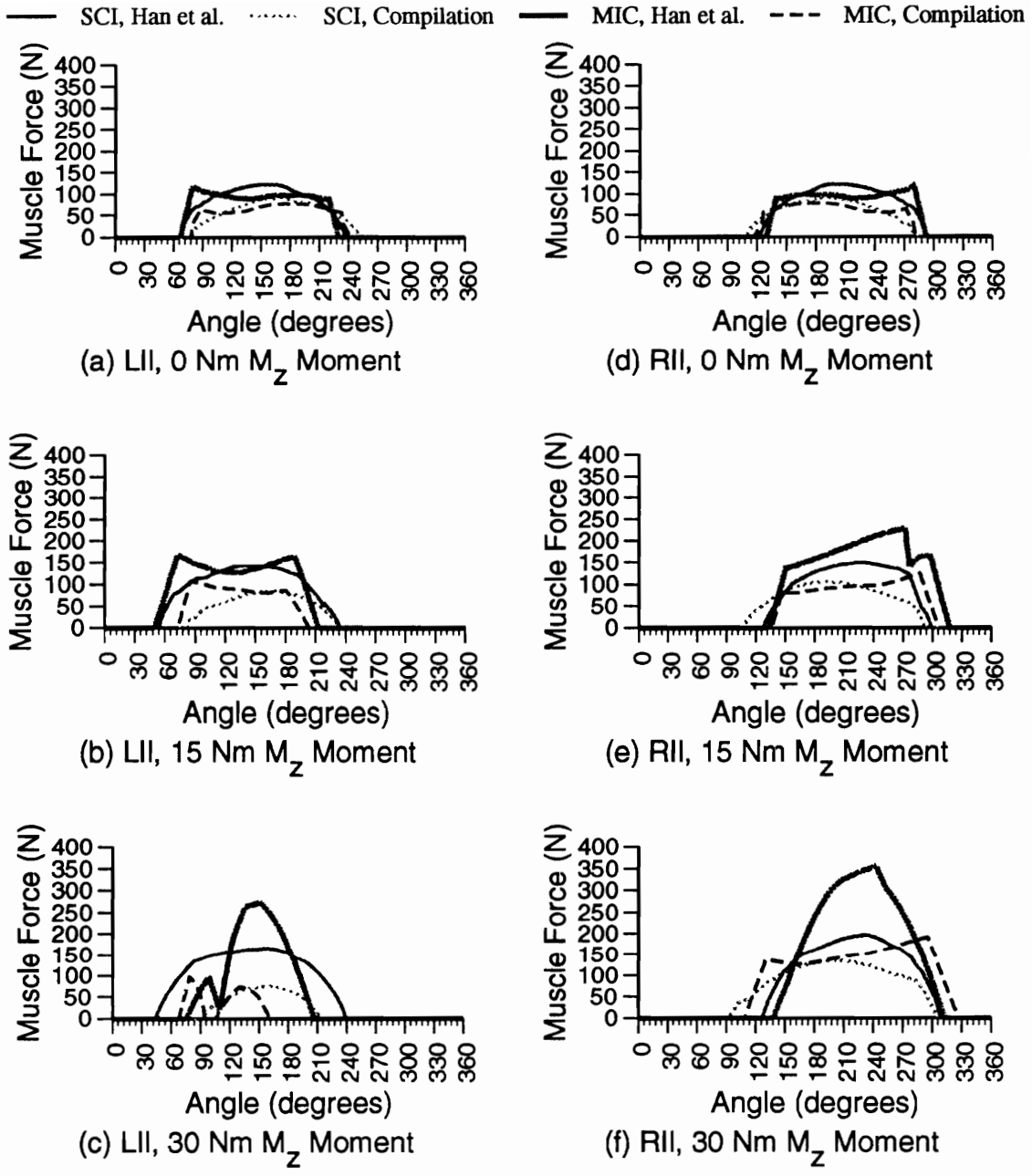

Figure 4.12 Left and right iliocostalis muscle forces for 18-muscle inputs predicted by angle of rotation of a load which generates a resultant 30 Nm M_x-M_y moment. An angle of 0 degrees corresponds to 30 Nm M_x and 0 Nm M_y. The four lines on each graph represent the SCI and MIC models combined with muscle geometries reported by Han et al. (1992) and a compilation of other studies.

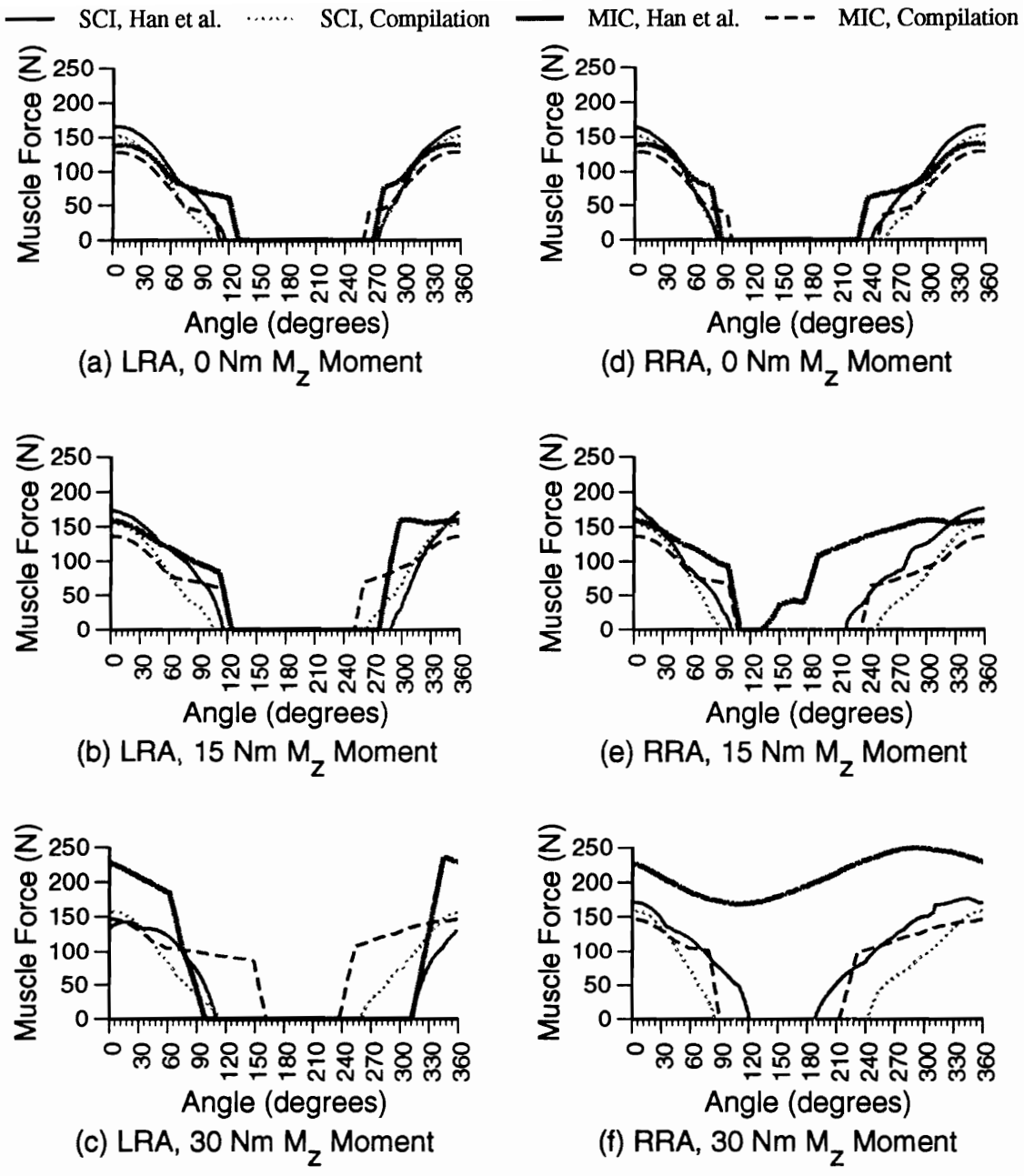

Figure 4.13 Left and right rectus abdominus muscle forces for 18-muscle inputs predicted by angle of rotation of a load which generates a resultant 30 Nm M_x-M_y moment. An angle of 0 degrees corresponds to 30 Nm M_x and 0 Nm M_y. The four lines on each graph represent the SCI and MIC models combined with muscle geometries reported by Han et al. (1992) and a compilation of other studies.

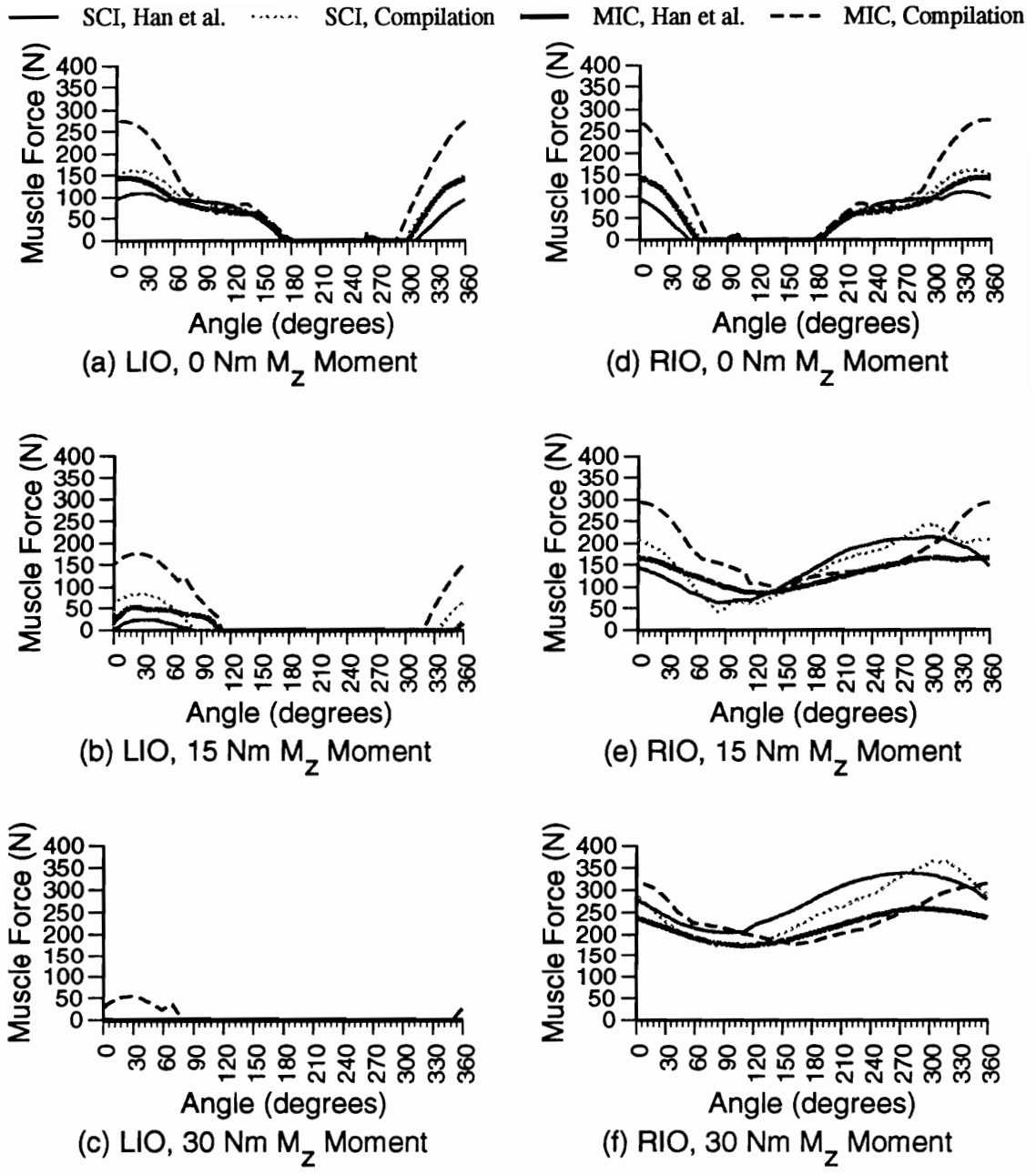

Figure 4.14 Left and right internal oblique muscle forces for 18-muscle inputs predicted by angle of rotation of a load which generates a resultant 30 Nm M_x-M_y moment. An angle of 0 degrees corresponds to 30 Nm M_x and 0 Nm M_y. The four lines on each graph represent the SCI and MIC models combined with muscle geometries reported by Han et al. (1992) and a compilation of other studies.

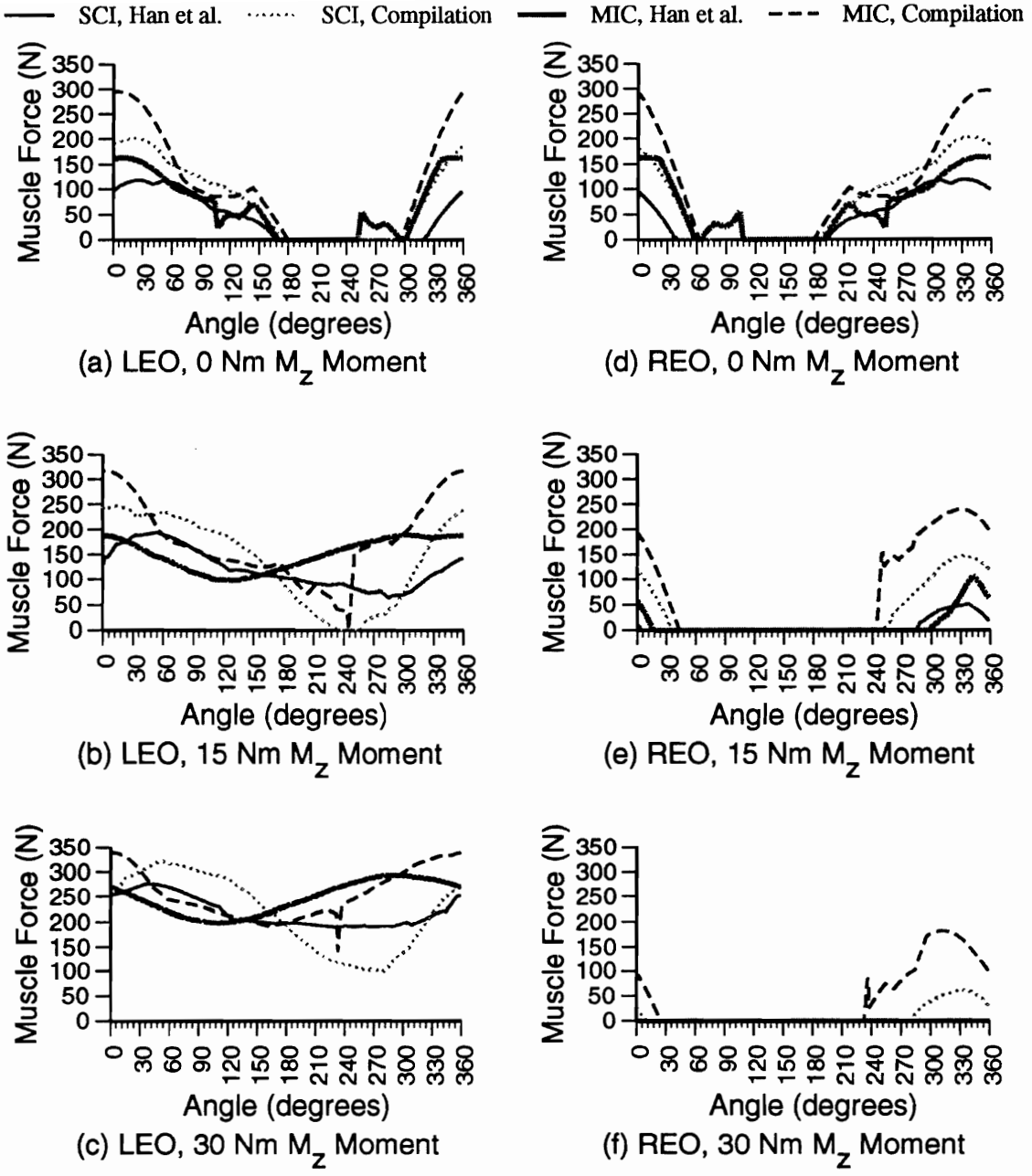

Figure 4.15 Left and right external oblique muscle forces for 18-muscle inputs predicted by angle of rotation of a load which generates a resultant 30 Nm M_x-M_y moment. An angle of 0 degrees corresponds to 30 Nm M_x and 0 Nm M_y. The four lines on each graph represent the SCI and MIC models combined with muscle geometries reported by Han et al. (1992) and a compilation of other studies.

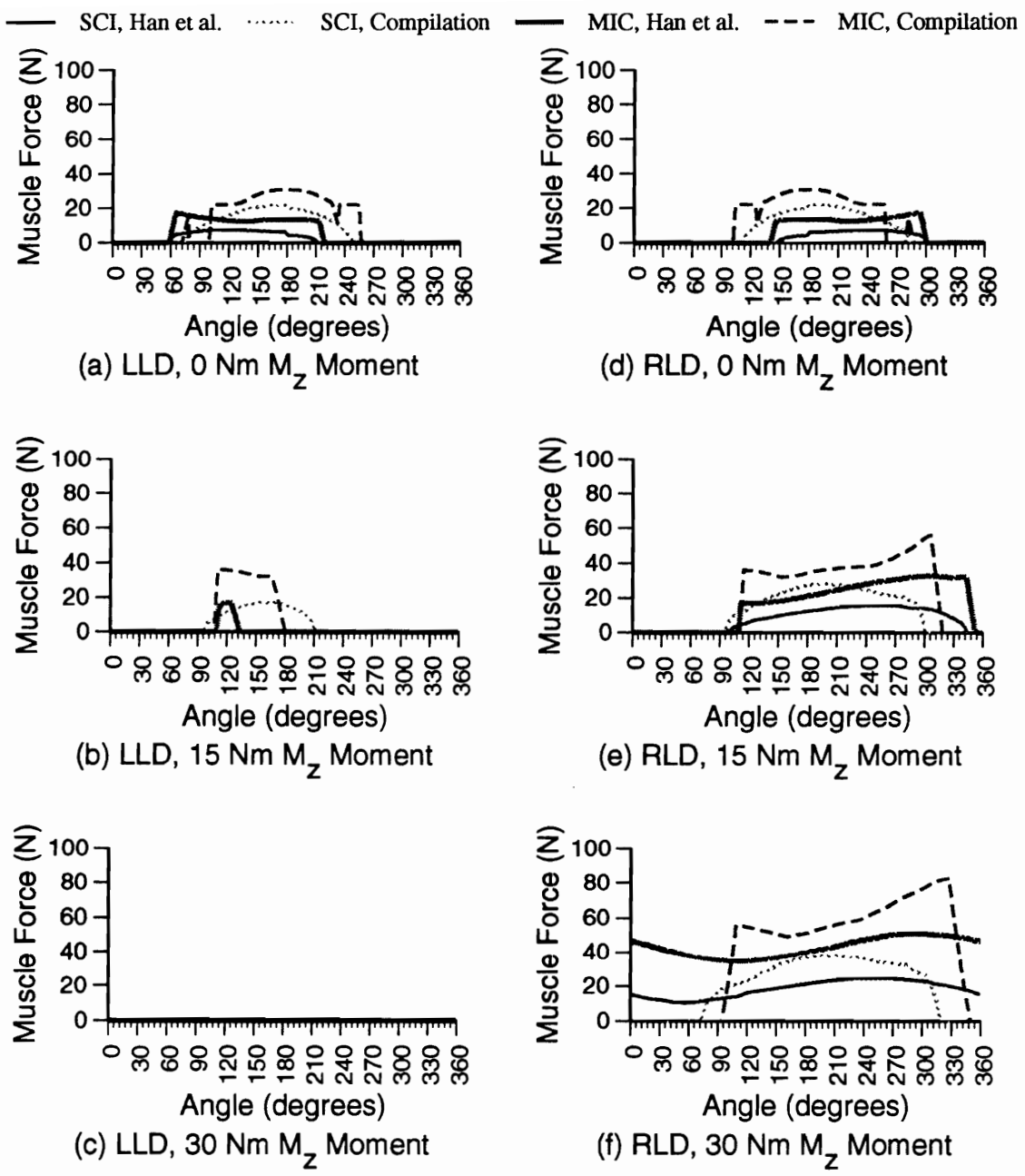

Figure 4.16 Left and right latissimus dorsi muscle forces for 18-muscle inputs predicted by angle of rotation of a load which generates a resultant 30 Nm M_x-M_y moment. An angle of 0 degrees corresponds to 30 Nm M_x and 0 Nm M_y. The four lines on each graph represent the SCI and MIC models combined with muscle geometries reported by Han et al. (1992) and a compilation of other studies.

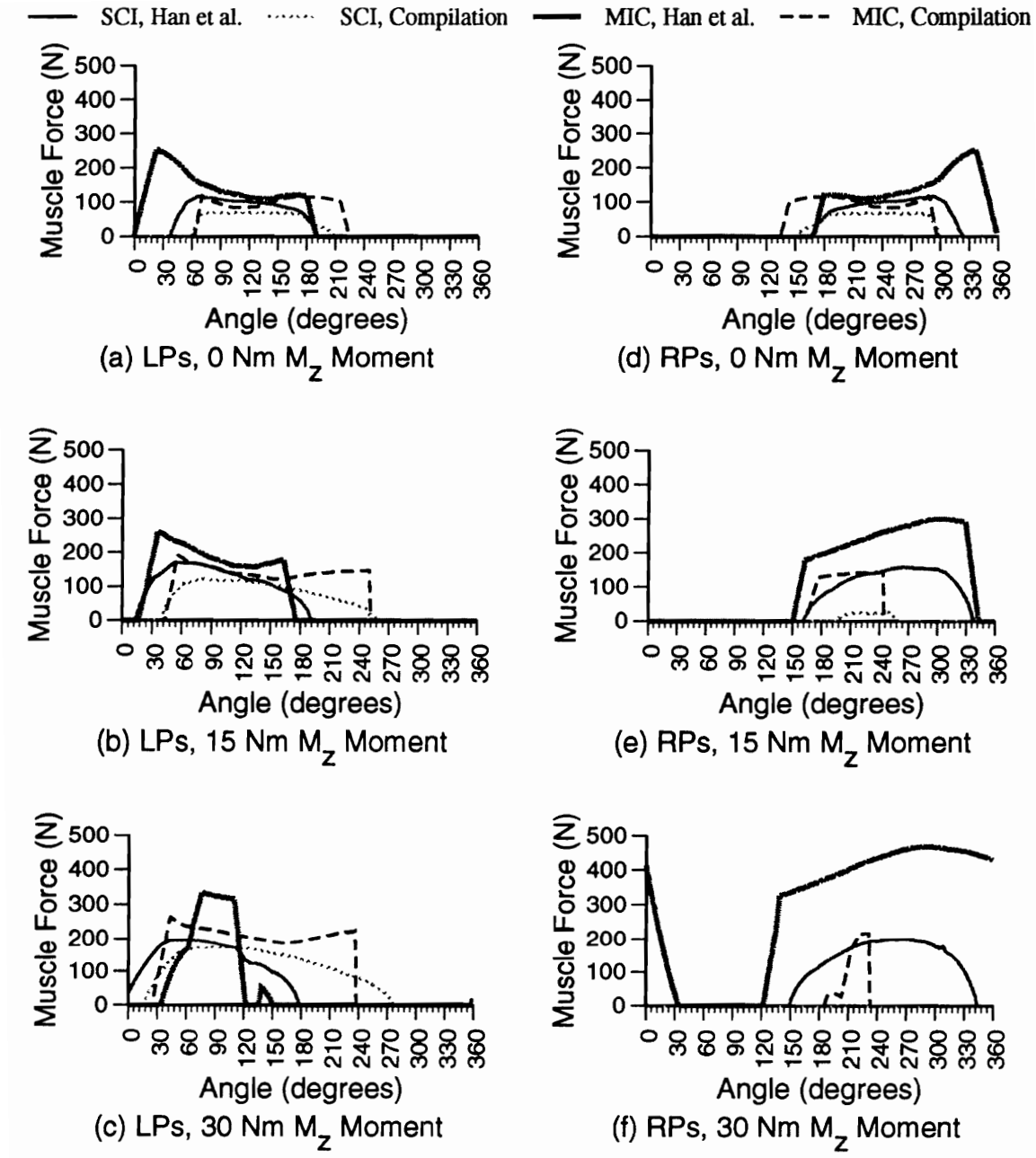

Figure 4.17 Left and right psoas muscle forces for 18-muscle inputs predicted by angle of rotation of a load which generates a resultant 30 Nm M_x-M_y moment. An angle of 0 degrees corresponds to 30 Nm M_x and 0 Nm M_y. The four lines on each graph represent the SCI and MIC models combined with muscle geometries reported by Han et al. (1992) and a compilation of other studies.

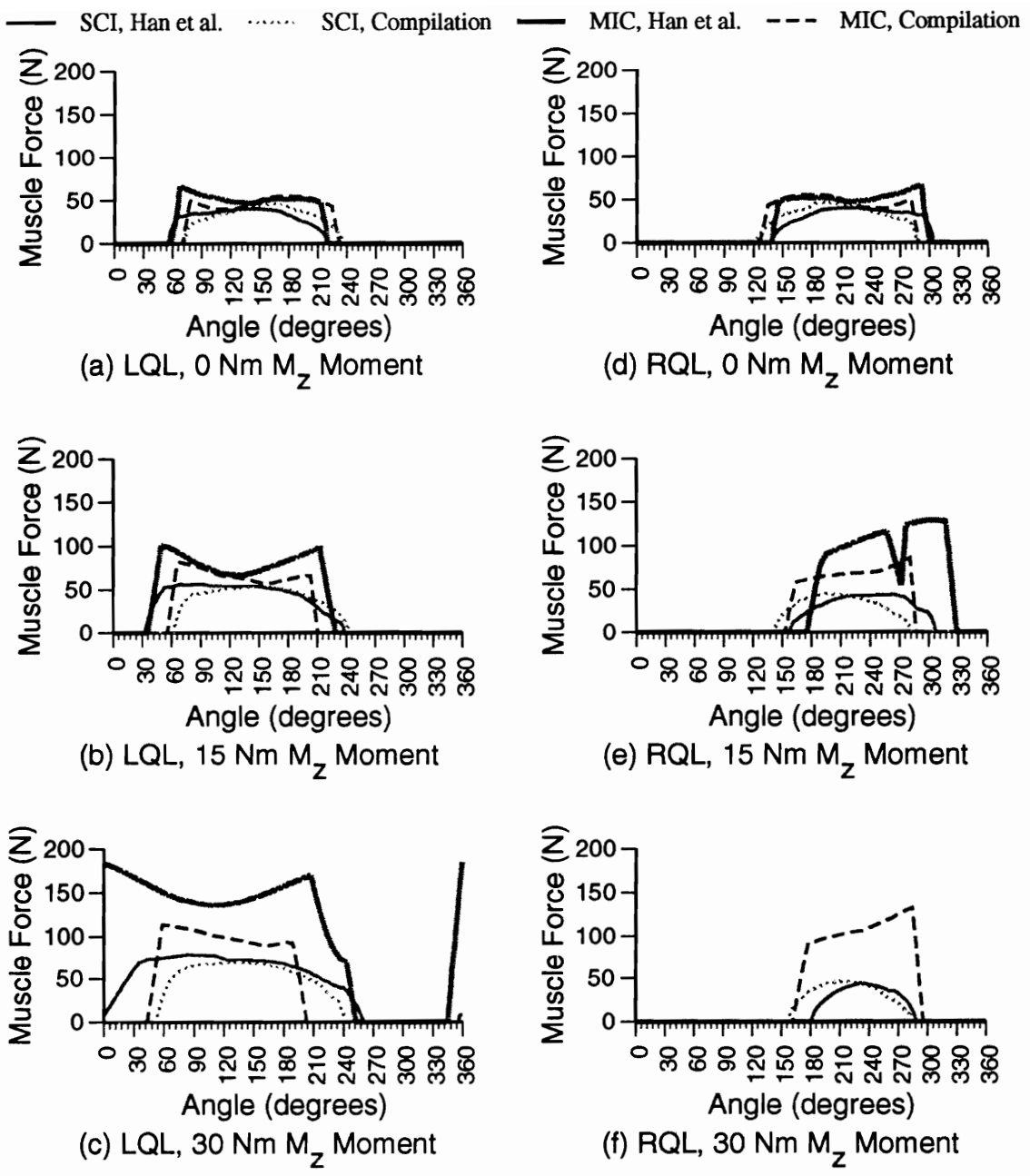

Figure 4.18 Left and right quadratus lumborum muscle forces for 18-muscle inputs predicted by angle of rotation of a load which generates a resultant 30 Nm M_x-M_y moment. An angle of 0 degrees corresponds to 30 Nm M_x and 0 Nm M_y. The four lines on each graph represent the SCI and MIC models combined with muscle geometries reported by Han et al. (1992) and a compilation of other studies.

4.3.2 Compression Predictions

To calculate compression force on the L3/L4 disc, the muscle forces were multiplied my the unit force vector in the z-direction. Total compression force on the spine needs to have body weight and forces creating the external moments added. However, for a given subject the body weight and external forces will be constant so adding them to compression will add a constant. The compression forces due only to muscle forces for the 10 muscle models are shown in Figure 4.19. The compression force predicted by the MIC model was always greater than the SCI model when the same geometry was used. In general, the Han et al. geometry led to higher compression force prediction than the compilation geometry, but not at every angle.

To investigate differences in compression due to muscle forces, the mean compression forces predicted every 20 degrees (18 observations) were determined. Loading conditions every 20 degrees were used to test actual muscle activity which will be reported in Chapters 5 and 6.

For compression forces averaged by model, the MIC model resulted in higher compression that the SCI model, 898 and 678 N respectively. For compression forces averaged by geometry, the Han et al. geometry led to higher compression than the compilation geometry, 835 and 740 N respectively. For compression forces averaged by torsion level, higher torsion led to higher compression. Torsion of 30 Nm resulted in a mean compression of 1029 N which was higher than the mean compression of 750 N with 15 Nm torsion which was higher than the mean compression of 583 N with 0 Nm torsion.

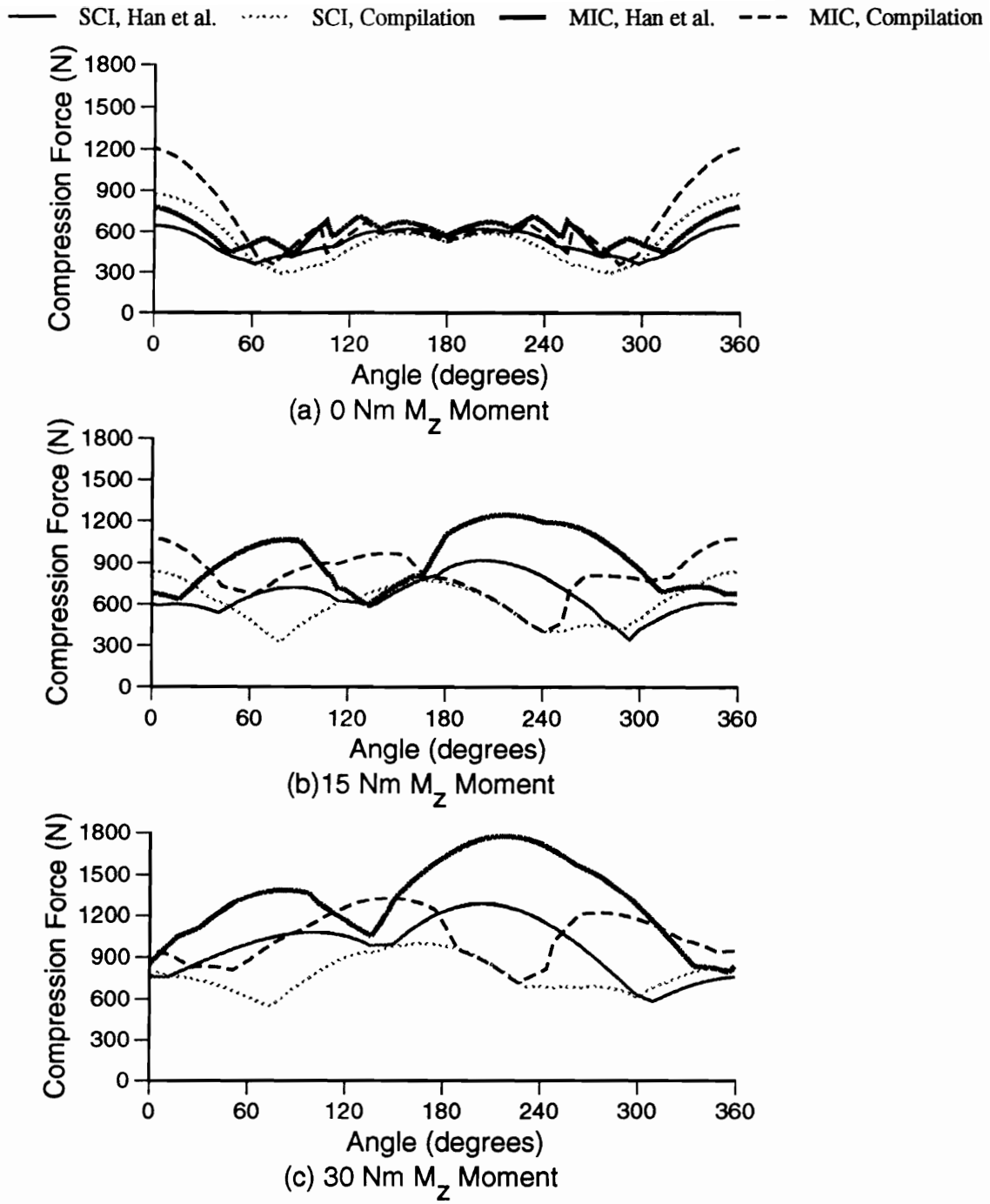

Figure 4.19 Compression force due only to muscle forces for 10-muscle inputs predicted by angle of rotation. The four lines on each graph represent the SCI and MIC models combined with muscle geometries reported by Han et al. (1992) and a compilation of other studies.

The mean compression forces by model and torsion are shown in Figure 4.20. The MIC model at each torsion predicted higher compression than the SCI model. The difference in compression between the models increased as torsion increased. At 0 Nm torsion, the difference in compression predictions was a mean of 113 N then increased to 233 N with 15 Nm torsion and increased further to 314 N with 30 Nm torsion.

The mean compression forces by geometry and torsion are shown in Figure 4.21. Little difference in compression predictions were found between the two geometries with 0 Nm torsion. At 15 and 30 Nm torsion, the Han et al. geometry led to higher compression predictions than the compilation geometry. The difference in compression predictions between the two geometries was a mean of 87 N with 15 Nm torsion and increased to 243 N with 30 Nm torsion.

4.4 Discussion

The combination of model and muscle geometry had a dramatic effect on whether the muscle was predicted to be active at varying external loads. Figures 4.1 through 4.4 show that the inputs affected whether a muscle was predicted active. Although the total number of active/inactive graphs are too numerous to discuss individually, several examples will be considered here. For example, Figure 4.2 shows the active regions for the Left Internal Oblique (LIO) muscle when 10 muscles were input to the models with 0 twisting moment. Shown on Figures 4.2(a) and 4.2(b), the MIC model was used with 10 muscles, but the muscle geometries were changed. The MIC model with the compilation geometry predicted the LIO to be active during left bending external moments

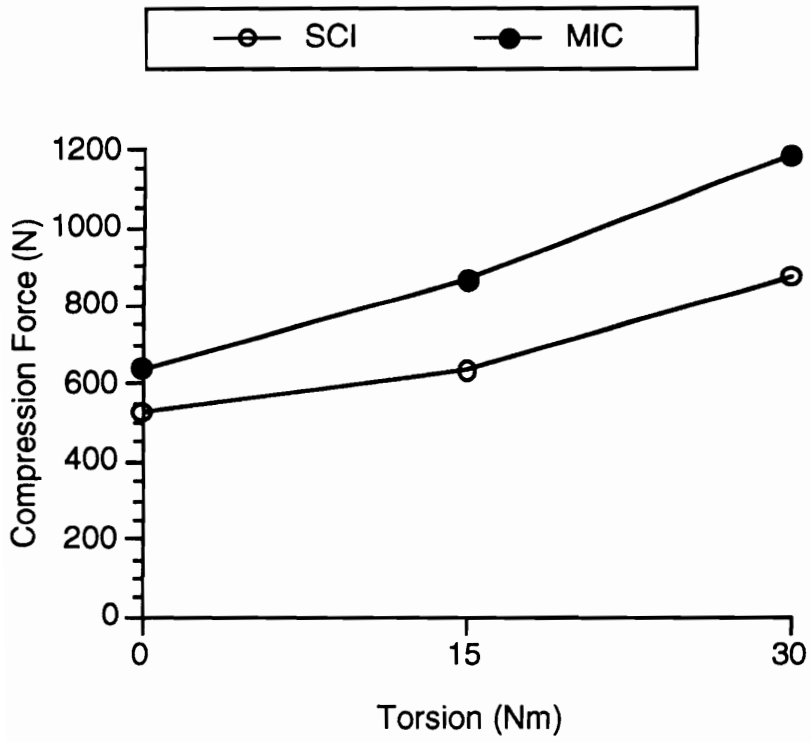

Figure 4.20 Mean compression force by model and torsion for muscle forces predicted every 20 degrees.

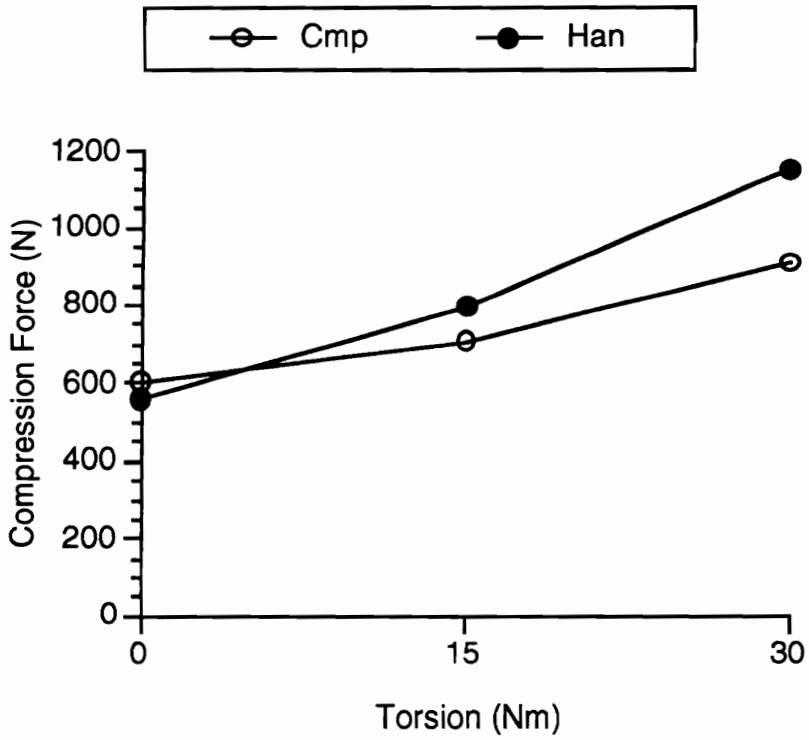

Figure 4.21 Mean compression force by geometry and torsion for muscle forces predicted every 20 degrees.

(M_y negative) and 0 flexion/extension moment and 0 twisting moment. However, when the same model was used, but the muscle geometry was changed to the Han et al. data set, under the same loading conditions, the muscle was predicted inactive. A similar result occurred if the geometric data set was held constant with the compilation geometry, but the model was changed from the MIC to SCI model. The MIC model with the compilation geometry predicted the LIO to be active during left bending external moments (M_y negative) and 0 M_x and M_z, but the SCI model with the same geometry predicted it inactive.

Figures 4.3 and 4.4 show the Left Rectus Abdominus (LRA) muscle for the 10- and 18-muscle models with 0 twisting moment, respectively. Figures 4.3(a) and 4.4(a) show the active regions for the MIC model using the compilation geometry and only the input of number of muscles was varied. Several combinations of external extension moments (positive M_x) and right bending moments were predicted active by the 10-muscle model. However, the 18-muscle model predicted the LRA to be active for a much smaller number of the same external moments.

Figure 4.5 provides a different representation of the erector spinae muscle activity range with 10 muscles. As the load was rotated about the body, the varying models predicted activity of the muscle to start at different angles. For example, with 0 Nm M_z the MIC model with Han et al. (1992) muscle geometry predicted activity of the left erector spinae to start at about 45 degrees. However, the other models and geometries did not predict activity until after 60 to 75 degrees of load rotation. The magnitudes of the predicted muscle forces

also varied between formulations. For example, the SCI model using the compilation geometry predicted the muscle force of the LES to be about 200 N for a load angle of 150 degrees and 30 Nm M_z. However, the SCI model using the Han et al. (1992) geometry predicted LES force of about 600 N for the same loading conditions.

Although only a few examples of the active/inactive graphs were discussed, observation of the other figures indicated that the inputs used to predict muscle activity affected whether the muscle was predicted to be active. Figures 4.5 to 4.18 show how the activity regions and magnitudes of the predicted muscle vary for M_x-M_y resultant moments of 30 Nm. The results of this investigation indicated that an experiment using human subjects should be undertaken. Actual human performance should be measured under loading conditions which differentiate the activity predicted by the model, number of muscles, and muscle geometries. The method in the current study to experimentally test the actual muscle activity will be discussed in the following chapter.

5. EXPERIMENT TO TEST OPTIMIZATION MODELS

5.1 Introduction

Optimization-based biomechanical models have been developed for the trunk region to estimate the internal forces in response to an external load. For a given task, the tension of the trunk muscles can be estimated and used to calculate the resultant forces on the spinal column. The compression and shear forces on the spinal discs can be estimated by summing the external and internal (muscular) forces.

Biomechanical optimization models of the trunk must be tested and validated for their accuracy in predicting muscle activity. Two models which have been proposed to predict the trunk muscle tensions are the Minimum-Intensity-Compression (MIC) model (Bean, Chaffin, and Schultz, 1988) and the Sum of the Cubed Intensities (SCI) model (Crowninshield and Brand, 1981). The formulations of these two models, the assumptions used to solve them, and examples of their implementation were discussed in Chapter 3.

Anatomical inputs are required by the MIC and SCI models to predict the muscle forces. If the joint contact and ligament forces are assumed negligible, as reviewed in section 2.7, the required inputs are the number of muscles, the moment arms to the vertebrae, the lines of action, and the cross-sectional areas. Chapter 2 reviewed the studies conducted to determine geometric parameters of the trunk muscles. From this review, sets of geometric inputs were determined, shown previously in Tables 2.16 - 2.19.

Chapter 4 reported on a computer simulation conducted to determine the effects of differing inputs into optimization-based trunk biomechanical models. The MIC and SCI models were included in the investigation. The number of muscles included in the development of the models was varied as well as the geometric parameters of the muscles included. These variables and their levels were discussed previously in Section 4.2.1. The inputs to trunk optimization models had a large effect on the prediction of muscle activity/inactivity for equal external loads.

One goal of this study was to add to the scientific data concerning the accuracy of competing optimization models and inputs used to predict trunk muscle activity. The actual physical exertions the subjects completed varied only in the external loads they were asked to resist. The varying external loads that the subjects resisted differentiated the predictions given by model combinations. This chapter reports on the methods used to empirically measure human trunk muscle performance during static exertions to resist external loads.

5.2 Loading Conditions to be Tested

In Chapter 4, graphs were generated showing the loading conditions for each muscle in which the muscle was predicted active (positive force). The regions of external loading which were predicted active changed dramatically with the change in model, muscle geometry inputs, and number of muscles in the model. To test the accuracy of the models and their associated inputs,

loading conditions were selected which differentiated the predictions of the manipulated variables.

Several loading conditions were selected which elicited differences in the predictions of the model. The set of loading conditions included both external flexion and extension moments. External flexion moments (negative M_x, see Figure 2.1) caused back muscles such as the erector spinae muscle, its constituents, or the latissimus dorsi to be more active. External extension moments caused more activity in the abdominal muscles.

To measure the muscle activity at several load conditions, weights were held about the body to generate a circle on the M_x-M_y loading plane. The moment arm was held constant, so several loading conditions were achieved as weights were moved around the body. For example, if a 75 N weight was held 40 cm in front of the L3/L4 disc, a 30 Nm flexion moment was imposed at the L3/L4 disc (not accounting for arm moments). If the load was rotated to the right maintaining the 40 cm distance, the flexion moment decreased and the right lateral bending moment increased. Instead of using a continuously rotating load which might induce dynamic loads and cause posture shifting of the subjects, discrete loading conditions were used for this study. For example, a weight was moved at 20 degree increments around the body over a series of trials. Figure 5.1 shows an example of the resulting moments for a 75 N load rotated every 20 degrees, 40 cm away from the body. These same loading conditions could be generated by using a larger load located closer to the body or a smaller load located further from the body. This study used discrete

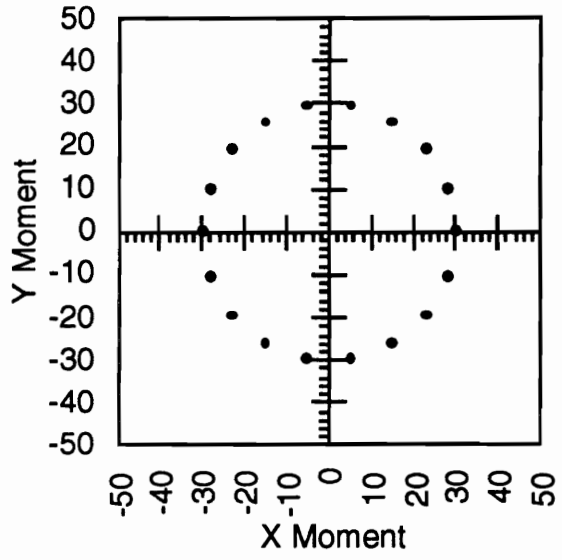

Figure 5.1 Example of resultant loading conditions from rotating a fixed weight a fixed distance around the body every 20 degrees. This method of generating loading conditions was used to test the predictions of varying models and inputs.

loading conditions around the body that differentiated the predictions of the modeling conditions.

5.3 Subjects

Twelve subjects participated in this study, six male and six female. The attributes of subjects which participated in the study are shown in Table 5.1. The subjects were compensated at a rate of $5.00 per hour for their participation in this experiment and were given a bonus of $5.00 for completing the entire experiment. Prospective subjects were screened for prior back disorders. The questionnaire used to screen subjects is shown in Appendix B. Subjects were allowed to participate only if they did not have a previous history

TABLE 5.1 Subject Characteristics

Attribute	Statistic	Males	Females	Combined
	Mean	21.33	21.00	21.17
Age (yrs)	Std Dev	3.56	2.28	2.86
	Range	18 - 28	19 - 24	18 - 28
	Mean	66.08	61.83	63.96
Mass (kg)	Std Dev	6.20	6.78	6.58
	Range	60 - 76.5	54 - 69.5	54 - 76.5
	Mean	174.33	168.5	171.42
Height (cm)	Std Dev	4.41	6.28	6.00
	Range	167 - 178.5	159 - 174	159 - 178.5

of back pain, back injury, or other disorders which would have prevented them from resisting torques applied to the torso.

5.4 Materials and Apparatus

5.4.1 External Loads Held by Hands

The subjects held weights in their hands while standing a in frame to create an equal resultant moment consisting of flexion/extension and lateral bending components. A drawing of the external loading frame system is shown in Figure 5.2. Extension moments were created by subjects holding a weight suspended over a pulley in front of the body which is the condition shown in

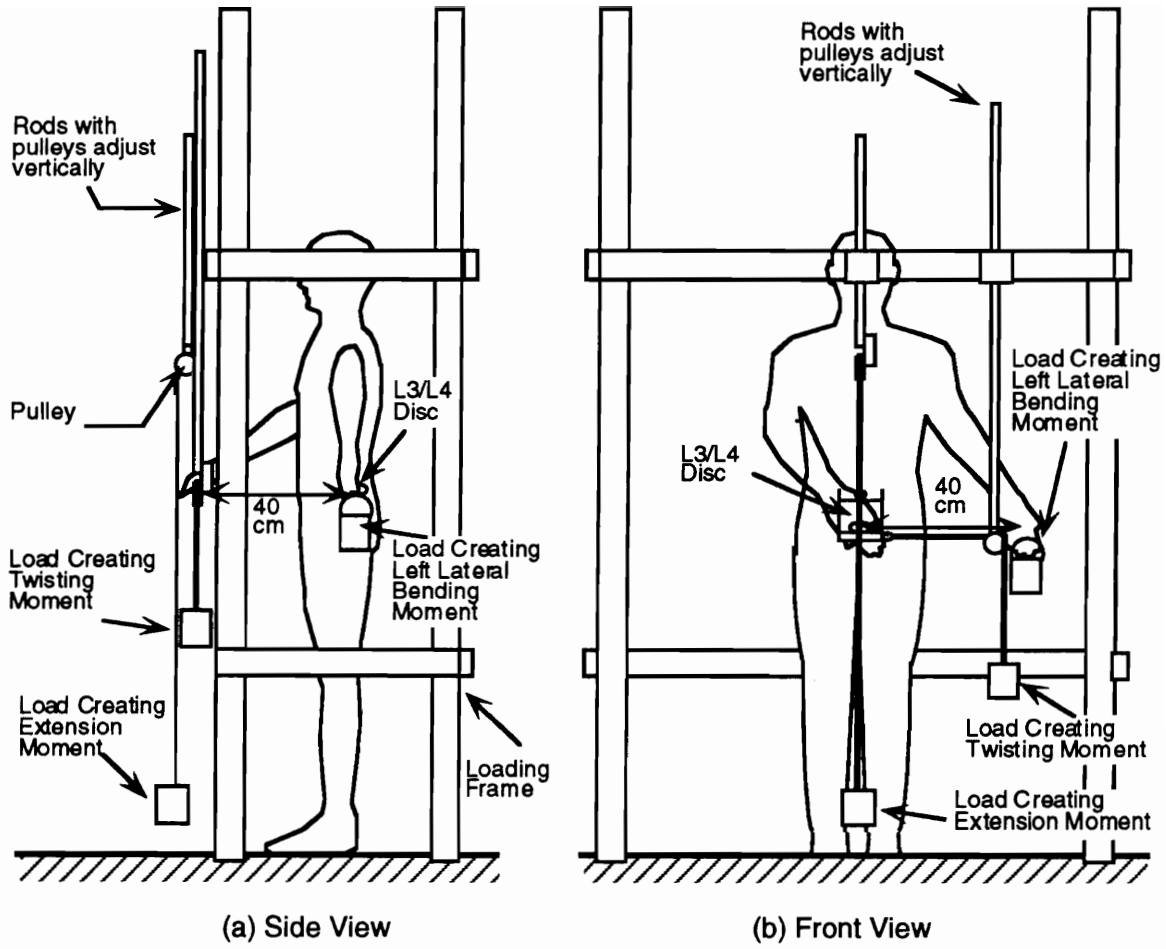

Figure 5.2 Load Application Mechanism indicates how an external extension moment, left bending moment, and torsion moment was applied. Flexion moments were generated by subjects lifting loads off the ground; (a) shows the side view of a subject standing in the frame, (b) shows the front view of a subject standing in the frame.

Figure 5.2. Flexion moments were created by subjects lifting a weight off the ground in front of the body. Lateral bending moments were created by lifting a weight with either the right or left hands. Twisting moments were generated by holding a weight suspending over a pulley laterally to the left of the mid-sagittal plane.

While in the loading frame, subjects had their hips restrained. A hip belt was worn by the subject which was tethered by straps to the four posts of the loading frame. The straps slid up and down on the loading frame to account for variable anthropometry of the subjects.

The lateral bending load was held 40 cm from the mid-sagittal plane for all subjects in the transverse plane of the L3/L4 disc. A plum bob was hung from the frame to indicate to the subject the position to hold the weight. To create a twisting moment, the height of the lateral pulley was adjusted to the height of the L3/L4 disc. The load to create the twisting moment was positioned at the L3/L4 height so no lateral bending moment was created from the load. The load to create a flexion/extension moment was held by the subjects with a handle. If the load was suspended over the pulley (external extension moment) the load was attached by a cable to the top of the handle. If the load was lifted off the ground (external flexion moment) the load was attached by a cable to the bottom of the handle. The handle was held 40 cm anterior to the frontal plane of the L3/L4 disc. The load creating the twisting moment was attached to the handle by a hook mounted in line with the handle grip. Since the torsion moment was held constant at 7.5 or 15 Nm, the weight suspended over the pulley was either 18.75 or 37.5 N due to the constant 40 cm moment arm.

A load located around the body every 20 degrees was generated by varying the weights lifted in the mid-sagittal and frontal plane. Suppose the load started in front of the subject in the mid-sagittal plane. Weight was lifted off the ground anterior to the frontal plane to create a 30 Nm flexion moment. To simulate a weight moving clockwise, the flexion moment was decreased by

lifting less weight in front (using the left hand), and the right lateral bending moment was created by lifting weight to the side with the right hand. The resultant flexion and right lateral bending moment was 30 Nm. The weights lifted in front (off the ground and over the pulley) and on both sides transmitted the M_x and M_y moments to the subject.

The free body diagram for the forces applied to the torso using the L3/L4 cutting plane is shown in Figure 5.3 for three different views. Figure 5.3 (a) shows that the horizontal distance of 40 cm from the L3/L4 disc to the flexion/extension force multiplied by the force generated the flexion/extension moment. The 40 cm moment arm was kept constant across subjects. The weight of the left and right arms created flexion/extension and lateral bending moments. Because of varying anthropometry and posture between subjects, the moments due to arms varied. To account for differences in arm anthropometry and posture, the forces applied over the pulley or lifted were varied to maintain constant flexion/extension and lateral bending moments across subjects. The procedure to account for arm weight will be discussed in Section 5.4.1.2.

Figure 5.3 (b) shows that the horizontal distance of 40 cm from the L3/L4 disc to the hand multiplied by the force generated the lateral bending moment. A moment arm of 40 cm was kept constant across subjects. The weight of the left and right arms created lateral bending moments. The procedure to account for arm weight will be discussed in Section 5.4.1.2.

Figure 5.3 (c) shows that the 40 cm distance from the L3/L4 disc to the hand multiplied by the force generated the torsional moment. The weight of the

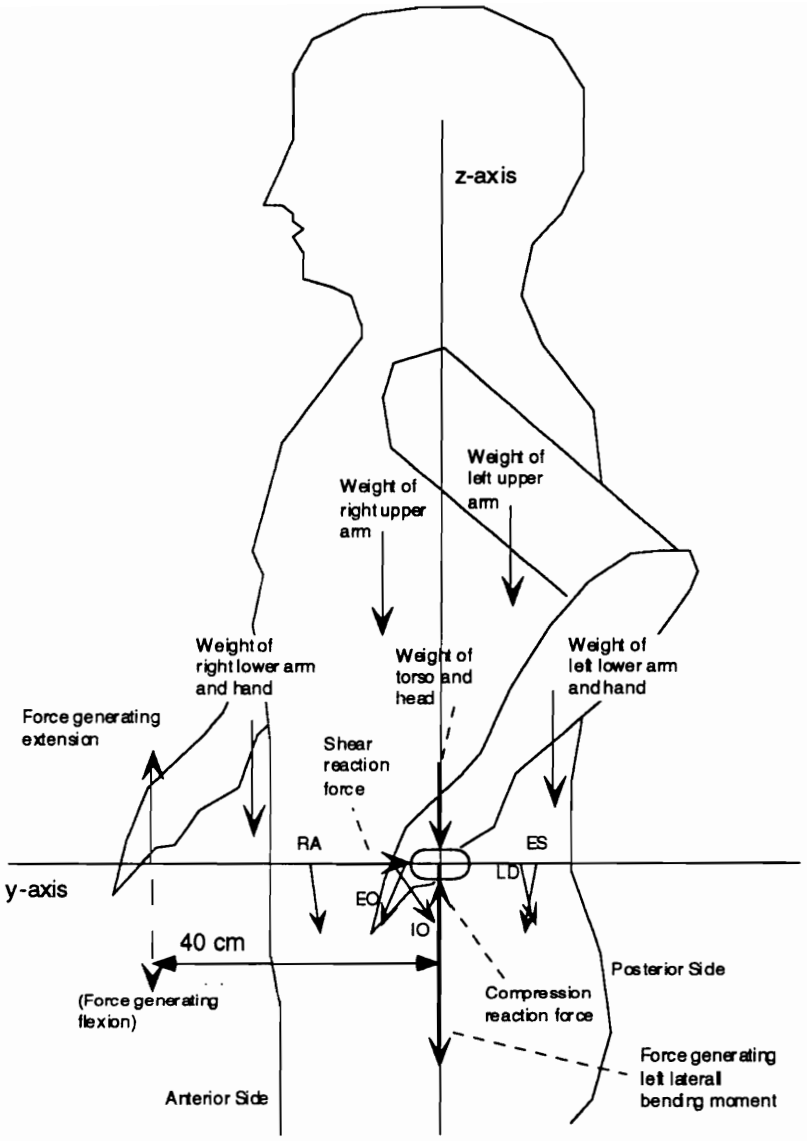

(a) Mid-Sagittal Plane View

Figure 5.3 Free body diagram of external and internal forces acting on body using L3/L4 cutting plane. The moment arms and lines action are from Han et al. (1992). (a) Mid-sagittal plane view; (b) Frontal plane view; (c) Transverse plane view.

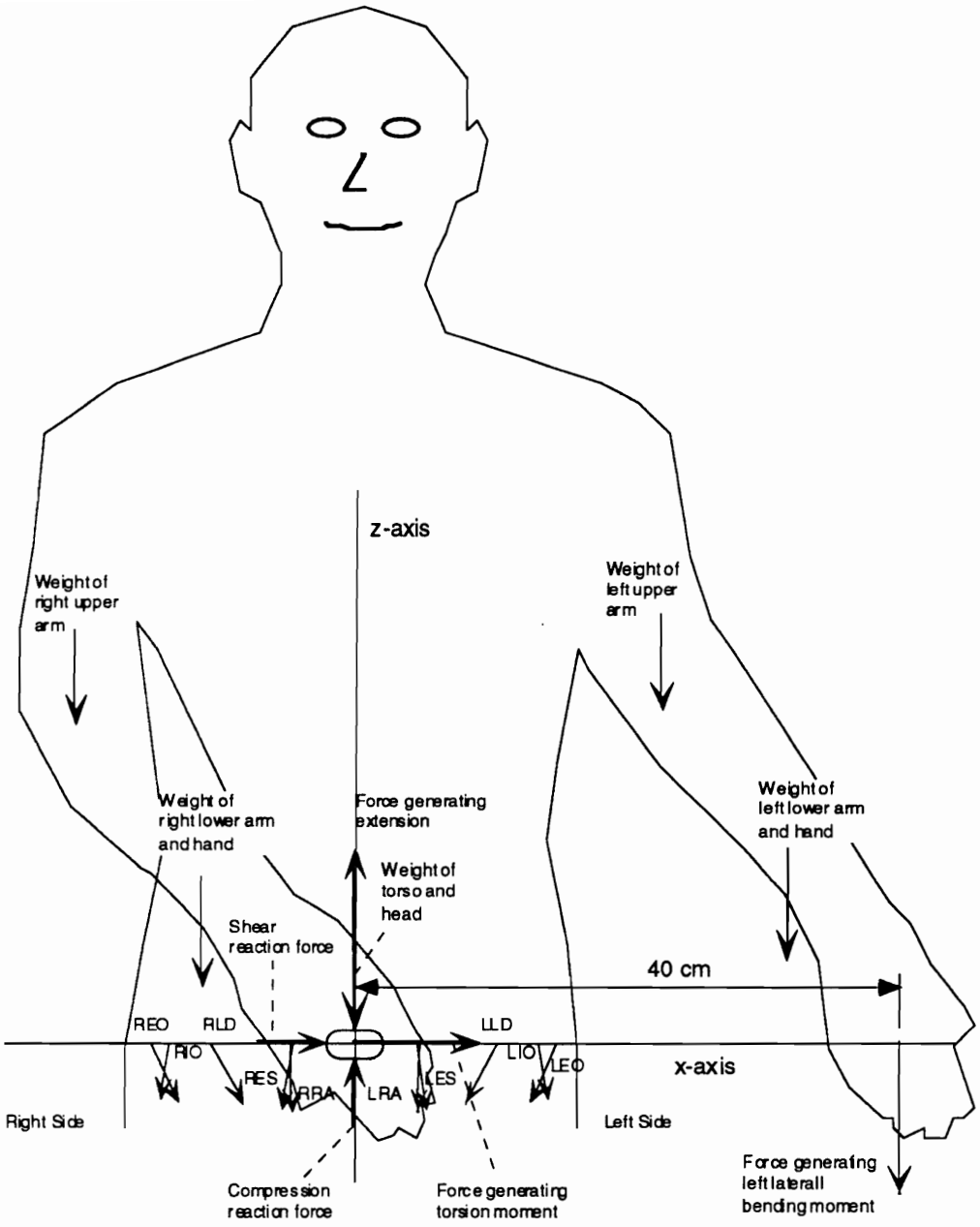

(b) Frontal Plane View

Figure 5.3 (Continued)

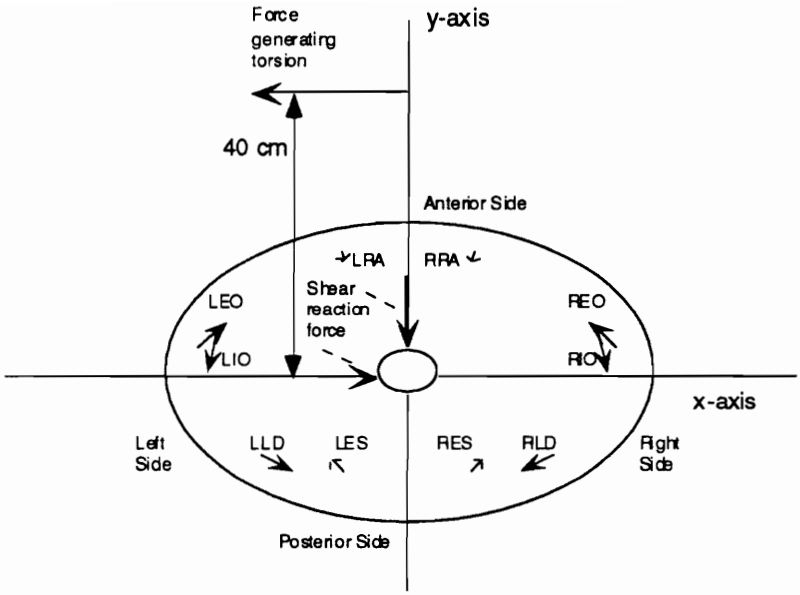

(c) Transverse Plane View

Figure 5.3 (Continued)

arms did not create torsional moment. The 40 cm distance was constant across subjects. Therefore, constant forces of 18.75 and 37.5 N were used to generate torsion moments of 7.5 and 15 Nm.

5.4.1.1 Positioning Subject to Hold Weights

A moment arm of 40 cm to the L3/L4 disc was used to calculate weights held in the hands to generate the flexion/extension, lateral bending, and torsion moments. An estimate of the location of the L3/L4 disc was calculated using the following regression equation ($R^2 = 0.61$) developed by Tracy et al. (1989).

$$\text{L3/L4 depth} = 36.2 + 0.256*(\text{Trunk Depth}) \qquad (5.1)$$

The variables L3/L4 depth and Trunk Depth were in units of mm, and the L3/L4 depth was measured from the posterior side.

The subject was positioned in the frame so that the estimated position of the L3/4 disc in the transverse plane was 40 cm from the hand position holding the loads in front of the body. The hip restraints maintained the position of the subject. The estimated depth of the L3/L4 disc also defined the frontal plane where the lateral loads were to be held. Plum bobs suspended from the frame marked the positions where the hands were held. The height of the plum bobs was set to the height of the L3 spinous process measured from the ground.

5.4.1.2 Estimating Moments Due to Arms

Using the hands to hold weights caused moments to be applied at the L3/L4 disc due to the weight of the arms. Since a constant 30 Nm resultant M_x-M_y moment was desired, the moments due to the arms were estimated. The position of the hands with respect to the L3/L4 disc was defined by where the loads were held. For example, assume the L3/L4 disc was at position (0,0,0) and a flexion and left lateral bending moment was applied. The right hand was at (0,40,0) and the left hand was at (-40,0,0) with coordinates in cm using the axes defined in Figure 2.1.

The length of the left and right lower and upper arms were measured for each subject as well as overall body weight. The weight of the lower and upper arms were estimated using the following percentages from Webb Associates (1978).

$$Wgt_{hand\&lower\ arm} = 0.023(\text{Total Body Weight}) \quad (5.2)$$

$$Wgt_{upperr\ arm} = 0.028(\text{Total Body Weight}) \quad (5.3)$$

The center of gravity for each arm segment was estimate from the following definitions taken from Clauser, McConville, and Young (1969).

Segment	Center of Gravity Definition	
forearm and hand =	67.7 % forearm length from elbow	(5.4)
upper arm =	43.6 % upper arm length from shoulder	(5.5)

The subjects were videotaped from the front, right, and left sides while performing a practice exertion. The angles of the forearm and upper arm were measured from the videotapes for the frontal and sagittal planes. Given the positions of hands, the length of the arm segments, and the angles of the arm segments, the positions of the elbows and shoulders were calculated. Using the estimates of arm segment center of gravity, the moment arm vector (r) from the L3/L4 was calculated. Using the estimates of arm segment weights (F), the moments due to the arms were determined (cross product of r and F).

The positions of the arms measured during the practice trial were assumed to be constant across all trials. Suppose the net moments due to the arms for weights held in front by the right hand and weights held to the side by the left hand were -4.3 Nm M_x and -4.9 Nm M_y. The arms created a net 4.3 Nm moment in flexion and 4.9 Nm moment in left lateral bending. Suppose an external moment condition of 23 Nm M_x (extension) and -19.3 Nm M_y (left lateral bending) was desired. The actual moments that need to be generated by the lifted weights were 27.3 Nm M_x and -14.4 Nm M_y. Therefore, a weight of 68.2 N (27.3 Nm divided by 0.4 m) was held over a pulley in front with the right hand

and 36.1 N (14.4 Nm divided by 0.4 m) with the left hand to the side. The moments had to be adjusted because the arms created a flexion moment aiding in the resistance of an applied extension moment. The arms also created a left bending moment which added to the left bending moment created by the weights.

5.4.2 External Loads Applied by Harness and Frame

A harness and frame were built to apply weights around the body to create an equal resultant moment consisting of flexion/extension and lateral bending components. The harness was worn only by male subjects. A drawing of the chest harness is shown in Figure 5.4. The hooks on the sides of the harness were mounted at a constant 40 cm distance from the mid-sagittal plane. Since the moment arm was constant, a constant force of 9.4 or 18.75 N was applied to each side hook to create a 7.5 or 15 Nm torsion moment. The force on each side created 3.75 or 7.5 Nm of torsion for a total of 7.5 or 15 Nm. Two bolts with padded 4 cm disks on the ends were mounted on the anterior side of the harness. These bolts were secured by tightening nuts on each side of the harness frame. The mounting bolts adjust laterally between spans of 15 to 35 cm. The adjustable mounting bolts allowed the harness to be fitted to the varying anthropometry of the subjects and positioned the anterior and posterior hooks and the lateral hooks in planes containing the L3/L4 disc. The lateral shoulder support bars were padded with a curvature to provide more surface area touching the shoulder.

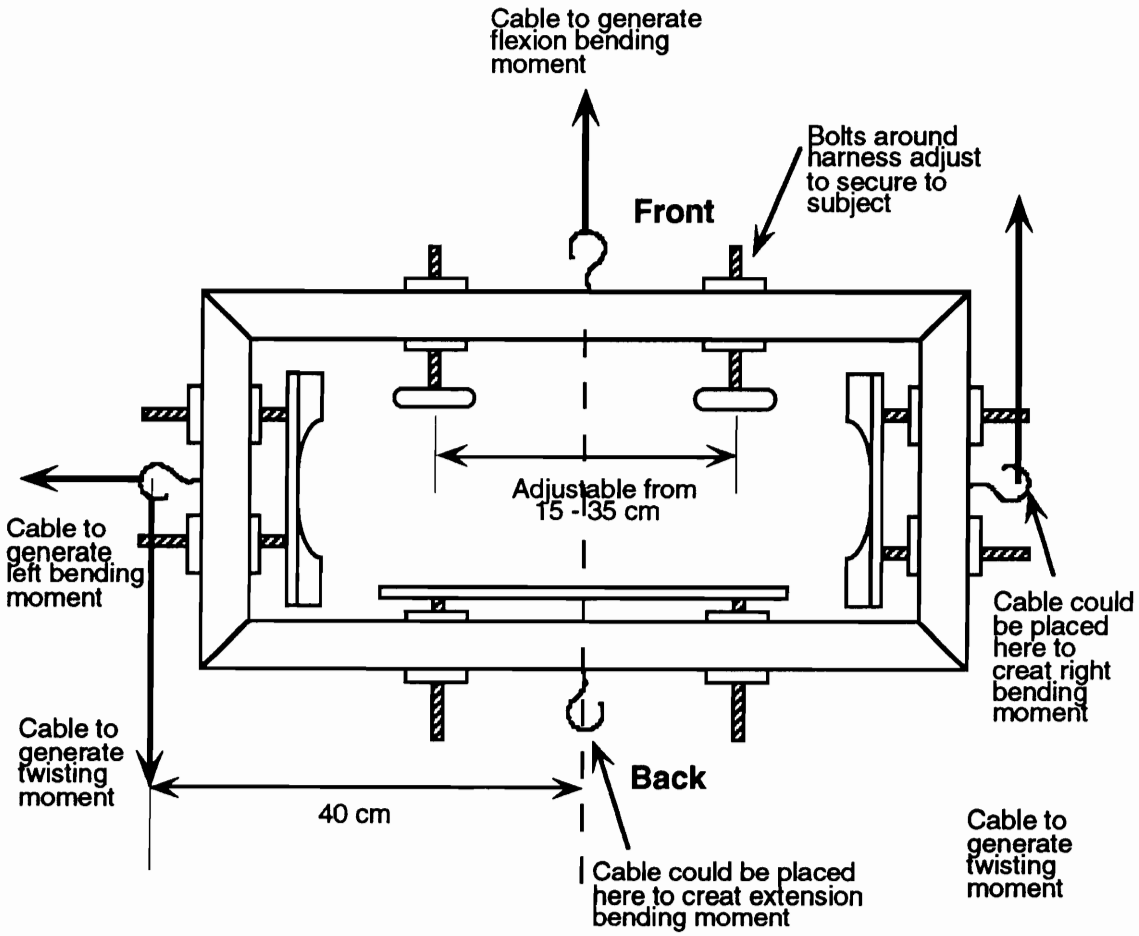

Figure 5.4 Chest Harness Worn by Subjects to Allow the Application of External Loads.

A loading frame was needed with the chest harness for application of external loads to the subjects. A drawing of the external loading system is shown in Figure 5.5. Moments were generated by suspending weights on cables over pulleys mounted on the frame and attaching to the chest harness worn by the subject. The twisting moment was generated by attaching 9.4 or 18.75 N weights to the lateral hooks on the chest harness. The distance from

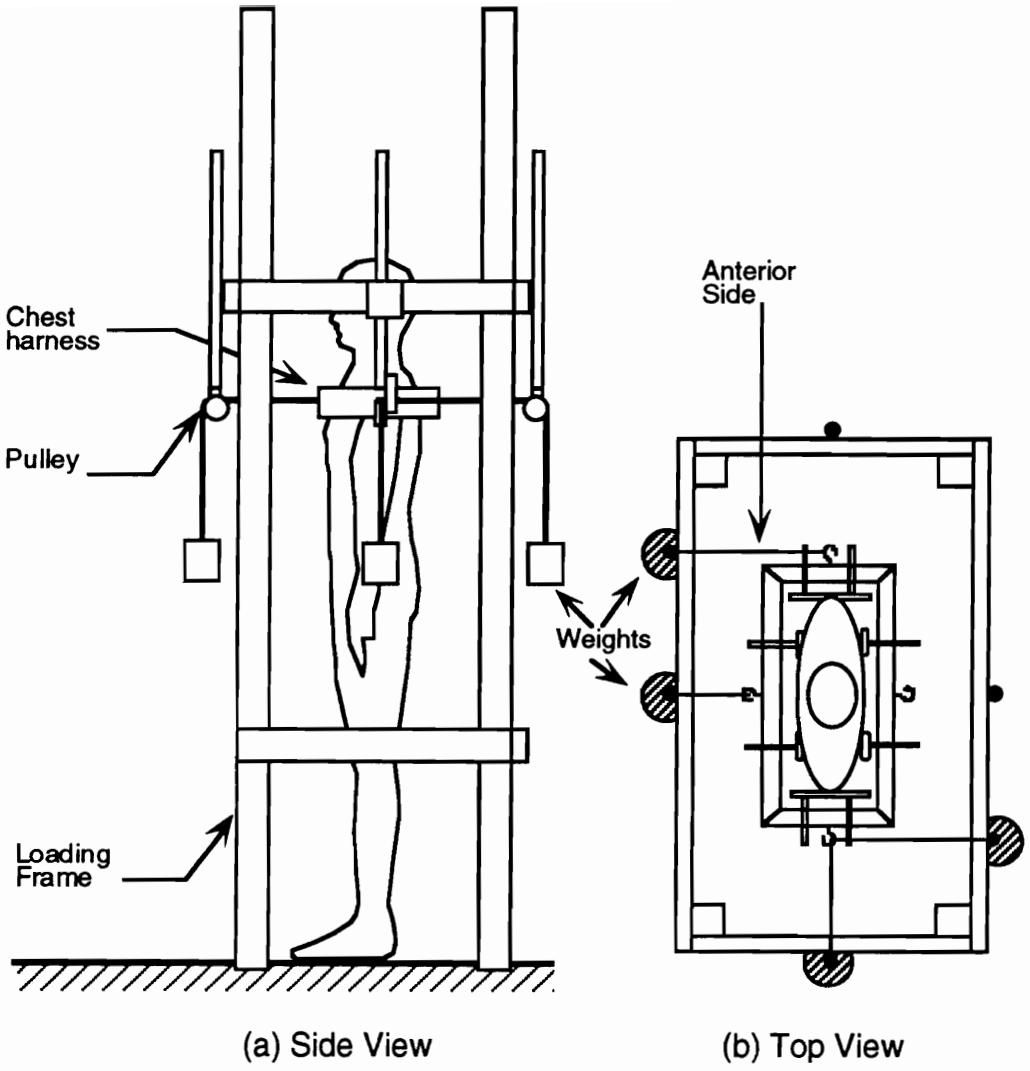

Figure 5.5 Load Application Mechanism, (a) shows the side view of a subject standing in the frame, (b) indicates how an external flexion moment, left bending moment, and torsion moment were applied.

the L3/L4 disc to the chest harness hooks determined the moment arm for the flexion/extension and lateral bending moments. While in the loading frame, subjects had their hips restrained. A hip belt was worn by the subject which was tethered by straps to the four posts of the loading frame.

A load moving around the body every 60 degrees was generated by varying the weights applied to the hooks in the mid-sagittal and frontal plane. Suppose the load started in front of the subject in the mid-sagittal plane. Weight was applied to the anterior hook to create a 30 Nm flexion moment. To simulate a weight moving clockwise, the flexion moment was decreased by applying less weight to the anterior hook, and the right lateral bending moment was created by applying weight to the right lateral hook. The resultant flexion and right lateral bending moment was 30 Nm. The line and pulley system located in front of, behind, and on both sides of the subjects transmitted the M_x, M_y, and M_z moments to the subject.

The free body diagram for the forces applied to the torso for a L3/L4 cutting plane is shown in Figure 5.6 for three different views. Figure 5.5, shown previously, indicated that the arms were positioned at the sides during harness trials. The arms should not have created moments about the L3/L4 disc for the harness trials. Weight adjustments were not needed to create the desired moments due to arm moments for harness loading as was necessary during hand loading trials. Figure 5.6 (a) shows that the vertical distance (d_1) from the L3/L4 disc to the harness hooks multiplied by the force generated the flexion/extension moment. Due to anthropometric differences, d_1 varied between subjects. The force applied over the pulleys was varied to maintain a constant flexion/extension moment across subjects. Figure 5.6 (b) shows that the vertical distance (d_1) from the L3/L4 disc to the harness hooks multiplied by the lateral force generated the lateral bending moment. The force applied over the pulleys was varied to maintain a constant lateral bending moment across

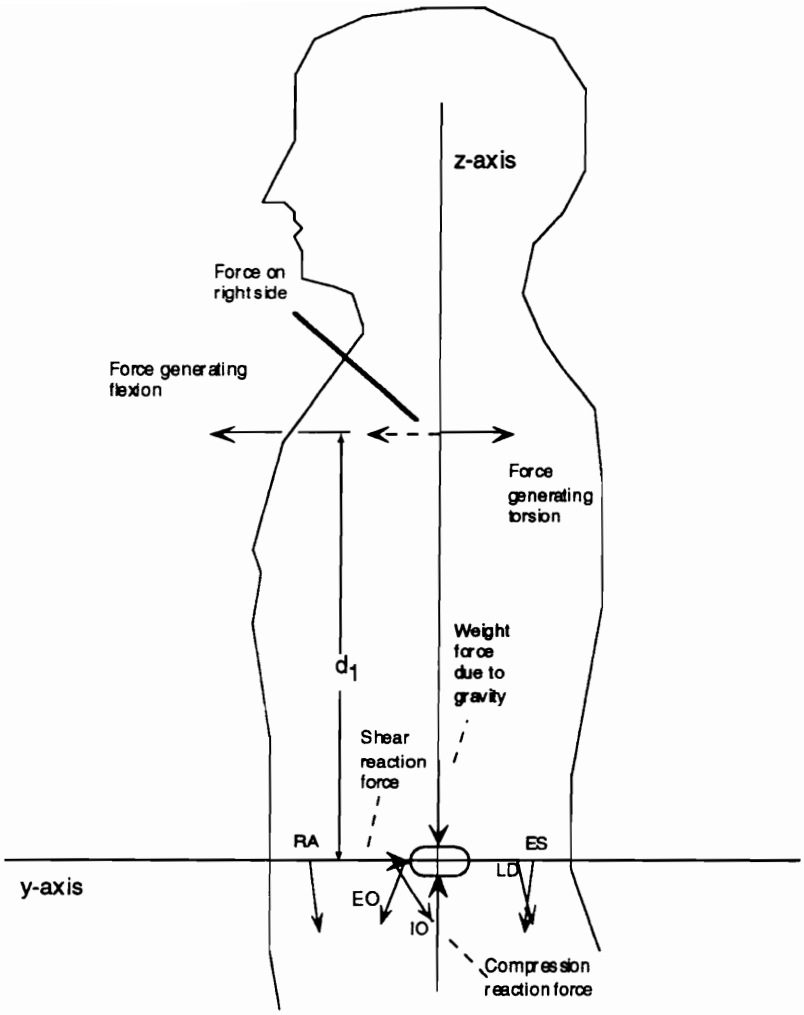

(a) Mid-Sagittal Plane View

Figure 5.6 Free body diagram of external and internal forces acting on body for a L3/L4 cutting plane. The moment arms and lines action are from Han et al. (1992). (a) Mid-sagittal plane view; (b) Frontal plane view; (c) Transverse plane view.

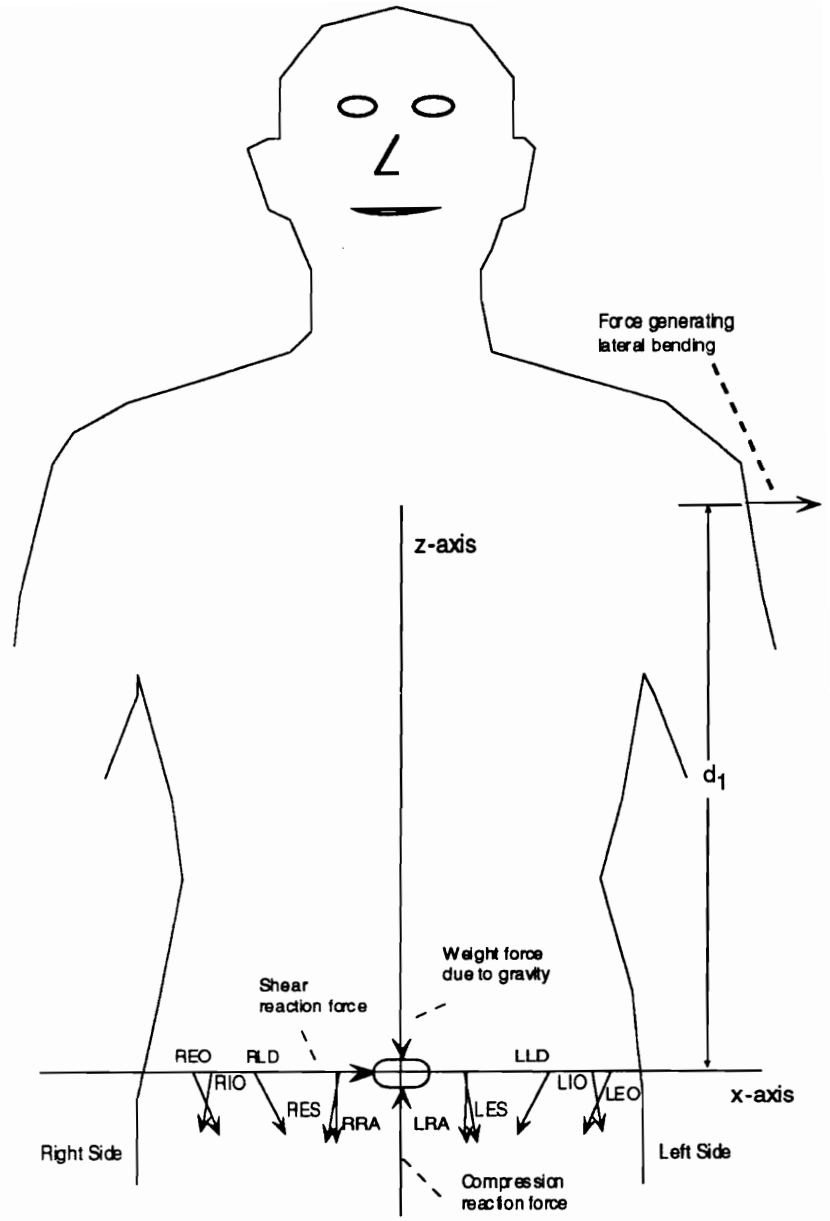

(b) Frontal Plane View

Figure 5.6 (Continued)

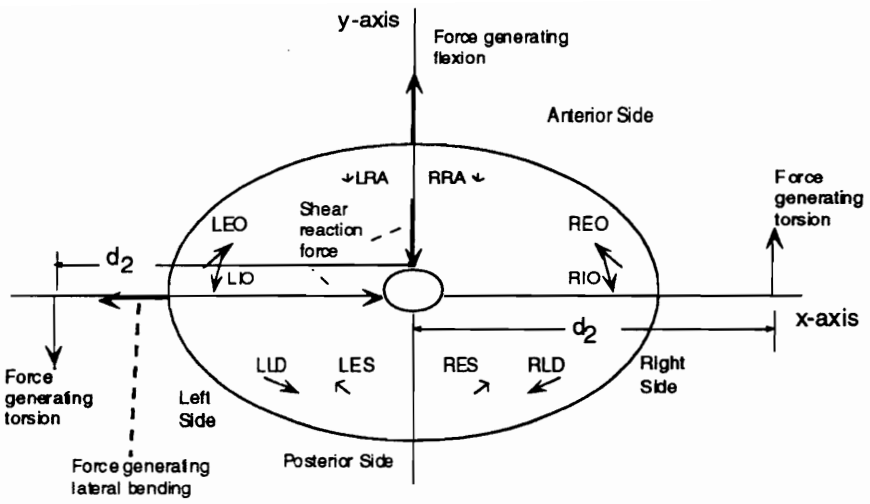

(c) Transverse Plane View

Figure 5.6 (Continued)

subjects. Figure 5.6 (c) shows that the horizontal distance (d_2) from the L3/L4 disc to the harness hooks multiplied by the force generated the torsional moment. The distance d_2 was a function of the harness used to apply loads not the subjects' anthropometry. The distance d_2 was constant across subjects at 40 cm, so a constant force was used.

5.4.3 Posture Monitoring

An upright posture was maintained by the subjects while the external loads were applied. Postures deviated from the upright posture would have caused the weight of the torso, head, and arms to generate moments about the L3/L4 joint in addition to the moments applied by the external load. To aid the subjects in maintaining an upright posture a light reflection system was

developed. A light emitter was mounted in front of the subject with the light beam in a plane parallel to the frontal plane. A second light emitter was mounted behind the subject with the light beam in a plane parallel to the frontal plane.

Both lights were mounted at the subject's suprasternale height. The lights were mounted at a width equal to the subjects' chest depth at the suprasternale plus 2 cm. This allowed an error of 1 cm on both sides of the chest. If the subject was in a neutral upright posture, both lights reflected back to their sensors, and LEDs in front of the subject illuminated indicating an upright posture. Figure 5.7 indicates the function of the posture system. As shown in Figure 5.7, if the subject's torso was flexed, the front light was blocked by the anterior side of the torso, and no light returned to the front sensor. The display to the subjects showed off for the front LED, but on for the rear LED, indicating they needed to adjust their posture by extending the torso. Also shown in Figure 5.7, if the subject's torso was extended, the rear light was blocked by the posterior side of the torso and no light returned to the rear sensor. The display to the subjects showed on for the front LED but off for the rear LED, indicating they needed to adjust their posture. If the subject's torso was twisted, both lights were blocked by the torso and no light returned to either sensor. The display to the subjects showed off for the front and rear lights and indicated they needed to adjust their posture.

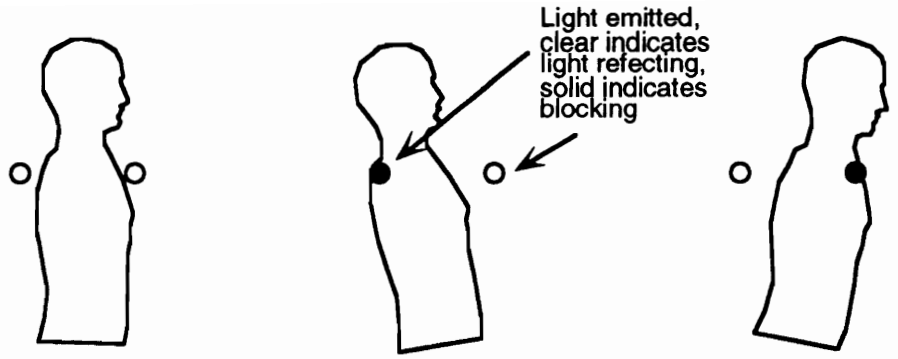

(a) Sagittal Plane View; left part shows posture system with both lights refecting because person is in an upright posture, center part shows rear light blocked by posterior side of body because torso is in extension. and right part shows front light blocked by anterior side of body because torso is in flexion.

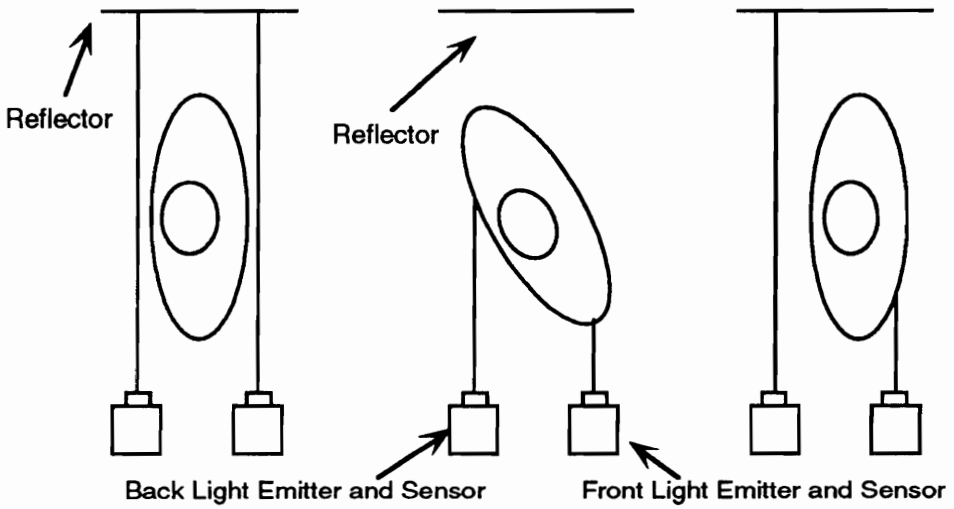

(b) Transverse Plane View; left part shows posture system with both lights refecting because person is in an upright posture, center part shows both lights blocked because the torso is twisted. and right part shows front light blocked by anterior side of body because torso is in flexion.

Figure 5.7 Posture monitoring system, (a) side view of a subject with upright and deviated postures, (b) top view of a subject with upright and deviated postures.

5.4.4 Electromyographic Instrumentation

The EMG activity of the muscles was recorded at eight locations using silver-silver chloride pre-gelled surface electrodes (model F1010 manufactured by Lead-Loc). The surface electrode locations for the four pairs of muscles were as follows: left and right erector spinae, 3 cm from midline at L3 spinous process; left and right rectus abdominus, 3 cm from midline at umbilicus level; left and right external oblique, 6 cm dorsal to the Anterior Superior Iliac Spine (ASIS) at umbilicus level (approximately 15 cm lateral to umbilicus; McGill, 1991); and left and right latissimus dorsi, over muscle belly at T9 level. The electrode pairs were oriented in the direction of the muscle fibers and separated by 2 cm. The locations of the electrode pairs followed those used by Hughes and Chaffin (1995), McGill (1991), Schultz et al. (1983), and Seroussi and Pope (1987) for the erector spinae, McGill (1991) for the rectus abdominus, Hughes and Chaffin (1995), Schultz et al. (1983), and Seroussi and Pope (1987) for the external oblique, and McGill (1991) for the latissimus dorsi. A single electrode was placed on the right acromion as the ground, and then connected to each of the two pre-amplifiers by a wire split from the ground.

Each electrode was connected to a pre-amplifier which amplified the signal 200 times by means of a snap wire 45 cm long. The pre-amplifiers were then connected to an amplify. The EMG signal was checked for amplification after the first maximum voluntary contraction trial. The EMG signals for the muscles were amplified to be in the range of approximately ±7.5 Volts (which was 75% of the analog-to-digital board range, ±10 Volts). A DC source

powered the amplifier instead of AC power for subject safety. The EMG signal was sampled at 500 Hz by a micro-computer through an analog-to-digital board installed in the computer.

5.5 Experimental Design

A computer simulation conducted to determine the effects of different inputs into optimization-based trunk biomechanical models was reported in Chapter 4. The goal of this experiment was to measure the actual muscular activity during different loading conditions. Model predictions were then compared to actual muscle activity. From the computer simulations, loading conditions were identified which differentiated the muscle predictions of the models.

5.5.1 Independent Variables

The experimental design for this study contained two parts. The first part consisted of comparing actual muscle activity to model predictions reported previously in Chapter 4. The second part consisted of comparing muscle activity when the external moments were generated through loads held in the hands versus loads applied with the harness system.

5.5.1.1 Actual Muscle Activity Compared to Model Predictions

Four factors were manipulated in this portion of the experiment, angle, muscle, torsion moment, and gender. The angle factor had 18 levels consisting

of varying 20 degree increments of x and y moments which had a resultant of 30 Nm. The 18 loading conditions were shown previously in Figure 5.1. The second factor, muscle, had eight levels which were the eight muscles monitored by EMG electrodes: left and right rectus abdominus (LRA, RRA), left and right external obliques (LEO, REO), left and right latissimus dorsi (LLD, RLD), and left and right erector spinae (LES, RES). The third factor, torsion moment, had two levels - 7.5 Nm and 15 Nm M_z. For the gender factor, six male and six female subjects participated in this part of the study.

5.5.1.2 Hand Moment Loading versus Harness Moment Loading

The experimental design contained four factors: angle, muscle, torsion moment, and apparatus. The angle factor had 6 levels consisting of 60 degree increments of x and y moments which had a resultant of 30 Nm. The 6 loading conditions were a subset of the 18 conditions shown previously in Figure 5.1. The second factor, muscle, had eight levels which were the eight muscles monitored by EMG electrodes: LRA, RRA, LEO, REO, LLD, RLD, LES, and RES. The third factor, torsion moment, had two levels - 7.5 Nm and 15 Nm M_z. The fourth factor, apparatus, had two levels consisting of loads applied via the hands and via the harness system.

Six male subjects participated in this part of the study. The harness was mounted below the suprasternale so that it did not interfere with the posture monitoring system (Section 5.4.3). The position of the harness precluded the use of female subjects given the posture monitoring system used for both loading apparatuses.

5.5.2 Dependent Variables

The dependent variable measured was raw EMG signal produced by the muscles under study. A filtering procedure to reduce ECG contamination required that raw EMG signal be collected. Filtering could not be performed on data that had already been processed. The raw EMG signal was filtered and reduced to compare to the muscle forces predictions of the models.

5.6 Protocol

The experiment was conducted in three sessions, the first one-hour long and the second and third three-hours long. In the first session, after the subjects had read and signed the informed consent form (Appendix A), they were screened using the questionnaire (Appendix B). Any participants who reported back pain in the last year were questioned further as to the degree of pain, and whether they were currently experiencing back pain. Those who had experienced no more than minor muscle soreness in the past three months, were not currently experiencing any back pain, and had no chronic back problems were accepted as participants in the experiment.

Anthropometric measurements were then taken on each participant: weight, stature, trochanterion height, L3 spinous process height from floor, waist depth at L3 spinous process, bicrestal breadth, height of suprasternale, chest depth at suprasternale, left and right lower arm length (elbow to ulnar styloid, Clauser et al., 1969), and left and right upper arm length. Next, the pulley suspending the weight for torsion was set to L3 spinous process height from the floor. The plum bobs for the front and left and right sides (marking placement for

the hands) were set at the L3 spinous process height. The estimate of the L3/L4 depth from the posterior side was then calculated.

The subject then stood in the frame so that the moment arms from the estimated L3/L4 position to the hand positions were 40 cm. The posture monitoring system was then set up so that the light width was equal to the chest depth at the suprasternale plus 2 cm and both lights were at the suprasternale height. The posture monitoring system was explained to the subjects and checked for accuracy. The subjects practiced flexing, extending, and twisting the torso to turn on and off the LEDs displayed in front of them. The subject was then instructed to position the hands at the markers when holding weights. Once the subject reached a posture so that both LED displays were lit, the subject held the weights for three seconds. Subjects were instructed not to adjust their posture if either LED light turned off after the start of the trial.

The subject was videotaped during a practice trial from the front, left, and right sides as weights were held in front with the right hand and to the left side with the left hand. The subject was videotaped again as weights were held in front with the left hand and to the right side with the right hand. The subject then completed practice trials simulating approximately the largest flexion/extension and left and right lateral bending moments. The exact weights to create 30 Nm resultant moments were not known until after the first session when moments due to arms were estimated. Therefore, the practice trials were an approximation to the experimental trials.

Between the first and second sessions, the videotapes were viewed to measure the angles of the left and right lower and upper arms. The moments

due to the arms were then estimated using the procedure discussed previously in Section 5.4.1.2. For two loading conditions (30 Nm M_x, 0 Nm M_y) and (-30 Nm M_x, 0 Nm M_y), the subject used both hands in front to hold the weights. The arms were assumed to be symmetrical so that there was no net lateral bending moment and only a flexion moment created by the arms. The desired resultant 30 Nm moments were then adjusted to account for arm moments. The weights needed to generate the adjusted moments (given a 40 cm moment arm) were calculated and measured.

Due to varying estimated arm moments, each subject lifted different weights. Paint cans were filled with lead shot and then sealed to accommodate the different weights required by each subject.

The preparation and procedure for the second and third sessions was the same. Before the start of each session, the EMG amplifier was calibrated. The pulley and plum bob height on the frame were set to the L3 height measured in the first session. The posture lights were also set to the height and width measured in the first session.

When the subject arrived for the second and third sessions, the L3 and T9 spinous processes and ASIS anatomical landmarks on the subject were located for preparation of electrode placement. The skin at the electrode placement was then prepared by shaving, if necessary, and cleaning with rubbing alcohol. The electrodes were then placed on the subjects in the eight trunk locations previously discussed in Section 5.4.4. The snap electrode leads were then connected to the pre-amplifiers and amplifier.

The muscle resting EMG level trial was measured as the subject lay on a bench on his/her back in a supine position. The subject was asked to stand in a upright posture as the EMG activity of the muscles was measured. The subject then performed six maximum voluntary contraction (MVC) trials reported by McGill (1991).

The first four MVC trials consisted of the subjects leaning the torso over the edge of a bench with the legs restrained and the hands placed behind the head. With the subject lying on the back supine, a flexor effort was obtained, and while lying on stomach prone an extension effort was measured. Lying on each side, the subject performed a right and left lateral bend. For the final two MVC trials, subjects were lying fully on the bench in a knee-bent sit-up position with the feet restrained. Hands were placed behind the head while the subject twisted the trunk to form an angle with the horizontal of approximately 30 degrees. The subject then attempted a maximum effort sit-up as the experimenter provided a matching resistance to the shoulders. For the final two MVC trials, the trunk rotated 30 degrees counter-clockwise and then 30 degrees clockwise on successive trials. The MVC trials had a duration of six seconds. During the first two seconds the subjects were instructed to build up to a maximum effort and then hold the effort for four seconds. The second through fifth seconds were used for data analysis.

Over the second and third sessions the subjects completed 36 experimental trials in which the they resisted externally applied moments using their hands. The 36 trials were composed of 18 combinations of M_x and M_y moments (20 degree increments of 30 Nm resultant moment) at each of two M_z

moments (7.5 and 15 Nm). Eighteen trials were completed each day with the torsion moment (M_z) blocked on days. All 18 combinations of M_x and M_y were completed in one day with 9 at 7.5 Nm M_z and 9 at 15 Nm M_z. The remaining 18 trials were completed on the final session. The order of the trials within the session were presented in random order.

Both male and female subjects completed the 36 hand loading trials over the final two sessions as described above. The males also performed an additional six trials in which they resisted external moments applied through the chest harness. Three of the male subjects started the first session with the harness trials, then completed the hand loading trials; the second session they started with the hand loading trials and then completed the harness trials. The other three male subjects followed an opposite pattern.

For the chest harness trials, the harness attachments were adjusted to center the front and rear hooks In the mid-sagittal plane and the lateral hooks in the frontal plane. The distance from the L3 spinous process to the harness hooks was then measured, because this distance affected the force applied to create constant moments across subjects, see Figure 5.6. The appropriate forces to generate the test conditions were then calculated. Each session, six of the same loading conditions used during hand loading were completed during harness loading, three with 7.5 Nm M_z and three with 15 Nm M_z.

For the experimental trials, the subject was placed in the loading frame, and the pulley heights were adjusted to be level with the harness on the subject or at the L3 height for the hand loading trials. The hip belt was then fitted to the subject and secured to the four posts of the loading frame. The estimate of the

L3/L4 disc location was then checked for correct positioning. The weights for the first trial were then attached to the harness hooks and placed over the pulleys or held by the hands. The weight calculated to be placed over the pulleys had been adjusted for pulley losses to create the appropriate force. The subjects then adjusted their posture to an upright position so that the reflector system to monitor posture turned on the LEDs in front of the subject. The subjects were then required to resist the moments for three seconds while the EMG signals were collected.

The subjects were given two minute rest breaks between trials. The succeeding experimental trials were then completed in random order until all conditions were finished.

The third session was conducted in the same manner as the second. Electrodes were placed according to markings on the subjects from the second session. Resting, standing, and MVC trials were completed followed by hand loading trials and harness trials (for male subjects).

6. RESULTS

A computer simulation conducted to determine the effects of different inputs into optimization-based trunk biomechanical models was reported in Chapter 4. Two optimization models, the MIC and SCI, were included in the investigation. The number of muscles included in the development of the models was varied as well as the geometric parameters of the muscles. The inputs to trunk optimization models affected the prediction of muscle activity/inactivity for equal external loads.

The method used in this study to empirically measure human trunk muscle performance during static exertions to resist external loads was discussed previously in Chapter 5. External loads were selected so that the varying models and inputs predicted activity of the muscles differently. Human muscle activity during exertions was compared to muscle predictions to measure the appropriateness of the models and associated inputs. This chapter reports the analysis and results of the data collected from the experiment.

6.1 Data Reduction

As stated in Section 5.4.4, the raw EMG signal was sampled at 500 Hz for 3 seconds during the static exertions. Because torso muscles were often contaminated with electrocardiographic (ECG) interference, the raw data was filtered to diminish the ECG signal within the EMG signal. Redfern, Hughes, and Chaffin (1993) suggested using a high pass filtering technique to remove the ECG contamination from the EMG signal. After testing high-pass cut-off

frequencies of 10, 30, and 60 Hz, Redfern et al. (1993) suggested using approximately 30 Hz as the cut-off frequency for surface electrodes. Because the current study collected EMG signals from trunk muscles using surface electrodes, a similar filtering technique was adopted.

Following Redfern et al. (1993), the EMG data collected for each muscle were high-pass filtered using a digital finite impulse response (FIR) filter with 100 coefficients based on a Hamming window design criteria. A cut-off frequency of 30 Hz was used as suggested by Redfern et al. (1993). Figure 6.1 shows the EMG data for the left erector spinae muscle from Subject 5 during a loading of 30 Nm M_x, 0 Nm M_y, and 7.5 Nm M_z. Figure 6.1(a) shows the raw unfiltered data; the spikes indicate ECG contamination. Filtered data with ECG impact reduced is shown in Figure 6.1(b).

A power spectral analysis of the EMG data for the left erector spinae muscle from Subject 5 during a loading of 30 Nm M_x, 0 Nm M_y, and 7.5 Nm M_z was performed. Figure 6.2(a) indicates much of the power of the data was below 30 Hz which was largely due to ECG contamination. Figure 6.2(b) shows that after filtering the ECG signal was diminished and low power remained for the LES above 30 Hz. The LES was expected to be inactive during the external extension load because the subjects recruited abdominal muscles for attempted flexion. Therefore, the low power of the LES after filtering was expected for the trial shown in Figure 6.2.

After filtering, the data was further processed by taking the root mean square (RMS) with a 60 ms time constant. Figure 6.1(c) shows the RMS values of the filtered EMG signal for the left erector spinae muscle from Subject 5

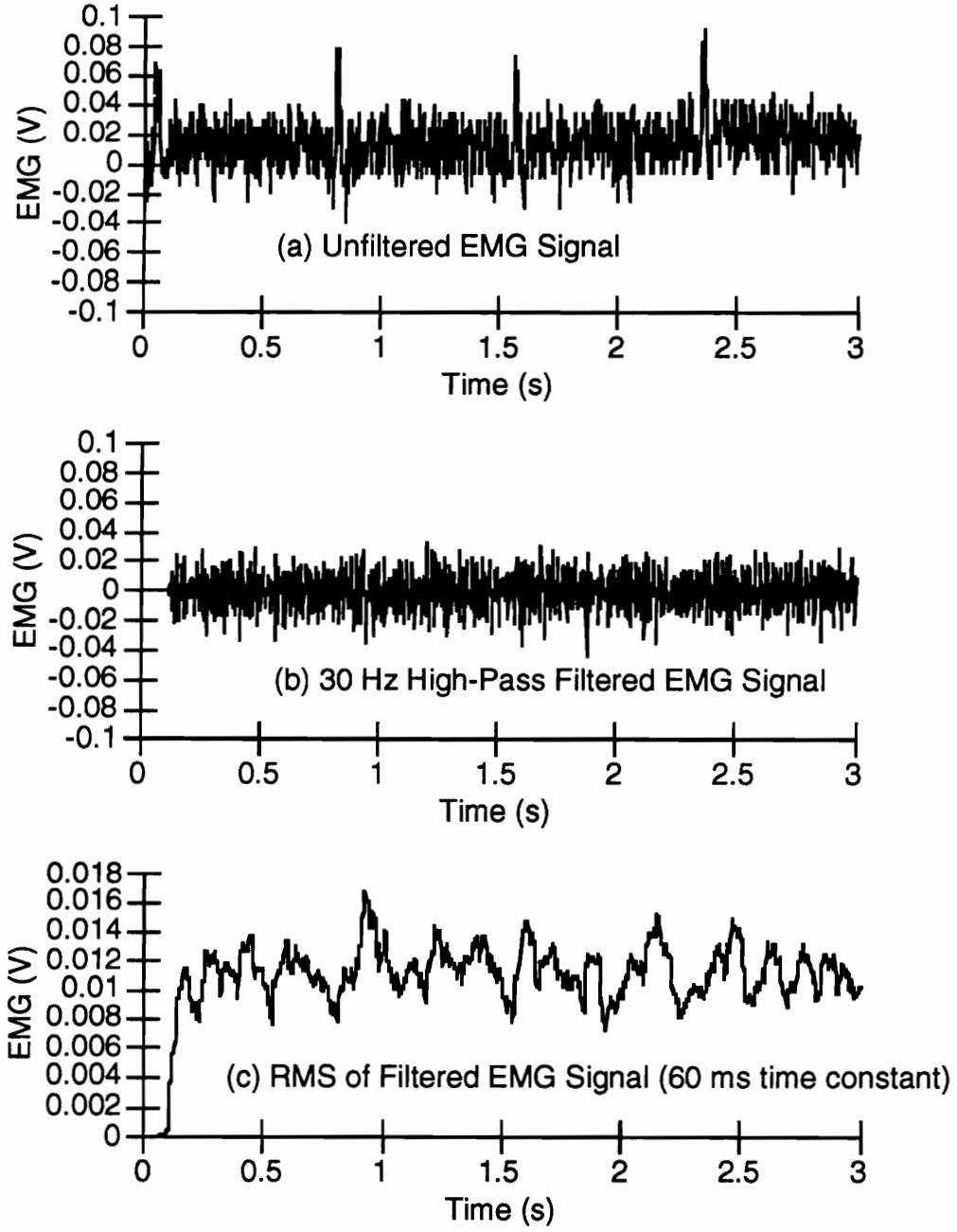

Figure 6.1 Raw and filtered data for the left erector spinae muscle from Subject 5 during a loading of 30 Nm M_x, 0 Nm M_y, and 7.5 Nm M_z. (a) unfiltered data with spikes showing ECG contamination. (b) filtered data with ECG impact reduced. (c) filtered data further processed by taking the RMS with a 60 ms time constant.

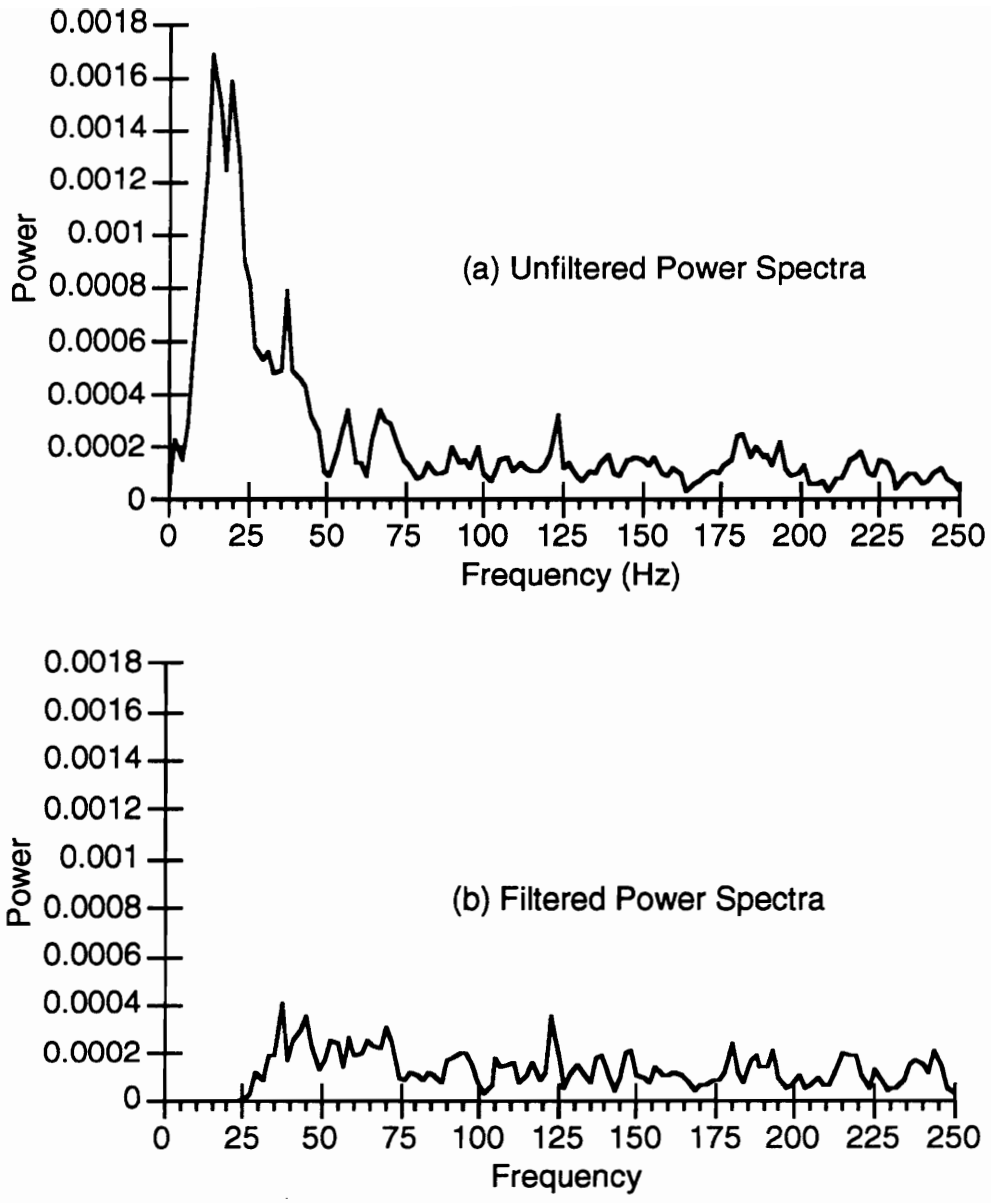

Figure 6.2 Power spectra for raw and filtered data for the left erector spinae muscle from Subject 5 during a loading of 30 Nm M_x, 0 Nm M_y, and 7.5 Nm M_z. (a) Power spectra for raw data, below 30 Hz the power is largely due to ECG contamination. (b) Power spectra for filtered data, power above 30 Hz due to muscle.

during a loading of 30 Nm M_x, 0 Nm M_y, and 7.5 Nm M_z. The mean RMS signal from 0.5 to 2.5 seconds was then taken as a representation of the activity of the muscle. For example, the mean RMS value for the LES of Figure 6.1(c) is 0.0115 volts.

Resting, standing, and maximum voluntary contraction (MVC) trials (Section 5.6) were filtered and processed using the same method as the experimental trials. The second to fifth seconds of the resting, standing, and MVC trials were used for filtering and processing. The maximum mean RMS value was then determined for each muscle across all the MVC trials.

The maximum mean RMS value for each muscle and mean resting RMS values were then used to normalize the RMS values determined for the hand loading and harness loading trials. The EMG signal measured during the loading trials was normalized using the following equation used by Lavender, Tsuang, Hafezi, Andersson, Chaffin, and Hughes (1992), Mirka (1991), and Seroussi and Pope (1987) :

$$EMG_{normalized} = \frac{EMG_{Test\ Trial} - EMG_{Resting}}{EMG_{Max.} - EMG_{Resting}} \qquad (6.1)$$

The normalization procedure defined the muscle activity for each hand and harness loading trials as a percentage of the maximum EMG level.

6.2 Measured Muscle Activity For Loads Held with Hands

During the experiment each subject performed static exertions to resist 18 combinations of 30 Nm resultant flexion/extension (M_x) and lateral bending

moments (M_y). All the 18 combined M_x and M_y were presented at two levels of torsion moment (M_z), 7.5 and 15 Nm.

The measured activity was viewed as a function of load angle. External loads were moved about the person so that the resultant M_x-M_y moment was 30 Nm. The percent measured muscle activity was plotted versus the angle of rotation. Figure 6.3 shows the measured muscle activity of each muscle for a male subject, number 1. Figure 6.4 shows the measured muscle activity of each muscle for a female subject, number 8.

6.3 Correlation Between Measured and Predicted Activity

To evaluate the accuracy of the four model and geometry combinations, the actual muscle activity was correlated with predicted activity. The muscle force predicted by each model combination at the 18 loading angles was used as the regressor variable to predict percent muscle activity measured in the experiment. A linear model was assumed between model muscle force and measured muscle activity. The regression models were developed for each combination of subject, muscle, and torsion moment so 18 observations were included in each regression equation. The R^2 values (percent of variation explained by the model) are shown for each model in Table 6.1 for male subjects and Table 6.2 for female subjects.

Three examples of actual and predicted muscle activity versus load angle were graphed. The three examples were selected for their range of R^2 values. Figure 6.5 shows the RRA muscle for subject 5 with 15 Nm torsion which contains a predictor with R^2 equal to 0.96. Figure 6.6 shows the REO

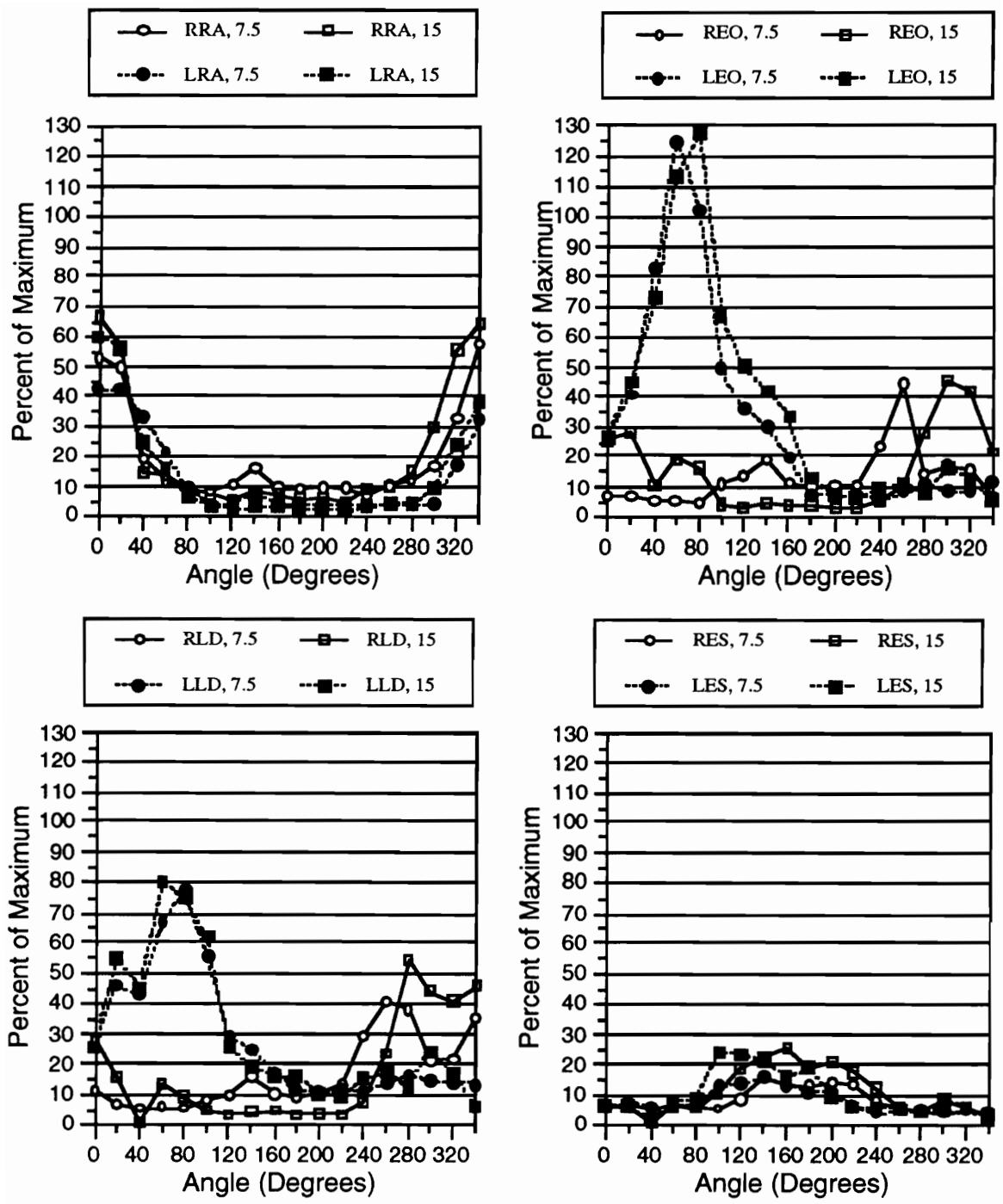

Figure 6.3 Normalized muscle activity as a function of load angle and torsion moment, Subject 1 (male). An angle of 0 degrees corresponds to external 30 Nm M_x and 0 Nm M_y. (subject attempted flexion); an angle of 180 degrees corresponds to external -30 Nm M_x and 0 Nm M_y. (subject attempts extension).

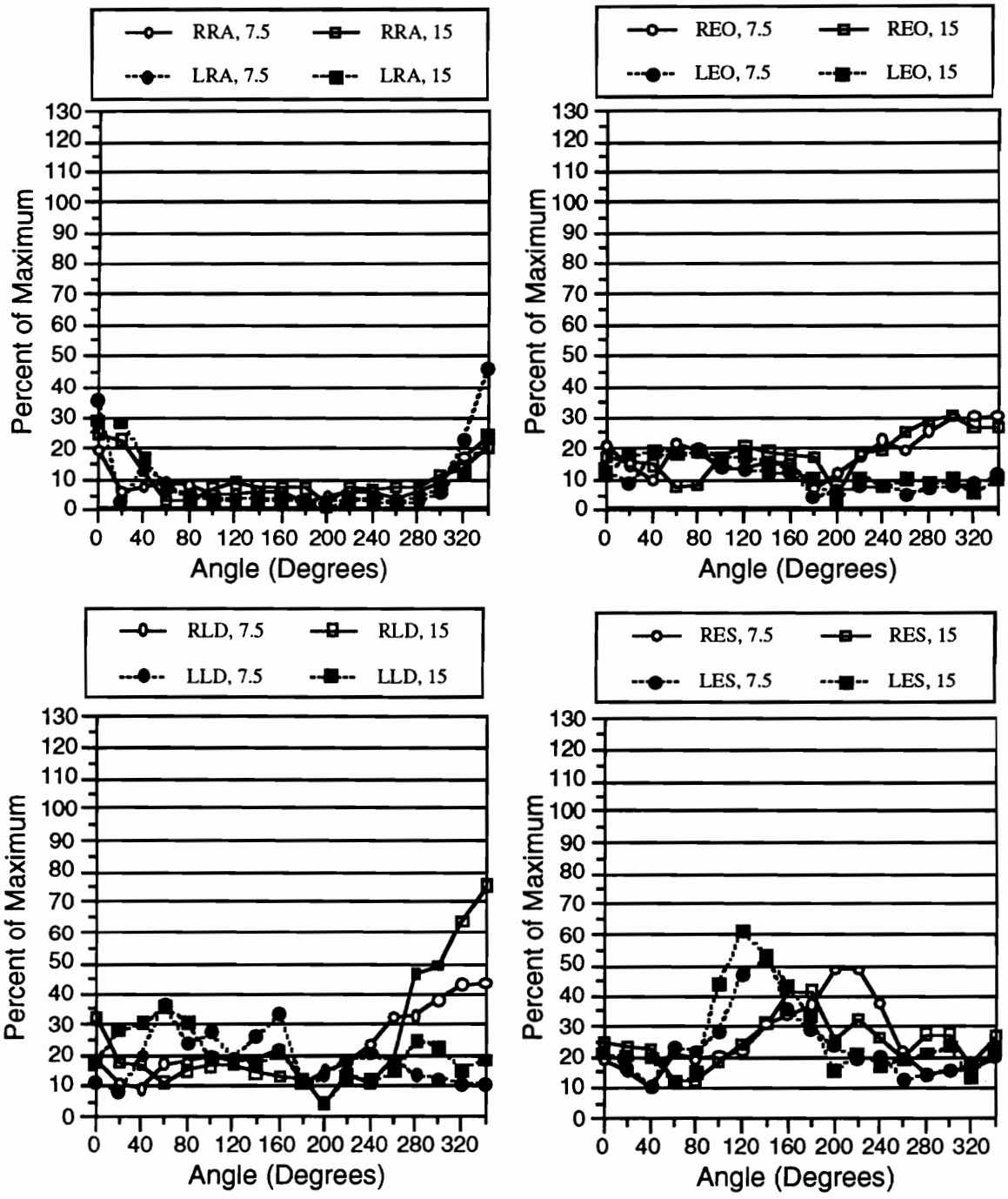

Figure 6.4 Normalized muscle activity as a function of load angle and torsion moment, Subject 8 (female). An angle of 0 degrees corresponds to external 30 Nm M_x and 0 Nm M_y. (subject attempted flexion); an angle of 180 degrees corresponds to external -30 Nm M_x and 0 Nm M_y. (subject attempts extension).

TABLE 6.1 R^2 Values Using Predicted Muscle Force of the Models to Predict Percent Muscle Activity for Male Subjects.

		7.5 Nm Torsion				15 Nm Torsion			
Sub	Muscle	MIC-C	MIC-H	SCI-C	SCI-H	MIC-C	MIC-H	SCI-C	SCI-H
1	RRA	0.73	0.18	0.78	0.69	0.73	0.13	0.82	0.70
1	LRA	0.58	0.71	0.84	0.81	0.40	0.45	0.86	0.64
1	REO	0.00	0.06	0.03	0.00	0.68	0.67	0.66	0.60
1	LEO	0.25	0.13	0.47	0.76	0.24	0.09	0.54	0.73
1	RLD	0.10	0.38	0.06	0.39	0.01	0.20	0.08	0.10
1	LLD	0.09	0.00	0.02	0.00	0.09	0.03	0.02	0.00
1	RES	0.72	0.23	0.75	0.37	0.46	0.12	0.65	0.19
1	LES	0.77	0.73	0.71	0.79	0.81	0.66	0.66	0.68
2	RRA	0.88	0.44	0.91	0.88	0.49	0.00	0.64	0.33
2	LRA	0.72	0.77	0.98	0.90	0.46	0.55	0.86	0.73
2	REO	0.55	0.46	0.58	0.40	0.08	0.20	0.04	0.08
2	LEO	0.72	0.29	0.89	0.94	0.41	0.42	0.88	0.76
2	RLD	0.05	0.04	0.22	0.02	0.15	0.65	0.07	0.34
2	LLD	0.13	0.09	0.00	0.10	0.36	0.21	0.27	0.00
2	RES	0.10	0.38	0.19	0.42	0.73	0.65	0.91	0.77
2	LES	0.04	0.11	0.07	0.10	0.87	0.52	0.94	0.87
3	RRA	0.82	0.35	0.87	0.82	0.79	0.29	0.90	0.79
3	LRA	0.51	0.79	0.76	0.83	0.54	0.62	0.85	0.76
3	REO	0.36	0.29	0.41	0.42	0.48	0.35	0.39	0.30
3	LEO	0.28	0.04	0.59	0.67	0.43	0.13	0.71	0.84
3	RLD	0.01	0.07	0.08	0.03	0.00	0.08	0.26	0.02
3	LLD	0.04	0.00	0.03	0.01	0.07	0.12	0.19	0.00
3	RES	0.49	0.53	0.66	0.68	0.40	0.38	0.54	0.51
3	LES	0.63	0.38	0.74	0.64	0.67	0.51	0.73	0.61
4	RRA	0.80	0.24	0.80	0.69	0.78	0.17	0.85	0.62
4	LRA	0.62	0.69	0.87	0.79	0.40	0.50	0.81	0.67
4	REO	0.28	0.61	0.39	0.39	0.40	0.41	0.20	0.06
4	LEO	0.15	0.05	0.41	0.58	0.49	0.00	0.43	0.63
4	RLD	0.00	0.22	0.05	0.12	0.01	0.33	0.08	0.14
4	LLD	0.06	0.00	0.01	0.00	0.42	0.19	0.18	0.00
4	RES	0.70	0.51	0.83	0.69	0.06	0.10	0.04	0.09
4	LES	0.42	0.23	0.45	0.46	0.12	0.11	0.11	0.18
5	RRA	0.93	0.46	0.94	0.90	0.90	0.34	0.96	0.83
5	LRA	0.73	0.91	0.83	0.95	0.58	0.86	0.75	0.91
5	REO	0.25	0.60	0.37	0.49	0.48	0.70	0.31	0.33
5	LEO	0.51	0.15	0.80	0.89	0.42	0.25	0.80	0.80
5	RLD	0.01	0.13	0.07	0.08	0.05	0.39	0.01	0.28
5	LLD	0.20	0.10	0.02	0.10	0.02	0.01	0.01	0.00
5	RES	0.79	0.84	0.80	0.87	0.91	0.65	0.96	0.75
5	LES	0.85	0.82	0.84	0.90	0.91	0.80	0.85	0.85
6	RRA	0.64	0.21	0.59	0.56	0.30	0.00	0.27	0.13
6	LRA	0.68	0.73	0.86	0.83	0.37	0.51	0.64	0.63
6	REO	0.33	0.71	0.43	0.56	0.25	0.39	0.24	0.22
6	LEO	0.38	0.10	0.66	0.70	0.29	0.31	0.70	0.68
6	RLD	0.04	0.37	0.00	0.31	0.20	0.37	0.00	0.29
6	LLD	0.23	0.05	0.00	0.01	0.31	0.03	0.05	0.00
6	RES	0.72	0.50	0.80	0.68	0.61	0.24	0.71	0.37
6	LES	0.51	0.38	0.66	0.57	0.57	0.39	0.71	0.57

TABLE 6.2 R^2 Values Using Predicted Muscle Force of the Models to Predict Percent Muscle Activity for Female Subjects.

		7.5 Nm Torsion				15 Nm Torsion			
Sub	Muscle	MIC-C	MIC-H	SCI-C	SCI-H	MIC-C	MIC-H	SCI-C	SCI-H
7	RRA	0.52	0.18	0.59	0.52	0.17	0.00	0.19	0.03
7	LRA	0.48	0.54	0.73	0.66	0.31	0.24	0.56	0.33
7	REO	0.08	0.34	0.13	0.34	0.06	0.28	0.03	0.19
7	LEO	0.37	0.09	0.65	0.82	0.46	0.18	0.78	0.89
7	RLD	0.00	0.21	0.05	0.14	0.00	0.24	0.10	0.06
7	LLD	0.00	0.05	0.08	0.03	0.20	0.02	0.00	0.00
7	RES	0.69	0.45	0.81	0.63	0.38	0.24	0.44	0.30
7	LES	0.65	0.53	0.76	0.76	0.66	0.47	0.72	0.60
8	RRA	0.49	0.19	0.56	0.55	0.72	0.04	0.74	0.49
8	LRA	0.35	0.38	0.54	0.46	0.43	0.46	0.87	0.63
8	REO	0.52	0.64	0.59	0.77	0.51	0.63	0.40	0.40
8	LEO	0.39	0.13	0.61	0.77	0.34	0.13	0.60	0.70
8	RLD	0.00	0.22	0.03	0.11	0.01	0.15	0.18	0.02
8	LLD	0.14	0.16	0.10	0.18	0.00	0.00	0.03	0.00
8	RES	0.67	0.55	0.82	0.71	0.43	0.14	0.45	0.19
8	LES	0.62	0.53	0.55	0.69	0.68	0.36	0.54	0.45
9	RRA	0.55	0.10	0.59	0.51	0.45	0.02	0.58	0.39
9	LRA	0.50	0.59	0.74	0.70	0.02	0.22	0.04	0.19
9	REO	0.00	0.03	0.01	0.04	0.57	0.54	0.61	0.62
9	LEO	0.29	0.09	0.50	0.56	0.55	0.00	0.49	0.74
9	RLD	0.03	0.05	0.10	0.01	0.00	0.29	0.06	0.08
9	LLD	0.00	0.00	0.02	0.00	0.09	0.01	0.02	0.00
9	RES	0.64	0.80	0.68	0.79	0.63	0.77	0.61	0.78
9	LES	0.83	0.59	0.74	0.83	0.18	0.36	0.09	0.10
10	RRA	0.78	0.26	0.85	0.75	0.42	0.06	0.55	0.47
10	LRA	0.54	0.70	0.77	0.80	0.43	0.61	0.79	0.74
10	REO	0.00	0.01	0.00	0.00	0.33	0.33	0.32	0.22
10	LEO	0.39	0.02	0.62	0.68	0.57	0.00	0.58	0.63
10	RLD	0.01	0.09	0.00	0.10	0.02	0.10	0.26	0.01
10	LLD	0.09	0.06	0.00	0.02	0.12	0.05	0.01	0.00
10	RES	0.30	0.23	0.42	0.35	0.07	0.25	0.07	0.18
10	LES	0.40	0.38	0.47	0.46	0.75	0.40	0.72	0.74
11	RRA	0.02	0.07	0.01	0.01	0.75	0.38	0.83	0.70
11	LRA	0.47	0.66	0.67	0.72	0.38	0.57	0.75	0.69
11	REO	0.49	0.68	0.50	0.73	0.12	0.16	0.06	0.05
11	LEO	0.16	0.01	0.46	0.61	0.41	0.00	0.53	0.88
11	RLD	0.03	0.31	0.00	0.21	0.00	0.10	0.19	0.03
11	LLD	0.18	0.19	0.08	0.23	0.02	0.03	0.00	0.00
11	RES	0.45	0.46	0.48	0.48	0.18	0.43	0.11	0.36
11	LES	0.65	0.48	0.71	0.74	0.35	0.15	0.44	0.25
12	RRA	0.24	0.06	0.26	0.23	0.07	0.00	0.03	0.01
12	LRA	0.83	0.49	0.59	0.58	0.24	0.23	0.63	0.38
12	REO	0.10	0.23	0.12	0.19	0.02	0.00	0.00	0.03
12	LEO	0.43	0.17	0.60	0.62	0.11	0.27	0.43	0.47
12	RLD	0.09	0.07	0.19	0.01	0.08	0.30	0.02	0.21
12	LLD	0.26	0.35	0.12	0.42	0.08	0.00	0.00	0.00
12	RES	0.01	0.07	0.00	0.05	0.46	0.22	0.55	0.30
12	LES	0.05	0.11	0.02	0.08	0.55	0.26	0.58	0.53

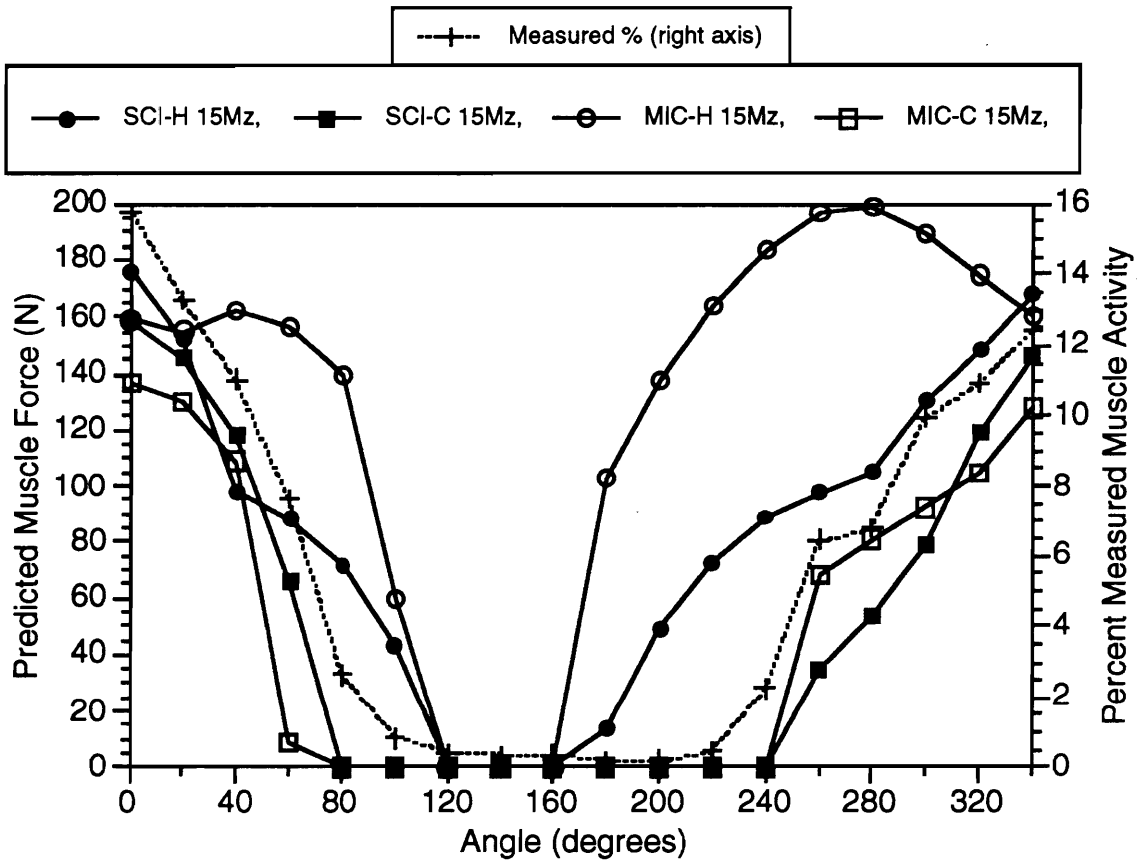

Figure 6.5 Model predictions and actual percent activity for RRA with 15 Nm torsion, Subject 5. Model predictions are in N and use left y-axis, while actual activity is in percent and uses right y-axis.

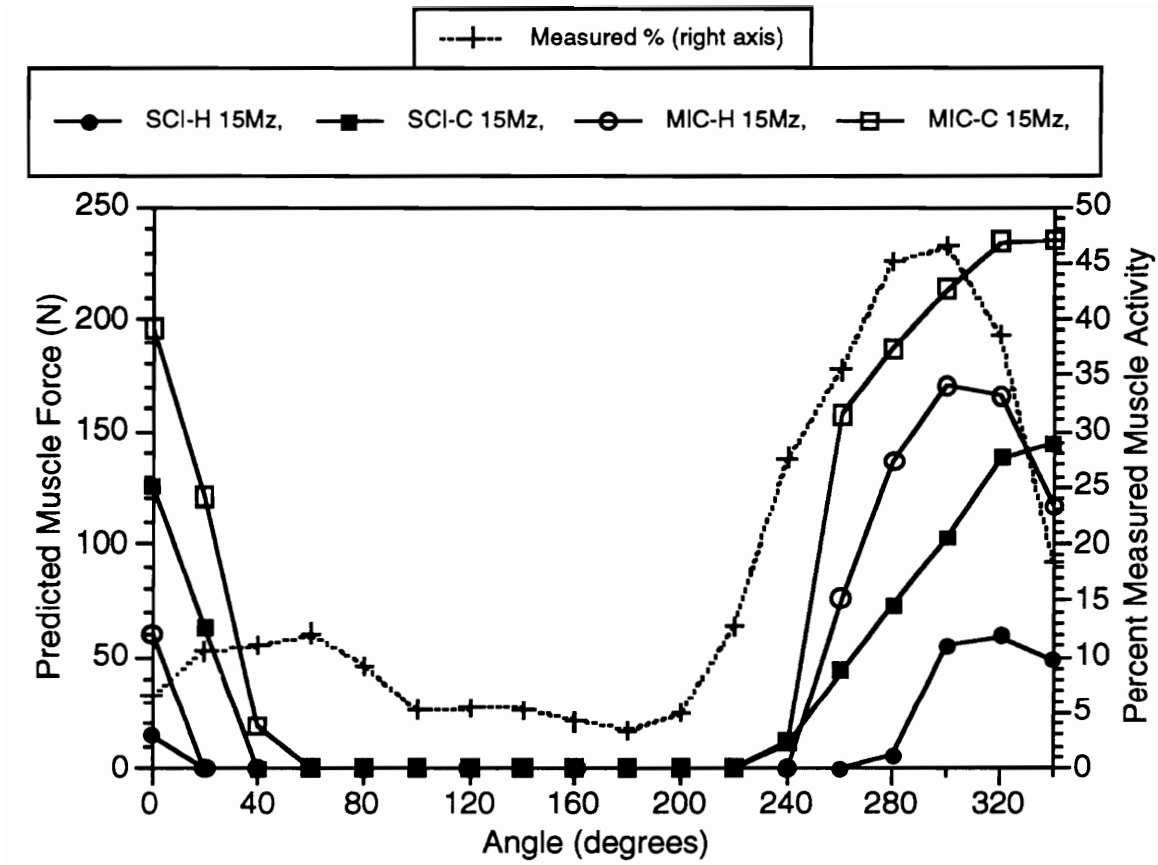

Figure 6.6 Model predictions and actual percent activity for REO with 15 Nm torsion, Subject 5. Model predictions are in N and use left y-axis, while actual activity is in percent and uses right y-axis.

muscle for subject 5 with 15 Nm torsion which contains predictors with R^2 ranging from to 0.30 to 0.70. Figure 6.7 shows the RLD muscle for subject 5 with 15 Nm torsion which contains predictors with R^2 as low as 0.01.

An R^2 value of 0.5 indicated that 50% of the variance in actual muscle activity was accounted for by the muscle force predictions of the models. Table 6.3 lists the number of times each model's forces predicted the percent activity with an R^2 greater than or equal to 0.5 collapsed across torsion moment and muscles. For every subject, the SCI model had the most regression models with R^2 greater than 0.5. For subjects 1, 2, 7, 8, 10, and 12, the SCI with the compilation geometry predicted activity of the most muscles with R^2 of at least 0.5. For subjects 4, 9, and 11, the SCI with the Han et al. (1992) geometry predicted activity of the most muscles with R^2 of at least 0.5. For subjects 3, 5, and 6, both SCI models predicted activity of the same number of muscles with R^2 of at least 0.5.

Table 6.4 lists the number of times each model's forces predicted the percent activity with an R^2 greater than or equal to 0.5 collapsed across subjects. The percent activity of RRA, LRA, LEO, RES, and LES were most often predicted with an R^2 greater than 0.5 (up to 12 times out of 12). The REO was only predicted with an R^2 greater than 0.5, 2 to 5 times. The model/geometry combinations predicted the RLD or LLD activity with an R^2 of at least 0.5 for only 1 case across all subjects and models.

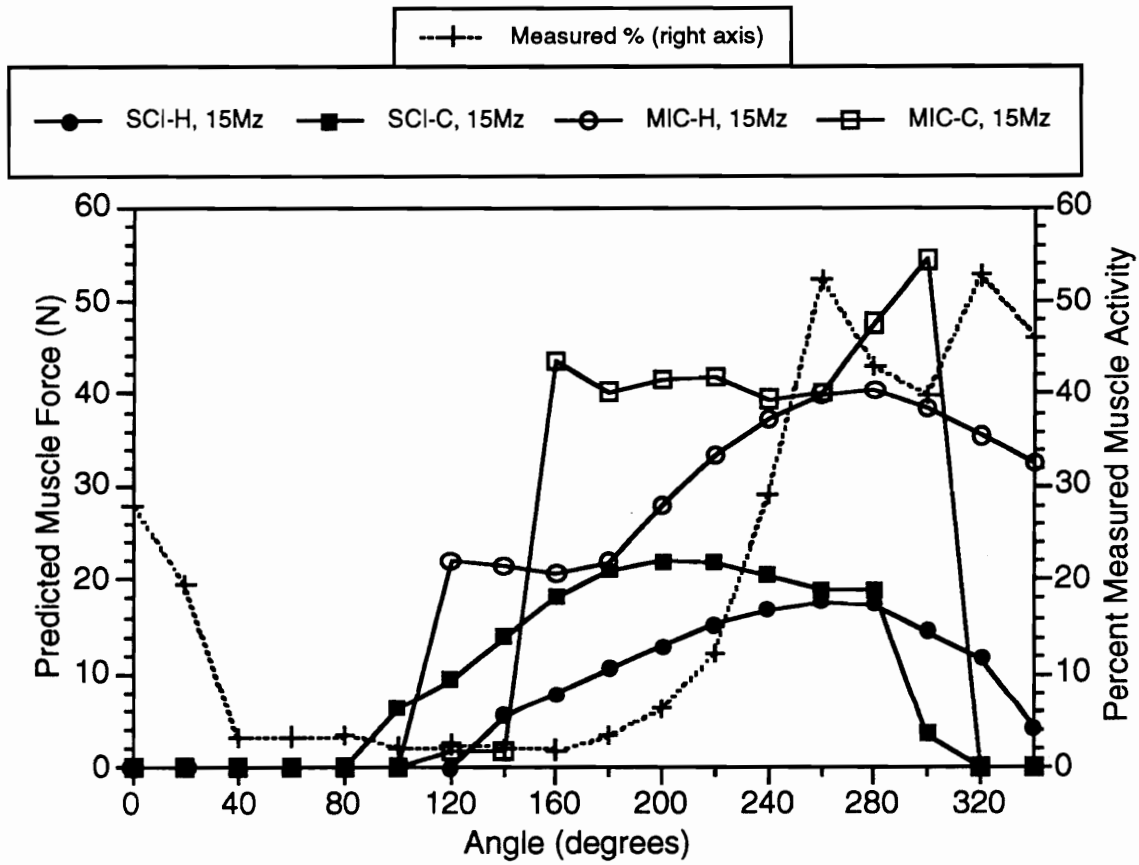

Figure 6.7 Model predictions and actual percent activity for RLD with 15 Nm torsion, Subject 5. Model predictions are in N and use left y-axis, while actual activity is in percent and uses right y-axis.

TABLE 6.3 Number of Times Out of 16 Each Model's Forces Predicted Percent Activity with an R^2 Greater Than or Equal to 0.5, Collapsed Across Torsion Moments

Subject	MIC-C	MIC-H	SCI-C	SCI-H
1	7	4	10	9
2	6	5	9	7
3	6	4	10	10
4	4	4	5	7
5	9	8	10	10
6	6	3	9	9
7	4	2	8	7
8	6	4	10	7
9	6	5	7	8
10	4	2	7	6
11	2	3	6	7
12	2	0	5	3

TABLE 6.4 Number of Times Out of 12 Each Model's Forces Predicted Percent Activity with an R^2 Greater Than or Equal to 0.5, Collapsed Across Subjects.

	7.5 Nm Torsion				15 Nm Torsion			
Muscle	MIC-C	MIC-H	SCI-C	SCI-H	MIC-C	MIC-H	SCI-C	SCI-H
RRA	9	0	10	10	6	0	9	5
LRA	8	10	12	11	2	7	11	9
REO	2	5	3	3	3	4	2	2
LEO	2	0	8	12	2	0	9	11
RLD	0	0	0	0	0	1	0	0
LLD	0	0	0	0	0	0	0	0
RES	7	5	8	7	4	3	7	4
LES	8	5	8	8	9	4	9	8

6.3.1 ANOVA of R^2 for 10-Muscle Models

The R^2 values were analyzed using a five-way mixed-factor Analysis of Variance (ANOVA). The within factors were muscle with eight levels and torsion moment with two levels. The between factors were geometry with two levels - compilation and Han, model with two levels - MIC and SCI, and gender with two levels. The ANOVA results for the R^2 values are shown in Table 6.5. The results indicated significance ($p<0.05$) for five main effects, five two-way interactions, and one three-way interaction.

The significant main effects indicated males were predicted better than females, 0.44 and 0.33 mean R^2 respectively. The SCI model, mean R^2 equal

TABLE 6.5 ANOVA Results for R^2 Values of Actual Activity Predicted by Model Forces.

Source	df	SS	MS	F-Value	P-Value	Greenhouse-Geisser
Between						
Geo	1	0.3012	0.3012	4.30	0.0445	
Mdl	1	2.0264	2.0264	28.96	0.0001	
Gen	1	2.1368	2.1368	30.53	0.0001	
Geo*Mdl	1	0.1707	0.1707	2.44	0.1262	
Geo*Gen	1	0.0197	0.0197	0.28	0.5986	
Mdl*Gen	1	0.0049	0.0049	0.07	0.7937	
Geo*Mdl*Gen	1	0.0007	0.0007	0.01	0.9233	
S/Geo,Mdl,Gen	40	2.7994	0.0700			
Within						
Mscl	7	25.8235	3.6891	117.40	0.0001	0.0001
Mscl*Geo	7	2.1053	0.3008	9.57	0.0001	0.0001
Mscl*Mdl	7	4.2260	0.6037	19.21	0.0001	0.0001
Mscl*Gen	7	1.0178	0.1454	4.63	0.0001	0.0009
Mscl*Geo*Mdl	7	1.5477	0.2211	7.04	0.0001	0.0001
Mscl*Geo*Gen	7	0.2056	0.0294	0.93	0.4800	0.4524
Mscl*Mdl*Gen	7	0.0939	0.0134	0.43	0.8852	0.8092
Mscl*Geo*Mdl*Gen	7	0.0749	0.0107	0.34	0.9348	0.8692
Mscl*S/Geo,Mdl,Gen	280	8.7981	0.0314			
Mz	1	0.2856	0.2856	15.90	0.0003	0.0003
Mz*Geo	1	0.1048	0.1048	5.83	0.0204	0.0204
Mz*Mdl	1	0.0191	0.0191	1.06	0.3087	0.3087
Mz*Gen	1	0.0419	0.0419	2.33	0.1348	0.1348
Mz*Geo*Mdl	1	0.0251	0.0251	1.40	0.2442	0.2442
Mz*Geo*Gen	1	0.0004	0.0004	0.02	0.8830	0.8830
Mz*Mdl*Gen	1	0.0005	0.0005	0.03	0.8746	0.8746
Mz*Geo*Mdl*Gen	1	0.0011	0.0011	0.06	0.8077	0.8077
Mz*S/Geo,Mdl,Gen	40	0.7186	0.0180			
Mscl*Mz	7	0.7837	0.1120	2.89	0.0062	0.0327
Mscl*Mz*Geo	7	0.0709	0.0101	0.26	0.9680	0.8717
Mscl*Mz*Mdl	7	0.1204	0.0172	0.44	0.8735	0.7417
Mscl*Mz*Gen	7	0.2927	0.0418	1.08	0.3758	0.3632
Mscl*Mz*Geo*Mdl	7	0.0214	0.0031	0.08	0.9992	0.9789
Mscl*Mz*Geo*Gen	7	0.0420	0.0060	0.16	0.9932	0.9401
Mscl*Mz*Mdl*Gen	7	0.0188	0.0027	0.07	0.9995	0.9829
Mscl*Mz*Geo*Mdl*Gen	7	0.0358	0.0051	0.13	0.9958	0.9530
Mscl*Mz*S/Geo,Mdl,Gen	280	10.8324	0.0387			

0.44, predicted muscle activity better than the MIC model, as indicated by the mean R^2 being equal to 0.33. The compilation geometry had a higher mean R^2 equal 0.41 than the Han geometry, mean R^2 equal 0.37. The higher torsion trials of 15 Nm were not predicted as well by the models as lower torsion trials, 0.37 and 0.40 mean R^2 respectively. For the muscle main effect, a Least Significant Difference post-hoc test was used to determine significant differences. The LRA was predicted significantly higher than all muscles (mean R^2 0.62), followed by the LES muscle (mean R^2 0.53), followed by the RRA, RES, and LEO muscles which were not significantly different from each other (mean R^2 of 0.48, 0.48 and 0.46, respectively), followed by the REO muscle, (mean R^2 0.32), and finally the RLD and LLD muscles were significantly worse than all other muscles but not different from each other (mean R^2 of 0.12 and 0.08, respectively).

The Muscle x Gender interaction is shown in Figure 6.8. Male muscle activity was predicted better for the RRA, LRA, REO, LES, and RES by 8 to 25 %. In females, no muscles were predicted better.

The Muscle x Geometry interaction is shown in Figure 6.9. The compilation geometry predicts the activity of the RRA, LES, and RES better than the Han et al. geometry by 8 to 26 %. The RLD was predicted better by the Han et al. geometry, but overall R^2 was low, 0.06 to 0.18.

The Muscle x Model interaction is shown in Figure 6.10. The SCI model predicted the activity of the RRA, LRA, LEO, LES, and RES better than the MIC model by 7 to 42 %. The five muscles predicted better by the SCI model also

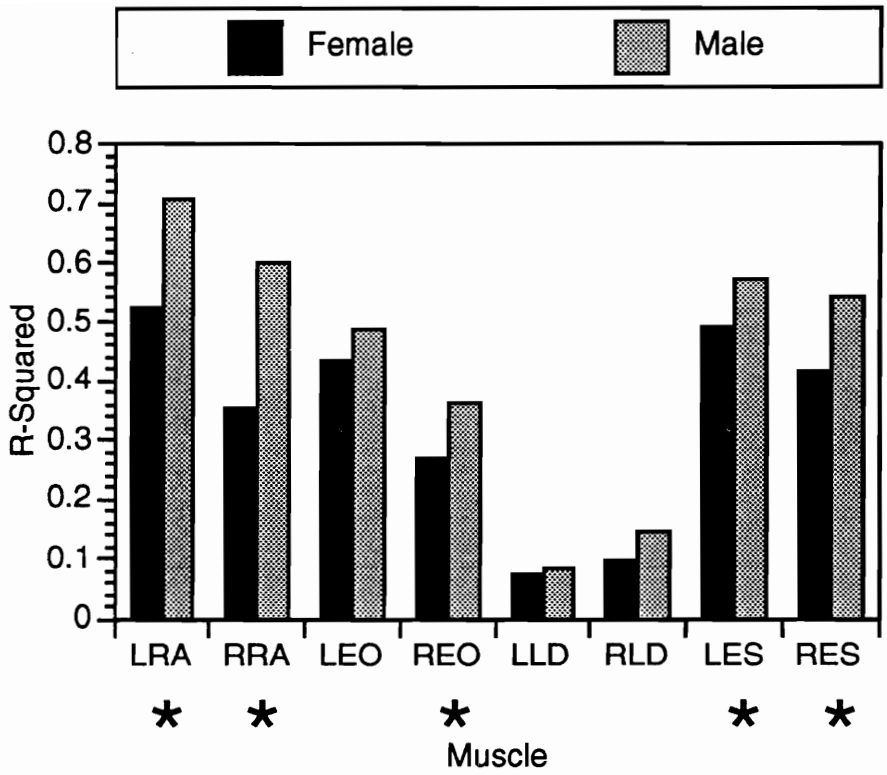

Figure 6.8 Muscle x Gender interaction for ANOVA of R^2 for 10-muscle Models. Asterisks below muscles indicate significant differences between gender using Least Significant Difference post-hoc test.

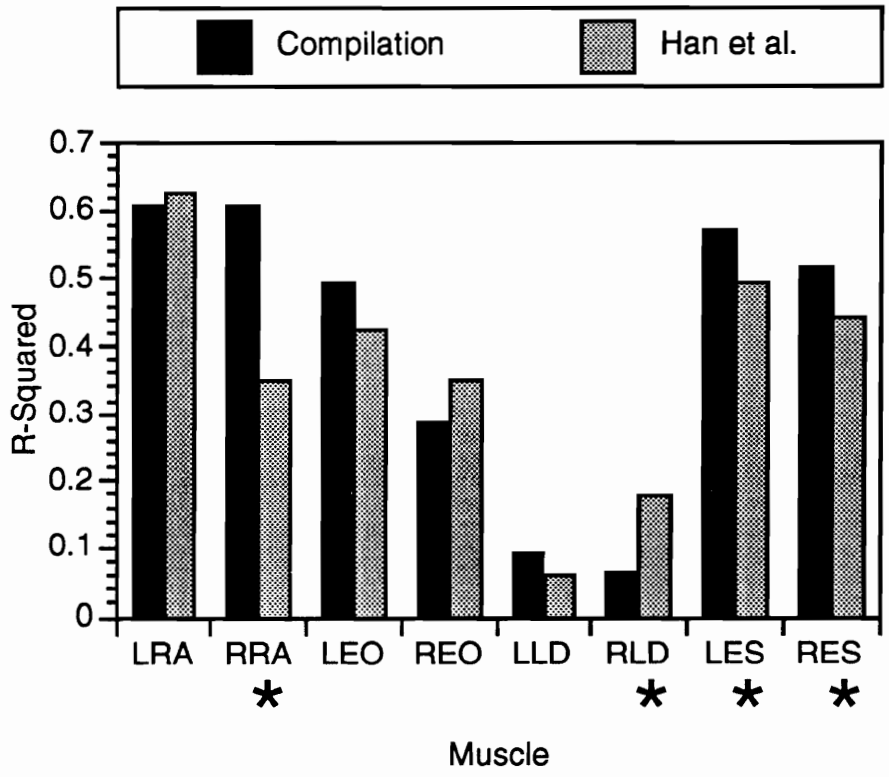

Figure 6.9 Muscle x Geometry interaction for ANOVA of R^2 for 10-muscle Models. Asterisks below muscles indicate significant differences between the geometries using Least Significant Difference post-hoc test.

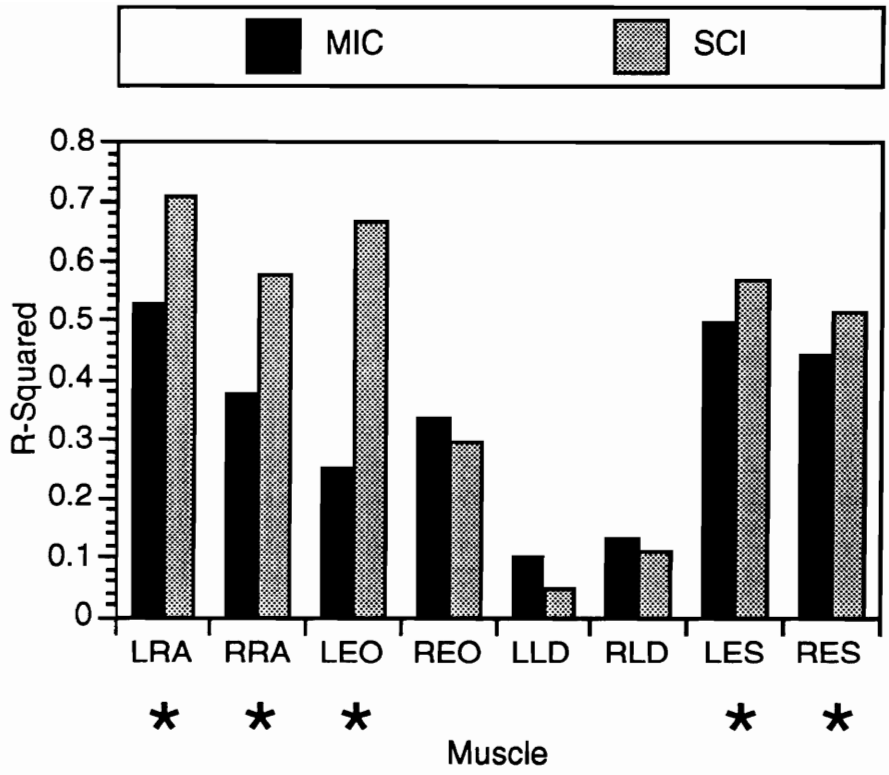

Figure 6.10 Muscle x Model interaction for ANOVA of R^2 for 10-muscle Models. Asterisks below muscles indicate significant differences between the models using Least Significant Difference post-hoc test.

had the five highest mean R^2 values. No muscle was predicted better by the MIC model.

The Muscle x Torsion interaction is shown in Figure 6.11. At the lower torsion level of 7.5 Nm, the activity of the RRA, LRA, and RES were predicted better than for torsion of 15 Nm by 9 to 15 %.

The Torsion x Geometry interaction is shown in Figure 6.12. The predictions using the compilation geometry did not significantly differ between 7.5 and 15 Nm torsions. The predictions using the Han et al. geometry significantly decreased from 7.5 to 15 Nm torsion by 6%.

The Muscle x Geometry x Model interaction is shown in Figure 6.13. For each muscle, significant differences between the four model and geometry combinations were identified. The SCI-C model predicted the activity of the LRA, RRA, LLD, LES, and RES better than or equal to the other models; the SCI-C predicted the LEO with mean R^2 equal 0.61 worse only than the SCI-H model and predicted the REO and RLD worse than only the MIC-H model. The SCI-H model predicted the activity of the LRA, LEO, REO, LLD, RLD, LES, and RES better than or equal to the other models; the SCI-H predicted the RRA with mean R^2 equal 0.53 worse only than the SCI-C.

6.3.2 ANOVA of R^2 for Comparing 10- Versus 18-Muscle Models

When the models included 18 muscles instead of 10, the erector spinae was divided into the multifidus, longissimus, and iliocostalis. To compare the 18-muscle formulation with the 10-muscle formulation, the actual activity of six muscles were included in the analysis. When the models included 18 muscles

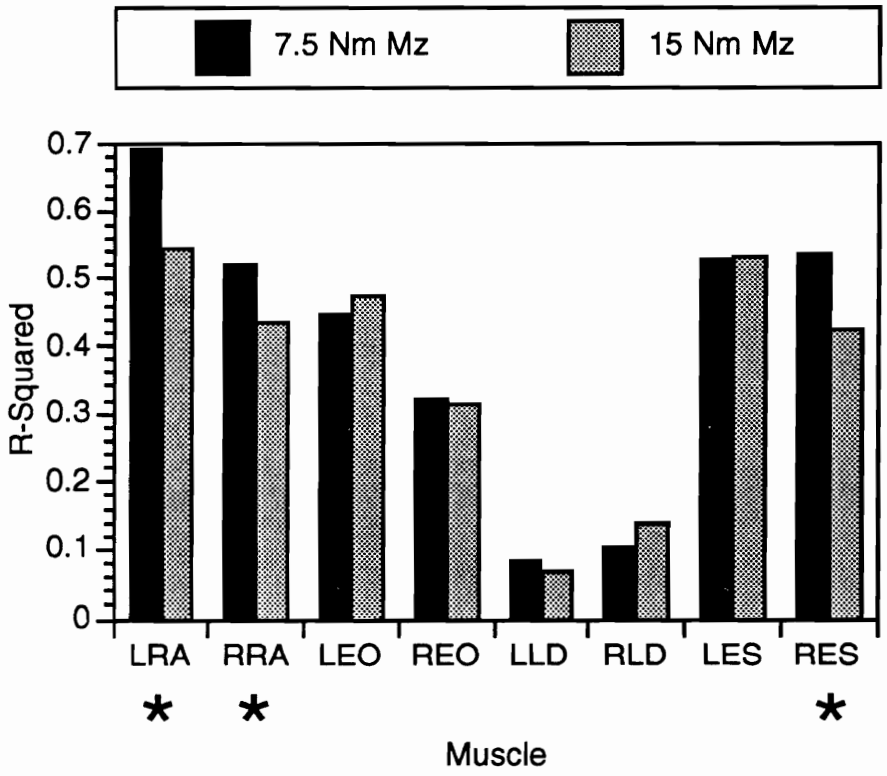

Figure 6.11 Muscle x Torsion interaction for ANOVA of R^2 for 10-muscle Models. Asterisks below muscles indicate significant differences between torsion levels using Least Significant Difference post-hoc test.

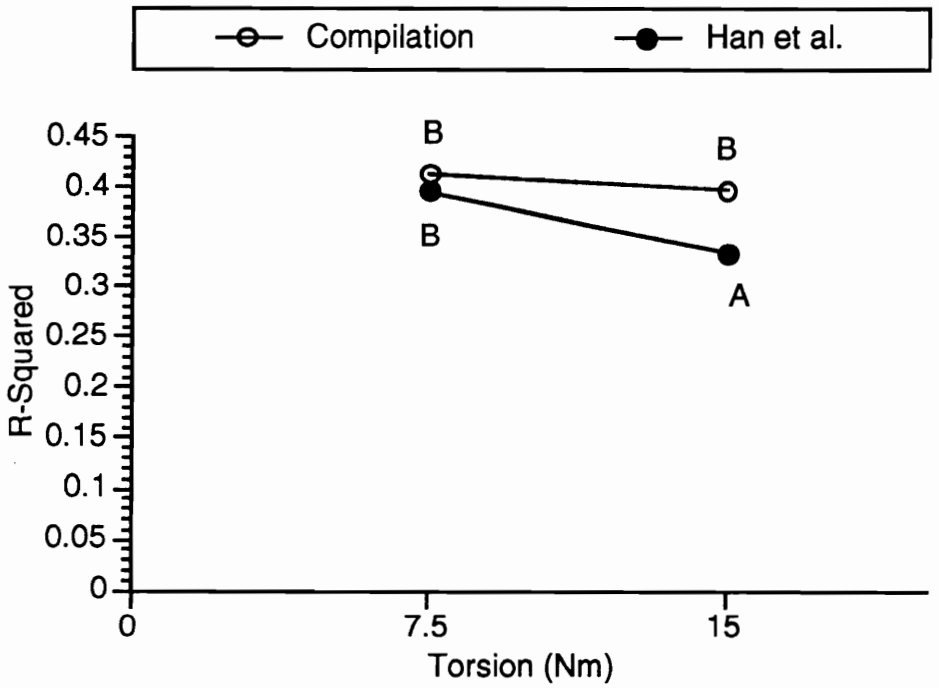

Figure 6.12 Torsion x Geometry interaction for ANOVA of R^2 for 10-muscle Models. Means marked with same letters are not significantly different using Least Significant Difference post-hoc test.

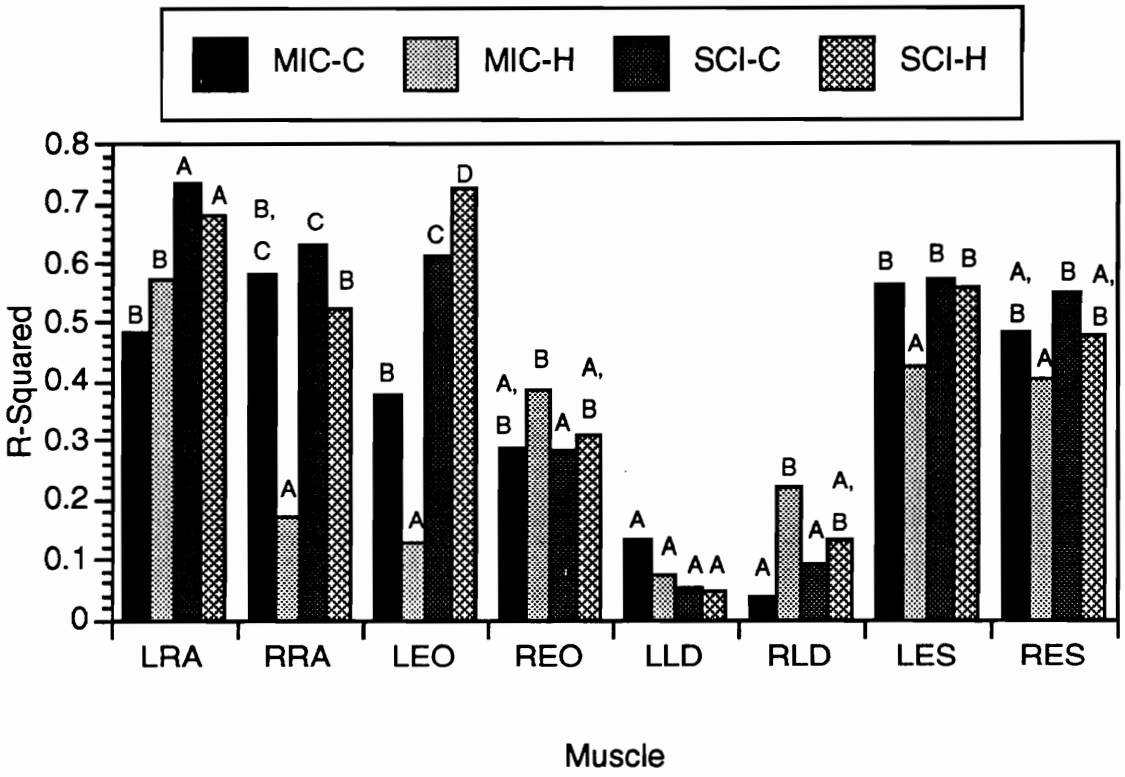

Figure 6.13 Muscle x Geometry x Model interaction for ANOVA of R^2 for 10-muscle models. Means marked with same letters within each muscle are not significantly different using Least Significant Difference post-hoc test.

instead of 10, the erector spinae was divided into the multifidus, longissimus, and iliocostalis. The LRA, RRA, LEO, REO, LLD, and, RLD were the muscles whose geometries did not change from 10- to 18-muscle formulations and were measured experimentally. The analysis reported in this section differs from the previous one because six muscles were included in the ANOVA instead of eight as well as adding the number of muscles factor.

The R^2 values were analyzed using a six-way mixed-factor Analysis of Variance (ANOVA). The within factors were muscle with six levels (LRA, RRA, LEO, REO, LLD, and, RLD) and torsion moment with two levels. The between factors were number of muscles with two levels - 10 and 18, geometry with two levels - compilation and Han, model with two levels - MIC and SCI, and gender with two levels. The ANOVA results for the R^2 values indicated significance ($p<0.05$) for three interactions containing the number of muscles factor. Only interactions containing the number of muscles factor were considered further. The effects of the other factors were analyzed and reported in the previous Section 6.3.1.

The Muscle x Number of Muscles interaction is shown in Figure 6.14. The 10-muscle models predicted the activity of the LEO and REO better than the 18-muscle models by about 8%. The 18-muscle models predicted the LRA better than the 10-muscle model by 5%. The RRA, LLD, and RLD were predicted equally well by both 10- and 18-muscle models.

The Muscle x Geometry x Number of muscles interaction is shown in Figure 6.15. For the LRA and LLD, the geometry and number of muscle combinations predicted similarly well. For the RRA and RLD, number of

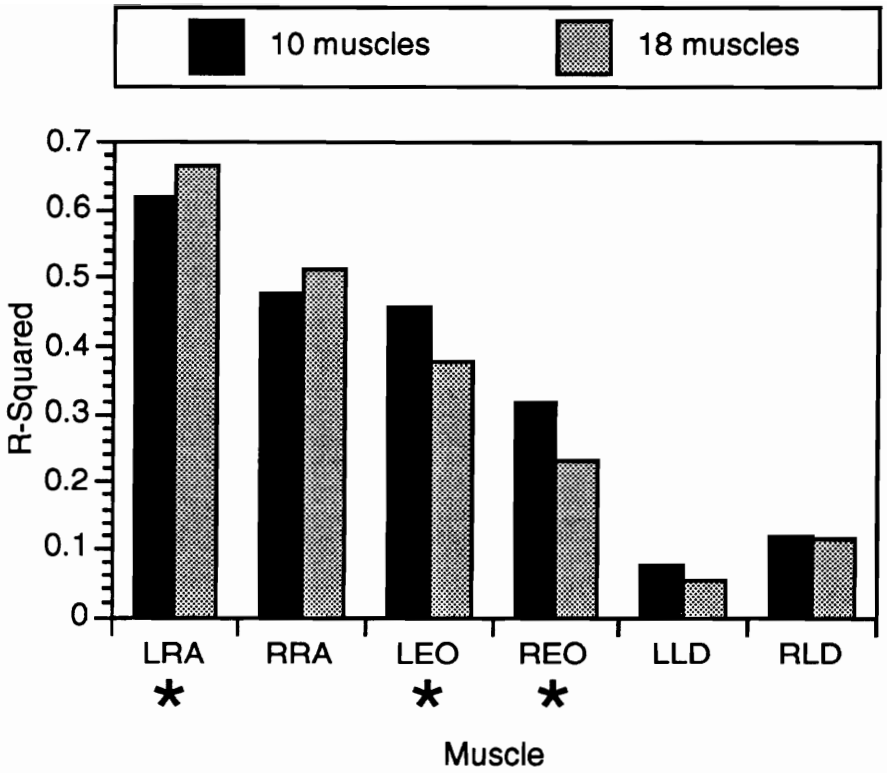

Figure 6.14 Muscle x Number of Muscles interaction for ANOVA of R^2 for 10- versus 18-muscle models. Asterisks below muscles indicate significant differences between number of muscles using Least Significant Difference post-hoc tests.

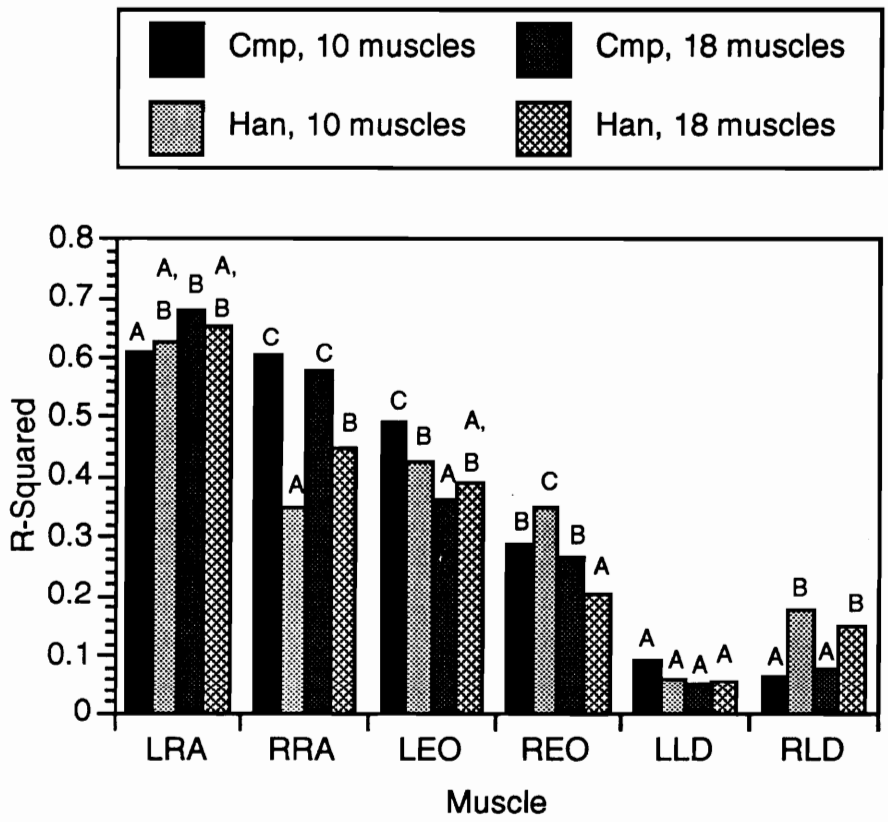

Figure 6.15 Muscle x Geometry x Number of Muscles interaction for ANOVA of R^2 for 10- versus 18-muscle models. Means marked with same letters within each muscle are not significantly different using Least Significant Difference post-hoc tests.

muscles did not have a large effect, the compilation geometry resulted in better predictions for the RRA and Han et al. better for the RLD. For the LEO and REO, the 10-muscle models generally resulted in better predictions.

The Muscle x Model x Geometry x Number of Muscles interaction is shown in Figure 6.16. Including 18 muscles in the models resulted in significantly better predictions for the MIC-C predicting the LRA and MIC-H predicting the RRA. Neither of the MIC-C predicting the LRA or MIC-H predicting the RRA cases were the highest predictions for the respective muscles. Including 10 muscles in the models resulted in significantly better predictions for the MIC-C predicting the LEO and MIC-H predicting the REO. Although the MIC-C predicting the LEO had lower mean R^2 values, the MIC-H predicting the REO (with 10 muscles) was the highest R^2 for the REO. For the LLD and RLD, the number of muscles did not result in any significant difference across the model combinations.

6.4 Hand Versus Harness Loading

The six male participants in this study completed static physical exertions in response to external loads which were applied using two methods: loads attached to a harness and loads held with the hands. The moments created at the L3/L4 disc were equivalent for both methods across 12 different loading conditions, 6 angles of a 30 Nm resultant M_x-M_y moment at two levels of M_z. The percent muscle activity was analyzed using a four-way within-subjects Analysis of Variance (ANOVA). The four within-subjects factors were muscle

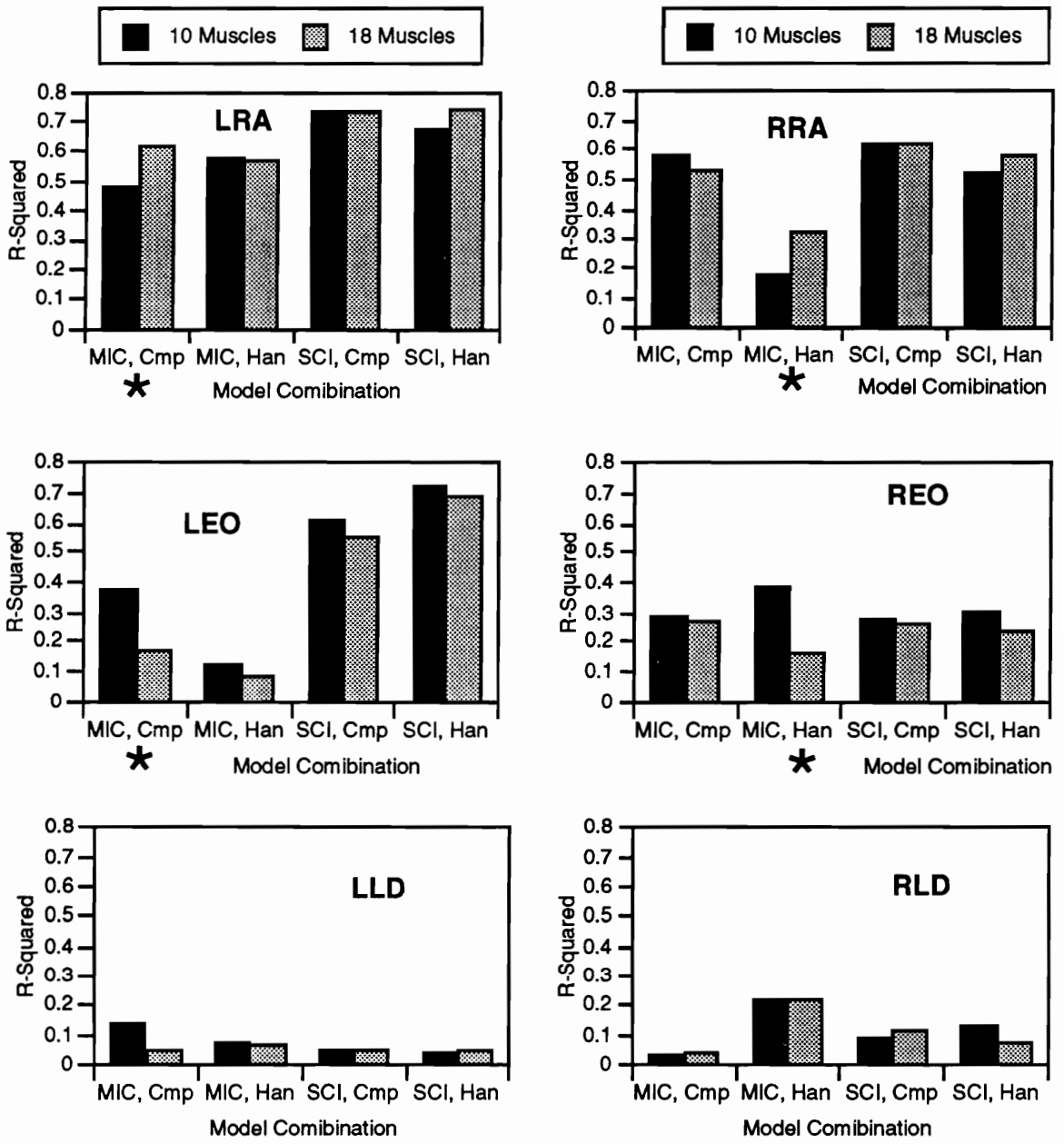

Figure 6.16 Muscle x Model x Geometry x Number of Muscles interaction for ANOVA of R^2 for 10- versus 18-muscle models. Asterisks below model combinations indicate significant differences between number of muscles using Least Significant Difference post-hoc tests.

with eight levels, angle of load with six levels, torsion moment with two levels, and apparatus with two levels - hand and harness.

The ANOVA results for the hand versus harness loading are shown in Table 6.6. The results indicated significance ($p<0.05$) using the Greenhouse-Geisser correction for three main effects, two two-way interactions, and one three-way interaction. The effects and interactions of interest were those including the apparatus factor. The apparatus main effect indicated that hand loading led to significantly higher mean activity than harness loading, 16.8 to 13.6%.

The Muscle x Apparatus interaction is shown in Figure 6.17. The LRA, RLD, and LLD muscles had significantly higher percent activity for the hand loading trials than the harness loading trials by 4 to 14%. The remaining five muscles had no significant differences in mean muscle activity between hand and harness loading.

The Angle x Muscle x Apparatus interaction is shown in Figure 6.18. The importance of this interaction was to identify at each level of angle and muscle if a significant difference between harness and hand loading existed. Table 6.7 lists the conditions in which a significant difference between hand and harness loading existed, using a Least Significant Difference post-hoc test. Hand loading resulted in higher mean percent activity for all significant differences except one. For the RRA, hand loading led to 13% higher activity at 0 degrees, and for the LRA hand loading led to about 17 and 8 percent higher activity at 0 and 60 degrees, respectively. At 60 and 120 degrees, the LEO had higher activity for hand loading by about 10 and 24 %, but at 300 degrees harness

TABLE 6.6 ANOVA Results for Hand Versus Harness Loading

Source	df	SS	MS	F-Value	P-Value	Greenhouse-Geisser
Between						
S	5	11541.3	2308.3			
Within						
Ang	5	2991.6	598.3	4.84	0.0031	0.0433
Ang*S	25	3089.1	123.6			
Mz	1	1379.6	1379.6	4.82	0.0797	0.0797
Mz*S	5	1432.6	286.5			
App	1	2881.1	2881.1	11.62	0.0191	0.0191
App*S	5	1239.9	248.0			
Mscl	7	20649.7	2950.0	5.63	0.0002	0.0072
Mscl*S	35	18354.5	524.4			
Ang*Mz	5	738.2	147.6	0.60	0.7014	0.5055
Ang*Mz*S	25	6167.0	246.7			
Ang*App	5	3831.6	766.3	4.23	0.0064	0.0683
Ang*App*S	25	4530.3	181.2			
Mz*App	1	184.7	184.7	4.87	0.0785	0.0785
Mz*App*S	5	189.8	38.0			
Ang*Mscl	35	50896.9	1454.2	17.67	0.0001	0.0001
Ang*Mscl*S	175	14400.3	82.3			
Mz*Mscl	7	903.9	129.1	1.61	0.1655	0.2437
Mz*Mscl*S	35	2809.4	80.3			
App*Mscl	7	6594.6	942.1	10.04	0.0001	0.0015
App*Mscl*S	35	3285.1	93.9			
Ang*Mz*App	5	933.3	186.7	2.35	0.0706	0.1441
Ang*Mz*App*S	25	1987.6	79.5			
Ang*Mz*Mscl	35	1713.1	48.9	1.37	0.0952	0.2837
Ang*Mz*Mscl*S	175	6235.5	35.6			
Ang*App*Mscl	35	16939.2	484.0	4.90	0.0001	0.0463
Ang*App*Mscl*S	175	17298.5	98.8			
Mz*App*Mscl	7	277.9	39.7	1.28	0.2871	0.3180
Mz*App*Mscl*S	35	1082.9	30.9			
Ang*Mz*App*Mscl	35	2747.1	78.5	2.25	0.0003	0.1516
Ang*Mz*App*Mscl*S	175	6097.8	34.8			

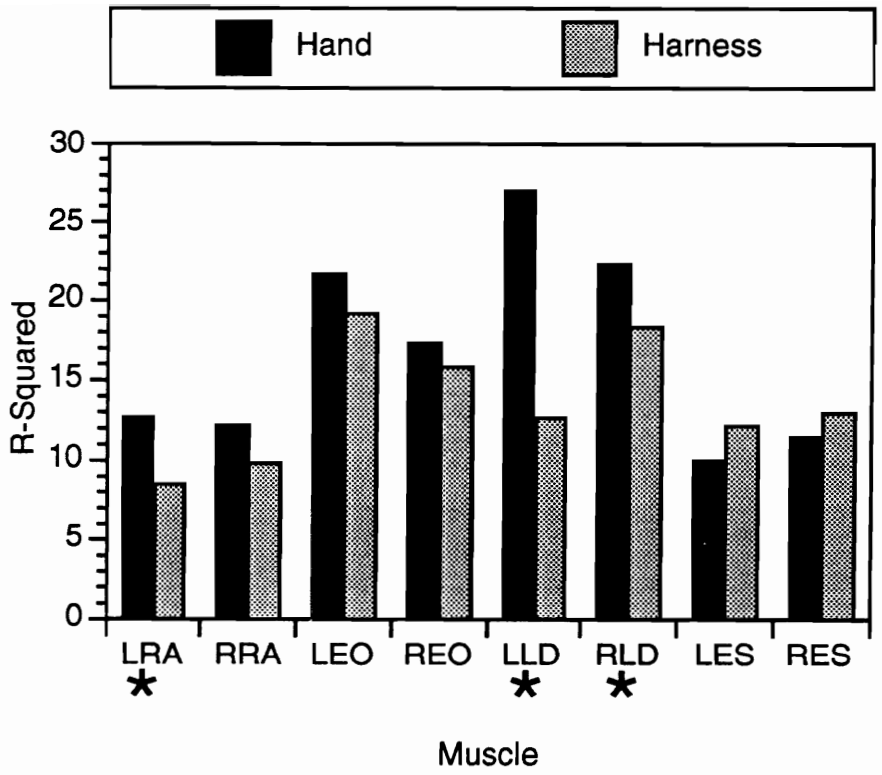

Figure 6.17 Muscle x Apparatus interaction for ANOVA of hand versus harness loading. Asterisks below muscles indicate significant differences between apparatus using Least Significant Difference post-hoc tests.

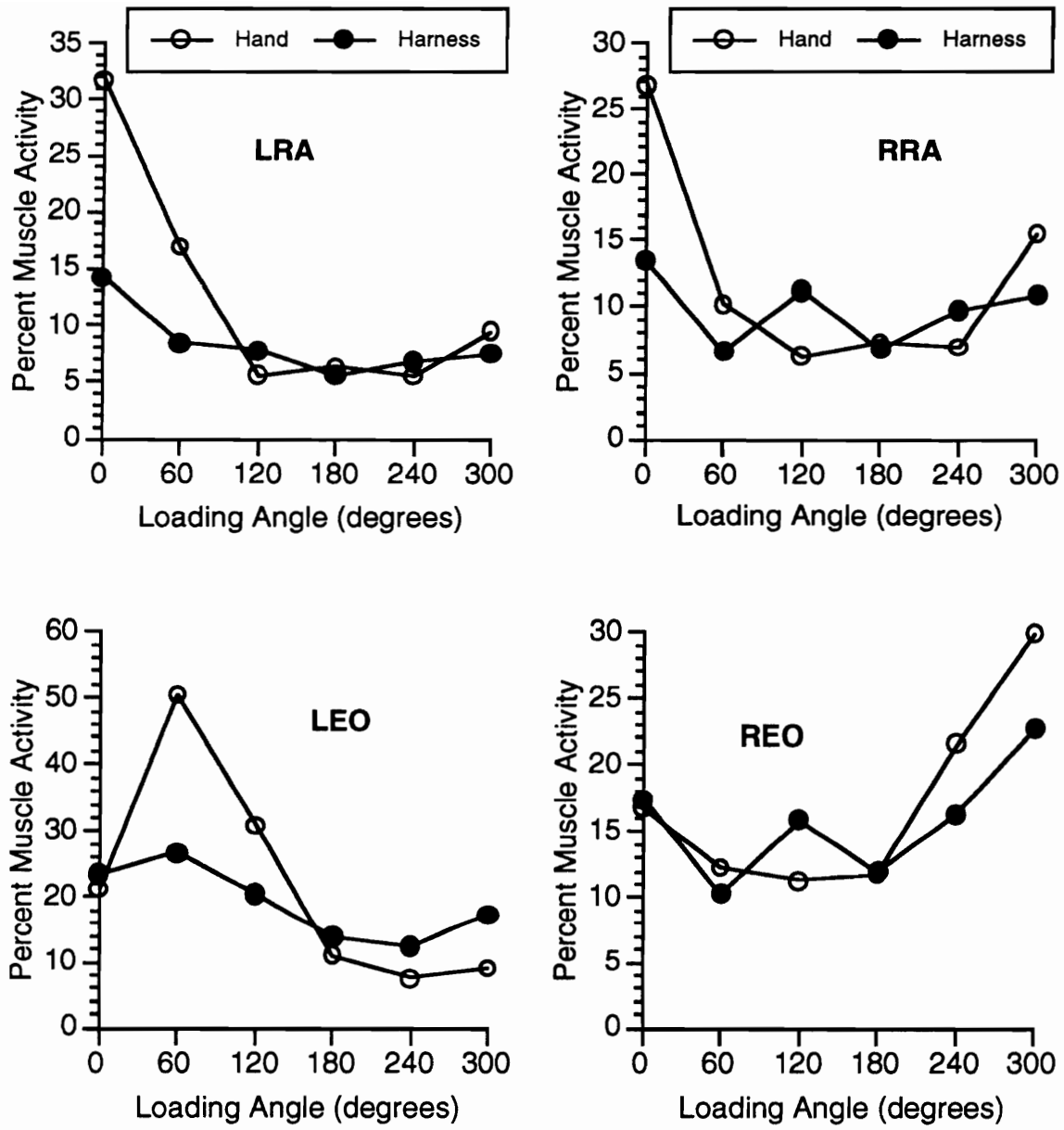

Figure 6.18 Angle x Muscle x Apparatus interaction for ANOVA of hand versus harness loading. Significant differences between apparatus are shown in Table 6.7.

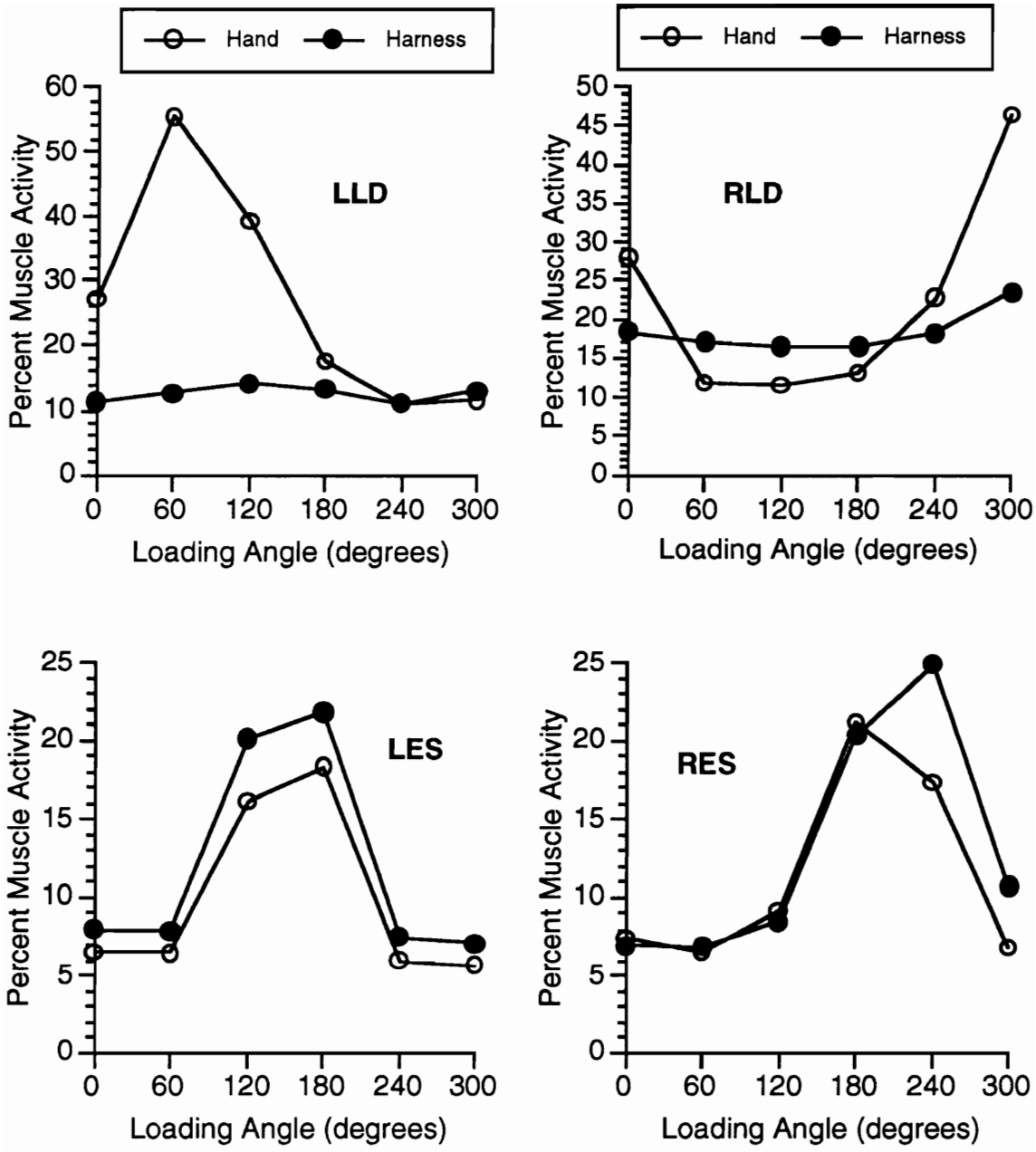

Figure 6.18 (continued)

TABLE 6.7 Significant differences between hand and harness loading at each angle and muscle condition using Least Significant Difference post-hoc tests.

Muscle	Angle Hand > Harness (degrees)	Angle Hand < Harness (degrees)
RRA	0	none
LRA	0, 60	none
REO	none	none
LEO	60, 120	300
RLD	0, 300	none
LLD	0, 60, 120	none
RES	none	none
LES	none	none

loading resulted in 8% higher mean muscle activity. The RLD and LLD had large increases in muscle activity during hand loading. At 0, 60, 120 degrees, LLD had about 16, 43, and 25% higher activity for hand loading, and at 0 and 300 degrees the RLD had about 9 and 23% higher activity for hand loading. The REO, LES, and RES had no significant differences in percent activity between hand and harness loading at any angles.

7. DISCUSSION

A computer simulation conducted to determine the effects of different inputs into optimization-based trunk biomechanical models was reported in Chapter 4. Two optimization models, the MIC and SCI, were included in the investigation. The number of muscles included in the development of the models was varied as well as the geometric parameters of the muscles. The inputs to trunk optimization models affected the prediction of muscle activity/inactivity for equal external loads.

The method used in this study to empirically measure human trunk muscle performance during static exertions to resist external loads was discussed in Chapter 5. External loads were selected so that the varying models and inputs predicted activity of the muscles differently. Chapter 6 reported the results of human muscle activity during the exertions compared to muscle predictions to measure the appropriateness of the models and associated inputs. This chapter discusses the implications of the experimental method, analysis, and results of the data collected from the experiment.

7.1 Impact of Changing Models and Muscle Inputs

The results of the computer simulations indicated that the choice of model, muscle geometry, and number of muscles had a significant affect on the predicted muscle forces. Figures 4.5 - 4.18, shown previously, indicated the differences in predicted force magnitudes as the model, muscle geometry, and number of muscles changed. Hughes (1995) pointed out that the differences in predictions due to changes in models may be due to differences in the way

large muscle intensities are penalized. The SCI model penalizes large muscle intensities by generating large objective function values. Synergistic load sharing between muscles is predicted to lower the objective function. However, muscles with shorter moment arms are recruited, increasing the force to resist external moments. Hughes (1995) went on to point out that the MIC model forces even more load sharing between muscles by requiring the lowest possible intensity. Using the lowest possible intensity increases the predicted muscle forces. The use of two different models partially accounted for the differences in predicted muscle forces, but varying muscle geometry and number of muscles also accounted for different muscle forces.

The choice of muscle geometry also created differences in muscle force predictions. Two major differences existed between the two muscle geometry sets. First, the line of action for the erector spinae differed in direction between the geometry sets. For the Han et al. geometry, the erector spinae acted toward the spinal disc in the sagittal plane and away from the disc in the frontal plane. For the compilation geometry, the erector spinae acted away from the spinal disc in the sagittal plane and toward the disc in the frontal plane. Second, the cross-sectional areas for all muscles were smaller for the Han et al. muscle set. The erector spinae, rectus abdominus, internal obliques, external obliques, and latissimus dorsi were 74, 71, 34, 30, and 24 percent smaller, respectively for the Han et al. geometry. Of particular interest was the dis-proportionate percent reduction for the obliques and latissimus dorsi.

The changes in line of action possibly caused changes in muscle force prediction as the torsion moment increased from 0 to 30 Nm. Using the Han et

al. geometry, the LES counteracted the external moment, but for the compilation geometry the LES added to the external torsion. Therefore, as shown previously in Figure 4.5, the LES muscle was predicted with increasingly larger forces by both the MIC and SCI models with the Han et al. geometry because the LES resisted the external torsion.

The lower cross-sectional areas of the oblique muscles with the Han et al. geometry was a possible cause for the differences in muscle force predictions, as well. If equal forces were predicted for the oblique muscle, but the cross-sectional area was different, then the intensity predicted for the oblique muscle changed. The differences in oblique forces shown in Figures 4.7 and 4.8 do not differ drastically within the same model having different geometries. The differences in force predictions of the obliques were largely due to model differences. However, when the Han et al. geometry was used the intensity for equal force predictions was higher. Therefore, when the MIC model was used the minimum intensity for a feasible solution will be higher for the Han et al. geometry then the compilation geometry.

Since the obliques have a large torsion generating component, they were recruited more as the external torsion increased. The LEO and RIO were predicted to increase in force from 0 to 30 Nm torsion (the REO and LIO decreased). As the forces for the LEO and RIO increased, the MIC model generated a higher minimum intensity for the LEO and RIO to counteract the torsion particularly with the Han et al. geometry. The higher minimum intensity allowed the MIC model to allocate more force to muscles with large moment arms used to counteract other moments. For example, the erector spinae has a

larger moment arm than the latissimus dorsi to counteract external flexion moments. Figure 4.5 shows that the RES was predicted with higher force for the MIC model with Han et al. geometry than the MIC model with compilation geometry as torsion increased. Figure 4.6 shows that since LES was predicted with higher forces due to higher intensities, less force was allocated to the LLD and RLD for the MIC model with Han et al. geometry than the MIC model with compilation geometry. Conversely, lower intensities with the compilation geometry led to more synergistic activity in the LES, RES, LLD, and RLD for the MIC model. Generally higher forces were predicted with the MIC model with compilation geometry for the LLD and RLD than with the MIC model with Han et al. geometry.

Changing the number of muscles input into the models can have an effect on the muscle force predictions, as well. In the current study, the 10 muscle model was expanded to 18 muscles by adding the psoas and quadratus lumborum and dividing the erector spinae into three components. Adding the psoas and quadratus lumborum allowed for more predicted synergistic muscle activity. The multifidus, longissimus, and iliocostalis (components of the erector spinae) had different direction vectors from each other and the erector spinae. Different direction vectors led to the recruitment of parts of the erector spinae to resist external moments that the grouped erector spinae would not resist. For example, with the Han et al. geometry, the grouped left erector spinae counteracted a external counter-clockwise torsion moment. However, when the erector spinae was divided, not all of its components resisted the same external moments as the grouped line of action.

The changes in muscle force predictions were a combination of the model used and differences in muscle geometry sets. A single factor did not account for the differences. Implementation of an optimization model to analyze industrial tasks required that a model, muscle geometry set, and number of muscle be selected.

7.2 Effect of Models and Muscle Inputs on Compression Prediction

Hughes (1995) showed that the MIC model led to the highest prediction of compression forces. He used the compilation geometry with 10 muscle input into the model. Hughes (1995) concluded that job analysis based on the MIC model led to conservative estimates of spinal compression. Figure 4.19, shown previously, indicated that higher predicted compression forces were also predicted when the Han et al. geometry was used instead of the compilation geometry. Higher compression forces might be caused by the disproportionate changes in oblique area discussed in the previous section. Another possible explanation is the generally shorter moment arms for the Han et al. geometry than the compilation geometry. Proportional shorter moment arms will lead to higher muscle force prediction to maintain equal moments.

In general, the highest and therefore most conservative estimates of compression forces resulted from the MIC model with Han et al. geometry. However, the predictions of the MIC model with the Han et al. geometry were not the most accurate when considering the mean R^2 values in predicting actual muscle activity.

7.3 Female Subjects and Model Predictions

The model combinations generally provided poorer predictions of females' actual muscle activity. The muscle geometry inputs were largely based on male subjects, which could have resulted in poorer predictions for females. The Han et al. muscle geometry included information from four female and six males in the data set. The Han et al. geometry contained disproportionately smaller cross-sectional areas for the obliques. The oblique areas reported by Han et al. (1992) were close to the cross-sectional areas reported by Chaffin et al. (1990) for 96 elderly women. The lack of a complete muscle geometry for females may have resulted in poorer predictions from the models.

The computer simulation used to predict muscle forces and compression did not include a geometry set for females. Hughes (1995) reported the MIC model provided conservative compression force estimates. Hughes (1995) used the compilation geometry which was based on data collected on males. The Han et al. geometry set might be closer to the muscle geometries of females, since it included four female subjects. If the Han et al. geometry has geometry closer to females, then muscles such as the obliques might be smaller for females. The Han et al. geometry predicted higher compression forces, and therefore would provide a more conservative estimate of compression for females then the compilation geometry.

7.4 Accuracy of Model Predictions

Regression techniques were used to assess the accuracy of model predictions. The muscle forces generated from the models were used to predict the percent activity of the subjects' muscles during loading. In general, the regression technique assessed the models' accuracy, as demonstrated by Figures 6.5 - 6.7. When a model predicted activity for a muscle, yet the actual activity was at a low percentage, the correlation was poor. When the active and inactive regions of the models did not match high and low percentages of activation, the percent of variation (R^2) described by the model was low. When R^2 values were approximately 0.5, the relative active and inactive regions corresponded between the models and actual activity. However, differences in the active and inactive regions and differences in magnitudes lowered R^2. Using regression analysis accounted for the differences in percent activity across the muscles and subjects. For example, the LES and RES muscles for Subject 1 reached a level of about 25% activity while the same muscles for Subject 8 reached a level of 60%. If both subjects exhibited the same relative changes in actual muscle activity, the correlation between predicted muscle force and actual activity were similar for both subjects.

The RRA, LRA, LEO, RES, and LES were predicted with an R^2 greater than 0.5 for 8 or more subjects by at least one of the models, shown previously in Table 6.4. The RLD and LLD were predicted with an R^2 greater than 0.5 only 1 time out of 96 total regression models. The activity measured for the latissimus dorsi seemed to be shifted from the model predictions. Figure 7.1 shows the predictions for the SCI model with compilation geometry and actual

activity for subjects 1 through 6. On Figure 7.1, good correlation would correspond to the shape of the actual activity and the predicted forces being approximately the same. However, the shape of the actual activity did not correspond to the shape of predicted activity so the correlation was poor. The model predicted activity from 100 to 300 degrees. Subjectively, the actual

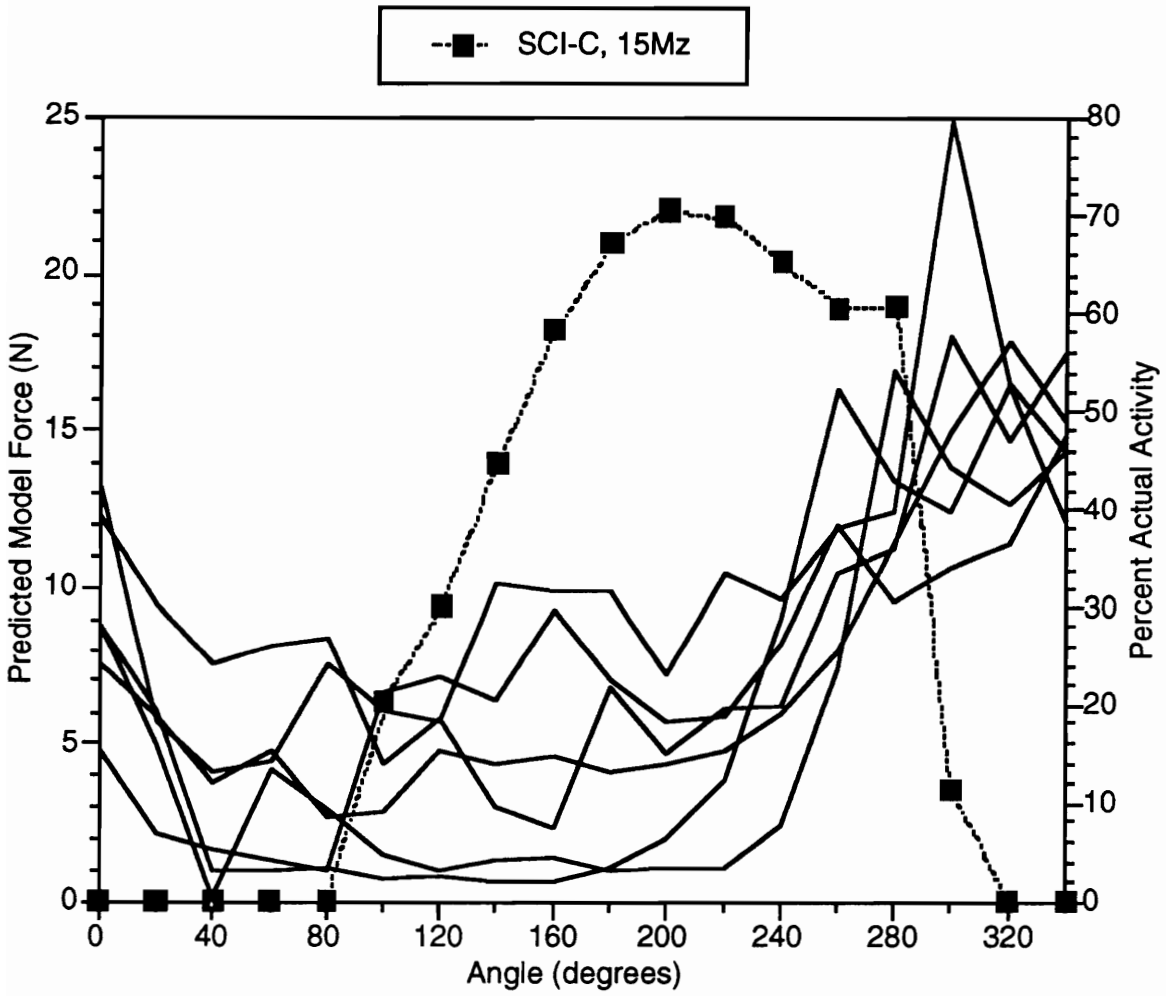

Figure 7.1 SCI-C Model predictions and actual percent activity for RLD with 15 Nm torsion, Subjects 1 through 6. Model predictions are in N and use left ordinate, while actual activity is in percent and uses right ordinate.

activity was from approximately 220 to 40 degrees (inactive 60 to 220 degrees). It appears that the predictions for activity were shifted about 100 degrees from actual, which caused the low R^2 in the regression equations.

The number of times a model predicted actual muscle activity across subjects with R^2 greater than 0.5 was shown previously in Table 6.4. The SCI model with the compilation geometry (SCI-C) predicted the most subjects accurately for RRA, LRA, RES, and LES at both torsion moments. The SCI-C model predicted fewer subjects accurately for the LEO muscle than the SCI-H model, 8 to 12 and 9 to 11 for two torsion levels. The SCI-C model predicted more subjects accurately than either MIC model, with only 0 to 2 subjects accurately predicted. The SCI-C model only predicted 3 subjects accurately for the REO muscle. However, the most subjects accurately predicted by any model was 5 by the MIC-H model.

7.4.1 Ten Muscle Models

To determine differences in the accuracy of the models an ANOVA was conducted on the R^2 values of each regression. The ANOVA showed relative differences between the models, but did not indicate if a model accurately predicted the activity of a muscle. For example, the MIC-H predicted the RLD with significantly higher R^2 than the MIC-C model. However, the mean R^2 was 0.22 for the MIC-H predicting the RLD, and predicted the RLD with R^2 greater than 0.5 for only one subject.

An ANOVA of R^2 values for 10-muscle models was conducted. The SCI model with either geometry had significantly higher R^2 values for some

conditions, but was never significantly worse. The SCI model with the compilation geometry had significantly higher R^2 values for several conditions, and was significantly worse for conditions with overall low R^2 values.

The LRA, RRA, LES, RES, and LEO muscles were predicted well by the SCI-C model with mean R^2 of 0.73, 0.63, 0.58, 0.55, and 0.61, respectively. The REO was predicted moderately by SCI-C, mean R^2 equal 0.28. The LLD and RLD were not predicted accurately by SCI-C (or any model), mean R^2 equal 0.05 and 0.09 respectively.

Three other studies have used regression techniques to compare the accuracy of model predictions with actual muscle activity. Hughes and Chaffin (1995), Hughes, Chaffin, Lavender, and Andersson (1994), and Zetterberg et al. (1987) compared actual muscle activity to model predictions. The mean R^2 values reported by each study by model and muscle are shown in Table 7.1. Hughes et al. (1994) compared model predictions of the MIC and SCI using compilation geometry to actual activity during flexion/extension and lateral bending moments. In general, the R^2 values were higher because they were for mean subject activity, but showed the same trends. The LLD and RLD were predicted poorly and the LES, RES, LRA, and RRA among the better predictions.

Hughes and Chaffin (1995) had subjects resist loads which caused attempted flexion combined with attempted counter-clockwise twisting. R^2 values of zero indicated that model predicted inactivity for all loading conditions. Non-zero R^2 values correspond well to those obtained in the present study. The LRA and RRA were predicted very well. Hughes and Chaffin (1995) found

TABLE 7.1 R^2 Values for muscle force prediction found by four studies,

	Zetterberg et al. (1987)	Hughes et al.(1994)		Hughes and Chaffin (1995)		Present Study	
Muscle	MIC-C	MIC-C	SCI-C	MIC-C	SCI-C	MIC-C	SCI-C
LES	0.86	0.86	0.96	0.40	0.00	0.56	0.58
RES	0.86	0.55	0.64	0.00	0.00	0.48	0.55
LRA	0.81	0.79	0.98	0.84	0.99	0.48	0.73
RRA	0.86	0.89	0.90	0.71	0.96	0.58	0.63
LEO	0.18	0.82	0.72	0.51	0.43	0.38	0.61
REO	0.51	0.75	0.71	0.97	0.86	0.29	0.28
LLD		0.00	0.08	0.32	0.32	0.13	0.05
RLD		0.32	0.33	0.00	0.00	0.04	0.09

better prediction for the REO than the LEO while the present study found opposite results. The difference might be due to the opposite direction of the torsion moments; Hughes and Chaffin had subjects attempt counter-clockwise twisting while the present study required subjects to attempt clockwise twisting.

Zetterberg et al. (1987) used wire electrodes to monitor the activity of muscles during pure flexion, extension, right lateral bending, or left lateral bending tasks. Three other lifting tasks were also completed by the subjects. The most accurate predictions were for the LES, RES, LRA, and RRA muscles which matches the results of the current study.

7.4.2 Comparing 10- Versus 18-Muscle Models

To compare the accuracy of the models using 18 muscles instead of 10 an ANOVA was conducted on the R^2 values of each regression. The interactions involving number of muscles were of interest to elicit differences from the ANOVA using only 10-muscle models. Increasing the number of muscle from 10 to 18 was for predictions of muscles for the MIC or SCI models. The regression equations to predict actual muscle activity still contained only one variable, the predicted muscle force of each model. Expanding the number of muscles included in the model would be useful if accuracy of the predictions improved or EMG signals of more muscles were monitored. The results of the ANOVA comparing 18- and 10-muscle models indicated that for the best geometries and models expanding from 10 to 18 muscles did not improve accuracy of the predictions.

The Muscle x Number of Muscles interaction revealed that for the LEO and REO, the 10-muscle model was better, and was significantly worse for the LRA, yet had a high mean R^2 equal 0.62. The Muscle x Geometry x Number of Muscles interaction indicated cases where the 18-muscle models were significantly better. However, 18 muscle models did not lead to higher R^2 values than the compilation geometry with 10 muscles, with the exception of the RLD which was predicted with low R^2 values. Finally, the Muscle x Model x Geometry x Number of Muscles interaction indicated that the cases in which 18 muscles improved accuracy were for the RRA with the MIC-H model and for LRA for MIC-C model. However, for both cases the improvement was for models with the lowest R^2 for the RRA and LRA, respectively.

7.5 Apparatus Used to Apply Moments

The ANOVA to assess differences between hand and harness loading indicated several significant main effects and interactions. Only those interactions including the apparatus factor were considered further. For example, the muscle main effect was significant, but further analysis would not reveal any differences between hand and harness loading.

The three-way interaction of Angle x Muscle x Apparatus indicated cases in which hand and harness loading differed significantly. The erector spinae muscles did not vary between hand and harness loading, indicating apparatus did not create changes in erector spinae activity. The LRA had significantly higher activity at 0 and 60 degrees for hand loading. The RRA had significantly higher activity at 0 degrees for hand loading. Differences in the rectus abdominus due to loading apparatus are difficult to explain. One possibility was that the estimation of arm moments was inaccurate. Arm moments were not considered for harness loading because subjects held their arms at their sides. Incorrect arm moments could have caused lower external extension moments than estimated, increased attempted flexion, and therefore increased rectus abdominus activity. At symmetrical loadings, inaccurate arm moments would have decreased external flexion moment, decreased attempted extension, and decreased erector spinae activity. However, no differences were found between hand and harness loading at 180 degrees. Harness loading should have been significantly higher for the erector spinae at 180 degrees if inaccurate arm moments caused the difference in the rectus abdominus. A

possible explanation for higher rectus abdominus activity, was to counteract higher latissimus dorsi activity at 0 and 60 degrees.

Hand loading created significantly higher LEO activity than harness loading at angles of 60 and 120 degrees. The LEO differences were also difficult to explain. The hand loading results seemed to agree with the assumed line of action of the LEO. An angle of 60 degrees corresponded to external moments with components causing extension, right lateral bending, and counter-clockwise twisting. An angle of 120 degrees corresponded to external moments with components causing flexion, right lateral bending, and counter-clockwise twisting. With the LEO active, the assumed line of action of the LEO would create attempted flexion, left lateral bending, and clockwise twisting. Since the LEO moment components closely counteract the external moment components it would seem it should have high activity. Harness loading led to higher LEO activity for at 300 degrees.

For the LLD and RLD, hand loading created significantly higher activity than harness loading. The higher activity in hand loading appeared to be due to the role of the latissimus dorsi in shoulder stability. At 0 degrees, both the left and right arms were used to hold down the weight suspended over the pulley. The attempted movement to hold the weight uses the LLD and RLD equally. With the harness, no shoulder moments were created, and therefore latissimus dorsi activity to stabilize the shoulder were not necessary as with the hand loading. At 60 degrees, the difference between hand and harness loading increased for the LLD, but became insignificant for the RLD. Only the left arm was used to hold down the weight suspended over the pulley at 60 degrees.

Although the total weight suspended over the pulley was lower at 60 degrees than 0 degrees, the individual left arm moments were approximately equal as the load was distributed from both hands to just the left arm. At 120 degrees, the difference between hand and harness loading was equal to approximately the difference at 0 degrees. The left arm load for the LLD at 120 degrees required lifting. For the RLD, at 300 degrees, only the right arm was used to hold down the weight suspended over the pulley so RLD was significantly higher for hand loading than harness loading. The differences between hand and harness loading were larger for the LLD than the RLD possibly due to subjects being right-handed. It could also be attributed to the attachment of the weight to create torsion moment. The weight causing torsion pulled the left arm away from the mid-sagittal plane of the body, while it pulled the right arm toward the mid-sagittal plane of the body. The line of action of the latissimus dorsi at the shoulder level might account for differences in its activity.

The experimental method could have contributed to large differences found between the hand and harness loading conditions for the LLD and RLD. External extension moments (subject attempted flexion) were created by holding a weight suspended over a pulley in front of the subject. Tasks involving external extension moments often involve loads applied behind people such as carrying weight in a back pack. Moments applied via a back pack would probably not contain the shoulder moments and LLD activity resulting from the current experimental method. However, differences between hand and harness loading were also found for the LLD during external flexion moments (subject attempted extension). The moments in the experimental

method were applied in a similar manner to lifting tasks. Models and experiments which do not consider the role of the latissimus dorsi in shoulder stability may underestimate its activity.

Torres, Hughes, and Chaffin (1990) applied external flexion moments (subjects attempted extension) at 25, 50, 75, and 100% of maximum effort using hand and harness loading. Torres et al. (1990) measured the EMG activity of the eight muscles also measured in the current study. They calculated the linear regression between moment at the L3/L4 and normalized EMG signals. They reported equal regression slopes for both hand and harness loading for the LES, RES, and RLD. However, the slopes were greater for hand loading for the LLD, LRA, RRA, LEO, and REO. Their results that the LES and RES muscle activity do not change with loading apparatus agreed with the present study. In addition, different slopes for the LLD, LRA, RRA, and LEO agreed with differences in loading conditions found in the present study. However, Torres et al. (1990) found the RLD not to change while the present study found differences and REO activity to change while the present study found no differences. The differences in the studies might be attributed to loading conditions. Torres et al. (1990) used moments in only one direction while moments in all three directions were investigated in the present study. In general, both studies found increased activity in muscles during hand loading, but no changes in erector spinae activity.

7.6 Determining Actual Active and Inactive Regions for Muscles

An attempt was made in this study to classify the actual percent muscle activities as either inactive or active. The actual muscle activity/inactivity regions could then have been compared to predicted activity/inactivity regions to determine the accuracy of competing models. Three criteria were suggested to define actual activity and inactivity for each muscle. The first criterion used the mean RMS EMG level measured for each muscle during the resting trial. Three standard deviations of the RMS EMG signal were then added to the mean. The mean resting EMG level plus three standard deviations was then normalized to the maximum EMG. The actual percent muscle activity was then compared to the resting plus three standard deviations percentage. If actual muscle activity was greater than resting plus three standard deviations, the muscle was considered active.

The second criterion to define active/inactive regions used the mean RMS EMG level measured for each muscle during the standing trial. The mean standing EMG was then normalized to the maximum EMG. The actual percent muscle activity was then compared to the standing percentage. If actual muscle activity was greater than standing, the muscle was considered active.

The third criterion also used the mean RMS EMG level measured for each muscle during the standing trial, but three standard deviations of the RMS EMG signal during standing were added to the mean. The mean standing EMG level plus three standard deviations was then normalized to the maximum EMG. The actual percent muscle activity was then compared to the standing plus

three standard deviations percentage. If actual muscle activity was greater than standing plus three standard deviations, the muscle was considered active.

None of the three criteria consistently established active and inactive regions for each muscle across subjects. For example, the resting plus three standard deviations criterion determined every loading condition to be active for one subject yet found most conditions inactive for another subject. Each subject seemed to vary on the criterion (if any) for effectively judging active/inactive regions. The active and inactive regions determined using each criterion could not be used for further analysis.

During pilot studies a fixed percentage of maximum such as 10% was considered as a method to establish activity regions. Using fixed percentage as a cut-off to define active and inactive was also inconsistent across subjects.

The difficulty in establishing a percentage to classify the activity of muscles appeared to be due to differences in EMG levels from the MVC trials. For example, for subject 1 the Rectus Abdominus (RA) muscles reached a maximum of about 70%. For subject 5, the RA muscles reached a maximum of only about 20%. During the MVC trials for subject 1, the maximum RA EMG value ranged from 1.8 to 2.8. During the MVC trials for subject 5, the maximum RA EMG value ranged from 2.7 to 4.1. Therefore, when the trial EMG signals were normalized the percentages were lower for subject 5.

An objective criterion to judge active versus inactive muscles was not determined. Subjective determination would be required to test the active and inactive matches of actual activity to model predictions. The method suggested

by Ladin et al. (1989) to test matches using a Chi-square statistic required determination of actual active and inactive regions.

An experiment reported by Lavender et al. (1992) measured the muscular activity of eight muscles as a 100 N load was rotated around the body. The load was applied over a 180 degree arc every 15 degrees to the right starting in the mid-sagittal plane in front of the subject and ending in the mid-sagittal plane behind the subject. Right lateral bending moments combined with flexion or extension moments were created. With no torsion moment, the angle that the muscles were predicted active do not vary with the magnitude of the moment created about the L3/L4 disc and can be applied to the model predictions of this study. Lavender et al. (1992) tested the activity of the left and right side latissimus dorsi (LLD, RLD), left and right erector spinae (LES, RES), left and right external oblique (LEO, REO), and left and right rectus abdominus (LRA, RRA) using t-tests on the EMG signals.

A procedure reported by Ladin et al. (1989) was followed to test the model predictions for active and inactive regions. For each of the 13 loading conditions tested by Lavender et al. (1992), the predictions of activity or inactivity of four model combinations were generated: MIC-H, MIC-C, SCI-H, and SCI-C. Table 7.2 shows the number of loading conditions predicted correctly and incorrectly by the MIC-H condition for the RES. The numbers along the diagonal represent correct predictions (muscle predicted active and experiment shown active, and muscle predicted inactive and experiment shown inactive). Numbers in the lower left and upper right corners represent conditions in which the model predicts inactivity and experiment show activity,

TABLE 7.2 Predictions of MIC-H Condition Compared to Results of Lavender et al. (1992) for RES

	Experimental On	Experimental Off
Predicted On	5	0
Predicted Off	2	6

and model predicts activity and experiment show inactivity, respectively. Chi-Square Tests for 2x2 contingency tables (Siegel and Castellan, 1988) were conducted on the model and experimental contingency tables to test if the models were predicting muscle activity correctly a significant number of times. Significance was found for the MIC-C predicting the RES, REO, and RRA, MIC-H predicting the RES and RRA, SCI-C predicting the REO and RRA, and SCI-H predicting the RES and RRA. When correct and incorrect predictions for each model were combined across muscles, all four model combinations predict a significant number of muscle activities correctly.

None of the left side muscles were ever significantly predicted by any of the four model combinations. Only the right side muscles were predicted correctly in some cases by the models. Forces were only applied to the right side of the body by Lavender et al. (1992), which might account for the findings.

Difficulties existed in applying the data reported by Lavender et al. (1992) to the model predictions. First, the loading conditions selected were all less than 15 % of maximum voluntary contractions. Some conditions with higher mean EMG signals than succeeding conditions were tested as zero due to high

variability. The lower EMG values were then found significant due to lower variability. Loading conditions at higher percentages of MVC might reduce muscles being shown to switch back and forth from active to inactive. Second, the sample size of 13 used in the contingency tables was fairly low so that 3 incorrect predictions by the model would cause it to be insignificant.

Lavender et al. (1992) used t-tests to determine if the mean activity at a particular loading condition was greater than zero. The same method was attempted for the current study. However, some conditions with higher mean EMG signals than succeeding conditions were tested as zero due to high variability, a problem similar to the results of Lavender et al. (1992). In the present study, one subject's normalized activity was at 20% and another subject's was at 80%. The variability was high so that the confidence intervals encompassed zero. Consistent predictions of active and inactive regions were not found in the current study.

7.7 Possible Experimental Errors

7.7.1 Posture and Arm Moment

During the static exertions, subjects were asked to maintain an upright posture. Subjects could have used the position of their torso to counteract the external loads reducing muscle activity if posture was not controlled. With the posture control system used in this study, subjects were given an error of ± 1 cm at the suprasternale height. Moments due to torso position error were estimated

to be from 1.6 to 2.3 Nm. Therefore, torso position errors could have increased or decreased static exertions by at most approximately 2.3 Nm.

The moments due to arms were estimated using the procedure discussed previously in Section 5.4.1.2. Error in the estimates of arm moments could also have occurred. The position of the lower and upper arms were determined from measuring lengths of the segments and their angles and projecting them from assumed hand positions. The position of the hands was fixed by hanging markers from the loading frame. Although subjects were instructed on the position of their hands some placement error could have occurred. The angles of the arm segments which were viewed from videotape could have had measurement error. Changing the measurement angles by up to 10 degrees had a small effect on the estimated moments. Also, the moments due to arms were estimated, following the first session, to determine weights for the final two sessions. This was necessary because loading moments were kept constant across subjects; arm moments could not be estimated after the trials were finished. Subjects could have varied their arm positions between trials with different weights. However, because hand and L3/L4 positions were fixed, the changes in arm positions were considered small.

7.7.2 Trials to Determine Maximum Voluntary Contraction

The maximum voluntary contraction (MVC) trials used in the current studied were patterned after those reported by McGill (1991). The MVC trials did not seem to consistently elicit the maximum EMG signal for each muscle. For some loading conditions during the experiment, the actual muscle activity

surpassed 100%, for example the LEO for subject 1 shown previously in Figure 6.3. However, the REO for subject 1 reached 50% at its highest level. For the remaining subjects, the LEO and REO attained approximately equal percent activity. Selecting MVC trials which will establish maximum EMG signals for each subject was difficult. However, in assessing the accuracy of model predictions, the regression analysis used was not affected by percentages over 100.

8. CONCLUSIONS

This dissertation investigated optimization-based biomechanical models using three unique approaches. First, the muscle geometric inputs (moment arms, lines of action, and cross-sectional areas) were varied. Past investigations had primarily used one set of muscle geometries. Second, combinations of all three moments, torsional, flexion/extension, and lateral bending, were investigated. Computer simulations of optimization models were used to predict muscle forces under loading conditions including all three moments. Combinations of the three moments were also applied to subjects to empirically determine the activity of muscles and test the accuracy of optimization-based models and inputs. Third, the experimental method included application of moments to subjects through loads held by the hands and loads attached to a harness mounted at the shoulder level.

8.1 Objectives

The first objective was to summarize the current knowledge of muscle moment arms from the vertebrae, lines of action, and cross-sectional areas. Two muscle geometry sets were generated as shown previously in Tables 2.16 - 2.19. The second objective was to summarize the assumptions for solving optimization models applied to the trunk, which was accomplished in Chapter 3.

The third objective was to investigate the effect of input parameters on the muscle force predictions of trunk optimization models with three sub-hypotheses. The conclusions of the third objective, from the results reported in Chapter 4, are as follows:

- Hypothesis 3.1 is accepted. Under identical loading conditions the Minimum Intensity Compression (MIC) and Sum of the Cubed Intensities (SCI) models predicted muscles with the same geometries to be active or inactive differently.

- Hypothesis 3.2 is accepted. The muscle geometries sets generated from the literature, Han et al. (1992) and a compilation from other authors, resulted in the same muscle being predicted active and inactive using the same model, MIC or SCI, with identical loading conditions.

- Hypothesis 3.1 is accepted. As the number of muscles included in the model changed from 10 to 18, muscles with the same geometries were predicted active and inactive differently by the same model, MIC or SCI.

The fourth objective was to experimentally test the predictions of combinations of competing models, number of muscles, and muscle geometry against actual muscle activity. As reported in Chapter 5, the method to test the fourth objective included measuring the EMG signals of eight muscles: Left and Right Rectus Abdominus (LRA, RRA), Left and Right External Oblique (LEO, REO), Left and Right Latissimus Dorsi (LLD, RLD), and Left and Right Erector Spinae (LES, RES). The conclusions determined from the results, reported in Chapter 6, are as follows:

- Hypothesis 4.1 stated that either the MIC or SCI model would predict actual muscle activity significantly better. The hypothesis is accepted. The SCI model provided overall better predictions than the MIC model.

- Hypothesis 4.2 stated that either the Han et al. or compilation geometry would predict actual muscle activity significantly better. The hypothesis is accepted. The geometry reported by a compilation of authors resulted in slightly better predictions than the Han et al. (1992) geometry

- Hypothesis 4.3 stated that one of the four combinations of model and geometry set would predict actual muscle activity significantly better. The hypothesis is accepted. The SCI model with the compilation geometry predicted muscle activity better than or equal to the other three muscle and geometry combinations. Across subjects, the SCI-C model should be used to predict muscle forces. However, the SCI-C model predicts LLD, RLD, and REO muscle with mean R^2 equal to 0.05, 0.09, and 0.28 respectively.

- Hypothesis 4.4 stated that one of two numbers of muscles used in the MIC and SCI models, 10 or 18, would predict actual muscle activity significantly better. The hypothesis is rejected. Expanding the number of muscles from 10 to 18 did not substantially increase accuracy of the

model predictions for six identical muscles included in both sets: LRA, RRA, LEO, REO, LLD, and RLD.

Additional conclusions from the results of the experiment are as follows:

- The LRA, RRA, LEO, LES, and RES were predicted well by at least one of the four model combinations for all of the subjects, up to an R^2 equal to 0.96 for the RRA of subject 5 and 0.98 for the LRA of subject 2.

- The LLD and RLD were not predicted well for any subject by any of the models with mean R^2 equal to 0.08 and 0.12 respectively. The latissimus dorsi plays a role in shoulder stability associated with holding weights in the hands, but not accounted for in trunk optimization models.

- The models predicted actual muscle activity better for males than females, for the LRA, RRA, REO, LES, and RES, accounting for 8 to 25% more of the variation.

- The models predicted moments with 7.5 Nm torsion better than moments with 15 Nm torsion.

The fifth objective was to test if moments applied using a shoulder harness versus weight held with the hands would affect muscle activity. Twelve

different moments were applied equivalently using the harness or hands. The EMG signals of eight muscles were measured: LRA, RRA, LEO, REO, LLD, RLD, LES, and RES. The hypothesis was that differences would occur between the two methods. The hypothesis is accepted because significant differences were found in the experiment. The following conclusions were determined from the results reported in Chapter 6.

- For weights held by the hands with the shoulder in flexion, the LLD and RLD showed much higher activity for hand loading than harness loading. The latissimus dorsi was apparently used in shoulder stability to counteract moments imposed during hand loading. Harness loading did not impose shoulder moments reducing the activity of the latissimus dorsi.

- Hand loading created much higher activity than harness loading for the following conditions. 0 degrees - LRA, RRA, LLD, RLD; 60 degrees - LRA, LEO, LLD; 120 degrees - LEO, LLD; and 300 degrees - RLD. Torsion existed with each angle. Zero degrees corresponded to attempted flexion, 60 degrees to attempted flexion and left lateral bending, 120 degrees to attempted extension and left lateral bending, and 300 degrees to attempted flexion and right lateral bending.

- In general, hand loading led to higher muscle activity than harness loading. Only the LES and RES muscles had equal activity between hand and harness loading across different moment conditions.

8.2 Future Research

The experimental method and results of this study point to several areas for future research, four of which are discussed below.

1) The number of muscles included in the model. This study included 10 and 18 muscles in different predictions. No improvement was found in the prediction of the six muscles measured which were common to each model development. Further study on the effects of including more muscles and sub-dividing muscles would help establish what muscles need to be included in an optimization-based trunk model.

2) Hand Loading. Large increases in latissimus dorsi activity were found as loads were shifted from harness loading to hand loading. Some of this increase could have been an artifact of the experimental method. External loads creating extension (subject required to attempt flexion) were applied by holding a weight in front of the body suspended over a pulley. External extension loads created by a more realistic task such as weight in a backpack would assist in evaluating the use of the latissimus dorsi. This study used hand loading, which was closer to an industrial task than harness loading. However, hand loads were applied using different weights held in each hand at different positions. Two handed

loading, which more closely resembles industrial tasks, needs to be studied further.

3) Gender Differences. The model developments required geometric inputs of muscle moment arms, lines of action, and cross-sectional areas. The geometric inputs reported in the literature were largely based on male subjects. A separate complete geometry of the muscles was not generated for females in this study because it was not available. However, the predictions of the models were better for males than females probably because the model parameters were based on male data. As separate muscle geometry for females becomes available, models which account for gender might improve predictions for females.

4) Maximum Voluntary Contraction (MVC) Trials. The MVC trials used in this study were the same as reported by McGill (1991). McGill (1991) also reported that for some muscles a single MVC could not be identified that would consistently elicit the maximum EMG signal. Development of a standard MVC protocol would be helpful future research. The differences in normalization of EMG data across subjects in this study might have been reduced with more defined MVC trials.

9. REFERENCES

An, K.N., Kwak, B.M., Chao, E.Y., and Morrey, B.F. (1984). Determination of muscle and joint forces: A new technique to solve the indeterminate problem. *Journal of Biomechanical Engineering, 106*, 364-367.

Anderson, C.K., Chaffin, D.B., Herrin, G.D., and Matthews, L.S. (1985). A biomechanical model of the lumbosacral joint during lifting activities. *Journal of Biomechanics, 18*(8), 571-584.

Anderson, J.E. (1978). *Grant's atlas of anatomy.* Baltimore: Williams and Wilkins Company.

Andersson, G.B.J., Pope, M.H., Frymoyer, J.W., and Snook, S. (1991). Epidemiology and cost. In M.H. Pope, G.B.J. Andersson, and D.B. Chaffin (Eds.), *Occupational low back pain* (pp 95-113). Boston: Mosby Year Book.

Andrews, J.G., and Hay, J.G. (1983). Biomechanical considerations in the modeling of muscle function. *Acta Morphol. Neerl.-Scand., 21*, 199-223.

Bazaraa, M.S., Jarvis, J.J., and Sherali, H.D. (1990). *Linear programming and network flows.* New York: Wiley.

Bazaraa, M.S., Sherali, H.D., and Shetty, C.M. (1993). *Nonlinear programming, theory and algorithms.* New York: Wiley.

Bean, J.C., Chaffin, D.B., and Schultz, A.B. (1988). Biomechanical model calculation of muscle contraction forces: a double linear programming method. *Journal of Biomechanics, 21*(1), 59-66.

Bogduk, N. (1980). A reappraisal of the anatomy of the human lumbar erector spinae. *Journal of Anatomy, 131*(3), 525-540.

Bogduk, N., Macintosh, J.E., and Pearcy, M.J. (1992a). A universal model of the lumbar back muscles in the upright position. *Spine, 17*(8), 897-913.

Bogduk, N., Pearcy, M., and Hadfield (1992b). Anatomy and biomechanics of psoas major. *Clinical Biomechanics, 7*, 109-119.

Bouisset, S. (1973). EMG and muscle force in normal motor activities. In J.E. Desmedt (Ed.), *New developments in electromyography and clinical neurophysiology* (pp 547-583). Brussels: Karger, Basel.

Bouisset, S., Lestienne, F., and Maton, B. (1977). The stability of synergy in agonists during the execution of a simple voluntary movement. *Electroencephalography and Clinical Neurophysiology, 42*, 543-551.

Bozec, S., Maton, B., and Cnockaert, J.C. (1980). The synergy of elbow extensor muscles during static work in man. *European Journal of Applied Physiology, 43*, 57-68.

Cappozzo, A., Felici, F., Figura, F., and Gazzani, F. (1985). Lumbar spine loading during half-squat exercises. *Medicine and Science in Sports and Exercise, 17*(5), 613-620.

Chaffin, D.B., and Andersson, G.B.J. (1991). *Occupational Biomechanics.* New York: Wiley.

Chaffin, D.B., Redfern, M.S., Erig, M., and Goldstein, S.A. (1990). Lumbar muscle size and locations from CT scans of 96 women of age 40 to 63 years. *Clinical Biomechanics, 5*, 9-16.

Cholewicki, J. and McGill, S.M. (1996). Mechanical stability on the in vivo lumbar spine: implications for injury and chronic low back pain. *Clinical Biomechanics, 11*(1), 1-15.

Clauser, C.W., McConville, J.T., and Young, J.W. (1969). Weight, volume, and centers of mass segments of the human body. (Tech. report AMRL-TR-69-70). Ohio: Aerospace Medical Research Laboratories.

Crowninshield, R.D. (1978). Use of optimization techniques to predict muscle forces. *Journal of Biomechanical Engineering, 100*, 88-92

Crowninshield, R.D., and Brand, R.A. (1981). A physiologically based criterion of muscle force prediction in locomotion. *Journal of Biomechanics, 14*(11), 793-801.

Dul, J., Townsend, M.A., Shiavi, R., and Johnson, G.E. (1984). Muscular synergism - I. on criteria for load sharing between synergistic muscles. *Journal of Biomechanics, 17*(9), 663-673.

Dumas, G.A., Poulin, M.J., Roy, B., Gagnon, M., and Jovanovic M. (1988). A three-dimensional digitization method to measure trunk muscle line of action. *Spine, 13*(5), 532-541.

Eycleshymer, A.C., and Schoemaker, D.M. (1911). *A cross-section anatomy.* New York: Appleton-Century Crofts.

Gracovetsky, S., Farfan, H.F., and Lamy, C. (1977). A mathematical model of the lumbar spine using an optimized system to control muscles and ligaments. *Orthopedic Clinics or North America, 8*(1), 135-153.

Han, J.S., Ahn, J.Y., Goel, V.K., Takeuchi, R., and McGowan, D. (1992). CT-Based geometric data of human spine musculature. Part I. Japanese patients with chronic low back pain. *Journal of Spinal Disorders, 5*(4), 448-458.

Hughes, R.E. (1991). *Empirical evaluation of optimization-based lumbar muscle force prediction models.* Unpublished doctoral dissertation, University of Michigan, Ann Arbor, MI.

Hughes, R.E. (1995). Choice of optimization models for predicting spinal forces in a three-dimensional analysis of heavy work. *Ergonomics, 38*(12), 2476-2484.

Hughes, R.E. and Chaffin, D.B. (1995). The effect of strict muscle stress limits on abdominal muscle force predictions for combined torsion and extension loadings. *Journal of Biomechanics, 26*(5), 527-533.

Hughes, R.E., Chaffin, D.B., Lavender, S.A., and Andersson, G.B.J. (1994). Evaluation of muscle force prediction models of the lumbar trunk using surface electromyography. *Journal of Orthopaedic Research, 12*, 689-698.

Johnson, C.A. (1992). *Optimization-based biomechanical evaluation of isometric exertions on a brake wheel.* Unpublished master's thesis, Virginia Polytechnic Institute and State University, Blacksburg, VA.

Kroemer, K.H.E., Kroemer, H.J., and Kroemer-Elbert, K.E. (1990). *Engineering physiology, bases of human factors/ergonomics.* New York: Van Nostrand Reinhold.

Ladin, Z., Murthy, K.R., and De Luca, C.J. (1989). Mechanical recruitment of low-back muscles: theoretical predictions and experimental validation. *Spine, 14*(9), 927-938.

Lavender, S.A., Tsuang, Y.H., Hafezi, A., Andersson, G.B.J., Chaffin, D.B., and Hughes, R.E. (1992). Coactivation of the trunk muscles during asymmetric loading of the torso. *Human Factors, 34*(2), 239-247.

Macintosh, J.E., and Bogduk, N. (1986). The biomechanics of the lumbar multifidus. *Clinical Biomechanics, 1*(4), 205-213.

Macintosh, J.E., and Bogduk, N. (1987). The morphology of the lumbar erector spinae. *Spine, 12*(7), 658-668.

Macintosh, J.E., and Bogduk, N. (1991). The attachments of the lumbar erector spinae. *Spine, 18*(7), 783-792.

Macintosh, J.E., Bogduk, N., and Pearcy, M.J. (1993). The effects of flexion on the geometry and actions of the lumbar erector spinae. *Spine, 18*(7), 884-893.

Macintosh, J.E., Valencia, F., Bogduk, N., and Munro, R.R. (1986). The morphology of the human lumbar multifidus. *Clinical Biomechanics, 1*(4), 196-204.

Marras, W.S. (1988). Predictions of forces acting upon the lumbar spine under isometric and isokinetic conditions: a model-experiment comparison. *International Journal of Industrial Ergonomics, 3*, 19-27.

Maton, B., and Bouisset, S. (1977). The distribution of activity among the muscles of a single group during isometric contraction. *European Journal of Applied Physiology, 37*, 101-109.

McGill, S.M. (1991). Electromyographic activity of the abdominal and low back musculature during the generation of isometric and dynamic axial truck torque: Implications for lumbar mechanics. *Journal of Orthopaedic Research, 9*, 91-103.

McGill, S.M., and Hoodless, K. (1990). Measured and modeled static and dynamic axial truck torsion during twisting in males and females. *Journal of Biomedical Engineering, 12*, 403-409.

McGill, S.M., and Norman, R.W. (1986). Partitioning of the L4-L5 dynamic moment into disc, ligamentous, and muscular components during lifting. *Spine, 11*(7), 666-678.

McGill, S.M., and Norman, R.W. (1987). Effects of an anatomically detailed erector spinae model on L4/L5 disc compression and shear. *Journal of Biomechanics, 20*(6), 591-600.

McGill, S.M., Patt, N., and Norman, R.W. (1988). Measurement of the trunk musculature of active males using CT scan radiography: Implications for force and moment generating capacity about the L4/L5 joint. *Journal of Biomechanics, 21*(4), 329-341.

McGill, S.M., Santaguida, L., and Stevens, J. (1993). Measurement of the trunk musculature form T_5 to L_5 using MRI scans of 15 young males corrected for muscle fibre orientation. *Clinical Biomechanics, 8*, 171-178.

Mirka, G.A. (1991). The quantification of EMG normalization error. *Ergonomics, 34*(3), 343-352.

Moga, P.J., Erig, M., Chaffin, D.B., and Nussbaum, M.A. (1992). A comparison of torso muscle fiber-line and centroid-line inclination angles relative to the L3-L4 interspace. (submitted).

Moga, P.J., Erig, M., Chaffin, D.B., and Nussbaum, M.A. (1993). Torso muscle moment arms at intervertebral levels T10 through L5 form CT scans on 11 male and 8 female subjects. *Spine, 18*, 2305-2309.

Nachemson, A.L., and Evans, J.H. (1968). Some mechanical properties of the third human lumbar interlaminar ligament (ligamentum flavum). *Journal of Biomechanics, 1*, 211-220

Németh, G., and Ohlsén, H (1986). Moment arm lengths of trunk muscles to the lumbosacral joint obtained in vivo with computed tomography. *Spine, 11*(2), 158-160.

Nussbaum, M.A. and Chaffin, D.B. (1995). Development and evaluation of a scalable and deformable geometric model of the human torso. *Clinical Biomechanics, 11*(1), 25-34.

Nussbaum, M.A., Chaffin, D.B., and Rechtien, C.J. (1995). Muscle lines-of-action affect predicted forces in optimization-based spine muscle modeling. *Journal of Biomechanics, 28*(4), 401-409.

Panjabi, M.M., Krag, M.H., White, A.A., and Southwick, W.O. (1977). Effects of preload on load displacement curves of the lumbar spine. *Orthopedic Clinics of North America, 8*, 181-192.

Pederson, D.R., Brand, R.A., Cheng, C., and Arora, J.S. (1987). Direct comparison of muscle force predictions using linear and nonlinear programming. *Journal of Biomechanical Engineering, 109*, 192-199.

Pedotti, A., Krishnan, V.V., and Stark, L. (1978). Optimization of muscle-force sequencing in human locomotion. *Mathematical Biosciences, 38*, 57-76.

Penrod, D.D., Davy, D.T., and Singh, D.P. (1974). An optimization approach to tendon force analysis. *Journal of Biomechanics, 7*, 123-129.

Rab, G.T., Chao, E.Y.S., and Stauffer, R.N. (1977). Muscle force analysis of the lumbar spine. *Orthopedic Clinics of North America, 8*(1), 193-199.

Redfern, M.S. (1988). *Electromyographic (EMG) signal processing and biomechanical modeling of lower leg muscles.* Unpublished doctoral dissertation, University of Michigan, Ann Arbor, MI.

Redfern, M.S., Hughes, R.E., and Chaffin, D.B. (1993). High-pass filtering to remove electrocardiographic interference from torso EMG recordings. *Clinical Biomechanics, 8*, 44-48.

Reid, J.G., and Costigan, P.A. (1985). Geometry of adult rectus abdominus and erector spinae muscles. *The Journal of Orthopaedic and Sports Physical Therapy, 6*(5), 278-280.

Reid, J.G., Livingston, L.A., and Pearsall, D.J. (1994). The geometry of the psoas muscle as determined by magnetic resonance imaging. *Arch Phys Med Rehabil, 75*, 703-708.

Reilly, C.H. and Marras, W.S. (1989). Simulift: a simulation model of human trunk motion. *Spine, 14*(1), 5-11.

Schultz, A.B., and Andersson, B.G.J. (1981). Analysis of loads on the lumbar spine. *Spine, 6*(1), 76-82.

Schultz, A., Andersson, G., Örtengren, R., Haderspeck, K., and Nachemson, A. (1982). Loads on the lumbar spine. *The Journal of Bone and Joint Surgery, 64-A*(5), 713-720.

Schultz, A., Cromwell, R., Warwick, D., and Andersson, G. (1987). Lumbar trunk muscle use in standing isometric heavy exertions. *Journal of Orthopaedic Research, 5*, 320-329.

Schultz, A.B., Haderspeck, K., Warwick, D., and Portillo, D. (1983). Use of lumbar trunk muscles in isometric performance of mechanically complex standing tasks. *Journal of Orthopaedic Research, 1*, 77-91.

Schultz, A.B., Haderspeck-Grib, K., Sinkora, G., and Warwick, D.N. (1985). Quantitative studies of the flexion-relaxation phenomenon in the back muscles. *Journal of Orthopaedic Research, 3*(2), 189-197.

Schultz, A.B., Warwick, D.N., Berskon, M.H., and Nachemson, A.L. (1979). Mechanical properties of human lumbar spine segments - part I: responses in flexion, extension, lateral bending, and torsion. *Journal of Biomechanical Engineering, 101*, 46-52.

Seireg, A., and Arvikar (1973). A mathematical model for evaluation of forces in lower extremities of the musculo-skeletal system. *Journal of Biomechanics, 6*, 313-326.

Seroussi, R.E. and Pope, M.H. (1987). The relationship between trunk muscle electromyography and lifting moments in the sagittal and frontal planes. *Journal of Biomechanics, 20*(2), 135-146.

Siegel, S. and Castellan, N.J. (1988). *Nonparametric statistics for the behavioral sciences.* New York: McGraw-Hill.

Stokes, I.A.F. and Gardner-Morse, M. (1995). Lumbar spine maximum efforts and muscle recruitment patterns predicted by a model with multijoint muscles and joints with stiffness. *Journal of Biomechanics, 28*(2), 173-186.

Takashima, S.T., Singh, S.P., Haderspeck, K.A., and Schultz, A.B. (1979). A model for semi-quantitative studies of muscle actions. *Journal of Biomechanics, 12*, 929-939.

Torres, B.A., Hughes, R., and Chaffin, D.B. (1990). *Comparison EMG study between harness and hand loading of the torso* (Technical Report). Ann Arbor, MI: University of Michigan, Center for Ergonomics.

Tracy, M.F., Gibson, M.J., Szypryt, E.P., Rutherford, A., and Corlett, E.N. (1989). The geometry of the muscles of the lumbar spine determined by magnetic resonance imaging. *Spine, 14*(2), 186-193.

Tsuang, Y.H., Novak, G.J., Schipplein, O.D., Hafezi, A., Trafimow, J.H., and Andersson, G.B.J. (1993). Trunk muscle geometry and centroid location when twisting. *Journal of Biomechanics, 26*(4/5), 573-546.

Tveit, P., Daggfeldt, K, Hetland, S, and Thorstensson, A. (1994). Erector spinae lever arm length variations with changes in spinal curvature. *Spine, 19*(2), 199-204.

Webb Associates (1978). *Anthropometric source book volume I: Anthropometry for designers.* NASA Reference Publication 1024. Washington, D.C.: National Aeronautics and Space Administration.

Williams, H.P. (1985). *Model building in mathematical programming.* Chichester: Wiley.

Williams, P.L., Warwick, R., Dyson, M., and Bannister, L.H. (1989). *Gray's anatomy.* Edinburgh: Churchill Livingstone.

Van der Helm, F.C.T. and Veenbaas, R. (1991). Modelling the mechanical effect of muscles with large attachment sites: Application to the shoulder mechanism. *Journal of Biomechanics, 24*(12), 1151-1163.

Yettram, A.L., Bai, B., Jackman, M.J. (1980). Equilibrium analysis for the forces in the human spinal column and its musculature. *Spine, 5*(5), 402-411.

Zetterberg, C., Andersson, G.B.J., and Schultz, A.B. (1987). The activity of individual trunk muscles during heavy physical loading. *Spine, 12*(10), 1035-1040.

APPENDIX A: Informed Consent

Informed Consent Form
Trunk Muscle Activity During Physical Exertion
Principal Investigator: Dr. Karl H. E. Kroemer
Investigator: Mark L. McMulkin

I. The Purpose of this Research

You are invited to participate in a study about trunk muscle activity during physical exertion. The purpose of this study is to determine if actual muscle activity during physical exertion matches the muscle activity predicted by models of the same physical activity. A total of 12 subjects will participate in this experiment.

II. Procedures

You will participate in three sessions of research. The first session will last about one hour, during which several body dimensions such as height and weight will be measured. You will also be given practice on the experimental trials during which posture will be measured by video tape. At the start of the second and third sessions, you will be fitted with several pieces of equipment. First, pairs of electrodes will be attached to eight locations around your trunk at approximately the waist level. To attach the electrodes your skin must be prepared by cleaning it with rubbing alcohol and possibly removing the hair around the electrode sites. Once the electrodes have been fitted, you will be asked to perform six maximum voluntary trunk physical exertions.

Following the maximum voluntary contraction efforts, the experimental trials will begin. You will be placed in a wooden loading frame. During the exertions, you will wear a hip belt attached to the frame to provide support. For six trials, a chest harness will be fitted to your shoulder region. This harness will be used to apply weights requiring you to make physical exertions of the trunk. For 18 trials you will asked to lift weights with your hands and maintain an upright posture. The frame allows weight to be either attached to the chest harness or lifted with your hands so that you will have to resist twisting movements, forward and backward movements, and side to side movements. The weights should require moderate physical activity of your trunk muscles. You will be asked to perform 30 exertions during the second and third sessions (the maximum effort trials, the harness trials, and the hand loading trials). Two minute rest periods will be provide between each exertion.

III. Risks

A screening questionnaire will be used to eliminate participants at risk for back injury or pain. Still, the possible risk or discomfort to you as a participant may be some fatigue and low back pain. Two minute rests between each trial will be provided to minimize fatigue. The electrodes are placed on your skin using an adhesive much like a bandage. Removal of the electrodes can cause brief skin irritation similar to removing a bandage. Electrode placement may also require hair removal which would be accomplished by an electric razor. The use of an electric razor will minimize the possibility of any cuts.

IV. Benefits of this Project

Your participation in the project will provide information on the accuracy of models used to predict trunk muscle activity during physical exertion. In addition, this research may lead to the development of models which determine if tasks may cause back injuries.

No guarantee of benefits has been made to encourage you to participate.

V. Extent of Anonymity and Confidentiality

Your individual results from this study will be kept strictly confidential. At no time will the researchers release your individual results of the study to anyone other than individuals working on the project without your written consent. The information you provide will have your name removed and only a subject number will identify you during analysis and any written reports of the research. Consolidated results from all the subjects with no individual identification may be reported in technical reports, conference proceedings, or journal articles.

You will be videotaped during each session. The video tape will be used after the experiment to analyze posture of the arms and torso. The tapes will be stored in an office (Whittemore 550); only the researchers will review the tapes for posture analysis. The tapes will be erased after May 1996.

VI. Compensation

If you decide to participate in this experiment, you will be paid $5.00 per hour, for an estimated total of $35 to $40, plus a $5.00 bonus for completing the third session. You will be paid at the end of the third session.

VII. Freedom to Withdraw

You are free to withdraw from this study at any time without penalty. If at any time during the experiment, you feel discomfort, fatigue, aches, or any other sensations that make it advisable to stop, alert the experimenter. Only you can be the judge of any onset of discomfort. If you choose to withdraw, you will be compensated for the portion of time that you completed. If you are found to be at risk for back injuries based on a screening questionnaire, or if electrodes are found not to work with you, you will be asked to withdraw from the experiment, and will be compensated for the time you have participated.

VIII. Approval of Research

This project has been approved, as required, by the Institutional Review Board for projects involving human subjects at Virginia Polytechnic Institute and State University and by the Department of Industrial and Systems Engineering.

IX. Subject's Responsibilities

I voluntarily agree to participate in this study. I have the responsibility to report honestly on the "Participant Screening Questionnaire" or during the experiment any conditions that may put me at risk for a back injury, or any other conditions of risk in this study.

X. Subject's Permission

I have read and understand the "Informed Consent Form" and conditions of this project. I have had all my questions answered. I hereby acknowledge the above and give my voluntary consent for participation in this project.

If I participate, I may withdraw at any time without penalty. I agree to abide by the rules of this project.

_____ _____

Signature Date

Should I have any questions about this research or its conduct, I will contact:

Mark L McMulkin Investigator	231-5359 Phone
Dr. Karl H. E. Kroemer Faculty Advisor	231-5677 Phone
Dr. Ernest R. Stout Chair, IRB Research Division	231-9359

APPENDIX B: Participant Physical Fitness Questionnaire

Participant Screening Questionnaire

Subject's Name:_____
Telephone Number:(_____)_____
Gender:_____ Date of Birth:_____

Please describe any physical activities you presently participate in on a regular basis:

_____;_____times per week

_____;_____times per week

Please answer Yes or No to the following questions.

Have you ever had a hernia?_____

Have you ever had a back injury or back or spine operation?_____

Have you had any noticeable back pain during the last year?_____

Have you ever had any joint dislocations, broken bones, or other physical injuries in the last year? _____

Have you ever had any other serious musculoskeletal injury?_____

Can you think of any injury, or illness you might have which could be aggravated by physical activity or participation in this experiment?_____

If yes, please explain:_____

_____

_____

_____
Signature and Date

VITA

Mark Lee McMulkin was born on May 17, 1966 in Great Bend, Kansas. He received a B.S. degree in Mechanical Engineering from the University of Idaho in May 1989. He received an M.S. degree in Industrial and Systems Engineering, Human Factors option from Virginia Polytechnic Institute and State University (Virginia Tech). While pursuing his M.S. and Ph.D. at Virginia Tech, he worked as a Graduate Research Assistant and Teaching Assistant. His research has included work on an alternative keyboard (the Ternary Chord Keyboard), finger speed, and railroad car wheel and lever brakes. He has been teaching assistant for graduate statistic and training courses and has taught a course titled Introduction to Industrial Engineering. He has authored or co-authored three journal articles and four proceedings papers in the Human Factors field. He is a member of the Human Factors and Ergonomics Society, the Ergonomics Society, Institute of Industrial Engineers, and Tau Beta Pi.